NASA CR 65540

HOUSTON RESEARCH INSTITUTE, INC.

DESIGN AND ENGINEERING DIVISION OF HOUSTON RESEARCH INSTITUTE, INC.,

6001 GULF FREEWAY, HOUSTON, TEXAS 77023, 713 WA 8-5001

FINAL REPORT

DESIGN DATA FOR ABLATORS

PART III: MATHEMATICAL MODEL FOR DECOMPOSITION OF PHENOL-FORMALDEHYDE ABLATORS

Design and Engineering

Research and Development

Economics, Marketing and Management Services

Presented to:

NASA Manned Spacecraft Center
(Contract No. NAS 9-2516)

31 March 1965

HOUSTON RESEARCH INSTITUTE, INC.
5417 CRAWFORD STREET
HOUSTON 4, TEXAS

o FINAL REPORT o

DESIGN DATA FOR ABLATORS
PART III
MATHEMATICAL MODEL FOR DECOMPOSITION OF PHENOL-FORMALDEHYDE ABLATORS

By

Charles E. Mauk
H. William Prengle, Jr.
W. A. Hoppe
M. S. Bawa

Presented to:

NASA Manned Spacecraft Center
(Contract No. NAS 9-2516)

31 March 1965

Approved:

Copy No._____
(-19,700)

H. William Prengle, Jr.
Vice President, Technical Director

TABLE OF CONTENTS

		Page
	ABSTRACT	1
I.	NOMENCLATURE	4
II.	INTRODUCTION AND LITERATURE SEARCH	
	A. Purpose of the Work	8
	B. The Ablation Phenomenon	8
	C. Literature Survey	10
III.	CHARACTERIZATION OF THE ABLATION SUBSTANCE	
	A. Structure of Phenol-formaldehyde Resin	21
	B. Curing of Phenol-formaldehyde Resin	22
	C. Water and Air Adsorption by Cured Phenol-formaldehyde Polymer	28
	D. Preliminary Characterization of the Epoxy-Novolak	29
IV.	EXPERIMENTAL INVESTIGATION	
	A. Review of Equipment in Literature	32
	B. Operation of Kinetic Equipment	40
	C. Operation of Auxiliary Equipment	47
V.	KINETIC MODEL	
	A. Chemical Reactions in the Solid Phase	52
	B. Solution of the Mass Diffusion Equation	56
	C. Possible Polymer Reactions	62
	D. Oxygen Evolved into the Gas Phase	66
	E. Carbon Evolved into the Gas Phase	69
	F. Hydrogen Evolved into the Gas Phase	70
	G. Total Weight Loss	71
VI.	ANALYSIS OF THE DATA	
	A. Weight Loss Data	73
	B. Solid Phase Property Changes	81
	C. Disappearance of Oxygen and Carbon from the Solid	84
	D. Rate and Transport Constants	92
VII.	PF PYROLYSIS GAS SPECIES	101
VIII.	CALCULATIONAL MODEL	110
	A. Working Equations	112
	B. Calculated TGA Curves	114
	C. In Situ Decomposition	122

Page

IX. LITERATURE CITED 124

o APPENDIX o

A. EXPERIMENTAL PROCEDURES 128

B. EXPERIMENTAL DATA 132

C. COMPUTER PROGRAMS 183

D. CALCULATION OF KINETIC AND DIFFUSION PARAMETERS 210

E. EXPERIMENTAL EQUIPMENT 215

LIST OF TABLES

TABLE		Page
I.	Major PF Decomposition Products	12
II.	Product Analysis - Polybenzyl Pyrolysis	15
III.	Translational and Vibrational Energies	19
IV.	Water Adsorption-Desorption on Phenol-formaldehyde Resin	29
V.	Water Adsorption on Epoxy Novolak Resin	31
VI.	Material Balance on C-1 Resin	85
VII.	Experimental Values of λ's and k's as a Function of Temperature	94
VIII.	Experimental Values of α's and μ's as a Function of Temperatures	95
IX.	Temperature Function Parameters for λ's and α's.	99
X.	Comparison of Gaseous Species	108
B-1	Thermal Decomposition Data, PF (378°C)	133
B-2	Thermal Decomposition Data, PF (387°C)	133
B-3	Thermal Decomposition Data, PF (382°C)	134
B-4	Thermal Decomposition Data, PF (436°C)	138
B-5	Thermal Decomposition Data, PF (533°C)	138
B-6	Thermal Decomposition Data, PF (571°C)	138
B-7	Thermal Decomposition Data, PF (498°C)	139
B-8	Thermal Decomposition Data, PF (605°C)	141
B-9	Thermal Decomposition Data, PF (666°C)	145
B-10	Thermal Decomposition Data, PF/Q (388°C)	146
B-11	Thermal Decomposition Data, EPN (316°C)	148
B-12	Thermal Decomposition Data, EPN (388°C)	150

		Page
B-13	Tar Analysis, PF Runs	152
B-14	Analysis of Residual Gas, PF Runs	154
B-15	Physical Properties of Solid (PF)	156
B-16 to B-40 (incl.)	Mercury Porosimeter Determination of Pore Volume, Surface Area, and Permeability	157-181
B-41	Magnitude of Diffusivities	182

LIST OF FIGURES

FIGURE		Page
1.	Infrared Spectrogram of Phenol-formaldehyde Film	24
2.	Infrared Spectrogram of Powered Phenol-formaldehyde Resin	26
3.	Phenol-formaldehyde Characterization Plot	27
4.	Epoxy Novolak Characterization Plot	30
5.	Kinetic Equipment (flow diagram)	41
6.	Kinetic Equipment (overall photo)	42
7.	Pyrolysis Furnace Interior (photo)	44
8.	Vacuum Desorption Apparatus (photo)	48
9.	Karl-Fisher Apparatus (photo)	49
10.	Winslow Mercury Porosimeter (photo)	51
11.	Visualization of the Porous Solid	53
12.	Diffusion Attenuation, $\eta(\alpha, \tau_m)$	61
13.	Weight Loss, PF Resin	74
14.	C/H/O Loss Distribution, PF (382°C)	75
15.	C/H/O Loss Distribution, PF (498°C)	76
16.	C/H/O Loss Distribution, PF (605°C)	77
17.	Effect of Quartz Fibers on PF Decomposition	78
18.	Weight Loss, EPN Resin	79
19.	C/H/O Loss Distribution, EPN (316°C)	80
20.	Physical Properties of Solid (function of weight loss)	82

FIGURE		Page
21.	Pore Size Distributions	83
22.	Oxygen Disappearance	86
23.	Oxygen Disappearance Mechanism	88
24.	Carbon Disappearance	89
25.	Carbon Disappearance, by the Model	91
26.	Rate and Transport Parameters, Oxygen Disappearance	96
27.	Rate and Transport Parameters, CH_2 - Disappearance	97
28.	Rate and Transport Parameters, Ring Disappearance	98
29.	Gas Species Distribution, 382°C	102
30.	Gas Species Distribution, 498°C	103
31.	Gas Species Distribution, 605°C	104
32.	Solid and Gas Phase Reaction Mechanism	105
33.	Visualization of the Ablation Process	111
34.	Effect of Heating Rate on TGA Curve	119
35.	Effect of Adsorbed Water on TGA Curve	120
36.	Effect of Quartz Content on TGA Curve	121
37.	Flow Chart for HRI65R002	185
38.	Flow Chart for HRI65R003	193
39.	Flow Chart for HRI65R004	196
40.	Flow Chart for HRI65R005	204
41.	Gas Chromatograph (photo)	216
42.	Pyrolysis Furnace (photo)	217
Dwg.	C-1001-19,700 Karl Fisher Apparatus	218
Dwg.	C-1002-19,700 Vacuum Desorption Apparatus	220

HOUSTON RESEARCH INSTITUTE, INC.
5417 CRAWFORD STREET
HOUSTON 4, TEXAS

FINAL REPORT

DESIGN DATA FOR ABLATORS

PART III

MATHEMATICAL MODEL FOR DECOMPOSITION OF PHENOL-FORMALDEHYDE ABLATORS

31 March 1965

ABSTRACT

An experimental study is described, the overall purpose of which was to arrive at a mathematical model for future design calculations which describes the chemical decomposition of phenol-formaldehyde (PF) ablators.

In order to determine the mechanism of pyrolysis the experimental work was accomplished at isothermal conditions. Data were obtained over a range of temperatures from 382 - 666°C (712-1199°F) for PF polymers. The effect of quartz fibers on the decomposition of PF polymers was determined. Also, several preliminary low temperature isotherms (316 and 388°C) were determined for epoxy-novolak resins.

Conclusions from the study as pertains to phenol-formaldehyde ablators are as follows:

1. Adsorption of water and air from the atmosphere by PF polymers cannot be neglected since it can amount to as much as 11 w%. Such amount has an important effect on the weight loss characteristics during the initial stages of decomposition.

2. In order to achieve maximum cross-linkage of the PF polymer, the curing procedure is important. A thin-film combination vacuum-heating curing procedure was found to give satisfactory and reproducible results; chain-ending alcoholic-OH was reduced to a minimum.

3. The degassing or outgassing of PF polymers over extended periods of time, observed by numerous investigators, is due in a substantial measure to the above mentioned adsorbed water and air and chain-ending alcoholic -OH groups.

4. For purposes of decomposition kinetics the PF polymer structure may be visualized as,

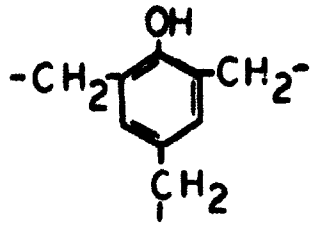

or $[(CH_2)_{3/2} - (C_6H_2) - (OH)]_m$

5. A six-step decomposition model, including a single desorption step and characterized by four rate constants, was found to describe satisfactorily the breakdown or pyrolysis of PF polymer. The model first visualizes breakout of phenolic-OH from the structure, followed by breakout of the $-CH_2$ bridges and then ring fragments. At low temperatures, phenolic-OH fracture is fastest but at higher temperatures the $-CH_2$ breakout becomes more rapid. Rate constants for the reactions follow the Arrhenius equation. The threshold or incipient reaction temperature is about 233°C (387°F).

6. At low temperatures, reaction first occurs rapidly on the surface of the solid (in the pores), but then becomes rate limited by solid phase diffusion of the product species from the bulk to the surface; the effect is quantitatively described and characterized by diffusivities of the expected magnitude - this is probably the most significant discovery made in the study.

At high temperatures, the transport effects are reduced by higher diffusivity values.

7. Once the product species have diffused from the bulk solid phase to the surface, transport is further limited by a concentration buildup at the surface, since there is insufficient sweep gas to keep the concentration at a low value.

8. At low temperatures the product species are H_2O, CO, CO_2, and a trace of H_2; attaining these molecular configurations by further reaction of OH, CH_2, H in the solid and gas phases.

9. At high temperatures the same product species appear and in addition, CH_4, C_2H_6, C_3H_8, monoaromatics and polyaromatic appear; the latter by fragmentation of the PF structure.

10. TGA curves can be computer calculated using the model for different heating rates, water content, quartz content,

and different temperature ranges. The calculated curves appear to be excellent simulations of experimental data.

11. Measurements of the physical characteristics of the PF solids (undecomposed resin and chars) indicate that the pores are large and the surface area is small compared to catalyst substances. Properties of the charred material are not substantially different than the undecomposed resin.

12. The addition of quartz fibers either during the curing process or after curing to produce a mixture has little or no chemical effect on the decomposition. The addition can be visualized as a dilution effect only.

Preliminary results on epoxy-novolak ablators indicate that, water adsorption is much less than for PF polymers, and is not a factor in the initial decomposition; and decomposition is much faster and occurs at lower temperature than for PF polymers.

I. NOMENCLATURE

The following is a listing of the nomenclature, symbols, and dimensional units used in the subsequent sections of this report.

Upper Case:

A, B, C, S, R	Symbolic designations for parts of the polymer, equation (V-25)
A_{λ_i}, A_{μ_i}, A_{α_i}	Arrhenius constants for λ_i, μ_i, α_i equations, min^{-1}
E_{λ_i}, E_{μ_i}, E_{α_i}	Activation energies for λ_i, μ_i, α_i equations, cal/g. mole
A_p	Surface area of pores, cm^2
C_i	Concentration of "i" th component, g. moles/cm^3
C_p	Heat capacity, c. l/gram
D	Diffusivity, cm^2/sec
K	Permeability, cm^2
L	Thickness of heat shield, cm
M	Molecular weight, grams/g. mole
R	Gas constant; 1.987 cal/g. mole - ^oK; 82.06 atm-cm^3/g. mole - ^oK
S	Surface area of solid element, cm^2
T	Temperature, ^oK
To	Initial temperature, ^oK
Tr	Threshold decomposition temperature defined by equation (VI-11); also reaction zone temperature, ^oK
Ts, Tcc, Tc, Tms	Temperature of surface, carbonizing char, char, metal surface, respectively, ^oK
V	Volume, cm^3
V_T, V_P	Total pore volume, cm^3/gram

W	Weight, gram
W_o	Initial weight, gram
(W/W_o)	Dimensionless weight
$\left(\frac{W_{PF}}{W_o}\right)$	Dimensionless weight of phenol-formaldehyde
$\left(\frac{W_{ox}}{W_o}\right)_g$, $\left(\frac{W_c}{W_o}\right)_g$, $\left(\frac{W_H}{W_o}\right)_g$	Dimensionless weight of elemental oxygen, carbon, and hydrogen respectively in the gas phase.
$\left(\frac{W_{ash}}{W_o}\right)$	Dimensionless weight of ash
$\left(\frac{W_{CO}}{W_o}\right)$, $\left(\frac{W_{CO_2}}{W_o}\right)$, $\left(\frac{W_{H_2O}}{W_o}\right)$, $\left(\frac{W_{H_2}}{W_o}\right)$	Dimensionless weight of carbon, carbon monoxide, carbon dioxide, water, and hydrogen respectively.
$\left(\frac{W_{CR}}{W_o}\right)$, $\left(\frac{W_{LAR}}{W_o}\right)$, $\left(\frac{W_{LHC}}{W_o}\right)$	Dimensionless weight of condensed rings, light aromatic rings, light hydrocarbon rings, respectively
X	Co-ordinate, cm
Z	Compressibility factor
α	Heating Rate, $dT/d\theta$, ^oC/min.
ρ	Dimensionless pressure

Lower Case:

a_i	Chemical activity of species "i", dimensionless
$\bar{d}$	Mean pore diameter, $\bar{d} = 4V_p/S$, microns
k_i	Kinetic rate constant for "i" th reaction, g. moles/sec - cm^3
$\bar{k}_i$	Effective kinetic rate constant, $\bar{k}_i = k_i \prod_j \gamma_j$, g. moles/sec - cm^3
k_s	Thermal conductivity of the solid, $\frac{cal/sec\text{-}cm^2}{cm - {}^oF}$

l, ℓ	Half thickness of solid element, cm
n, n_t	Number of moles, total moles
n_{ABC_o}, n_o	Initial moles of resin
n_{SRO}	Initial moles of water in resin
r	Kinetic rate, g. moles/sec-cm^3
t	Temperature, ^oC
u, w, x, y, z, η	Moles, in reaction material balances

Greek Letters:

$\alpha_i =$	$(l^2\lambda_i/D)^{\frac{1}{2}} = (\lambda_i/\mu_i)^{\frac{1}{2}}$
$\beta_1, \beta_2, \beta_3,$	Defined by equation (VIII-2)
γ_j	Activity coefficient of "j" component
ϵ	Porosity
η_i	Diffusion attenuation, defined by equation (VIII-6)
θ	Time, min.
Θ	Dimensionless time
$\lambda =$	$\bar{k}\ V/n_o$, reaction parameter, min^{-1}
$\mu =$	$D/l^2 = S^2\rho^2 D$, diffusion parameter, min^{-1}
ξ_i	Conversion function, defined by equation (VIII-3), (V-20), dimensionless
ξ_i^o	Ideal conversion, if all solid were on a surface, defined by equation (V-7)
π	Total pressure, atm.
ρ	Density, skeletal density, gram/cm^3

ρ_B	Bulk density, gram/cm^3
ρ_g	Gas density, $\rho_g = M\pi/ZRT$, gram/cm^3
ρ_s	Density of the solid, gram/cm^3
ρ_{so}	Initial density of the ablation material, gram/cm^3
τ	Dimensionless temperature, T/To
$\tau_m =$	$\mu\theta$, diffusion time, dimensionless
$\tau_k =$	$\lambda\theta$, kinetic time, dimensionless
ϕ_{125}	Defined by equation (VIII-2), (V-59)
$X =$	X/L, dimensionless

II. INTRODUCTION AND LITERATURE SURVEY

A. PURPOSE OF THE WORK:

The overall purpose of the study was to arrive at a mathematical model for future design calculations, which describes the chemical decomposition of phenol-formaldehyde (PF) ablators.

At the outset, it is important to note that the experimental approach was to study the decomposition under isothermal conditions; ample justification exists for this type of approach when studying kinetics and mechanisms, and the approach has proved successful once again.

Specifically, it was desired to:

1) - develop a suitable kinetic model for the primary decomposition of the polymer, including both chemical and physical phenomena; describing the weight loss of the solid and evolution of the gaseous species.

2) - determine the rate constants as a function of temperature.

3) - determine the transport parameters involved.

4) - develop a method for calculating a variable temperature (TGA) decomposition curve for the solid.

5) - determine the changes in the physical characteristics (density, pore volume, pore size, surface area, permeability, etc.) of the solid phase.

6) - determine the effect of quartz fibers on the degradation.

7) - conduct a preliminary decomposition of epoxy-novolak (EPN) polymer.

B. THE ABLATION PHENOMENON:

Numerous reports and papers have been found in the literature which describe the ablation phenomenon; good summaries are given by three papers: Sutton (51), Scala (41), and McAllister (33). Sutton's paper is outstanding for its experimental evaluation of several ablative materials with various reinforcements under simulated hypervelocity conditions. Scala presents mathematical models of each of the char regions and combines them to obtain an approximate overall solution. McAllister gives a very comprehensive description of ablation,

but the unique contribution is the collection of photomicrographs of the char structure. The general consensus throughout the literature is that an ablative material affords the best heat protection, and a phenolic resin with a silica type material used as reinforcement is an outstanding candidate for the best ablator.

During ablation, the ablator is normally pictured as being divided into several zones. The first zone is the unreacted material. The second zone, with which this investigation is at present primarily concerned, is the reaction zone in which the initial breakdown of the material is taking place, and the products of which are a carbonaceous char and several types of gases.

The third zone is the char zone from which the gas products have been eliminated. Gases from the reaction zone pass through the char zone on the way to the surface, but the temperature is not high enough to cause further decomposition.

In the fourth zone, the temperature is high enough to decompose the gas molecules into smaller species and as a result of this, carbon in the form of graphite is deposited on the structure of the char. If a silica type reinforcement is used a reaction between silica and carbon to form silicon carbide is possible in this zone. It is expected that this reaction absorbs energy at approximately 5,000 Btu per pound of silicon carbide formed.

At the surface, several things contribute to the loss of material. Carbon may be burning or subliming, silicon carbide may be subliming, or silica may be melting and flowing away under the force of the air flow. If the surface is at the temperature of melting silica, it will be approximately 1710^{o}C; subliming silicon carbide, 2200^{o}C; subliming graphite, 3650^{o}C. Since the radiation of energy is proportional to the fourth power of the absolute temperature, a graphite surface would radiate about twenty times as much energy as a silica surface having the same emissivity. The gas molecules are being injected into the boundary layer; this reduces the energy flow into the ablator. The flow of molten silica, or the deposition of carbon may plug the pores of the char so that the gases cannot escape, and as gas pressure builds up, the surface may be "exploded" away. If the surface is not strong enough, it may be torn away by air flow. It is obvious that some trade off must be made to determine the optimum surface conditions of strength and composition, and this should be the object of some future investigation.

C. LITERATURE SURVEY:

1. Decomposition Data - Ablators:

Numerous reports and papers have been examined (see Part I of this report) relating to ablation. A few reports are available which present elemental analysis of char or products, but only where molecular analysis of phenolic decomposition products is given are the results of use in this study. Applicable data can be found in three reports, Ouchi (38), Schmidt (43), and Friedman (3).

Ouchi (38) presents graphical results from pyrolysis of several kinds of phenolic resins which can best be interpreted as rates of production of each of the products at temperatures from 200-1000°C. Actually, the results are the amount of material generated over a 100° temperature increment as analyzed by a mass spectrometer or water absorption. Apparently nothing with a mass number higher than that of CO_2 could be analyzed. Because of the graphical presentation large temperature increments between samples, and no analysis of mass numbers greater than 44, the results are only qualitatively useful.

Schmidt (43) tabulates molecular analyses of pyrolytic products which were summarized from several papers by Madorsky and Straus of the National Bureau of Standards. The CTL 91-LD phenolic was heated in an electric furnace. The time to heat the material to the desired temperature was 2-5 minutes, and the temperature was held for 5-30 minutes. The material volatile at room temperature was analyzed by mass spectrometer. Material which could not be identified made up 50-70% of the products.

Friedmar (3) presents analyses of three fractions of the products from arc furnace pyrolysis of CTL 91-LD glass reinforced phenolic resin and nylon-phenolic resin. The nylon-phenolic results are not applicable to the problem, because it is not possible to tell which and how much of the decomposition products come from the nylon. Only three fractions are analyzed, volatile under vacuum at -195°C, -78°C, and room temperature, but this generally accounts for 85-90% of the weight loss. Results are tabulated as mole % averaged over several runs, and analysis was made for components as heavy as C_{10} aromatics. It is interesting to note that about 6 mole % ammonia was found in the phenolic products; this is thought to result from the decomposition of an additive put in by the manufacturer.

Lee (26) pyrolyzed a phenolic novolak in a flask heated with a heating mantle, and the material which was volatile below 120°C was passed directly into a mass spectrometer. As

would be expected with a novolak, more than 10 mole % of the material identified was formaldehyde (see Section III-A).

Table I shows the fraction of the components in the products from different sources (based on the components which were identified). A comparison of the results from the different reports may not be justified because of the differences of technique involved. Exposure time was a matter of seconds for Friedman, minutes for the results in Schmidt, hours for Ouchi and the time is not known for the results of Lee. The temperatures appear to be comparable, but Friedman had a steep temperature gradient across his sample, while Ouchi's temperature was changing throughout the run. Two of the reports deal with CTL 91-LD phenolic, but Ouchi manufactured his own and Lee used a material which is not very similar to the others. The results of Ouchi must be integrated to compare with the others.

The fact that Ouchi finds twice as much water as Friedman, while Schmidt reports none, seems to indicate that Ouchi's resin was not completely cured, and cross-linking with the evolution of water occurred during the pyrolysis. The hydrogen and carbon monoxide contents seem to be consistant, and except for Friedman, so does the methane; however, if Friedman's acetylene were converted to equivalent methane, the comparison would be much more favorable. The other components are of less importance. Except for the higher mass number products, the results of Ouchi seem quite comparable to those from Friedman or Schmidt. The product distribution shown in Table I emphasizes that the material used by Lee discourages quantitative comparison with the others.

2. Mechanisms - Pyrolysis of PF Resins:

During the investigation of the open literature, two papers were found which were concerned with the pyrolysis of phenol-formaldehyde (PF) resins as possible models for the structure of coal. The papers did not attempt to develop a kinetic model, but some mechanisms were proposed based on the experimental work of the authors. These mechanisms are given here for completeness, although their value is doubtful since they were not quantitatively confirmed.

Ouchi (38) deduces the following mechanisms of reaction:

1. Initial reactions of one of the forms,

$$2(-OH) \longrightarrow -O- + H_2O \qquad \text{(II-1)}$$

$$-OH + -CH_2- \longrightarrow \diagup\!\!\diagdown CH + H_2O \qquad \text{(II-2)}$$

TABLE I

MAJOR PF DECOMPOSITION PRODUCTS

	MOLE% OF IDENTIFIED COMPONENTS					
	LEE	SCHMIDT			FRIEDMAN	OUCHI*
COMPONENT	450°C	500°C	800°C	1200°C	700°C	700°C
HYDROGEN	0.5	0	66.7	66.9	34.7	34.3
METHANE	0.8	27.4	13.9	14.6	6.0	12.1
AMMONIA	0	0	0	0	6.2	0
WATER	10.5	0	0	0	18.9	42.6
ACETYLENE	0	0	0	3.5	6.7	0
CARBON MONOXIDE	40.2	12.8	8.6	3.8	15.4	9.9
CARBON DIOXIDE	30.6	1.4	0.4	1.3	0.6	0.7
ETHANE/ETHYLENE	0.5	0	1.6	2.7	1.9	0.4
PROPANE/PROPYLENE	1.7	0	0.1	0.2	0.6	0
BUTANES/BUTENES	0	0	3.4	0	0	0
ACETONE	0	31.0	0	0	0.3	0
PROPANOL	0	18.9	0	0	1.7	0
BENZENE	0	3.3	0.2	5.5	2.9	0
TOLUENE	1.5	5.2	0.3	0.6	0.7	0

* The results of Ouchi are integrated to 700°C to make them comparable.

2. Assuming that the ring is resistant to heat, the methane is formed from the methylene bridges and the following secondary reactions are proposed,

$$-CH_2- + H_2O \rightarrow CO + 2H_2 \qquad (II-3)$$

$$-CH_2- + H_2 \rightarrow CH_4 \qquad (II-4)$$

$$-CH_2- + -O- \rightarrow CO + H_2 \qquad (II-5)$$

$$2(-CH_2) \rightarrow C_2H_4 \qquad (II-6)$$

$$C_2H_4 + H_2 \rightarrow C_2H_6 \qquad (II-7)$$

$$CO + -O- \rightarrow CO_2 \qquad (II-8)$$

In the second step, the benzene nuclei are bonding directly to each other.

Wolfs (53) draws several interesting conclusions from a study of the carbonization of several phenolic resins formed with radioactive formaldehyde (temperature 400-600°C). The initial decomposition is a depolymerization by breaking the methylene bridges, so that the average number of carbon atoms per monomer unit is the same. Some monomer units become richer in hydrogen and polymerize to form "tar". Other monomer units loose hydrogen and go to form "semi-coke". A secondary reaction occurs when the semi-coke decomposes to volatile gases and carbon. Radioactivity indicates that the majority of the carbon in the volatile gases comes from the rings, while the original bridge carbon stays in the solid.

3. Mechanisms - Pyrolysis of Poly-Aromatics:

It is to be expected that a review of the literature on the pyrolysis of polyaromatics should lead to conclusions applicable to the aromatic ring structure of phenolic resins. A study of the pyrolysis of aromatic and polyaromatic compounds should lead to an understanding of the initial decomposition mechanisms of the resins. Outstanding in the literature is a series of papers by Greensfelder, Voge, and Good (16-18), which discuss decomposition products and mechanisms.

a. Pertinent Papers and Reports:

Anderson (2) conducted a TGA, up to 525°C of polybenzyl, the basic structure of which is represented as follows:

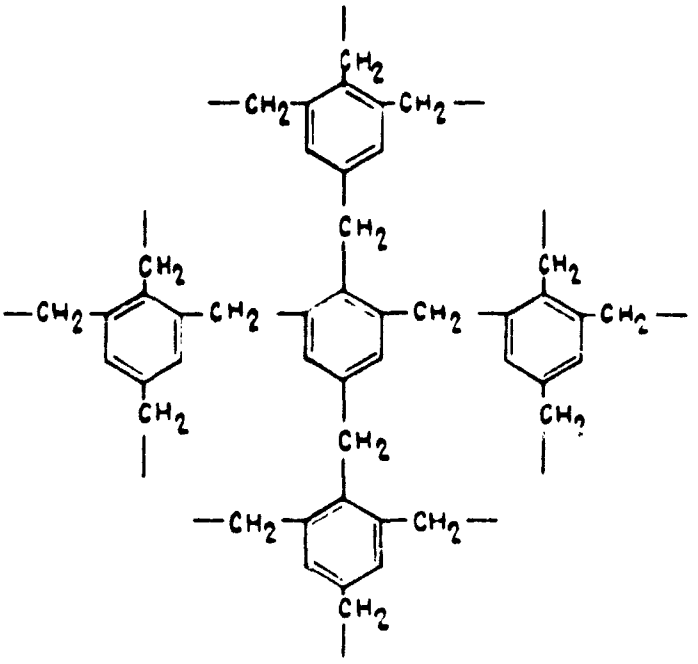

Comparison of the structure of polybenzyl with that of phenol-formaldehyde indicates that the polybenzyl investigation should have considerable bearing or a phenolic ablation study. Product analysis is shown in Table II.

If there were no preference for the breaking of bridge bonds, the product distribution relative to benzene should be:

	Molar Ratio
Benzene	1
Toluene	4
Xylenes	6
3 Methyl-groups-per-ring	4
4 Methyl-groups-per-ring	1

Since the experimental ratio of toluene to benzene is 3 to 1, the indication is that the bridge carbons are held preferentially in the residue. This idea is reinforced by the fact that 2, 3, or 4 methyl-groups-per-ring molecules are practically non-existent in the liquid product.

TABLE II

PRODUCT ANALYSIS-POLYBENZYL PYROLYSIS

COMPONENT	WT.% OF CHARGE	MOLAR RATIO
RESIDUE		
CONDENSATE (IN PYROLYSIS TUBE)	28.60	
VOLATILE LIQUID	4.00	
BENZENE	0.85	1.0
TOLUENE	3.11	3.1
XYLENES	0.04	

Lewis (27) sums up work with DTA, ESR (electron spin resonance), IR, UV, and x-ray on the pyrolysis products of acenaphthylene to propose a mechanism for its carbonization. the ESR technique was applied to solutions in m-quinquephenyl or biphenyl up to 300°C. The success of the investigation indicates the importance of free radical mechanisms not only in the carbonization of acenaphthylene, but also in the carbonization of several other aromatic compounds previously observed. The mechanism proposed is as follows:

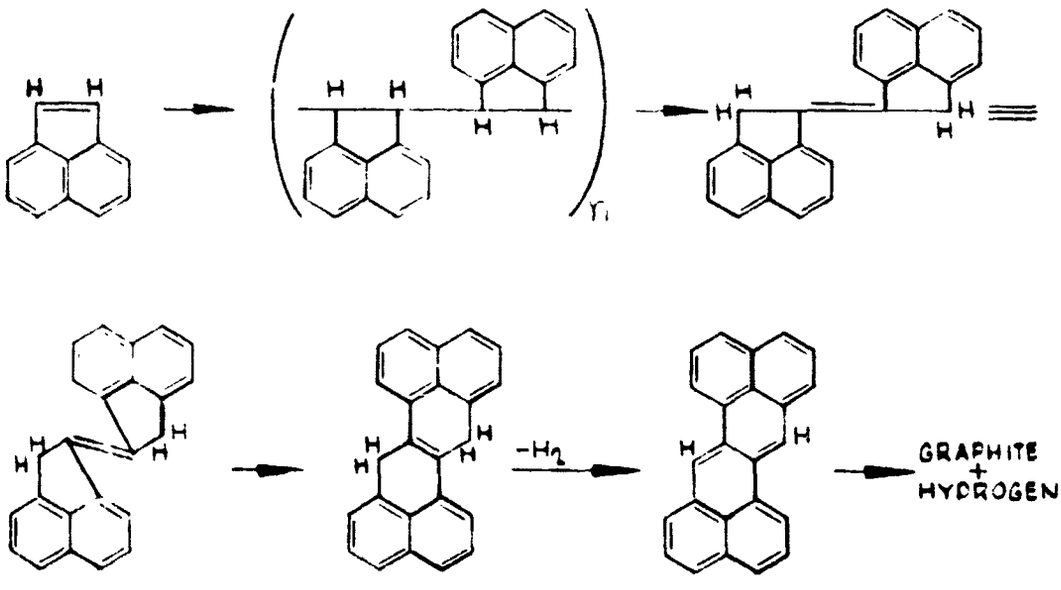

Equation (III-2) shows only the major changes, and free radicals are the intermediate products. It is interesting to note that lattice spacing for this synthetic graphite is 3.370 Å and that of natural Canadian graphite is 3.361 Å.

Meyer (34) performed a pyrolysis of toluene or deuterated toluene in an atmosphere of hydrogen or deuterium at 750°C. The indication was that hydrogen atoms are much more strongly fastened to the methyl groups than to the rings. The benzene, methane, and toluene formed were examined by mass spectrometer and IR. Conversion was about 2%.

Kinney (22) pyrolyzed benzene, naphthalene, anthracene, chrysene, and pyrene in a tubular quartz reaction at 800-1100°C at concentrations less than 5 mole % in nitrogen. Contact times were in the range of 1-50 seconds. Carbon formation is increased from the 1-ring to 2-ring to the 3-ring material, but the 4-ring materials drop off in carbon formation. This is probably because of geometrical consideration for the condensation. Packing the reactor with coke increases the carbon rate for all materials. Packing the reactor with quartz chips increases the production of biphenyl from benzene. Traces of acetylene are produced; a few wt% methane are formed; up to 60 mole % hydrogen is released as H_2 for 90 wt% conversion of benzene to carbon. The following mechanism is proposed for the condensation of benzene.

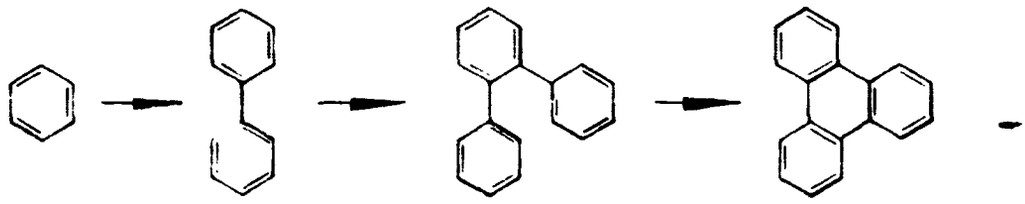

Stehling (50) pyrolyzed several hydrocarbons, each diluted with helium, at temperatures in the range 600-900°C. A cylindrical Vycor reactor was used, and contact time was in the range 4-10 seconds (held constant for a material for runs over the temperature range). Analytical results for acetylene appeared independent of whether the reactor walls were clean, polymer coated, or carbon coated. Other than carbon and hydrogen, benzene is the chief pyrolysis product of acetylene,

reaching a peak of 25% of acetylene feed at 800°C; naphthalene is about 5% (carbon basis); ethylene 9%, methane 5%; unconverted acetylene 23%. More hydrogen is produced from an acetylene-benzene mixture than from the components pyrolyzed separately under the same conditions. In the pyrolysis of benzene, decomposition of benzene was not detectable until 800°C, and at 900°C only 43% of the benzene decomposed.

Stehling concludes that:

1. Carbon formation cannot, in general, result from a mechanism of the type acetylenic ⟶ aromatic ⟶ carbon.

2. With high temperatures, and free radicals present, carbon formation is more likely to result from ring-opening and fragmentation of aromatics than from condensation.

3. A methyl group substituted on the aromatic rings has more effect on decomposition than a second ring.

Kinney (23) pyrolyzed benzene, acetylene, and diacetylene, 0.1 mole % in helium, at 1200°C in a porcelain tube at contact times up to 112 milliseconds. The major gas products for benzene are acetylene, diacetylene, methane, and hydrogen (not analyzed for) Extrapolation of the data toward zero contact time implies a mechanism of initial decomposition of the form,

$$C_6H_6 \longrightarrow HC \equiv CH + HC \equiv C\text{-}\ C \equiv CH + H_2 \qquad \text{(III-4)}$$

But because at the shortest experimental contact time, 4 milliseconds, the mole % of acetylene is twice that of diacetylene, the mechanism of Equation (III-5) may also be important. This is emphasized by the fact

$$C_6H_6 \longrightarrow 3\ HC \equiv CH \qquad \text{(III-5)}$$

that benzene was prepared quantitatively from acetylene nearly a century ago; the reverse reaction for Equation (III-5). After 4 milliseconds the diacetylene curve drops away much faster than does the acetylene (benzene pyrolysis products).

Since acetylene is an important product of diacetylene and vice-versa; and more than 90% of the diacetylene was pyrolyzed in 112 milliseconds, but less than 25% of the acetylene was pyrolyzed in the corresponding time period; the obvious conclusion is that the primary decomposition mechanism is the formation of diacetylene, which then decomposes to carbon.

b. Conclusions from Papers in the Literature:

Based on the results and mechanisms proposed in the

foregoing papers, certain conclusions can be drawn. A possible mechanism for the condensation of diacetylene is as follows, and appears justified by the results of Kinney:

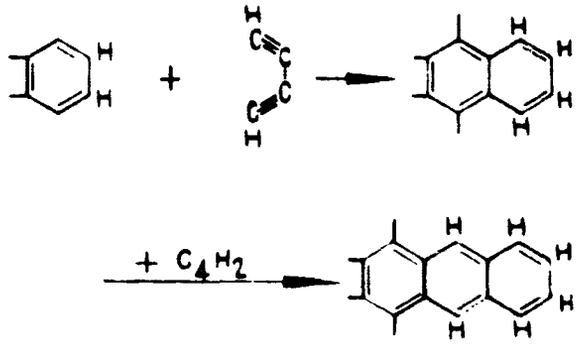

Since Stehling found that an olefinic-aromatic mixture had a higher hydrogen production rate (and consequently a higher carbon rate) than the sum of the separate rates, the use of an aromatic structure for the neucleus of condensation seems justified. In summary, it appears that the pyrolysis of aromatics to a graphite type carbon should follow two parallel mechanisms. The first is typified by the condensation of benzene, Equation (III-3), and is dominant at low temperatures, 800-1100°C, where there is less tendency for the ring to crack; or at high densities, where condensed aromatics, stabilized by additional resonant energy, form before the ring has a chance to break. The second mechanism is dominant at high temperatures, above 1100°C, where the ring breaks. The most likely path for the second mechanism is the breaking of the benzene ring to form acetylene, part of which immediately decomposes to form diacetylene and H_2. The diacetylene then condenses around an uncracked benzene neucleus, as shown in Equation (III-6). At the borderline, 1100°C region, both mechanisms may be active.

Below 800°C, benzene is relatively inert unless it is irradiated with light of wavelength less than 20 μ. The near infrared, which is the fundamental bond vibration region, is approximately 2-20 μ, and apparently strong radiation of the proper frequency can so excite the C-C bonds in the benzene ring that some of them break and acetylene is formed. This gives a clue as to why the rings might break at high temperature. One possibility is that the radiation from the reactor

wall might be strong at the frequency corresponding to the ring C-C stretch fundamental, but it is more likely that the bond is simply thermally excited to the breaking point. As an example of this, consider the change from 1000°C, where Kinney (1954) found ring condensation, to 1200°C, where Kinney (1960) found ring cracking. Table III compares the fraction energy change per degree of freedom for translation, $\frac{1}{2}kT$, and for vibration $h\nu_o / \exp(h\nu_o/kT) - 1$. From 1000°C to 1200°C, the C-C stretch increases 27% while the translation energy increases only 16%. Since the C-C bond in the benzene ring is not a single bond or a double bond, but something about halfway between, at 1000°C, a C 1½ C bond would have 0.786×10^{-13} ergs energy and at 1200°C, 1.040×10^{-13} ergs. This does not necessarily reflect the activation energy of bond breaking, but it is interesting to note that at approximately the point where ring breaking becomes significant, the vibrational energy of a C 1½ C bond becomes equal to the translational energy of one degree of freedom.

Since there are 6 C-C and 6 C-H bonds in a benzene molecule (plus 18 other bonding and stretching vibrational modes), while there are only 3 translational and 3 rotational degrees of freedom, it can be seen that at high temperatures much more of the energy goes into vibrational modes than translation and rotation.

TABLE III

TRANSLATIONAL AND VIBRATIONAL ENERGIES

	ENERGY/DEGREE OF FREEDOM		
	800°C	1000°C	1200°C
TRANSLATION ($\frac{1}{2}kT$)	0.740×10^{-13} erg	0.879×10^{-13} erg	1.019×10^{-13} erg
C-C STRETCHING (AROMATIC, 989 cm^{-1})	0.480kT	0.543kT	0.594kT
C-C STRETCHING (AROMATIC, 1618 cm^{-1})	0.280kT	0.351kT	0.427kT
C-H STRETCHING (AROMATIC, 3045 cm^{-1})	0.045kT	0.081kT	0.120kT

4. Kinetic Models Proposed Previously:

The only attempt at model development for the process appears to be that of Friedman (14). Previous work by other investigators indicated that the weight loss of a strictly subliming polymer was of the expected first order forms,

$$-\dot{W} = \bar{k}\, W$$

where "W" is the weight of material, and "$\bar{k}$" is the reaction rate constant. In his early work, Friedman recognized that in a charring ablation material, the filler and a portion of the material would end up as char and would not be available for reaction. It would therefore be more proper to write the previous equation as,

$$-\dot{W} = \bar{k}\, (W - W_c)$$

where "W_c" is the final weight of the char. In his 1961 report, Friedman recognizes that although no one knows in what form the kinetic equations of decomposition should appear, it is very unlikely that the overall or apparent equation would be of first order. He therefore proposed that the overall reaction rate would be of the form,

$$-\left(\frac{\dot{W}}{W_o}\right) = \bar{k}\left(\frac{W}{W_o} - \frac{W_e}{W_o}\right)^n$$

where "W_o" is the initial weight of material, and "n" is the pseudo order of the overall reaction. He also recognized that the reaction rate constant would be of the Arrhenius form,

$$\bar{k} = A \exp\left(-\Delta E/RT\right)$$

When evaluating the constants for a best fit of the results of a thermogravimetric analysis of fiberglass reinforced phenol-formaldehyde resin, $A = 10^{18}$ hr^{-1}, $\Delta E = 55{,}000$ cal./g. mole, and $n = 5$, were obtained. The final form of the overall kinetic equation, with these values for the constants, gives very reasonable reproduction of the data except for a very early loss of about 5% which occurred up to about 400°C. Incomplete cross-linking in the original material probably caused the initial loss as the cross-linkage was completed and water eliminated. A reaction order greater than three is virtually unknown in reaction kinetics, and Friedman says that the apparent fifth order probably results from a complex mechanism in the solid state of the highly cross-linked material.

Because Friedman's model is the only kinetic model in the literature, many investigators have used it in their overall model. However, to make a significant improvement, it is necessary to develop a kinetic model which describes the molecular processes involved.

III. CHARACTERIZATION OF THE ABLATION SUBSTANCE

A. STRUCTURE OF PHENOL-FORMALDEHYDE RESIN:

The literature indicates that the first step in the reaction of phenol with formaldehyde is the formation of phenol alcohols,

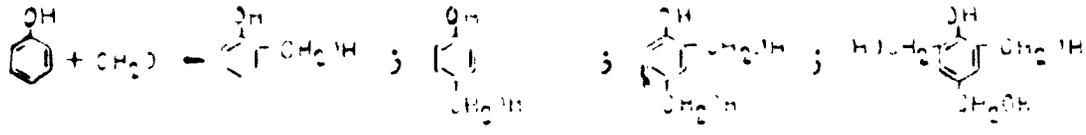

(III-1)

with the relative amounts of the mono-, di-, and tri-alcohols determined by the relative amounts of phenol and formaldehyde initially present. The next step in the series is a reaction such as,

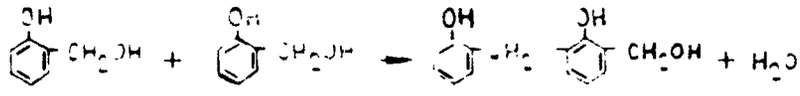

(III-2)

which is repeated to form a linear chain of ring structures connected by methylene bridges. In an acid catylized reaction, there is also the possibility of forming a methyl ether bridge,

(III-3)

however, with strong heating later in the cure, the methyl ether bridge decomposes to form a methylene bridge and a formaldehyde molecule. The linear polymer is fuseable and soluble in organic solvents, but three dimensional configurations of three bridges per ring are formed as the reactions

progress and these formations are infuseable and insoluble. The final stage might be visualized by the following two dimensional representation of the three dimensional structure:

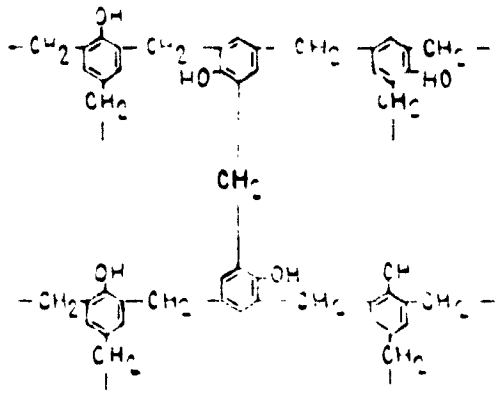

(III 4)

If an acid catalyst was used, then some of the methylene bridges, $-CH_2-$, will be methylene ether bridges, $-CH_2-O-CH_2-$, and only in an ideal case will there be three bridges on each ring. Some of the rings will have two bridges and either an alcohol group, $-CH_2OH$, or a hydrogen atom at the third position. Experimental evidence concerning the basic structure of the resin is reviewed by Cashwell (5).

B. CURING OF PHENOL-FORMALDEHYDE RESIN:

The "A" stage resin is made up essentially of the alcoholic condensation products of phenol and formaldehyde and is water soluble.

The "B" stage resin is made up of linear chains of alternating rings and methylene bridges and is fuseable and solvent soluble.

The "C" stage resin is essentially all cross linked and is infuseable and insoluble.

The stages are not clearly separated, but overlap so that the "A" stage resin will have not only phenol alcohols, but also some higher condensation products. In the "B" stage, some phenol alcohols will still be present, and an appreciable amount of cross linked material may be present. From 3 to 6% of the "C" stage resin may still be removed by extensive extraction with acetone.

To obtain a resin which has the best thermal stability, it is obvious that cross-linkage should be as extensive as possible.

The phenol-formaldehyde used in this investigation is EA-466 Phyophen (90-087), furnished by Reichhold Chemicals, Inc. (Carteret, New Jersey), which is a purple water solution of phenol alcohols (A stage). The initial proportion is 1½ moles of formaldehyde to one mole of phenol, which is the correct proportion for three bridges attached to each ring, plus a small amount of fixed alkali catalyst. Although this material is chosen to give the most complete cross-linkage possible for phenol-formaldehyde, three bridges per ring, the bridges may not all form if the curing is not carried out properly. Some measure of the extent of cross-linkage may be obtained by determining the amount of "alcoholic" hydroxide (-OH groups attached to the methylene groups as opposed to being attached directly to the ring). A titrametric method of determining alcoholic OH by acetylation with acetic anhydride is described in Appendix A. If the resin is polymerized and cured at 150°F for 12-24 hours, the solid material is relatively soft and the alcoholic OH is approximately 15% by weight (this corresponds roughly to one unformed bridge for each ring); but after "complete" curing, the resin is very hard and the alcoholic OH is less than 0.5% by weight. Since the complexity of the geometric structure prevents 100% cross-linkage, the alcoholic OH can never be reduced to zero.

Because of the possibility that the alcoholic OH analysis was indicating phenolic OH (hydroxide group attached directly to the ring) as well, the question arose as whether the 0.5% OH value resulted only because the extreme curing conditions had actually caused decomposition and loss of the phenolic OH (normally greater than 15% by weight). The question can be resolved by infrared spectroscopy. Figure 1 shows a spectrogram of a thin film of resin cured under relatively mild conditions, and a large adsorption peak occurs at the characteristic frequency for OH stretching, approximately 3300 $\bar{\nu}$. When the same film is subjected to additional curing under the more adverse conditions, substantially no change appears in the OH adsorption peak. This establishes that the alcoholic OH analysis does not include phenolic OH and that the phenolic OH is not lost under the most extreme conditions of curing which were used. Figure 1 also indicates the vibrational modes which have been assigned to the more important vibrational adsorption peaks.

It is very difficult to form a uniform resin film of the proper thickness to have the required degree of transparency, and when such a film is formed, it is very delicate. A method which is more practical with respect to physical manipulation involves grinding the solid material to a fine powder, mixing with potassium bromide, and pressing in a hydraulic press to

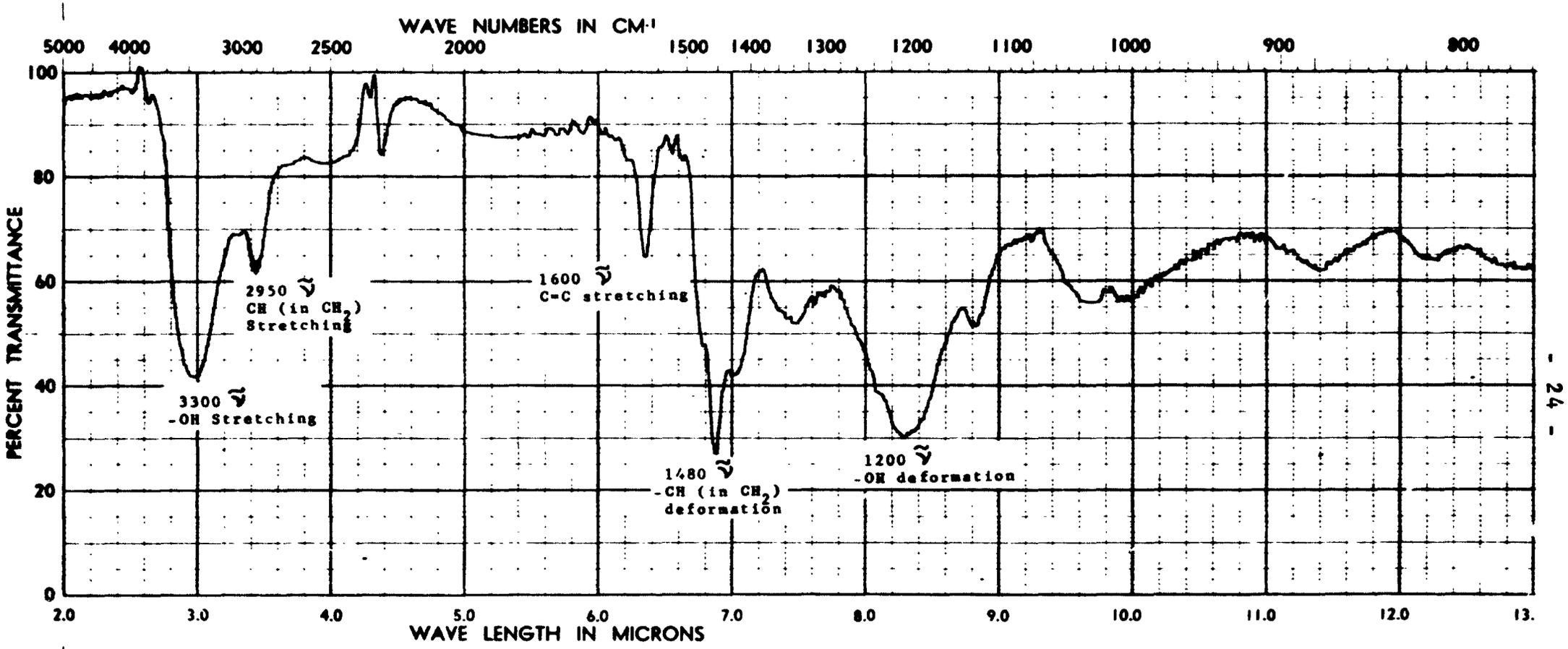

SAMPLE: Phenol-formaldehyde Resin Film

(0.0004 in. thick, cured at 250°F. for 20 min.)

Date: 2 Nov 1964; Scan: 25 min.

BAIRD MODEL A, IR SPECTROPHOTOMETER

(NaCl Prism) Single Beam Operation

FIGURE 1. INFRARED SPECTROGRAM OF PHENOL-FORMALDEHYDE FILM

form a pellet (described in more detail in Appendix A). The spectrogram of such a pellet is shown in Figure 2. The quality of the pellet spectrogram is almost as good as that of the film, but the practicality of the pellet technique justifies its use, particularly for the study of charred material.

Elemental analysis (described in Appendix A) is a method of obtaining the amounts of carbon and hydrogen in a sample directly and the amount of oxygen by difference. In principle, the comparison of the elemental analysis with the theoretical values calculated from the structural formula should give an indication of the degree of cure, but in a practical case, direct comparison of numerical values is not helpful until the cure is advanced as far as it can go. For relatively uncured material, the comparison should be made by means of a characterization plot, such as that given for phenol-formaldehyde in Figure 3. The apex of all the lines corresponds to the theoretical analysis of the resin; the lines to the right of this point correspond to decomposition of the resin and loss of the molecules with which the lines are labeled; this type of plot can be used to study the pyrolysis if the products are few and simple. The lines to the left correspond to adsorption (absorption, chemisorption) of the indicated molecules on the cured resin, and in the case of the uncured resin, the H_2O line corresponds to H and alcoholic OH which would be formed (and removed) as the cure progresses. In actual case this is found to be true, the analysis of the mildly cured resin falls along the H_2O line; and as the cure progresses, the analysis moves toward the theoretical point.

It is now possible to define the criteria for completely cured resin,

a. Elemental analysis to correspond to the theoretical structure, and

b. Alcoholic OH equal to zero.

Because of the random distribution in the geometrical structure, complete cross-linkage can not be achieved. The best alcoholic OH which could be obtained during this investigation was 0.43 weight %, and this could be reached only after curing under vacuum. The average elemental analysis of the resin (on an ash free basis) is: carbon 78.09 w% (80.32); hydrogen 5.47 w% (5.40); oxygen 16.44 w% (14.28). The values in the parentheses are the theoretical values based on the structure shown by Equation (III-4). The ash content is 2.60 w%.

This investigation has determined the following curing cycle to be adequate. The water solution of the resin is pored into

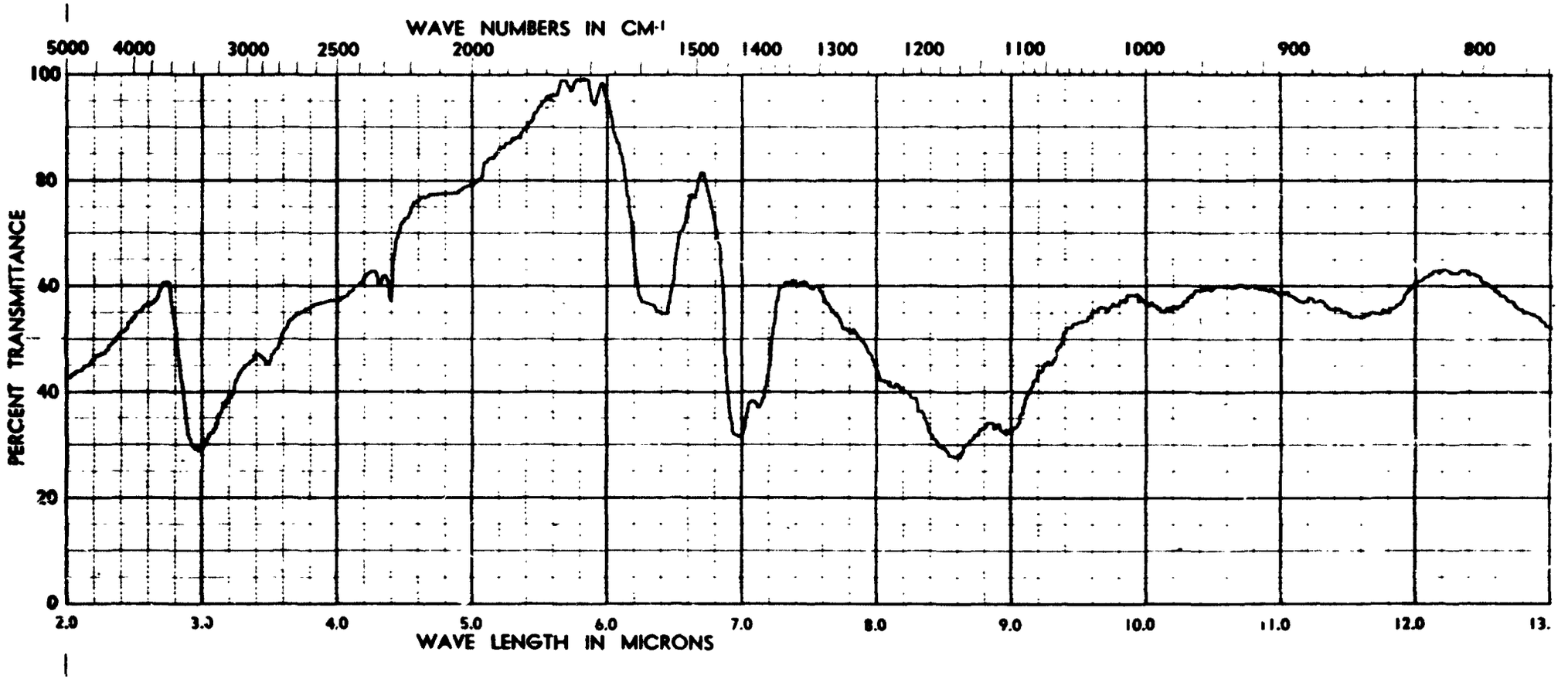

SAMPLE: Phenol-formaldehyde Resin in KBr Pellet

(4 mg. C-1 resin to 458 mg. KBr)

Date: 2 December 1964; Scan: 25 min.

BAIRD MODEL A, IR-SPECTROPHOTOMETER

(NaCl Prism) Single Beam Operation

FIGURE 2. INFRARED SPECTROGRAM OF POWDERED PHENOL-FORMALDEHYDE RESIN

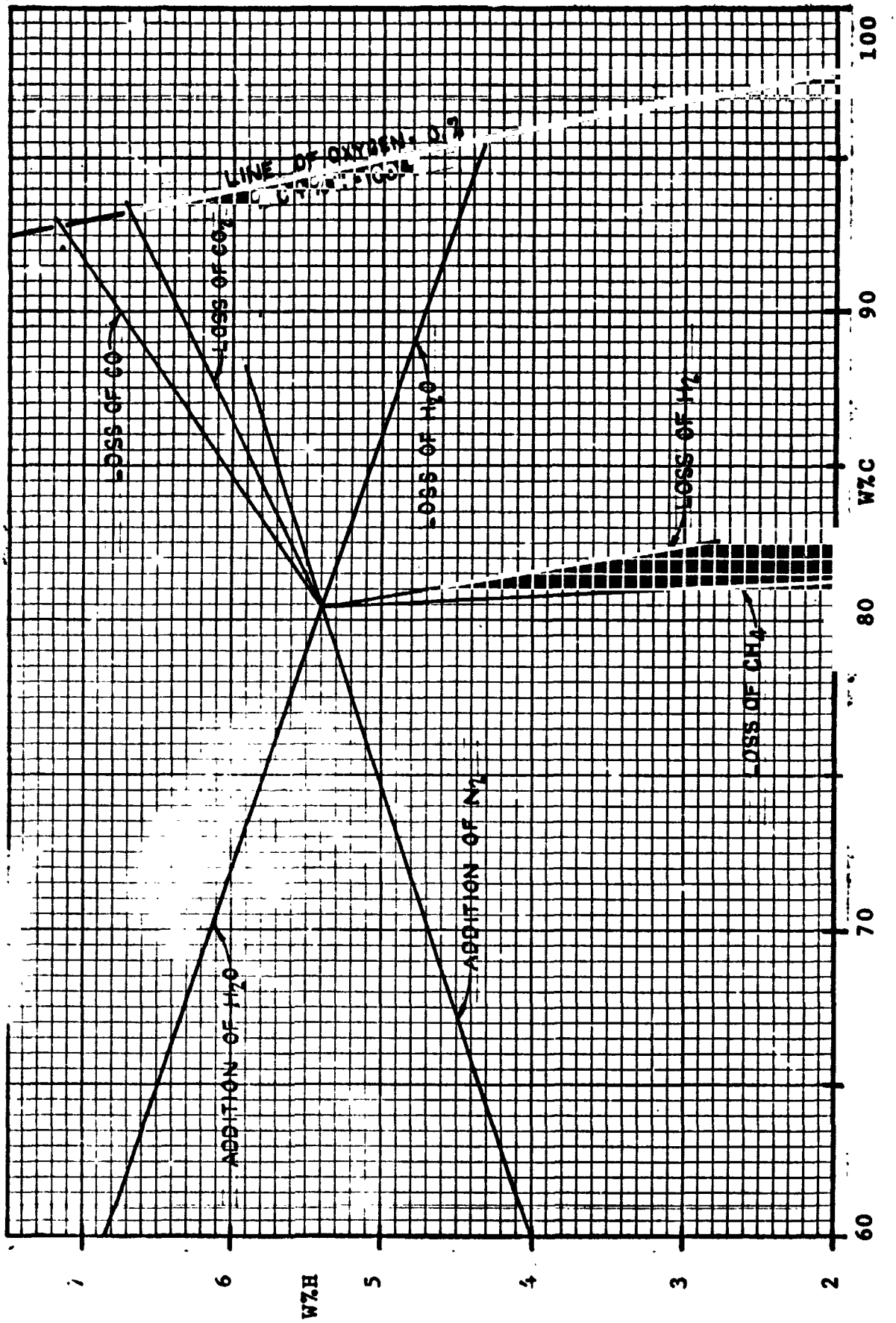

FIGURE 3 - PHENOL-FORMALDEHYDE CHARACTERIZATION PLOT

a shallow container to form a thin liquid film. This is heated at 310-330°F for 1/2 - 1 hours. The thin film of solid which results is crushed, then ground to pass through a 60 mesh screen. The fine particles are heated under vacuum (1-3 mm Hg absolute) at 350-400°F for about 24 hours or until the elemental analysis and the alcoholic OH analysis no longer improve.

C. WATER AND AIR ADSORPTION BY CURED PHENOL-FORMALDEHYDE POLYMER:

At an early stage of this investigation, it was found that the experimental results from the pyrolysis determinations were not consistent with what was expected. The difficulty was traced to the ability of the cured resin to adsorb appreciable amounts of water and/or air. A quantitative investigation of the magnitude of the phenomenon was attempted, and the results are as shown in Table IV. The freshly dried material was exposed at room temperature to an atmosphere saturated with water vapor for the indicated time, and the weight gain was noted. Dry sand exposed under the same conditions showed no gain in weight. Some of the samples were heated in an ordinary laboratory oven, and it was found that quantitative desorption could be accomplished in one hour at 212°F. A sample exposed at room temperature and an average relative humidity of 56% for 5 hours gained 7.68 weight % (dry basis).

A typical char was approximated by mixing together equal parts of pyrolysis residue from 25 min., 60 min., and 16½ hours runs at 497°C. The weight gain was found to be 15.49 wt. % (dry basis) at 715 min. exposure to 100% relative humidity at room temperature; 15.90% at 1250 min., and 16.28% at 2155 min.

Future work should include a more detailed investigation of the adsorption phenomenon, but because of time limitations this investigation could only attempt to minimize the effect. The technique found to be most effective is to place the freshly dried resin in a small bottle having a rubber stopper and a teflon stopcock. Samples are removed through the stopcock, and between samples, the bottle is stored in a desiccator. While in use, the resin is frequently re-dried under vacuum, but between dryings, the adsorbed material builds up on the resin surface. In one case, where the exposure to atmosphere is thought to be more extensive than usual, the resin lost 2.12 wt. % (dry basis) on being vacuum dried. Because of the difficulty of maintaining the resin free of all adsorbed materials, it was decided to keep the material as uniform and consistent as possible and allow for adsorbed material by the kinetic model (see Section V).

TABLE IV

WATER ADSORPTION-DESORPTION ON PHENOL-FORMALDEHYDE RESIN

Minutes Exposed to Humidity	% Adsorbed* at 100% Relative Humidity+	% Desorbed* in 1 Hour @ 212°F
20	1.43	1.43
40	2.97	2.97
50	3.21	3.28
120	5.70	5.64
450	10.55	
640	10.30	
700	10.72	
770	11.02	11.05
1320	11.00	
1320	10.95	

* Weight % based on dry resin
\+ Room Temperature

As part of the elemental analysis, the Karl Fisher apparatus (Section IV-C) is used to determine moisture in the resin and in the chars. The moisture varies with the amount of exposure to the atmosphere and the degree of humidity. For the resin, the maximum value found was 0.43 wt. %, but 0.21% is a more typical value. The chars sometimes have moistures as high as 2.5%, but usually stay in the range of 0.3-1.0%.

D. PRELIMINARY CHARACTERIZATION OF THE EPOXY-NOVOLAK:

The epoxy-novolak used in this investigation is 40.9 w% epoxy-novolak, 43.5 w% polysebacic anhydride, 7.3 w% 4-vinyl-cyclohexene dioxide, and 7.7 w% methyl NADIC anhydride, all co-polymerized together, with 0.5 w% catalyst, tridimethyl amino methyl phenol, in the form of a dark yellow, glassy slab. The slab was machined along one edge, and the resulting shavings were ground to pass through a 60 mesh screen, then vacuum dried at 1 mm Hg absolute pressure and 240°F for about 16 hours.

The elemental analysis on a dry, ash free basis for the epoxy is: carbon 69.5 wt. % (69.3); hydrogen 8.23% (7.26); and oxygen 22.3% (23.5); where the values in parentheses are the theoretical values calculated from the composition. The ash content is 0.18 w%. A characterization plot for the epoxy-novolak is given in Figure 4, but is not as useful as for the phenolic, because the structure can not be defined. Each of

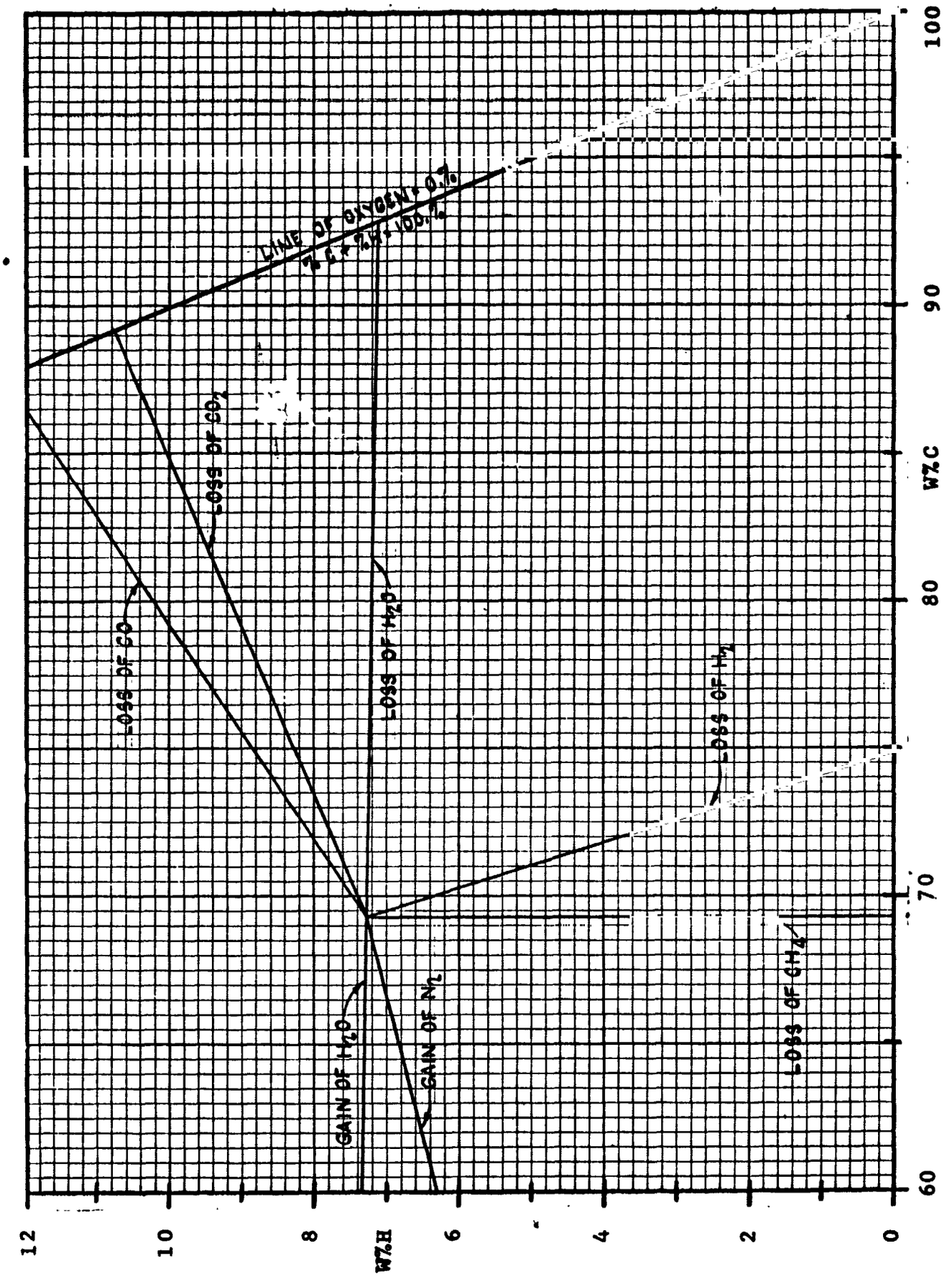

FIGURE 4 - EPOXY-NOVOLAK CHARACTERIZATION PLOT

the anhydrides can polymerize with each of the epoxy compounds, thus giving four different types of linkage, each of some unknown amount. In addition, there is no elimination of molecules during curing of the epoxy as there is with water from the phenolic, so that the curing can not be followed by elemental analysis. The assumption is made that the curing is complete as received.

The epoxy is much less adsorptive than the phenolic, as indicated by the epoxy adsorption values in Table V; phenolic material has a great many hydroxide groups and these tend to hydrogen-bond to water and possibly also to oxygen and nitrogen. The epoxy has only trace amounts of hydroxide from the catalyst, and consequently adsorption due only to the surface effects, which are much less than the hydrogen-bonding effects. The net result is that after the pyrolysis runs of the epoxy-novolak were completed, the unused material would desorb only 0.37 wt. % under vacuum (3 cm Hg abs.) at 240°F for 21 hours. In addition, the moisture by the Karl Fisher analysis never exceeded 0.11%.

TABLE V

WATER ADSORPTION ON EPOXY-NOVOLAK RESIN

Exposure Time	Relative Humidity (Room Temperature)	Weight % Gain* (Dry Basis)
25 min.	80.3%	0.74
7½ Hrs.	100%	0.84

* No additional gain was observed for additional exposure time.

Shavings of epoxy machined from a slab and ground up were a chalk white, loose, flakey powder. This powder darkened to a very light tan after vacuum drying. After pyrolysis at 569°F, the epoxy residue turned a straw color and formed a loose cake which could be easily broken up to the original texture. After pyrolysis at 730°F, the epoxy residue formed a dark brown cake of more tenacity, but which could still be broken up without much effort to form a powder of finer texture than the original.

IV. EXPERIMENTAL INVESTIGATION

A. REVIEW OF EQUIPMENT IN LITERATURE:

An evaluation of some of the techniques and equipment which have been used to more accurately define the ablation phenomenon of plastic materials indicates that the equipment can be divided into three broad categories: 1) Chemical Kinetic Equipment, 2) Physical Property Equipment, and 3) Re-entry Simulation Equipment.

The chemical kinetic equipment is used to investigate the nature of the chemical reactions involved in the degradation of ablation materials (i.e. determination of orders of reaction, activation energies, heats of reaction, chemical species formed, etc.). There has been very little detailed work in this area.

The physical property equipment is used to produce detailed information on the properties of the virgin materials and the chars formed during ablation. The equipment is divided into two general categories: 1) Thermal Properties Equipment (i.e. heat capacity, thermal conductivity, thermal diffusivity, etc.), 2) Basic Physical Property Equipment (i.e. density, surface area, pore size distribution, structural properties, etc.) The information is required to adequately define the heat and material balances and physical configuration of the mass during the ablation process.

Simulation equipment is used to reproduce or simulate as near as possible the actual conditions that are experienced during re-entry. By far, this is the largest group of experimental equipment which exists today. Simulation has been very necessary to provide quick approximations of designs for spacecraft heat shields, but the work is virtually useless when making a detailed kinetic study. Therefore, an evaluation of this equipment has not been made.

The purpose of the literature review was to determine the experience and equipment developed by others on chemical kinetic studies of ablation. From such information and our experience in reaction kinetic studies, a kinetics apparatus design was evolved.

The literature survey has revealed approximately nine basic methods of determining the reaction kinetic parameters of ablative systems. They are as follows:

1. Xenon Flash Lamp Pyrolysis
2. Transpiration Cracking in Char
3. Thermogravimetric Analysis, TGA

4. Differential Thermal Analysis, DTA
5. Isothermal Furnace Pyrolysis
6. Commercial Aerograph Pyrolyzer
7. Radio Frequency Apparatus
8. Electron Spin Resonance
9. Fluid Bed Pyrolysis

Certain general articles presented by D. L. Schmidt (42-44), Nelson (37), and Schwartz (45, 46) indicate that most if not all of the basic methods which are currently being used are included in the above list.

1. Kinetics Equipment

a. Xenon Flash Lamp Pyrolysis: This is one of the relatively newer techniques for investigating pyrolysis of plastics and has been described by Nelson (37) of Bell Telephone Laboratories; Martin (30), Rudkin (40), and Lincoln (28) of the U. S. Naval Radiological Defense Laboratory; Friedman (7, 32) of General Electric Space Sciences Laboratory; and Wacks (52) of National Bureau of Standards. The technique can be very valuable when determining reaction kinetic data over periods of one second to one millisecond. It has been used by Wacks, Friedman, and Martin in conjunction with either a time-of-flight mass spectrometer or a two-stage gas-liquid partition chromatograph to identify the pyrolysis products of ablative plastics. The system is apparently easy to calibrate for energy input (cal/cm^2) from calorimetric data on graphite or silver. This can be converted to rate of heat input by knowing the area of exposure and exposure time. Herein lies some of the problems of use. 1) The electrical circuit must be carefully designed and calibrated to produce a uniform, usable light pulse. 2) To reach very high temperatures the sample must be very finely divided - and a determination of the area exposed must be made. 3) With ablative materials, the change in chemical species and their unknown reaction rates make it extremely difficult to determine the temperature of reaction.

The technique has been used very successfully to determine the heat capacity, thermal conductivity, and thermal diffusivity of materials up to their decomposition temperature, and has been especially valuable in the field of ceramics at high temperatures. It was concluded that this technique was not ideally suited to the chemical kinetic study being contemplated.

It should be noted that the two analysis techniques discussed later (i.e. TOF or a conventional mass spectrometer and GLPC) can be used on any type of kinetics apparatus.

b. Transpiration Cracking in Chars: This apparatus was developed by the General Electric Space Sciences Laboratory

(49) and is used to study the secondary reactions that occur in the char layer of an ablating plastic. (i.e. methane cracking down to pyrolytic graphite and hydrogen). In basic principle, the method can be very useful in studying secondary pyrolysis reactions, but has numerous operating problems. Preliminary results indicated a very efficient cracking of the primary products, which was to be expected from general kinetic theory and what is known about thermal cracking of hydrocarbons.

c. Thermogravimetric Analysis (TGA): This is one of the most widely used kinetics apparatus. Its utility has been described by Schmidt (43) and has been discussed in detail by Coffman (6), Kotlensky (24), and Boguist (3). The method yields loss of weight data versus temperature profile data. During analysis, plastic samples are heated at a preselected rate of temperature rise (i.e. 3-6°C/min.) through and beyond their decomposition temperatures. Extensive use has been made of the Chevanard Thermobalance.

The technique is not suited for detailed kinetic studies because the temperature is varying with time, kinetic equations are complex even for isothermal data; consequently, the technique can not be used for mechanism studies. Isothermal gravimetric studies, on the other hand, are ideally suited for detailed kinetic studies. To complete the kinetic data required, some type of pyrolysis product analysis would have to be made.

d. Differential Thermal Analysis (DTA): This technique has been used quite extensively to determine the incipient reaction temperatures for ablative plastics. Schmidt (43), Boquist (3), and Mason (31) describe its use.

DTA studies are performed by comparing the temperatures of an inert reference substance (aluminum oxide, etc.) with that of an ablative plastic as the temperature is programmed on a continuous rise through and beyond the decomposition temperatures. Its major value is in defining the zones of temperature which require detailed kinetic study. The results of DTA experiment also indicate whether the reaction is exothermic or endothermic which in itself gives a clue to the type of mechanism involved at any particular temperature.

e. Isothermal Furnace Pyrolysis: This technique has been developed and used by Madorsky (29) of the National Bureau of Standards and the General Electric Space Sciences Laboratory (49). Schmidt (43) describes the details of some of this work.

Isothermal furnace pyrolysis provides one of the best bases for design of a kinetics apparatus. In kinetics

it is important, that the temperature of the reaction be held constant, that the temperature throughout the sample be the same, and that the exact value of the temperature be known. The degree of temperature control and the relatively large heat sink of the electrical furnace make it suitable to fulfill the above conditions.

Combination of a thermobalance (tungsten-spring or electronic) and an electrical furnace would provide weight loss versus time information under isothermal pyrolytic conditions. This information along with component analysis can be used to derive Arhennius-type plots and calculate activation energies of decomposition.

f. Commercial Aerograph Pyrolyzer with Hydrogen Flame Analyzer-JPL: This commercial pyrolyzer utilizes a glowing platinum coil to pyrolyze plastic samples. Its use has been described by Johnson (21) of the Jet Propulsion Laboratory. Its chief disadvantage is the lack of temperature control or method for measuring the temperature. Johnson (21) has used a very sensitive hydrogen flame ionization detector in conjunction with a Perkin-Elmer Chromatograph to identify pyrolysis products. He has indicated the presence of large numbers of pyrolysis products (40 to 50 for polystyrene pyrolysis).

The hydrogen flame detector, of course, will not indicate the presence of hydrogen, which is a distinct disadvantage since hydrogen may be an important product liberated by the condensation mechanisms of phenolic structures.

g. Radio Frequency Apparatus: This technique was developed to study the chemical reactivity effect of atomic-nitrogen with plastics in a non-hyperthermal environment. The system, as described by Mathews (10, 32), Lapple (25), and Mixer (35), simulates the hot gaseous air plasma which is highly reactive due to its dissociation into atomic species. The method is highly specialized and would find little use in basic in-depth kinetic studies of ablating plastics. Its value is primarily as a source of ionized species for special atmospheric studies and surface effect studies.

h. Electron Spin Resonance Apparatus: This technique has been used quite extensively by Singer and Co-workers (48) of the National Carbon Company to study the thermal decomposition reactions of organic compounds. The major advantage of the system is that it permits identification of radical intermediates formed during pyrolysis and allows the tracing of the mechanisms of the reactions involved. Its use to date has been limited to pure organic compounds; therefore, it is difficult

to judge what kind of potential value the technique has for determining the mechanisms of pyrolysis of ablative plastics. The complications presented by the polymers, either homogeneous or heterogeneous, could be formidable.

i. Fluid Bed Pyrolysis: This technique as described by Coffman (6) of the General Electric Company can be used only on thermoset resins. Thermoplastic polymers or thermosetting resins will not fluidize under high temperatures. One of its major advantages is the uniform and efficient mixing and heat transfer that is realized experimentally. One of the major disadvantages is the initial time response of the system. It is very difficult to bring the system to a desired temperature rapidly and adjust the fluidization at the same time. Another disadvantage is the time and care required in preparing the resin powder for use. For the most satisfactory fluidization the powder must be smaller than 200 but larger than 325 mesh sieve size (approx. .09mm avg. diameter). Even at this size a relatively large quantity of fluidization gas (helium) is required which makes subsequent analysis of the pyrolysis products difficult.

The method has some advantages, but also has some serious operational disadvantages which limit its usefulness.

2. Physical Propert Equipment

Equipment to determine the physical properties of ablative plastics and their chars has not been discussed to any great extent in the literature. Probably the main reason for this is that equipment developed for use in other fields (i.e. refractory metals, ceramics, etc.) can be adapted for use in this field.

There are two basic areas in which physical property equipment are required (i.e. Thermal Property and Basic Physical Property Equipment); of the two, the thermal property equipment is of primary interest. There are six basic types of physical property equipment discussed in the literature:

a. Heat Capacity Apparatus - SRI
b. Thermal Conductivity Apparatus - SRI
c. Thermal Diffusivity Apparatus
d. Mercury Porosimeter
e. Nitrogen Sorbtometer
f. Char Layer Pressure Drop Apparatus

Of these, only the heat capacity, thermal conductivity, and thermal diffusivity apparatii are of primary interest. The mercury porosimeter and nitrogen sorbtometer are standard,

commercial units which require no further discussion. The char layer pressure drop apparatus, developed to study spallation of charring ablators is not of primary interest and will not be discussed further.

a. Heat Capacity Apparatus: An apparatus for this type of measurement to 5000°F on refractory materials is described by Howse (19) of the Southern Research Institute. Use is made of a tube-type graphite furnace for heating the materials and an ice calorimeter for heat capacity determinations. This relatively simple system could be applied to any material that is inert at the maximum temperature of the determination. Therefore porous chars could be crushed and compacted for heat capacity measurements of the solid residue, and the effect of various gases taken into account theoretically by knowing the porosity of the original char and the heat capacity of the gases.

b. Thermal Conductivity: There are two basic methods of determining the thermal conductivity of an inert material. The equilibrium method is described by Howse (19) and the transient method by Nagler (36) of the Jet Propulsion Laboratory. The equilibrium method is by far the simplest and most economical method, therefore the discussion will be limited to the former.

A simple, well insulated, electrically heated system is used by Howse and coworkers (19). There are no particular advantages or disadvantages to the experimental technique used. The system is set up to provide measurement of the variables which define the thermal conductivity (i.e. $Q = k A \Delta T/\Delta X$) from Fourier's Equation.

c. Thermal Diffusivity Apparatus: There are two distinct techniques which have been advanced for measuring the thermal diffusivity of materials. They are based on the same principle of the transient heat flow equation which defines the thermal diffusivity as $\alpha = k/C_p\rho$, where k = thermal conductivity, ρ = density, and C_p = heat capacity.

Farmer (11) of the Nonmetallic Materials Laboratory describes the use of an arc imaging furnace as the source of a uniform radiant heat flux whereas Jenkins (20) of the U. S. Naval Radiological Defense Laboratory uses the Xenon flash lamp to accomplish the same thing but in a shorter period of time. The flash method tends to minimize heat losses because of the short period of measurement, but has the disadvantage of raising the front surface temperature to very high values, and makes it difficult to define an "effective temperature" for a measurement.

3. Analytical Equipment

Because of the importance of product analysis to a kinetic study, the more important analytical equipment and techniques were examined. X-ray and electron spin resonance are useful in deciding on mechanisms of reactions, but these techniques do not lend themselves to quantitative analysis. Therefore, they will not be considered further in this section.

Standard laboratory techniques can give important analytical information. Passing the pyrolysis gas through an absorption bulb filled with a drying agent will give the amount of water in the gas as the increased weight of the bulb. Similarly, carbon dioxide can be determined by another bulb filled with ascarite.

Another useful technique is the combustion of solid material (such as virgin ablator or pyrolysis residue) in pure oxygen. From subsequent analysis of the combustion products, the amount of carbon, hydrogen, and nitrogen which was in the original material can be determined. The amount of oxygen in the material must be determined by difference.

In principle, any type of analytical equipment could be used in conjunction with any type of pyrolytic equipment to make a kinetic study. In practice, it is found that the combinations used are rather restricted, not only because a type of equipment may not be suited for a particular type of material, but also because most investigators like to use directly coupled equipment. This imposes another restriction on both analysis and pyrolysis equipment in that the interface must be reasonably convenient.

Gas chromatography has found wide use in the analysis of pyrolysis products of ablative materials. It is possible to make quantitative determinations of compositions not only of that fraction of the products which are gases under normal conditions, but also for components of the liquid fraction which have an appreciable vapor pressure below 250°C, (the maximum operating temperature for most chromatograph columns). The chromatograph does not require a large sample of material, and time required for analysis can usually be made conveniently short. A marked disadvantage is the necessity of calibrating each type of fractionating column to be used to obtain the residence time which is characteristic of each of the components expected in the sample. Another disadvantage is that a type of column which can distinguish between members of one class of compounds, such as alcohols, will usually lump together indistinguishably the members of other classes, such as light gases or hydrocarbons. The last disadvantage can usually be overcome

by analyzing several identical samples on different columns, or by a series staging of different kinds of columns.

Infrared spectrophotometry has been surprisingly limited in application in the literature, although this may be because a good spectrophotometer plus accessories costs about ten times as much as a good chromatograph. It is possible to obtain spectrograms for the solid residue of pyrolysis as well as the gas and liquid products. The solid material is usually ground with KBr and the resulting mixture pressed into a pellet. Complex gas or liquid mixtures cannot be readily analyzed, but simple mixtures can be analyzed quantitatively.

IRS is outstanding for qualitative analysis. A compound may be identified exactly by comparing its spectrogram with those of pure materials until a match is found, but a skilled interpreter of spectrograms can identify a compound by its characteristic adsorption peaks even though he does not have a known spectrogram for comparison. This is especially useful when a chromatograph column cannot be calibrated with known substances; the unknown sample is injected into the chromatograph and adsorbed in the column, and as each fraction is desorbed from the column, it is collected and identified by obtaining its spectrogram.

An interesting study of the oxidative degradation of phenolic material has been made by Conley (8) using IRS. This was accomplished by forming a thin film of resin on a sodium chloride window (transparent to IR) and then curing the resin in place. A very similar technique could be used if the window and film combination can stand the thermal stresses involved at the higher temperatures necessary for non-oxidative decomposition (200°C maximum for oxidative and 400°C minimum for non-oxidative degradation).

Mass spectrometers, both conventional and time-of-flight, have found extensive use for the analysis of pyrolysis products, even though a good mass spectrometer may have an initial cost of more than 30 times that of a good chromatograph. The fast response of a M.S. (some can make a mass scan every 100 micro-sec.) make it imperative for the study of the very fast reactions. In general, pyrolysis reactions can be controlled at temperatures where the reaction rate is slow enough that IR or chromatography can be used for product analysis. It seems likely that in most cases where M.S. was used, it was used only because it was available and not because it was the best method of analysis.

A strong disadvantage of M.S. is that the apparatus must be calibrated to obtain a frequent spectrum for even fairly

simple molecules. The pattern of cracking depends on sample temperature; and since some mass spectrometers are constructed in a fashion that the sample temperature is not adjusted before a mass spectrum is obtained, it is often necessary to obtain the characteristic mass spectrum of each molecule at several temperatures before an analysis can be completed. When two molecules have the same mass number, interference occurs, and they can be distinguished only by their cracking patterns.

4. Conclusions From the Literature Concerning Experimental Kinetic Equipment

By far the best piece of analytical equipment to accomplish the required objectives is a gas chromatograph. An infrared spectrophotometer is not well suited for quantitative analysis of a complex mixture, although it is very useful for qualitative analysis. A mass spectrometer is much more expensive and has the advantage only of very fast analysis, but the pyrolysis rate can be controlled by the temperature so that speed of analysis is not critical. The literature indicates that the number of important decomposition products is small enough to allow satisfactory calibration of the chromatograph columns with known compounds or mixtures. In any experimental investigation, it is important that the temperature throughout the sample be the same, and to know the exact value of the temperature. These requirements eliminate all flash techniques (including arc imaging), the Aerograph, and radio frequency induction heating. The fluid bed apparatus has such a large throughput of gas that the decomposition gases are diluted beyond the range convenient for analysis. The pyrolysis equipment therefore appears to be limited to some type of electrical furnace. In any apparatus where the temperature is changing, no matter how uniformly there is always a temperature lag from the furnace to the sample and from the outer portion of the sample to the inner portions. Even when both sample and furnace are small, and the furnace temperature is known very accurately, as in TGA or DTA, the error in temperature may be significant in a kinetic study. Therefore, it is important for experimental reasons, as well as for reasons in kinetic theory, that the electrical furnace be operated isothermally.

B. OPERATION OF KINETIC EQUIPMENT:

A flow diagram of the kinetics equipment is presented as Figure 5, and a photograph of the operational configuration before unitizing appears as Figure 6. The object of the kinetics equipment is to accomplish pyrolysis in a tube furnace and analysis by chromatograph. The furnace and chromatograph themselves are described in Appendix E, where

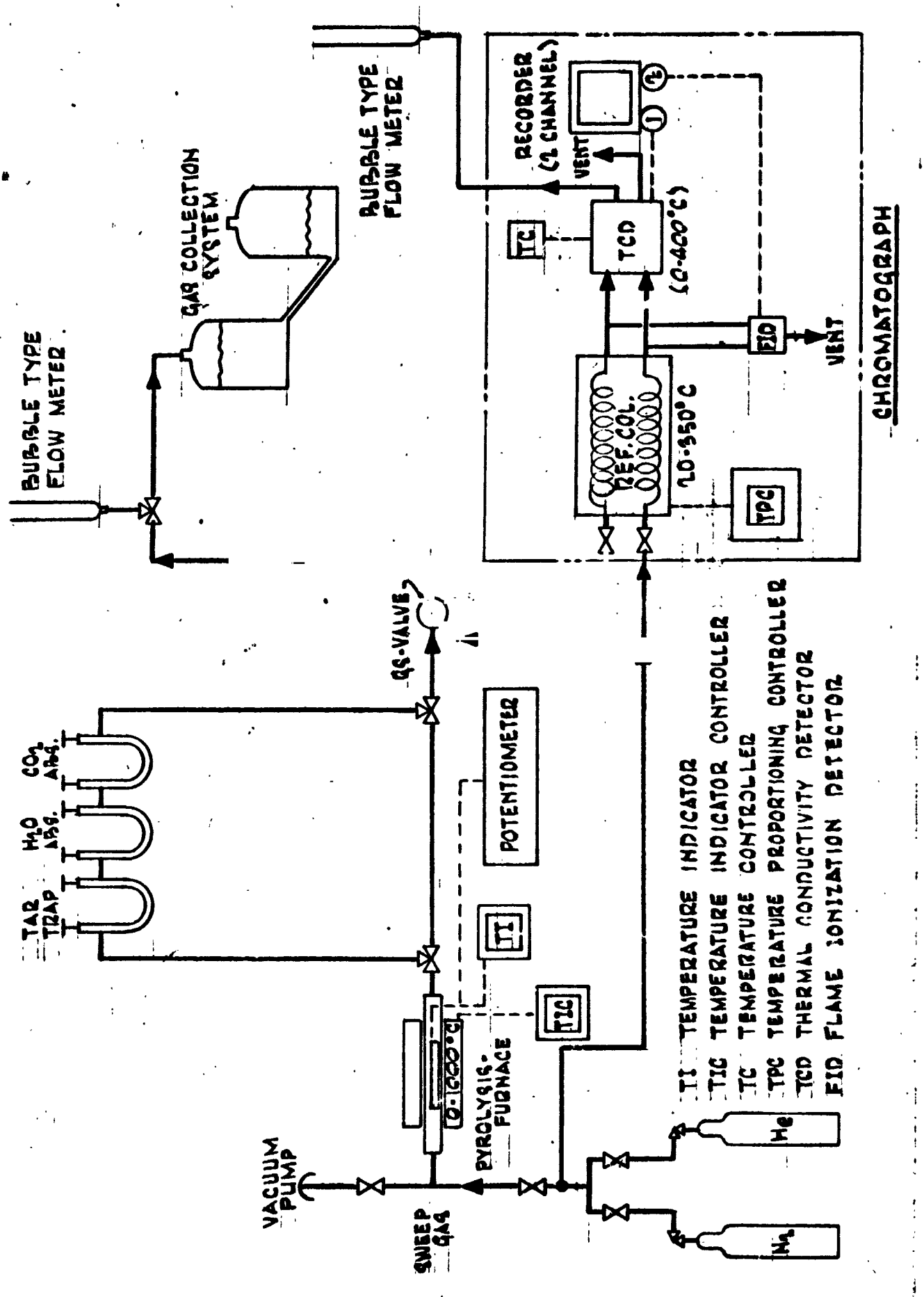

FIGURE 5 - KINETICS EQUIPMENT

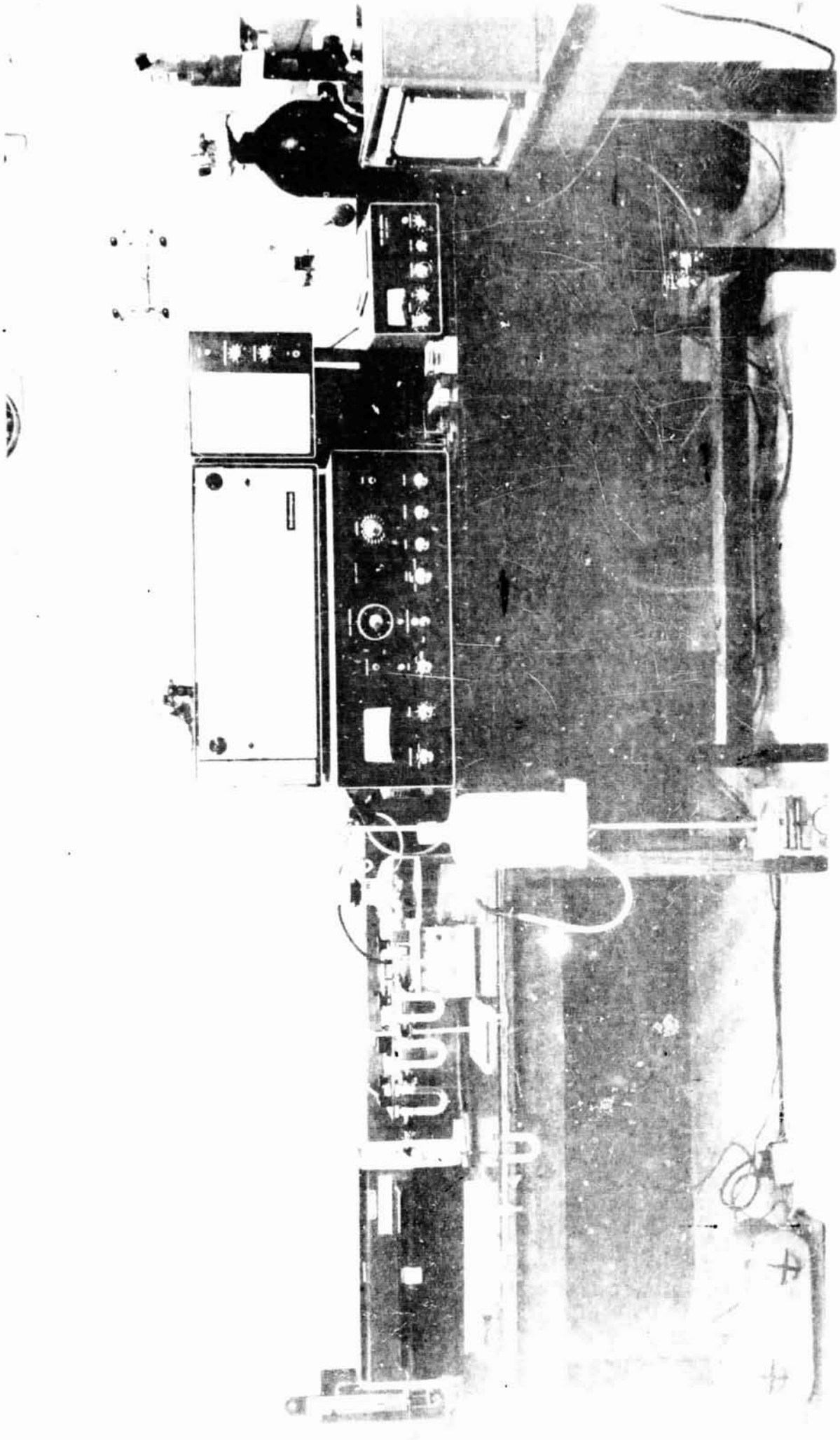

FIGURE 6 - KINETICS EQUIPMENT

descriptions of other major components occur.

Before a run can be made, the various components must be turned on and allowed to warm up. The recorder requires only a few minutes for its electronics to stabilize, but the chromatograph electronics require 1/2 to 1 hour. The temperature controller on the thermal conductivity detector oven is normally left activated, and the TCD oven is maintained at 300°C, except during extended shut-downs. The carrier gas is left flowing at a few cc. per minute all the time, but before an analysis is made, the carrier rate is adjusted, and balanced at 120 cc. per minute through each of the chromatograph columns, using the bubble flow meter temporarily attached to the TCD vents. Both nitrogen and helium are available as carriers, although helium is normally used for greater sensitivity in the TCD. The dual flames of the flame ionization detector must be ignited and allowed to reach thermal stability; this requires only a few minutes. The proper restrictors (hypodermic needles) are selected and attached to the vents of the TCD so that proper sensitivity in the FID can be maintained. The TPC on the column oven can be programmed and, therefore, has very quick response for heating, but 1/4 to 1/2 hour is required to cool the column oven from the high final temperature to the low initial temperature for the next analysis.

The temperature indicating controller on the pyrolysis furnace is left on all the time, and the furnace temperature is held constant, but when the temperature is changed to run a different isotherm, several hours may be required to reach thermal equilibrium at the new temperature. The indicator of the TIC is not sufficiently precise to obtain the temperature of pyrolysis, and it represents the temperature of the furnace, not of the pyrolysis tube. The pyrolysis temperature is determined by the emf from a thermocouple inserted in the tube, measured with a precision potentiometer. The temperature is taken before and after a run and only minor variation is observed. Temperatures could be taken during a run but no significant difference occurs. The sweep gas rate is adjusted to exactly 40 ml. per minute by a precision needle valve and is measured by a bubble flow meter. Both nitrogen and helium are available, but the sweep gas and carrier gas should be the same so that the sweep will not show up during the chromatographic analysis.

When the proper parameters have been preset and equilibrium established, the run can be started. A sample of about 1/4 gram of material is weighed by means of an analytical balance into a boat formed from steel shim stock. The configuration of the boat can be seen in Figure 7. The boat is placed into the cool end of the furnace tube, and the end of the tube is sealed

FIGURE 7 - PYROLYSIS FURNACE

with a soft rubber stopper through which passes a stainless steel push rod. The tube is evacuated to 1 mm. Hg or less to remove any oxygen present, and then flooded with the sweep gas. The adsorption tubes are removed and the initial weights obtained with an analytical balance. The adsorption tubes are replaced, the gas sampling valve positioned properly, the carrier gas is allowed to pass into the gas collection bottle, and the timer for the gas collection is started. The sample and boat are pushed to the center of the furnace tube, the push rod is withdrawn, and the pyrolysis timer is started. The push rod must be of non-magnetic material or the boat may be inadvertently pulled back or tipped over. After the required period of pyrolysis has elapsed, the boat is hooked by the push rod and pulled back into the cool zone of the tube, and the pyrolysis timer is stopped. With practice, the boat may be hooked blindly, but it is safer to open the top of the furnace as in Figure 7, so that the boat is visible and there is less chance for an accident. While the furnace is open, the temperature will drop, but this is so slight that the control temperature can be recovered within a few minutes after closing. The sweep gas is allowed to flow into the gas collection bottle for 10 minutes after the sample is removed from the hot zone to be sure that all of the pyrolysis products are removed from the tube, and the gas collection timer is stopped. When the sample boat has cooled, it is removed from the cool end of the tube and weighed on an analytical balance to determine the amount of residue or char remaining. The adsorption tubes are weighed to determine how much tar, water, and carbon dioxide were formed during pyrolysis.

During the course of the pyrolysis, the product gases are being swept through the adsorption tubes. The first adsorption tube contains only pyrex wool and is used as a trap for low volatility organic material of a tarry nature. To help prevent premature condensation of the tar, the exhaust end of the furnace tube and the side arm of the tar trap can be wrapped with heating tapes. To aid in condensing the tar in the trap, the adsorption tube can be immersed in a water bath, but the bath can not be so cold as to condense the water in the product gas; room temperature has been found to be a satisfactory temperature. The second tube is filled with anhydrous magnesium perchlorate to adsorb the water produced by pyrolysis. The third tube contains ascarite to adsorb the carbon dioxide produced by pyrolysis. From the adsorption tubes, the remaining pyrolysis gas flows through the gas sampling valve and into the gas collection bottle, where it displaces a brine solution. If a run of weight loss only is desired, the gas bypasses the adsorption tubes and exhaust directly into a vent.

The gas sample valve is designed so that in one position, the sample gas passes into the valve through the sample loop and out of the valve, while the chromatograph carrier gas passes into the valve, then into the chromatograph. In the other position, the sample gas passes straight through and the carrier gas passes through the sample loop before it enters the chromatograph. This allows the addition of a completely reproducible amount of gas each time, and the sample loops are replacable with sizes from 1/4 ml. to 25 ml. In principle, the gas exiting from the last adsorption bulb could be passed through the sample loop on the way to the gas collection bottle, and several times during the run, a sample could be sent directly into the chromatograph. In practice, this is not too successful, because the cycle time for running samples through the chromatograph is comparable with the average length of a pyrolysis run. However, it is hoped that proper choice of chromatographic parameters would reduce the cycle time to the point where this type of run would be practical.

The pyrolysis gas should not be allowed to sit very long before an analysis is made because the gas will be slightly soluble in the brine. The brine receiver bottle is lifted above the liquid level in the gas collection bottle, and some of the pyrolysis gas is displaced into the GS valve and through the sample loop. When the loop is thoroughly flushed, the GS valve is switched, the gas sample flows into the chromatograph, and the temperature program on the column oven is started. The program used is from 50°C to 275°C at the rate of 16°C per minute. The columns used are 6 ft. of 1/4 inch tubing packed with 60-100 mesh molecular sieve 5A. As each gas fraction reaches the end of the column, it is split, with the major portion going to the less sensitive TCD. During the run, the detector outputs must be continuously monitored and the attenuation controls adjusted to maintain the peaks of the chromatogram between 50-100% of full scale on the recorder chart. As each peak emerges, it is marked with its attenuation value. The mathematical area is the chart area multiplied by the attenuation factor multiplied by the dilution factor. The dilution factor is the sweep gas flow rate multiplied by the total gas collection time divided by the size of the sample loop. Each peak is related to the mass of the material for the peak by multiplying by the calibration factor. The calibration factor for each substance is determined by adding a known amount of material to the chromatograph and dividing the mass by the resulting chart area for the peak and dividing by the attenuation factor for the peak.

Gas analysis and weight loss runs were made at temperatures from 712°F to 1199°F and at times up to 80 minutes which

resulted in weight loss values up to nearly 40% for phenol-formaldehyde. For epoxy-novolak, runs were made at 569°F and 730°F at times up to 60 minutes and weight loss values went up to nearly 70% by weight.

C. OPERATION OF AUXILIARY EQUIPMENT:

The vacuum desorption apparatus is shown in Figure 8 and is described in more detail in Appendix E. The operation is very simple. A sample is weighed, if necessary, and placed in the vacuum oven. The oven is turned on and the temperature control set at an appropriate range. The valve between the oven and the atmosphere is closed off. The valve to the vacuum manifold is opened and the vacuum pump started. The oven door must be held closed until sufficient vacuum is built up to hold it closed. When the required vacuum is attained the oven-manifold valve is closed and the vacuum pump is shut off. Usually the amount of desorption is small enough so that the vacuum will be maintained for an extended period, but a fresh vacuum should be drawn at the end of the desorption period to remove any desorbed gases, and in extreme cases, it may be necessary to continuously evacuate the oven. At the end of a desorption run, the oven's valve to the atmosphere is opened to release the vacuum, and the sample is placed in a desiccator to cool before weighing. If the desorption treatment is the end step of a curing cycle, then after the required time, the oven is switched off and the resin is left inside to cool under vacuum.

The Karl Fisher apparatus is shown in Figure 9 and is described in detail in Appendix E. The associated calculations are described in Appendix A. The electronics do not require a warm up period and are ready to go as soon as the switch is turned on. The run starts with sufficient methanol in the beaker to cover the metal parts of the electrodes; at this point the meter reads about 10 milliamps. While the methanol is stirred by the magnetic stirrer, the Karl Fisher reagent is added from the automatic burette in 1/2 ml. portions. As each portion is added, the meter flicks over to 100 and drops rapidly back to the original reading. The drop becomes slower as the end point is approached, and the end point is taken as the titration for which the meter first requires 10 sec. to return to the original reading. During the titration the methanol solution goes from colorless to yellow to light orange. The color change has been used to determine the end point, but in this case, the use of an insoluble solid sample interferes with the visibility of the color change. After the blank end point

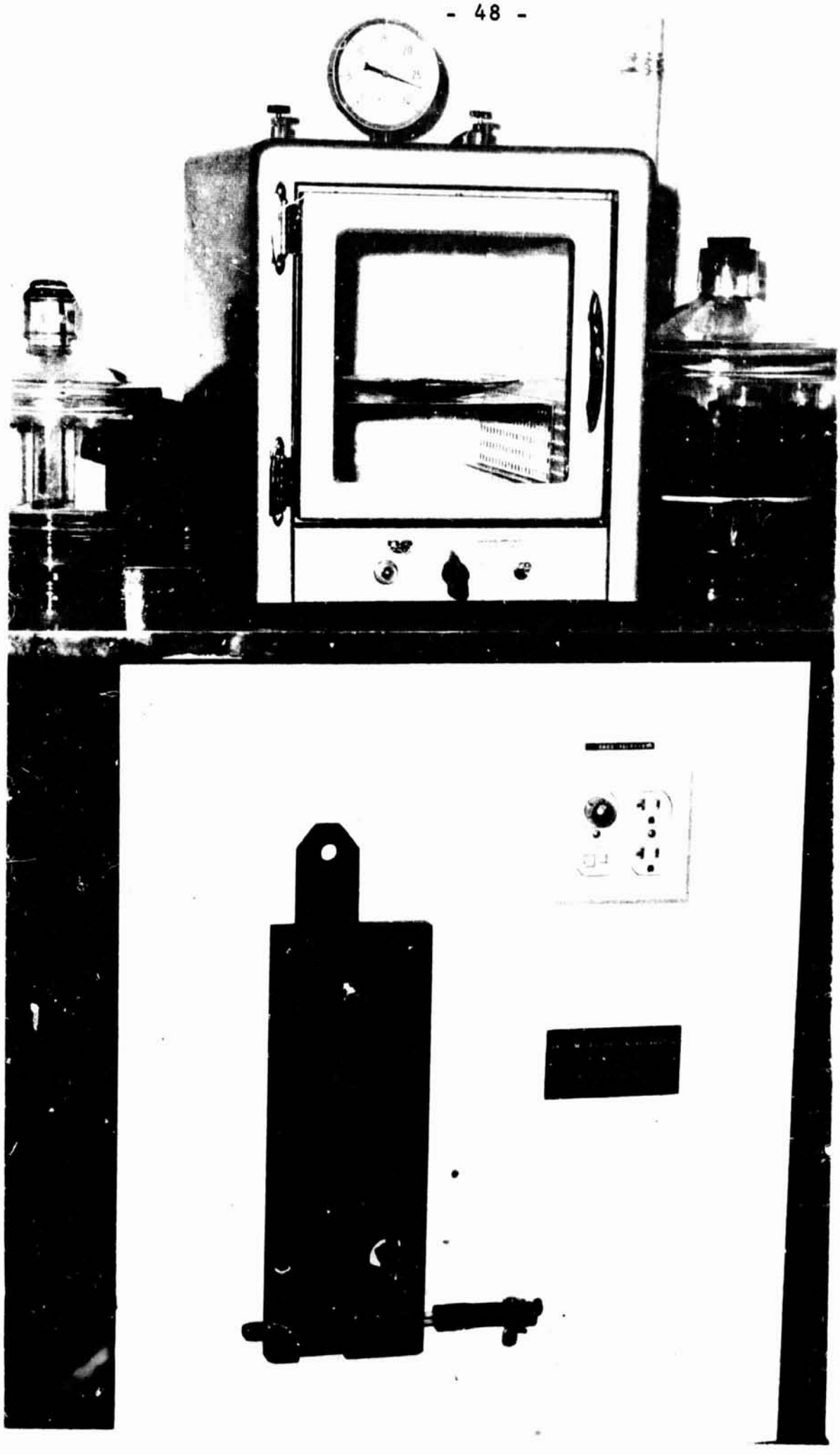

FIGURE 8 - VACUUM DESORPTION APPARATUS

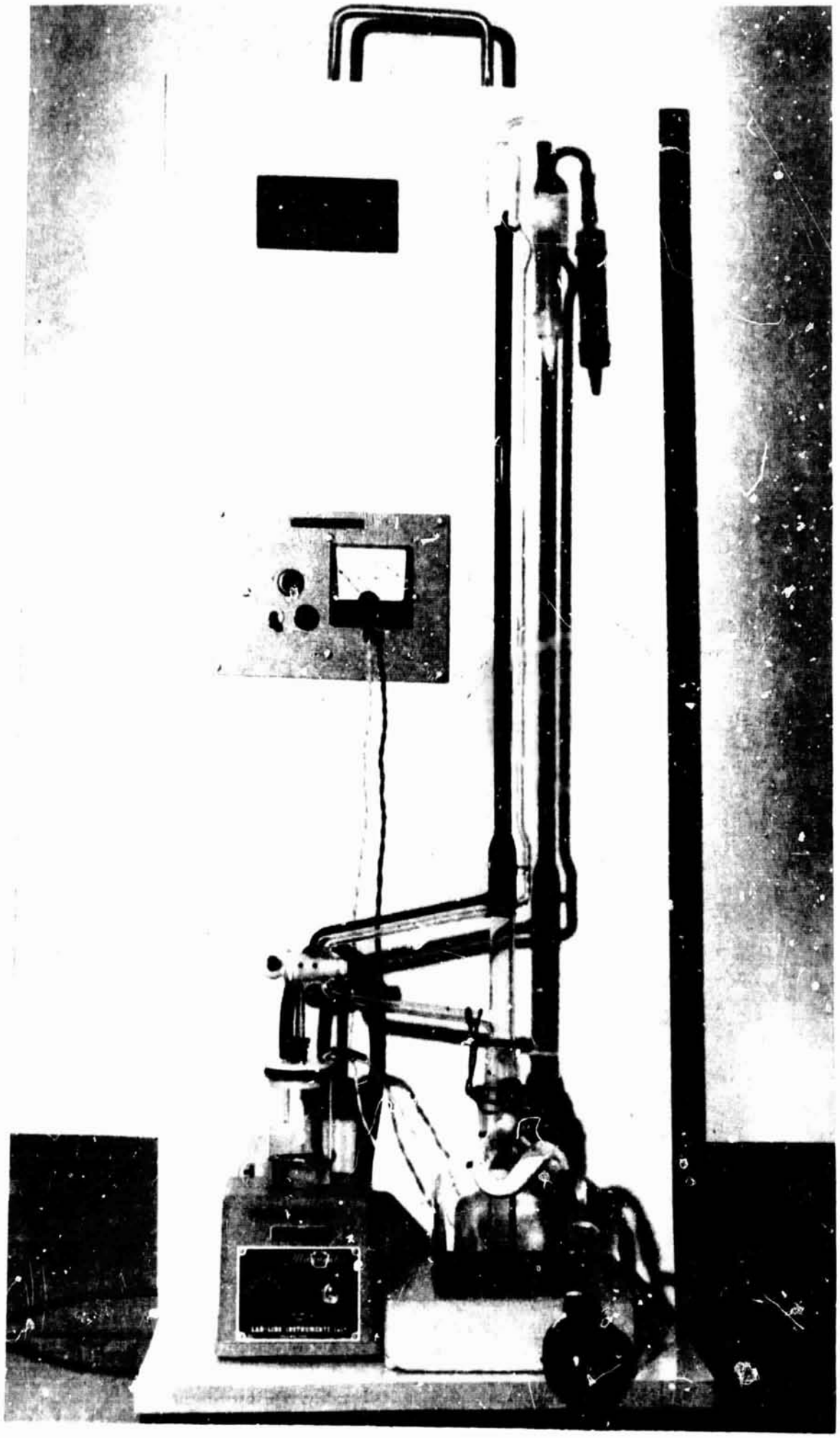

FIGURE 9 - KARL FISHER APPARATUS

is reached, the weighed solid sample is added to the beaker, and with stirring, additional KF reagent is added to reach the end point again. The water content of the sample is calculated from the amount of reagent added after the sample (Appendix A).

The Winslow Mercury Porosimeter, pictured in Figure 19, is a standard piece of equipment manufactured by American Instruments Co., Inc. Specifications are given in Appendix E. Detailed theory and operating procedures are given in company literature supplied with the equipment. Derivations by which surface area and permeability can be calculated from the pore diameter distribution data have been made, and calculations are performed by computer program HRI65R003, listed in Appendix C. The weighed sample is placed in the penetrometer which is a glass bulb with a graduated stem. The penetrometer is placed in the filling device, stem down, and the filling device is evacuated to 200 microns of Hg absolute. The stopcock is opened and mercury is forced into the filling device by atmospheric pressure until the lower part of the penetrometer stem is covered. Pressure is then slowly raised to 5 psia (as close as possible and recorded exactly) and mercury is forced up the stem and into the penetrometer bulb. The excess mercury is drained away. The pressure is increased to atmospheric in stages and the stem reading recorded at each stage. As the pressure goes up the mercury is forced into smaller and smaller pores, so that the stem reading represents the total pore volume of pores from infinite diameter down to D(microns) = 175./P(psia), where P has been corrected for the mercury head in the stem. When atmospheric pressure has been reached, the penetrometer is transferred to the high pressure container and the pressure increased until readings have been obtained up to 15,000 psig.

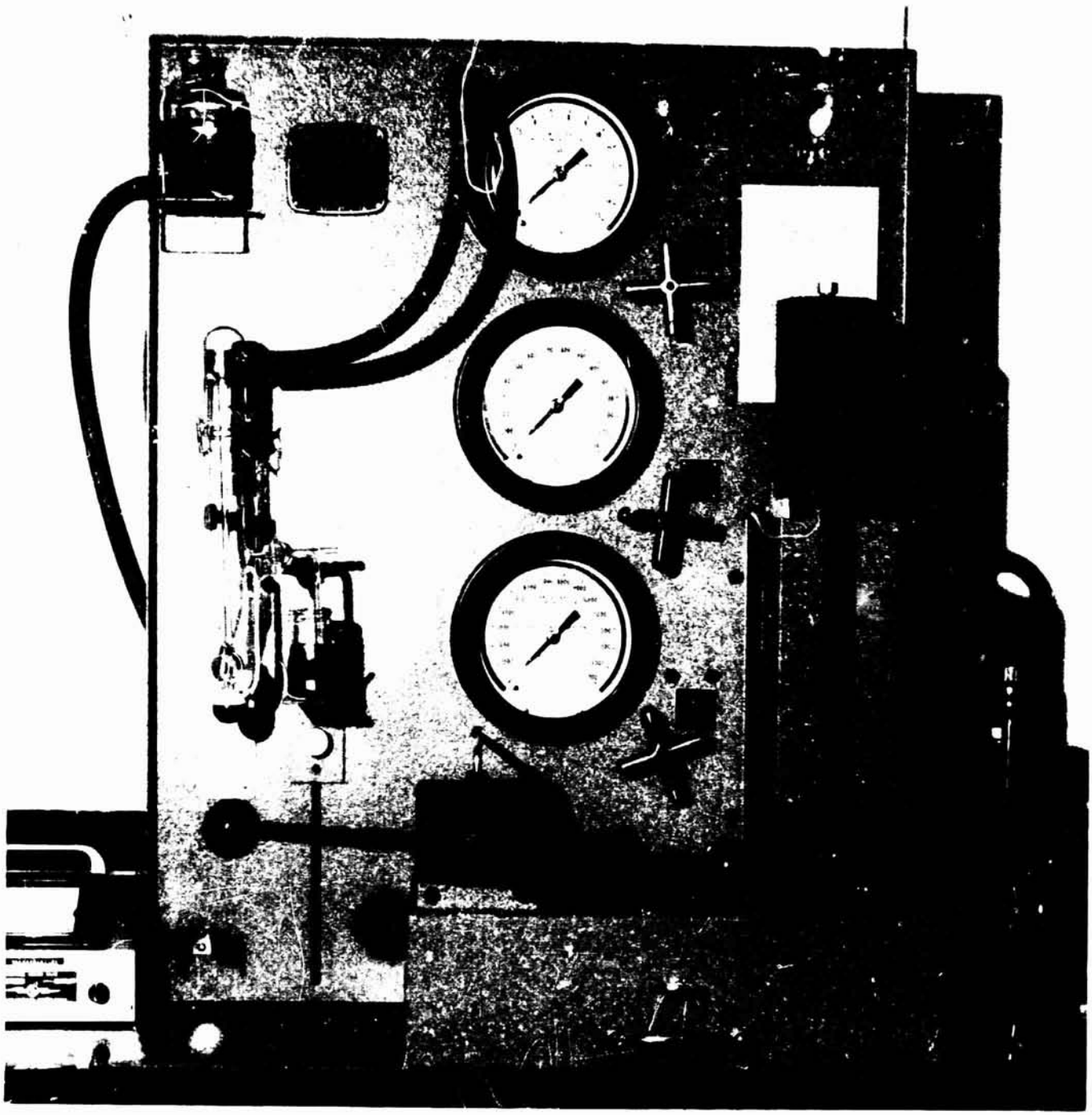

FIGURE 10 - WINSLOW MERCURY POROSIMETER

V. KINETIC MODEL

It is desired to formulate a mathematical model for the degradation of the solid polymer (a porous solid) in terms of the chemical reactions and the transport phenomena involved. Ideally, if the solid were completely contained on a surface then the product species would pass immediately into the gas phase and react further. Actually, the amount of surface area might be low and a substantial amount of mass would be within the bulk solid phase, where transport to the nearest surface would be a factor.

In any kinetic study two points of view are possible: mathematic description in terms of, 1) disappearance of the reactants, and 2) appearance of the product species. In the case involved here, the disappearance of the solid is of prime importance since it determines the basic energy utilization; on the other hand, the subsequent transpiration effects are dependent upon the product species and secondary reactions which occur.

Our primary concern in this report is the description of the initial solid phase degradation -- the chemical and physical processes involved.

A. Chemical Reactions in the Solid Phase:

Consider the necessary equations for a chemical reaction in a solid phase which produces a species which diffuses to the nearest surface and is then carried away by a sweep gas; the one-dimensional geometry can be visualized as shown in Figure 11. Assume a simple first order chemical reaction of A⟶B in the solid element δV, and diffusion of B in the x-direction only. The material balance equation for component B is given by,

$$\left\{\begin{matrix}\text{Mols B into } \delta V \\ \text{by diffusion} \\ \text{in } d\theta\end{matrix}\right\} + \left\{\begin{matrix}\text{Mols B produced} \\ \text{in } \delta V \text{ by reaction} \\ \text{in } d\theta\end{matrix}\right\} - \left\{\begin{matrix}\text{Mols B out of} \\ \delta V \text{ by diffu-} \\ \text{sion in } d\theta\end{matrix}\right\} = \left\{\begin{matrix}\text{Change of mols of} \\ \text{B in } \delta V \text{ in } d\theta\end{matrix}\right\} \quad \text{(V-1)}$$

$$-D\,dA\left(\frac{\partial C_B}{\partial x}\right)_1 d\theta + r_B\,d\theta\,\delta V + D\,dA\left(\frac{\partial C_B}{\partial x}\right)_2 d\theta = \left(\frac{\partial n_B}{\partial \theta}\right)_n d\theta \quad \text{(V-2)}$$

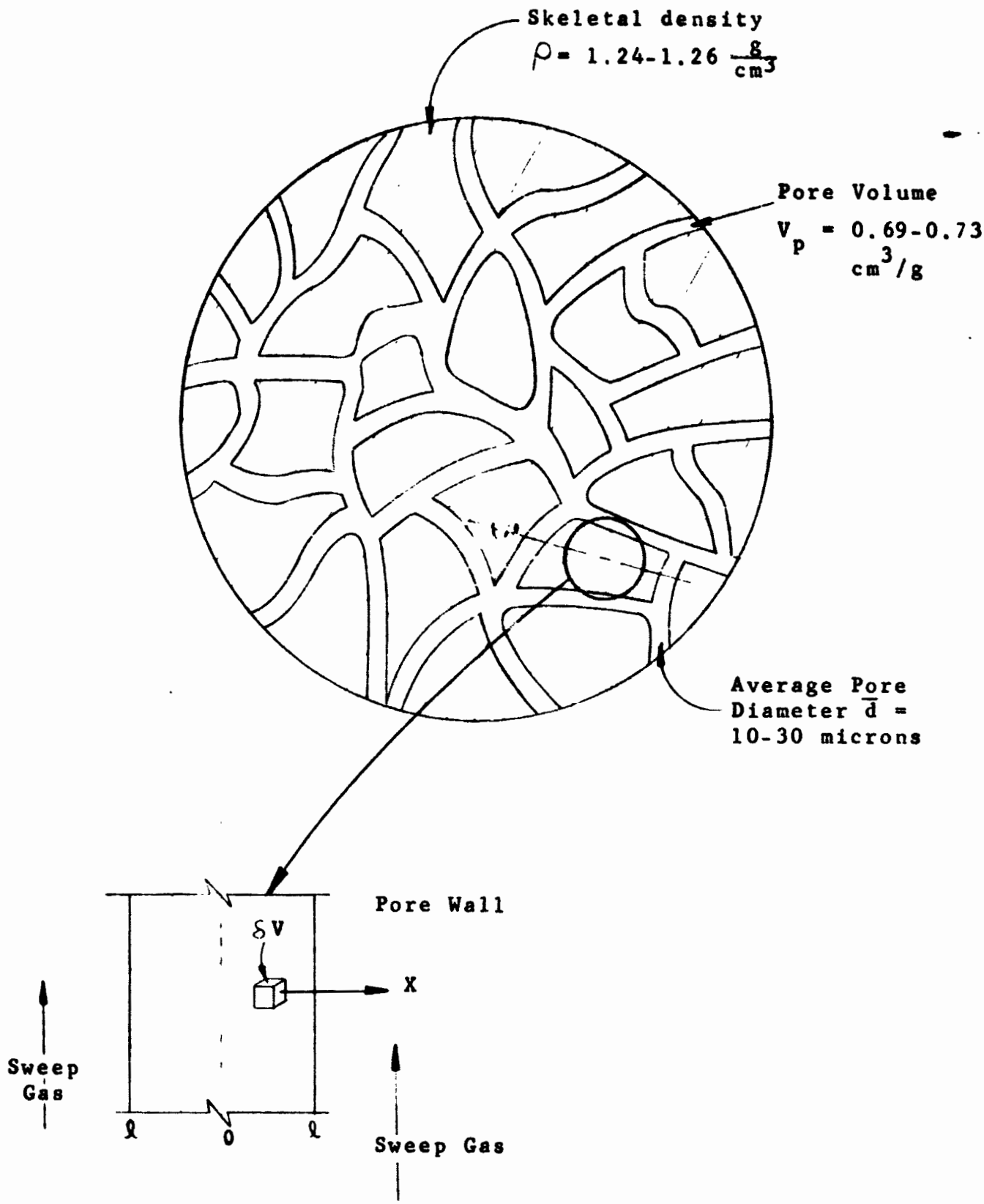

FIGURE 11 - VISUALIZATION OF THE POROUS SOLID

now $$\left(\frac{\partial C_B}{\partial x}\right)_2 = \left(\frac{\partial C_B}{\partial x}\right)_1 + \frac{\partial}{\partial x}\left(\frac{\partial C_B}{\partial x}\right)_1 dx$$

giving,

$$\left(\frac{\partial^2 C_B}{\partial x^2}\right) - \frac{1}{D\delta V}\left(\frac{\partial n_B}{\partial \theta}\right) + \frac{r_B}{D} = 0 \qquad \text{(V-3)}$$

since $(n_B/V) = C_B$ then,

$$\left(\frac{\partial^2 C_B}{\partial x^2}\right) - \frac{1}{D}\left(\frac{\partial C_B}{\partial \theta}\right) = -\frac{r_B}{D} \qquad \text{(V-4)}$$

For the reaction involved,

$$A \longrightarrow B$$

$$n_{A_0} - y \qquad y$$

$$\dot{j} = kVa_A = k\gamma_A V\left(\frac{n_{A_0} - y}{n_{A_0}}\right) \qquad \text{(V-5)}$$

(V-6)*

which upon integration gives,

$$\xi^{\circ}_{B} = \left(\frac{y}{rA_0}\right) = \left(1 - e^{\frac{-kV}{rA_0}\theta}\right) = \left(1 - e^{-\lambda\theta}\right)$$

(V-7)

Also,

$$C_B = \left(\frac{y}{V}\right) = \frac{rA_0}{V}\left(1 - e^{-\lambda\theta}\right)$$

(V-8)

and

$$r_B = \left(\frac{1}{V}\frac{\partial n_B}{\partial\theta}\right) = \dot{C}_B = ke^{-\lambda\theta}$$

(V-8)

Substituting (8) into (4) gives,

$$\left(\frac{\partial^2 C_B}{\partial x^2}\right) - \frac{1}{D}\left(\frac{\partial C_B}{\partial\theta}\right) = -\frac{kC}{D}e^{-\lambda\theta}$$

(V-9)

$$\left(\frac{\text{mols}}{\text{vol cm}^2}\right) - \left(\frac{\text{Sec mols}}{\text{cm}^2\ \text{vol sec}}\right) = -\left(\frac{\text{Sec mols}}{\text{cm}^2\ \text{sec vol}}\right)$$

Equation (9) is the differential equation to be solved; the boundary conditions are,

i) region, $0 < X < \ell$;

ii) when $\theta = 0$, $C_B = 0$, in the entire region, $X = 0 \rightarrow \ell$;

iii) the sweep gas rate is sufficiently high to make, $C_B = 0$, at. $X = \theta$, $\theta > 0$.

---

* A dot over a symbol indicates its time derivative.

B. Solution of the Mass Diffusion Equation:

We note a solution given for equation (V-9) by Carslaw and Jaeger (4) , p. 132, eq. 14):

$$\left(\frac{C_R V}{n A_0}\right)=\left[\frac{\cos x\,(\lambda/D)^{1/2}}{\cos \ell\,(\lambda/D)^{1/2}}-1\right] e^{-\lambda\theta} + \frac{4}{\pi}\sum_{r=0}^{\infty}\frac{(-1)^n e^{-\frac{(2n+1)^2\pi^2 D\theta}{4\ell^2}}\cos\left((2n+1)\frac{\pi x}{2\ell}\right)}{(2n+1)\left[1-\frac{(2n+1)^2\pi^2 D}{4\lambda\ell^2}\right]}$$

(V-10)

and,

$$\frac{V}{nA_0}\left(\frac{\partial C_R}{\partial X}\right)=\left(\frac{\sin x\,(\lambda/D)^{1/2}}{\cos \ell\,(\lambda/D)^{1/2}}\right)\left(\frac{\lambda}{D}\right)^{1/2} e^{-\lambda\theta} \frac{2}{\ell}\sum_{n=0}^{\infty}\frac{(-1)^n e^{-\frac{(2n+1)^2\pi^2 D\theta}{4\ell^2}}\sin\left((2n+1)\frac{\pi x}{2\ell}\right)}{\left(1-\frac{(2n+1)^2\pi^2 D}{4\lambda\ell^2}\right)}$$

(V-11)

At $X=\ell$,

$$\frac{V}{nA_0}\left(\frac{\partial C_R}{\partial X}\right)_{x=\ell}=\frac{2}{\ell}\sum_{n=0}^{\infty}\frac{(-1)^n e^{-\frac{(2n-1)^2\pi^2 D\theta}{4\ell^2}}\sin\left((2n+1)\pi/2\right)}{\frac{(2n-1)^2\pi^2 D}{4\lambda\ell^2}-1} - \left(\frac{\lambda}{D}\right)^{1/2} e^{-\lambda\theta}\tan\left(\frac{\ell^2\lambda}{D}\right)^{1/2}$$

(V-12)

The transport of B across the boundary at X = ℓ will be given by,

$$\dot{n}_B = -DS\left(\frac{\partial C_B}{\partial x}\right)_{x=\ell} \qquad \text{(V-13)}$$

now,

$$V = \frac{S}{\chi}(2\ell) \quad ; \ell = (V/S) = \left(\frac{1}{Sp}\right) \qquad \text{(V-14)}$$

Then,

$$\dot{n}_B = -\frac{DSnA_0}{V}\left[\frac{2}{\ell}\sum \cdots - \left(\frac{1}{\nu}\right)^{1/2} e^{-\lambda\theta} \tan\left(\frac{\ell^2\lambda}{D}\right)^{1/2}\right]$$

$$= \frac{-DSnA_0}{V\,V/S}\left[\sum \cdots - 1/2\left(\frac{\ell^2\lambda}{D}\right)^{1/2} e^{-\lambda\theta} \tan\left(\frac{\ell^2\lambda}{D}\right)^{1/2}\right]$$

$$= -\left(\frac{2DnA_0}{\ell^2}\right)\left[\sum \cdots - 1/2\,\alpha\, e^{-\lambda\theta} \tan\alpha\right]$$

$$\alpha \equiv \left(\frac{\ell^2\lambda}{D}\right)^{1/2} = \left(\frac{\ell^2 k V}{nA_0 D}\right)^{1/2} \qquad \text{(V-15)}$$

$$\frac{\ell^2}{2D n A_0}\int dn_B = \frac{\ell^2}{2D}\int_0^{\xi_B} d\xi_B = \int_0^{\theta}\left[\sum\cdots - \frac{\alpha}{2}\tan\alpha\, e^{-\lambda\theta}\right]d\theta$$

$$\frac{\ell^2}{2D}\xi_B = \left(\frac{\alpha}{2\lambda}\tan\alpha\right)\left(1-e^{-\lambda\theta}\right) + \left(\frac{4\ell^2}{\pi^2 D}\right)\sum_0^{\infty}\frac{\left(1-e^{\frac{-(2n+1)^2\pi^2 D\theta}{4\ell^2}}\right)}{(2n+1)^2\left(1-\frac{(2n+1)^2\pi^2 D}{4\ell^2\lambda}\right)}$$

$$\xi_B = \left(\frac{\tan\alpha}{\alpha}\right)\left(1-e^{-\lambda\theta}\right) + \frac{8}{\pi^2}\sum_0^{\infty}\frac{\left(1-e^{\frac{-(2n+1)^2\pi^2 D\theta}{\pi\ell^2}}\right)}{(2n+1)^2\left[1-\frac{(2n+1)^2\pi^2}{4\lambda^2}\right]} \qquad \text{(V-16)}$$

For convenience the following parameters are defined:

$$\left.\begin{array}{l}\text{Dimensionless}\\ \text{Diffusion}\\ \text{Time,}\quad \tau_m\end{array}\right\} \equiv \left(\frac{D}{\ell^2}\right)\theta = DS^2\rho^2\theta = \mu\theta$$

$\mu \equiv$ diffusion parameter

$$\left.\begin{array}{l}\text{Dimensionless}\\ \text{Kinetic Time,}\\ \tau_k\end{array}\right\} \equiv \left(\frac{kV}{nA_0}\right)\theta = \left(\frac{k M_0}{\rho}\right)\theta = \lambda\theta$$

$\lambda \equiv$ reaction parameter

$$\left.\begin{array}{l}\text{Reaction-Diffusion}\\ \text{Parameter,}\quad \alpha^2\end{array}\right\} \equiv \frac{\lambda}{\mu} = \left(\frac{\lambda\ell^2}{D}\right) = \left(\frac{k\lambda_0}{\rho^3\delta^2 D}\right) = \frac{\tau_k}{\tau_m} \qquad \text{(V-17)}$$

Equation (V-7) can be introduced into (V-16) giving,

$$\xi_B = \left(1 - 1 + \frac{\tan\alpha}{\alpha}\right)\xi_B^0 - \frac{8}{\pi^2}\sum_0^\infty \frac{\left(1 - e^{-\frac{(2n+1)^2\pi^2\tau_m}{4}}\right)}{(2n+1)^2\left(\frac{(2n+1)^2\pi^2}{4\alpha^2} - 1\right)}$$

$$= \xi_B^0 - \left[\frac{8}{\pi^2}\sum_0^\infty \cdots + \left(1 - \frac{\tan\alpha}{\alpha}\right)\xi_B^0\right]$$

(V-18)

From equation (V-7) and V-17) we note that,

$$\xi_B^0 = \left(1 - e^{-\lambda\theta}\right) = \left(1 - e^{-\tau k}\right) = \left(1 - e^{-\alpha^2\tau_m}\right)$$

(V-7)

and (V-18) becomes

$$\xi_B = \xi_B^0 - \left[\frac{8}{\pi^2}\sum \cdots + \left(1 - \frac{\tan\alpha}{\alpha}\right)\left(1 - e^{-\alpha^2\tau_m}\right)\right]$$

(V-19)

Let

$$\eta \equiv \left[\frac{8}{\pi^2}\sum_0^\infty \cdots + \left(1 - \frac{\tan\alpha}{\alpha}\right)\left(1 - e^{-\alpha^2\tau_m}\right)\right]$$

= Diffusion Attenuation (V-20)

Then,

$$\xi_B = \xi_B^0 - \eta\,(\tau, \tau_m)$$

(V-21)

Now consider η under certain limiting conditions; equation (V-20) can be simplified as follows, for $\alpha < 0.5$,

$$\eta \cong \frac{4}{\pi^2} \sum_{0}^{\infty} \frac{\left(1 - e^{-\frac{\pi^2}{4}(2n+1)^2 \tau_m}\right) 4\alpha^2}{(2n+1)^2 (2n+1)^2 \pi^2 \left(1 - \frac{4\alpha^2}{(2n+1)^2 \pi^2}\right)} + \left(1 - \frac{\alpha^2}{3}\right)\left(1 - e^{-\alpha^2 \tau_m}\right)$$

For $\tau_m > 0.3$,

(V-22)

$$\eta \cong \frac{32\alpha^2}{\pi^4}\left[\left(1 - e^{-\frac{\pi^2}{4}\tau_m}\right)\sum_{1}^{\infty} \frac{1}{(2n+1)^4}\right] - \frac{\alpha^2}{3}\left(1 - e^{-\alpha^2 \tau_m}\right)$$

$$\eta \cong \frac{\alpha^2}{3}\left[\frac{96}{\pi^4}\left(1 - e^{-\frac{\pi^2}{4}\tau_m}\right) - \left(1 - e^{-\alpha^2 \tau_m}\right)\right]$$

$$\eta \cong \frac{\alpha^2}{3}\left(e^{-\alpha^2 \tau_m} - e^{-\frac{\pi^2}{4}\tau_m}\right)$$

(V-23)

If α and Tm are small, a further simplification results.

$$\eta \cong \frac{\alpha^2}{3}\left[1 - \alpha^2 \tau_m - 1 + \frac{\pi^2}{4}\tau_m\right] = \frac{\alpha^2 \tau_m}{3}\left(\frac{\pi^2}{4} - \alpha^2\right)$$

$$(\alpha < 0.5\,;\ \tau_m < 0.5)$$

(V-24)

A plot of the computer calculated values of η, by equation (V-20) is presented by Figure 12.

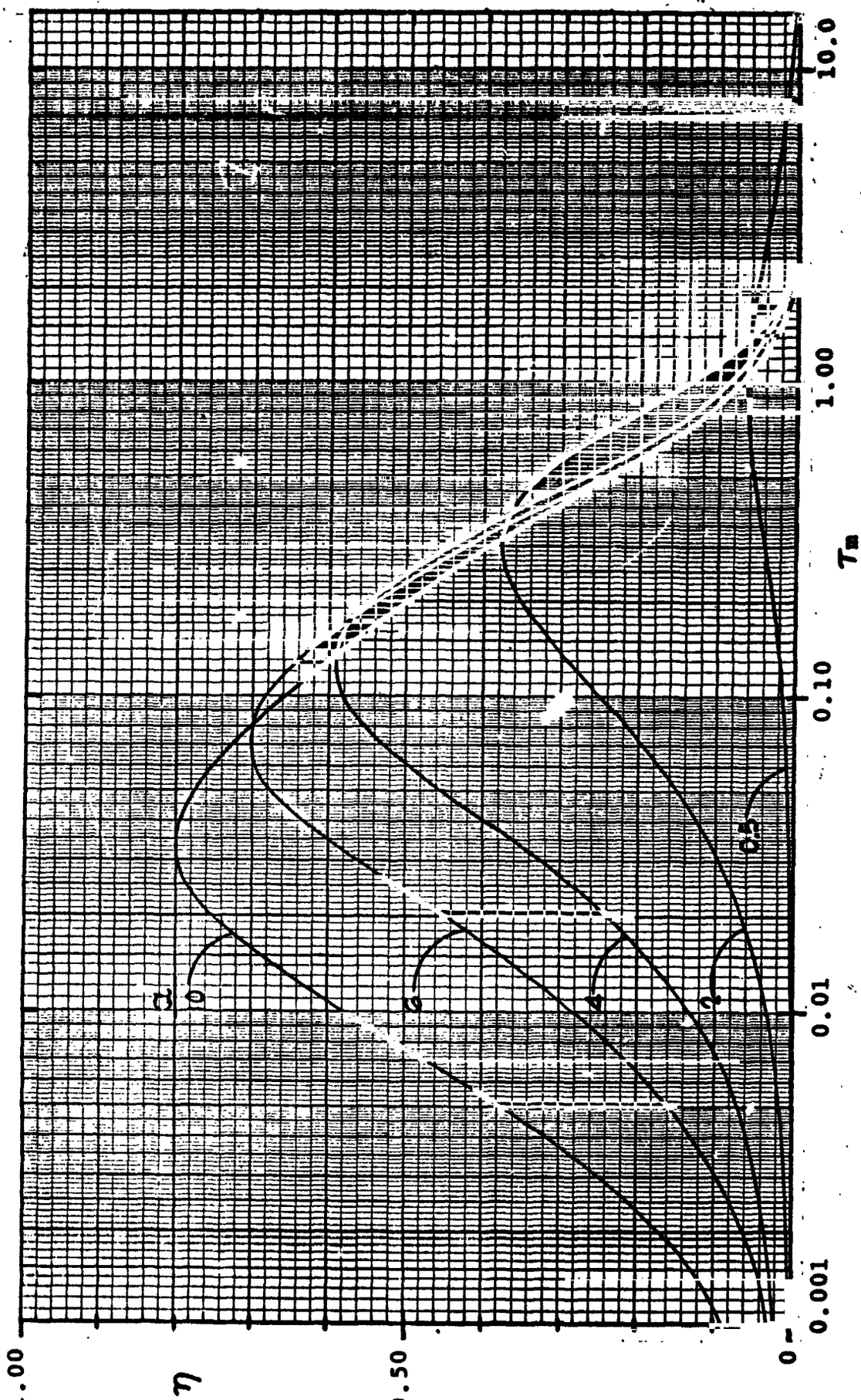

FIGURE 12 - DIFFUSION ATTENUATION, $\eta(\alpha, \tau_a)$

C. Possible Polymer Reactions:

Our present picture of the "cured" polymer substance is that there exists:

a) - a residual amount of adsorbed water, gases (O_2 & N_2), and unlinked alcoholic -OH groups (which are released as water when the substance is decomposed, SR ⟶ R + S);

b) - a basic polymer structure made up of individual units, which can be visualized as,

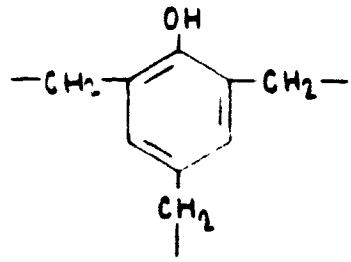

$(CH_2)_{3/2} \cdot (C_6H_2) \cdot OH$

A • B • C

(V-25)

c) - a residual amount of mineral "ash" (from the catalyst, polymer impurities, etc.).

As an elementary model, we propose the following reactions taking place in the thermal decomposition process:

1) - release of the adsorbed water, gases, and alcoholic -OH, which can be represented by,

$$SR_{(s)} \xrightarrow{ko} R_{(g)} + S_{(s)} \qquad \text{(V-26)}$$

2) - breakoff of the -OH and $-CH_2$ groups from the polymer unit by,

$$AB\,|\,C_{(s)} \xrightarrow{k_1} AB_{(s)} + C_{(g)} \qquad \text{(V-27)}$$

$$A\,|\,B\,C_{(s)} \xrightarrow{k_2} BC_{(s)} + A_{(g)} \qquad \text{(V-28)}$$

$$A\,|\,B_{(s)} \xrightarrow{k_3} B_{(s)} + A_{(g)} \qquad \text{(V-29)}$$

$$B\,|\,C_{(s)} \xrightarrow{k_4} B_{(s)} + C_{(g)} \qquad (V\text{-}30)$$

3) - breakout of larger fragments, especially at higher temperatures, from the ring, by

$$ABC_{(s)} \xrightarrow{k_5} A_{(g)} + B_{(g)} + C_{(g)} \qquad (V\text{-}30a)$$

4) - reaction in the gas phase of the fragments evolved.

For the weight loss by decomposition of the solid, the following equations apply.

$$(\dot{SR}) = -k_o V\, \alpha_{SR} \qquad (V\text{-}31)$$

$$(\dot{ABC}) = -(k_1 + k_2 + k_5) V\, \alpha_{ABC} \qquad (V\text{-}32)$$

$$(\dot{AB}) = V(k_1 \alpha_{ABC} - k_3\, \alpha_{AB}) \qquad (V\text{-}33)$$

$$(\dot{BC}) = V(k_2 \alpha_{ABC} - k_4\, \alpha_{BC}) \qquad (V\text{-}34)$$

Also for the gas species evolved,

$$\dot{R} = k_o V\, \alpha_{SR} \qquad (V\text{-}35)$$

$$\dot{C} = V(k_1 + k_5)\, \alpha_{ABC} + k_4 V\, \alpha_{BC} \qquad (V\text{-}36)$$

$$\dot{A} = V(k_2 + k_5)\, \alpha_{ABC} + k_3 V\, \alpha_{AB} \qquad (V\text{-}37)$$

$$\dot{B}_{(g)} = k_5 V\, \alpha_{ABC} \qquad (V\text{-}38)$$

By material balance,

$$SR_{(s)} \xrightarrow{k_o} S_{(s)} + R_{(g)}$$

$$(n_{SRo} - w) \qquad w \qquad w$$

$$ABC_{(s)} \xrightarrow{k_1} AB_{(s)} + C_{(g)}$$

$$(n_{ABCo} - x) \qquad x \qquad x$$

$$ABC_{(s)} \xrightarrow{k_2} BC_{(s)} + A_{(g)}$$

$(n_{ABCo}-x-y)$ $\quad$ y $\quad$ y

$$AB_{(s)} \xrightarrow{k_3} B_{(s)} + A_{(g)}$$

$(x-u)$ $\quad$ u $\quad$ $(u+y)$

$$BC \xrightarrow{k_4} B_{(s)} + C_{(g)}$$

$(y-\eta)$ $\quad$ $(\eta+u)$ $\quad$ $(\eta+x)$

$$ABC \xrightarrow{k_5} A_{(g)} + B_{(g)} + C_{(g)}$$

$(n_{ABCo}-x-y-z)$ $\quad$ $(z+u+y)$ $\quad$ z $\quad$ $(z+\eta+x)$

	$\theta:0$	$\theta:\theta$	MW (Approx.)
$SR_{(s)}$	n_{SRo}	$n_{SRo}-w$	130
$S_{(s)}$	0	w	112
$R_{(g)}$	0	w	18
$ABC_{(s)}$	n_{ABCo}	$n_{ABCo}-x-y-z$	112
$AB_{(s)}$	0	x-u	95
$C_{(g)}$	0	$x+\eta+z$	17
$BC_{(s)}$	0	$y-\eta$	91

$A_{(g)}$	0	z + u + y	21
$B_{(s)}$	0	η + u	74
$B_{(g)}$	0	z	74

$$n_{T(s)} = n_{ABCo} - z \cong n_o \text{ , because z is small}$$

$$n_{T(g)} = w + x + y + 3z + \eta + u$$

From equation (V-31),

$$\frac{dn_{ABC}}{d\theta} = -\frac{k_0 V n_{ABC}}{n_o} \; ; \; \left(\frac{n_{ABC}}{n_o}\right) = \left(\frac{n_{ABC}}{n_o}\right)_o e^{-\left(\frac{k_0 V}{n_o}\right)\theta}$$

(V-39)

From equation (V-32),

$$\frac{dn_{ABC}}{d\theta} = -k_{1+5} V \left(\frac{n_{ABC}}{n_o}\right) \; ; \; \left(\frac{n_{ABC}}{n_o}\right) = e^{-\left(\frac{k_{1+5} V}{n_o}\right)\theta}$$

(V-40)*

From equation (V-33),

$$\frac{dn_{AB}}{d\theta} + \frac{k_3 V}{n_o} n_{AB} = \left(\frac{k_1 V}{n_o}\right) n_{ABC} = k_1 V e^{-\left(\frac{k_{1+5} V}{n_o}\right)\theta}$$

integrating gives,

$$\left(\frac{n_{AB}}{n_o}\right) = \left(\frac{k_1}{k_{1+5} - k_3}\right)\left(e^{-\frac{k_3 V\theta}{n_o}} - e^{-\frac{k_{1+5} V\theta}{n_o}}\right)$$

(V-41)

* $k_{125} = k_1 + k_2 + k_5$

From equation (V-34),

$$\frac{dn_{BC}}{d\theta} + \frac{k_4 V}{n_0} n_{BC} = \frac{k_2 V}{n_0} n_{ABC} = k_2 V e^{-\left(\frac{k_{123} V}{n_0}\right)\theta}$$

integration gives,

$$\left(\frac{n_{BC}}{n_0}\right) = \left(\frac{k_2}{k_{125} - k_4}\right)\left(e^{-\frac{k_4 V \theta}{n_0}} - e^{-\frac{k_{125} V \theta}{n_0}}\right) \qquad (V-42)$$

From equation (V-38),

$$\frac{dn_{B(g)}}{d\theta} = k_5 V \frac{n_{ABC}}{n_0} = k_5 V e^{-\left(\frac{k_{125} V \theta}{n_0}\right)}$$

$$\frac{n_{B(g)}}{n_0} = \frac{k_5}{k_{125}}\left(1 - e^{-\frac{k_{125} V \theta}{n_0}}\right) = \frac{k_5}{k_{125}} \xi^{\circ}_{125} \qquad (V-43)$$

D. Oxygen Evolved into the Gas Phase:

The total oxygen evolved into the gas phase assuming a surface reaction with no diffusion attenuation, and assuming $k_1 = k_4$ and $k_2 = k_3$, is given by,

$$\dot{W}ox = 16\dot{C} + 16\dot{R} \qquad (V-44)$$

$$\frac{\dot{W}_{Ox}}{16V} = (k_1+k_5)\,a_{ABC} + k_2\,a_{BC} + k_0\,a_{SR}$$

$$= (k_1+k_5)\,a_{ABC} + k_1\,a_{BC} + k_0\,a_{SR}$$

$$= (k_1+k_5)\frac{n_{ABC}}{n_0} + k_1\frac{n_{BC}}{n_0} + k_0\frac{n_{SR}}{n_0}$$

$$= k_{15}\,e^{-\frac{k_{125}V\theta}{n_0}} + \left(\frac{k_1k_2}{k_{125}-k_2}\right)\left(e^{-\frac{k_2V\theta}{n_0}} - e^{-\frac{k_{125}V\theta}{n_0}}\right)$$

$$+ k_0\frac{n_{SR0}}{n_0}\,e^{-\frac{k_0V\theta}{n_0}}$$

$$= k_{15}\,e^{-\frac{k_{125}V\theta}{n_0}} + \left(\frac{k_1k_2}{k_{25}}\right)\left(e^{-\frac{k_1V\theta}{n_0}} - e^{-\frac{k_{125}V\theta}{n_0}}\right)$$

$$+ k_0\left(\frac{n_{SR0}}{n_0}\right)e^{-\frac{k_0V\theta}{n_0}}$$

$$\left(\frac{\dot{W}_{Ox}}{16V}\right) = k_0\left(\frac{n_{SR0}}{n_0}\right)e^{-\frac{k_0V\theta}{n_0}} + \frac{k_1k_2}{k_{25}}\,e^{-\frac{k_1V\theta}{n_0}}$$

$$+ \left(k_{15} - \frac{k_1k_2}{k_{25}}\right)e^{-\frac{k_{125}V}{n_0}\theta} \qquad \text{(V-45)}$$

$$\left(\frac{W_{ox}}{W_o}\right)_g = \frac{16V}{W_o}\left[k_o \frac{n_{s2o}}{n_o}\int_o^\theta e^{-\frac{k_o V\theta}{n_o}}\,d\theta + \frac{k_1 k_2}{k_{25}}\int_0^\theta e^{-\frac{k_1 V\theta}{n_o}}\,d\theta + \left(k_{15}\frac{-k_1 k_2}{k_{25}}\right)\int_0^\theta e^{-\frac{k_{125} V\theta}{n_o}}\,d\theta\right]$$

$$= \left(\frac{16 n_o}{W_o}\right)\left\{\left(\frac{n_{s2o}}{n_o}\right)\left(1-e^{-\frac{k_o V\theta}{n_o}}\right)+\left(\frac{1}{1+\frac{k_5}{k_2}}\right)\left(1-e^{-\frac{k_1 V\theta}{n_o}}\right)\right.$$

$$\left.+\underbrace{\left[\frac{1}{\left(1+\frac{k_2}{k_1+k_5}\right)}-\frac{1}{\left(1+\frac{k_5}{k_2}\right)\left(1+\frac{k_2}{k_1}+\frac{k_5}{k_1}\right)}\right]}_{\beta_1}\left(1-e^{-\frac{k_{125} V\theta}{n_o}}\right)\right\}$$

$$\left(\frac{W_{ox}}{W_o}\right)_g = \left(\frac{16 n_o}{W_o}\right)\left[\frac{n_{s2o}}{n_o}\xi_o + \frac{1}{\left(1+\frac{k_5}{k_2}\right)}\xi_1 + \beta_1 \xi_{125}\right] \qquad \text{(V-46)}$$

When the temperature is low $k_5 \cong 0$ and,

$$\left(\frac{W_{ox}}{W_o}\right)_g = \left(\frac{16 n_{s2o}}{W_o}\right)\xi_o + \left(\frac{16 n_o}{W_o}\right)\xi_1$$

(V-47)

Including the diffusion effect,

$$\left(\frac{W_{ox}}{W_o}\right)_g = \left(\frac{16 n_{s2o}}{W_o}\right)\xi_o + \frac{16 n_o}{W_o}\left(\xi_1^o - \eta_1\right)$$

(V-48)

E. Carbon Evolved into the Gas Phase:

(Assuming $k_1 = k_4$; $k_2 = k_3$) The total carbon (C) is given by,

$$\dot{W}_c = \frac{3}{2}(12)\dot{A} + 6(12)\dot{B}$$

(V-49)

$$\left(\frac{\dot{W}_c}{12V}\right) = \left[\frac{3}{2}(k_2 + k_5) + 6k_5\right] a_{ABC} + \frac{3}{2} k_3 a_{AB}$$

$$= [\,]\, e^{-\frac{k_{125} V\theta}{n_0}} + \frac{3}{2}\frac{k_2 k_1}{(k_{125} - k_2)}\left(e^{-\frac{k_2 V\theta}{n_0}} - e^{-\frac{k_{125} V\theta}{n_0}}\right)$$

$$= \left(\frac{3}{2} k_{25} + 6k_5 - \frac{3}{2}\frac{k_2 k_1}{k_{15}}\right) e^{-\frac{k_{125} V\theta}{n_0}} +$$

$$+ \frac{3}{2}\frac{k_1 k_2}{k_{15}} e^{-\frac{k_2 V\theta}{n_0}}$$

(V-50)*

$$\left(\frac{W_c}{W_o}\right)_g = \frac{12 n_o}{W_o}\left[\left(\frac{3}{2} k_{25} + 6k_5 - \frac{3}{2}\frac{k_1 k_2}{k_{15}}\right)\frac{1}{k_{125}}\left(1 - e^{-\frac{k_{125} V\theta}{n_0}}\right)\right.$$

$$\left. + \left(\frac{3}{2}\frac{k_1}{k_{15}}\right)\left(1 - e^{-\frac{k_2 V\theta}{n_0}}\right)\right]$$

$$\left(\frac{W_c}{W_o}\right)_g = \left(\frac{18 n_o}{W_o}\right)\left(\frac{k_1}{k_{15}}\right)\xi_{12} + \frac{18 n_o}{W_o}\left(\frac{k_2 + 5k_5 - \frac{k_1 k_2}{k_{15}}}{k_{125}}\right)\xi_{125}$$

$$= \left(\frac{18 n_o}{W_o}\right)\left(\frac{k_1}{k_{15}}\right)\xi_{12} + \left(\frac{18 n_o}{W_o}\right)\beta_2\, \xi_{125}$$

(V-51)

* $k_{15} = k_1 + k_5$; $k_{25} = k_2 + k_5$

When the temperature is low $k_5 \cong 0$ and,

$$\left(\frac{W_i}{W_o}\right)_g = \frac{18 n_o}{W_o} \xi_2 \qquad (V\text{-}52)$$

F. Hydrogen Evolved into the Gas Phase:

The total hydrogen (H) is given by (assuming $k_1 = k_4$, $k_2 = k_3$),

$$\dot{W}_H = 2(1)\ddot{R} + 3(1)\ddot{A} + 2(1)\dot{B}_{(g)} + 1(1)\ddot{C} \qquad (V\text{-}53)$$

$$\left(\frac{\dot{W}_H}{V}\right) = 2k_o a_{SR} + (k_1 + 3k_2 + 4k_5)\, a_{ABC} + 3k_2 a_{AB} + k_1 a_{Ei}$$

$$= 2k_o \left(\frac{n_{SRO}}{n_o}\right) e^{-\frac{k_o V\theta}{n_o}} + \left(k_1 + 3k_2 + 4k_5 - \frac{3k_1 k_2}{k_{15}} - \frac{k_1 k_2}{k_{25}}\right)$$

$$e^{-\frac{k_{125} V\theta}{n_o}} + \frac{3k_1 k_2}{k_{15}}\, e^{-\frac{k_2 V\theta}{n_o}} + \frac{k_1 k_2}{k_{25}}\, e^{-\frac{k_1 V\theta}{n_o}}$$

(V-54)

$$\left(\frac{W_H}{W_o}\right)_g = \frac{n_o}{W_o}\left[2\left(\frac{n_{SRO}}{n_o}\right)\left(1 - e^{\frac{-k_o V\theta}{n_o}}\right) + \frac{k_2}{k_{25}}\left(1 - e^{\frac{k_1 V\theta}{n_o}}\right)\right.$$

$$+ \frac{3k_1}{k_{15}}\left(1 - e^{\frac{k_2 V\theta}{n_o}}\right)$$

$$\left. + \left(\frac{k_1 + 3k_2 + 4k_5 - \frac{3k_1k_2}{k_{15}} - \frac{k_1k_2}{k_{25}}}{k_{125}}\right)\left(1 - e^{\frac{k_{125} V\theta}{n_o}}\right)\right]$$

$$\left(\frac{W_H}{W_o}\right)_g = \frac{n_o}{W_o}\left[2\left(\frac{n_{SRO}}{n_o}\right)\xi_o + \frac{k_2}{k_{25}}\xi_1 + \frac{3k_1}{k_{15}}\xi_2 + \beta_3\,\xi_{125}\right] \qquad \text{(V-55)}$$

When the temperature is low, $k_5 = 0$, and

$$\left(\frac{W_H}{W_o}\right)_g = \frac{n_o}{W_o}\left[2\left(\frac{n_{SRO}}{n_o}\right)\xi_o + \xi_1 + 3\,\xi_2\right] \qquad \text{(V-56)}$$

G. Total Weight Loss:

Obviously, the total weight loss is the sum of the total oxygen, carbon, and hydrogen evolved into the gas phase, and is given by the sum of equations, (V-46), (V-51), (V-55),

$$\left(1 - \frac{W}{W_o}\right) = \left(\frac{W_{ox}}{W_o}\right)_g + \left(\frac{W_c}{W_o}\right)_g + \left(\frac{W_H}{W_o}\right)_g \qquad \text{(V-57)}$$

$$\left(1 - \frac{W}{W_o}\right) = \left(\frac{18\,n_{SRO}}{W_o}\right)\xi_o + \left(\frac{17\,n_o}{W_o}\right)\left(\frac{k_2}{k_{25}}\right)\xi_1 + \left(\frac{21\,n_o}{W_o}\right)\frac{k_1}{k_{15}}\,\xi_2$$

$$+ \left(\frac{16\,n_o}{W_o}\right)\phi_{125}\,\xi_{125} \qquad \text{(V-58)}$$

$$\phi_{125} = \left(\beta_1 + \frac{9\beta_2}{8} + \frac{\beta_3}{16}\right)$$

(V-59)

If $k_5 = 0$ then,

$$\left(1 - \frac{W}{W_o}\right) = \left(\frac{18 n_{SRO}}{W_o}\right) \xi_0 + \left(\frac{17 n_o}{W_o}\right) \xi_1 + \left(\frac{21 n_o}{W_o}\right) \xi_2$$

(V-60)

An additional material balance equation is useful in the calculations,

$$\underset{(\theta=0)}{W_o} = W_{ABCO} + W_{ash} + W_{SRO}$$

$$= W_{ABCO}\left(1 + \frac{W_{ash}}{W_{ABCO}} + \frac{W_{SRO}}{W_{ABCO}}\right)$$

$$\left(\frac{W_o}{n_o}\right) = M_{ABC}\left(1 + \frac{W_{ash}}{W_{ABCO}} + \frac{W_{SRO}}{W_{ABCO}}\right)$$

(V-61)

VI. ANALYSIS OF THE DATA

A. WEIGHT LOSS DATA:

An overall view of the decomposition rate process can be obtained from the weight loss function, $(1 - W/W_o)$. Figure 13 presents the weight loss isotherms as a function of time over a range of 720°F to 1200°F. In making any mechanism study, it is imperative to "slow down" the reactions to rates such that the individual phenomena can be observed. In this study, for phenol-formaldehyde polymer, a temperature of 382°C (720°F) was a good threshold level. Six additional weight loss isotherms were obtained at higher temperatures, and at two particular temperatures, 498°C and 605°C, complete analyses including product species, were obtained. The material balanced curves and data are presented as Figures 14, 15, and 16, at 382°C, 498°C and 605°C, respectively. The detailed data for all runs are presented in Appendix B (Tables B-1 through B-14).

Obviously, the mechanism of weight loss must be the composite effect of breakup of the chemical structure of the polymer; i.e., the sum of the individual reactions involved. The fact emerges from the data that the oxygen is first to come out of the polymer $\left[\text{c.f. } \left(\frac{Wox}{Wo}\right) \text{ and } \left(\frac{Wc}{Wo}\right) \text{ at } 382°C\right]$.

The effect of quartz fibers on the decomposition of PF polymer was determined at 382°C and appears to be negligible; 28.8 w% quartz fibers were a) individually cured with the PF polymer and b) admixed with the cured polymer, the weight loss curves are presented in Figure 17. To illustrate that the effect is primarily dilution, a normalized curve is also plotted in Figure 17.

As part of the study preliminary isotherms were determined for the epoxy-novolak polymer described previously. The first isotherm was obtained at 388°C (730°F), but the weight loss in 15 minutes was found to be almost 50 w%. Lower temperatures were tried, and an isotherm obtained at 316°C (569°F) was more directly comparable to the PF polymer at 382°C. Figure 18 presents the results, and Figure 19 presents a preliminary mareriał balanced set of curves.

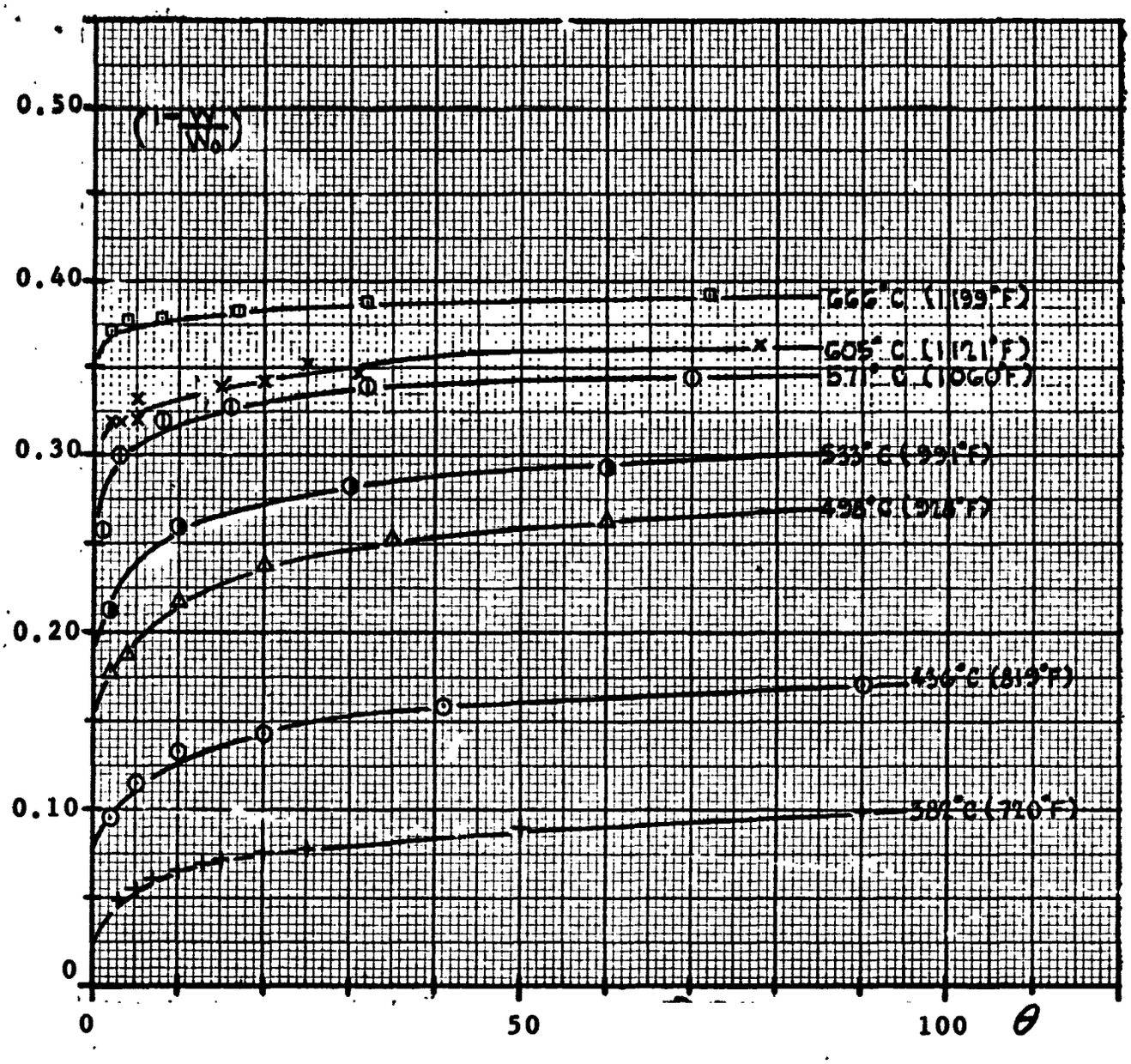

FIGURE 13 - WEIGHT LOSS, PF RESIN

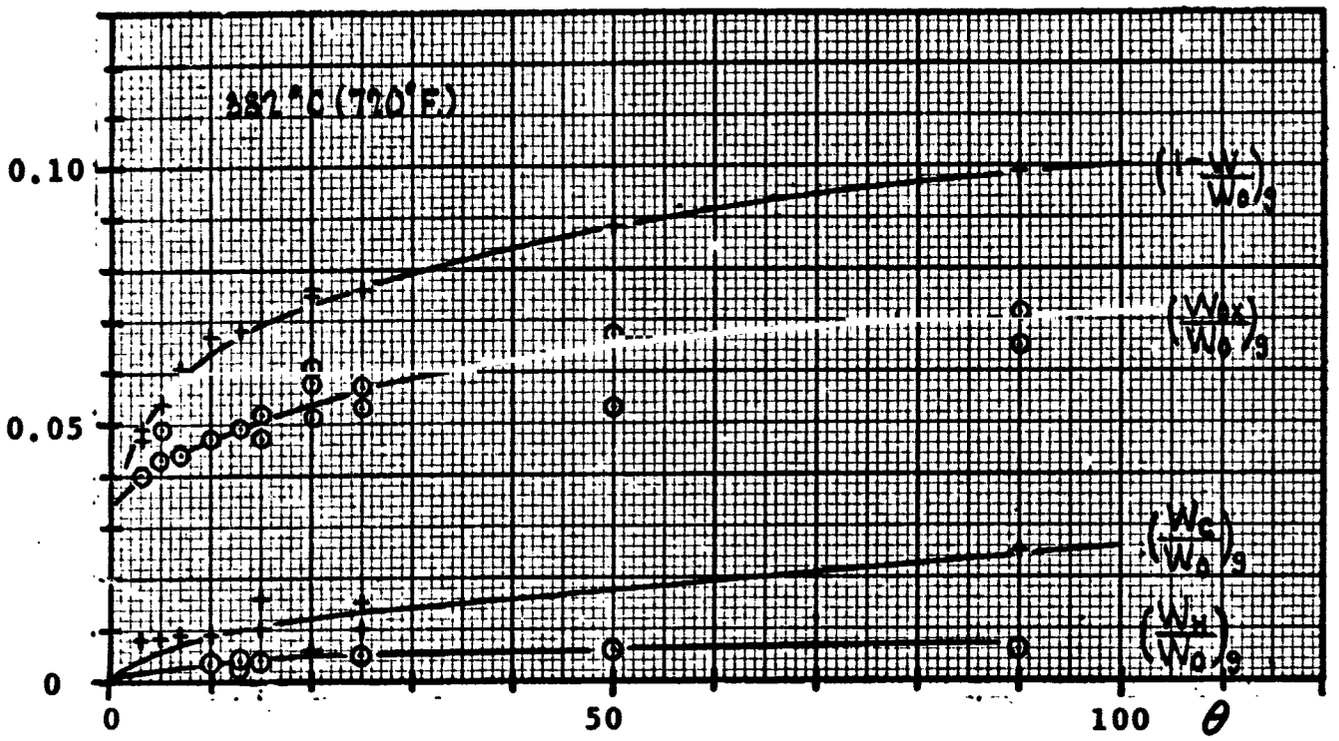

θ	$(1-\frac{W}{Wo})_g$	$(\frac{Wox}{Wo})_g$	$(\frac{Wc}{Wo})_g$	$(\frac{W_H}{Wo})_g$
0	0	0	0	0
3	0.048	0.0405	0.005	0.002
5	0.052	0.043	0.006	0.003
7	0.057	0.045	0.007	0.004
10	0.063	0.048	0.009	0.004
15	0.069	0.052	0.011	0.005
20	0.073	0.055	0.012	0.006
30	0.080	0.058	0.015	0.007
50	0.089	0.064	0.018	0.007
80	0.097	0.069	0.022	0.007
100	0.101	0.071	0.024	0.007

FIGURE 14 - C/H/O LOSS DISTRIBUTION, PF (382°C)

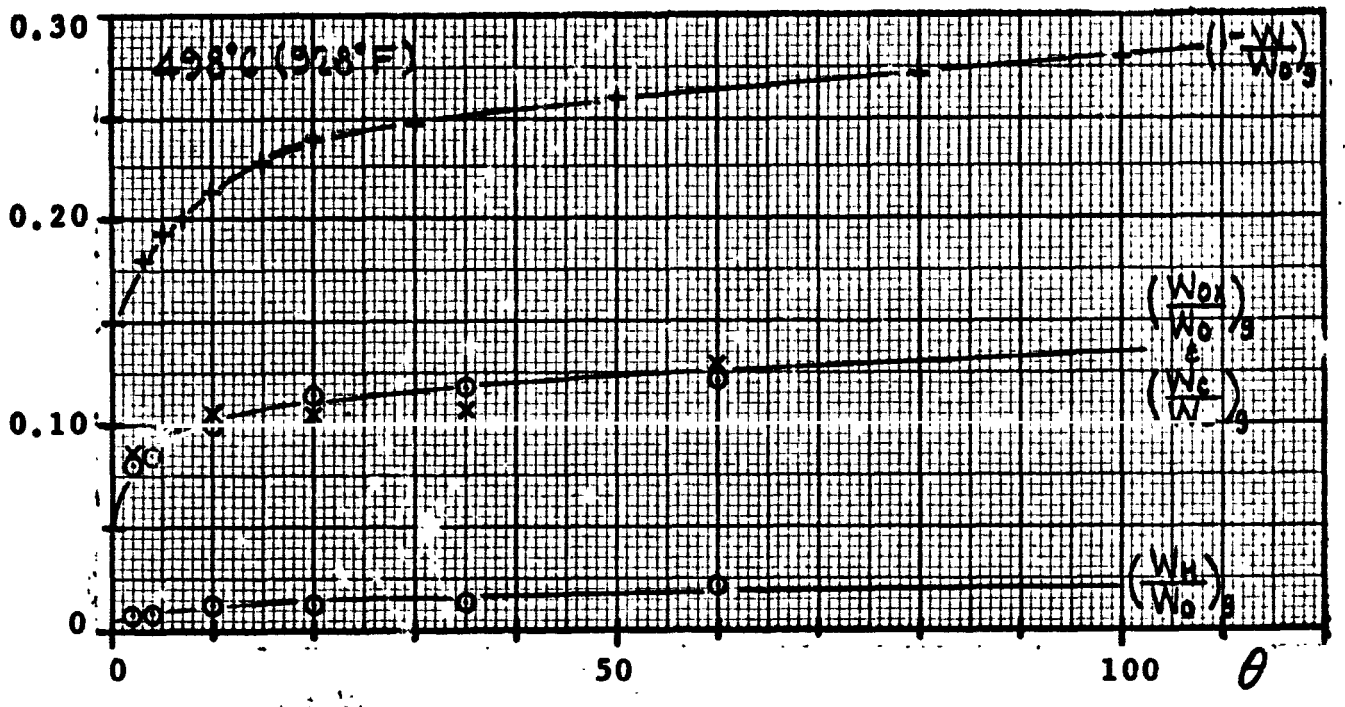

	$\left(\frac{1-W}{Wo}\right)$	$\left(\frac{Wox}{Wo}\right)_g$	$\left(\frac{Wc}{Wo}\right)_g$	$\left(\frac{W_H}{Wo}\right)_g$
0	0	0	0	0
3	0.178	0.0810	0.085	0.012
5	0.191	0.0900	0.088	0.013
7	0.200	0.0950	0.0950	0.014
10	0.213	0.1010	0.100	0.014
15	0.227	0.1060	0.106	0.015
20	0.240	0.1095	0.115	0.015
30	0.248	0.1150	0.118	0.016
50	0.260	0.122	0.122	0.016
80	0.272	0.130	0.125	0.017
100	0.280	0.135	0.127	0.018

FIGURE 15 - C/H/O LOSS DISTRIBUTION, PF (498°C)

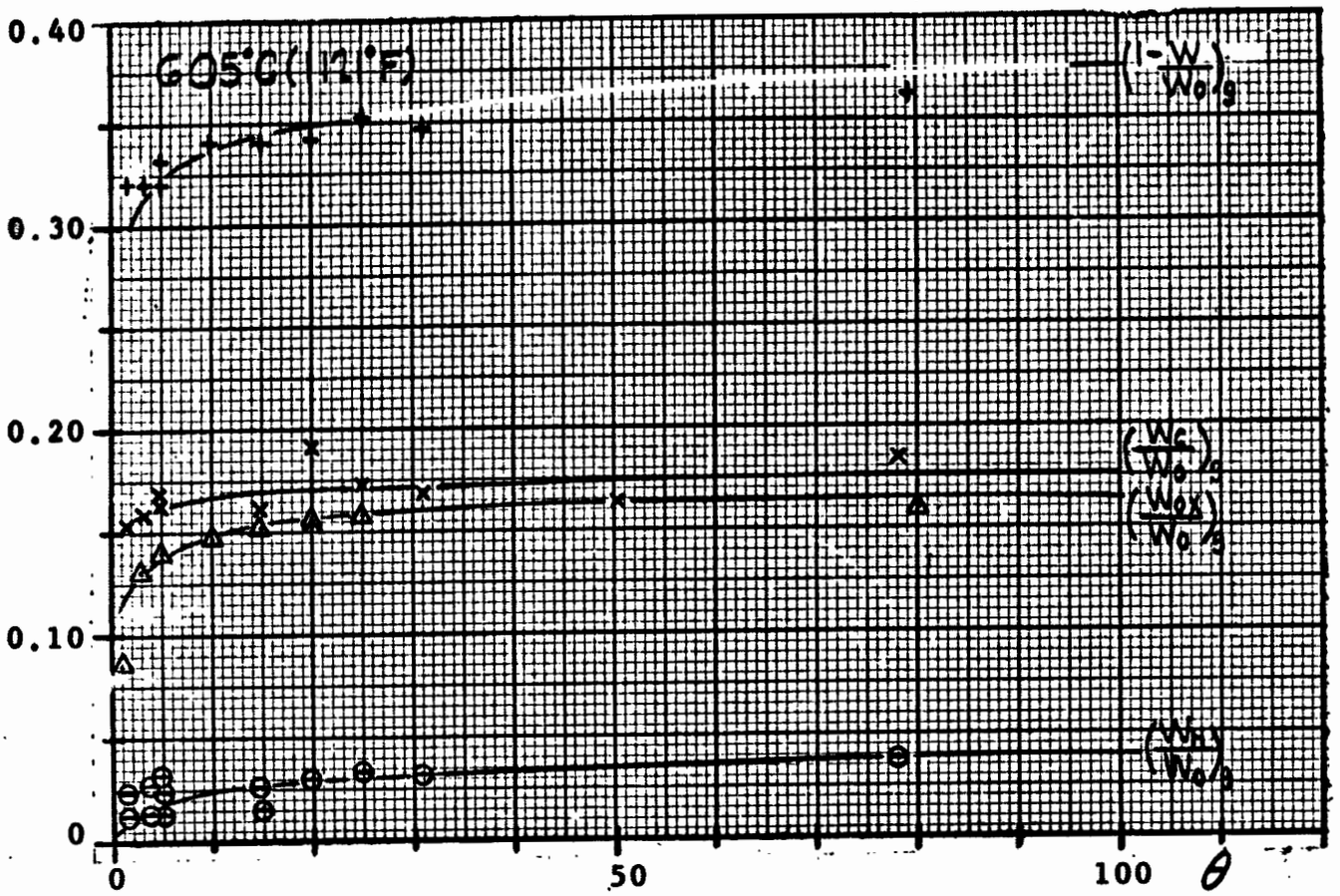

θ	$(1-\frac{W}{Wo})$	$(Wox/Wo)g$	$(Wc/Wo)g$	$(W_H/Wo)g$
0	0	0	0	0
3	0.310	0.133	0.161	0.016
5	0.320	0.139	0.161	0.020
7	0.331	0.143	0.163	0.023
10	0.336	0.147	0.164	0.025
15	0.343	0.152	0.165	0.026
20	0.349	0.156	0.166	0.027
30	0.355	0.160	0.165	0.030
50	0.363	0.162	0.166	0.035
80	0.371	0.163	0.171	0.037
100	0.376	0.163	0.174	0.039

FIGURE 16 - C/H/O LOSS DISTRIBUTION, PF (605°C)

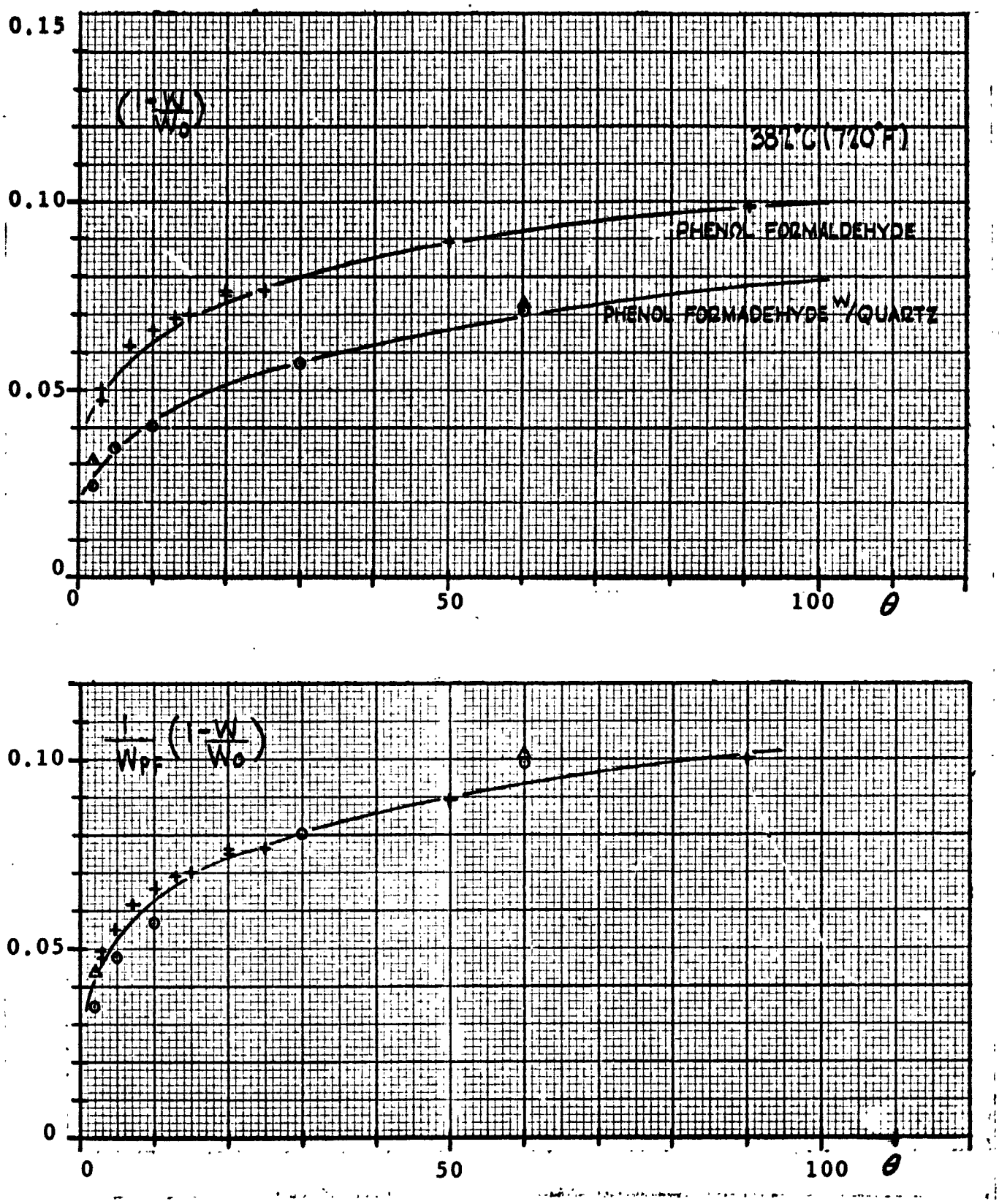

FIGURE 17 - EFFECT OF QUARTZ FIBERS ON PF DECOMPOSITION

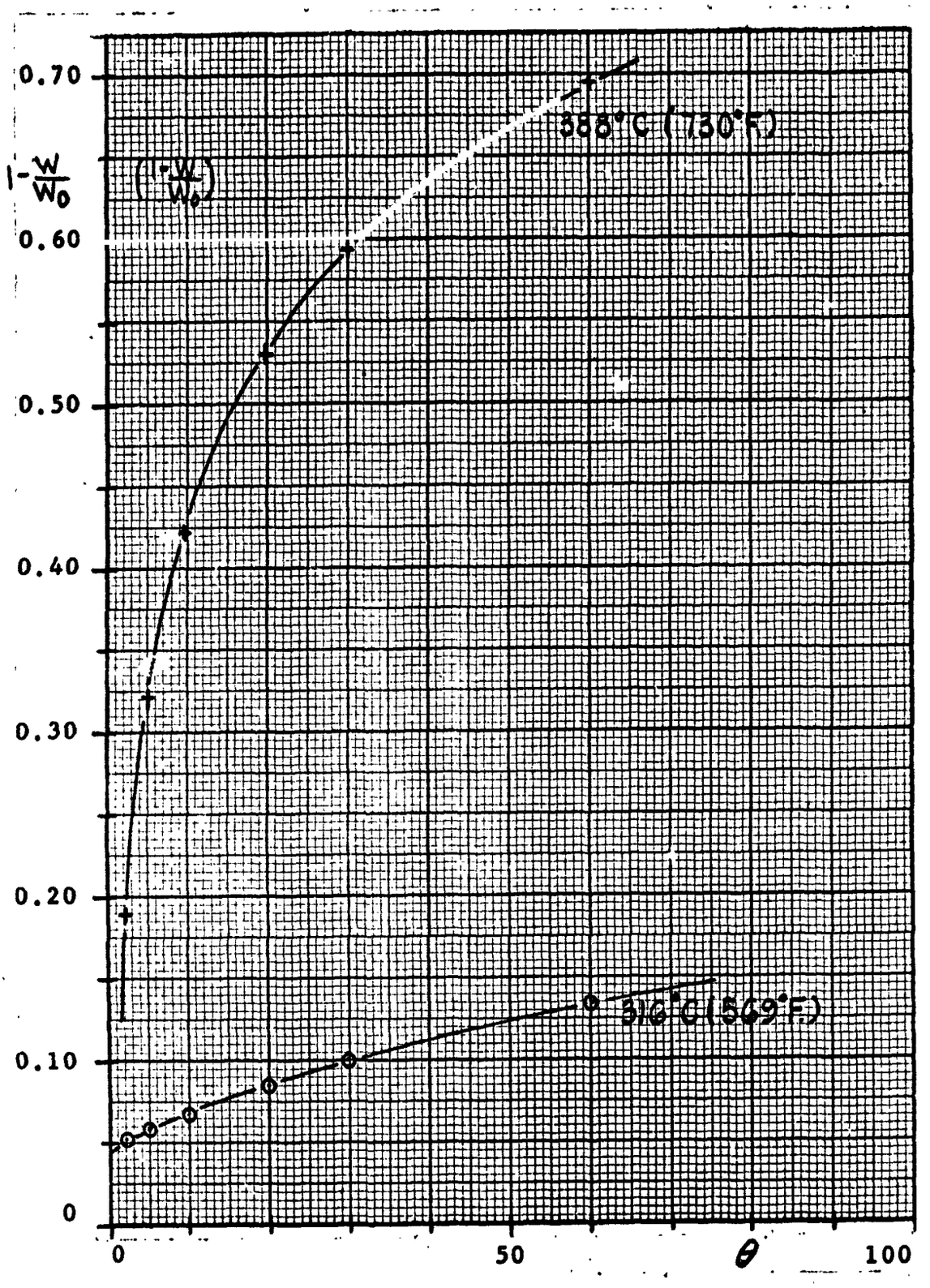

FIGURE 18 - WEIGHT LOSS, EPN RESIN

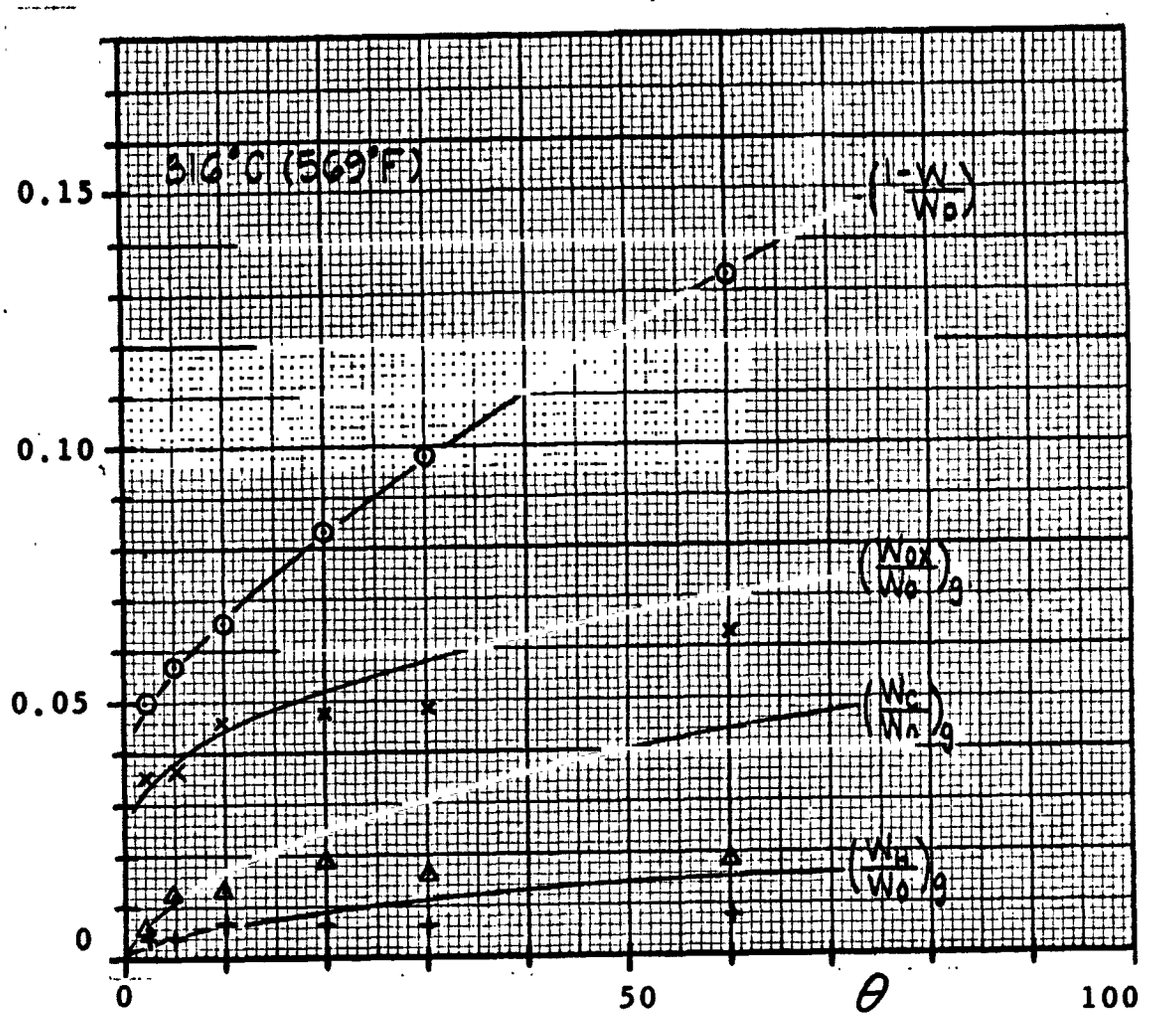

	$(1-\frac{W}{W_o})$	$(\frac{W_{ox}}{W_o})_g$	$(\frac{W_c}{W_o})_g$	$(\frac{W_H}{W_o})_g$
0	0	0	0	0
3	0.050	0.038	0.008	0.004
5	0.056	0.039	0.012	0.005
7	0.060	0.041	0.014	0.0055
10	0.066	0.044	0.016	0.006
20	0.083	0.051	0.024	0.008
30	0.095	0.056	0.029	0.010
50	0.120	0.066	0.039	0.014
60	0.130	0.070	0.045	0.015

FIGURE 19 - C/H/O LOSS DISTRIBUTION, EPN (316°C)

B. SOLID PHASE PROPERTY CHANGES:

The physical characteristics of the solid are important in understanding a) the solid reaction volume and b) the transport of the decomposition species to the surface. The properties of porosity, bulk density, skeletal density, pore volume, surface area, permeability as a function of weight loss, and the surface area and permeability distributions as a function of the pore volume for a given sample, were measured by means of a Winslow mercury porosiometer and an analytical balance. The detailed data are presented in Appendix B (Tables B-16 to B-40) and a summary of the pertinent values is given by Table B-15. A plot of the skeletal density, pore volume, surface area, average pore diameter, and permeability as a function of the weight loss is presented in Figure 20.

The skeletal density, ρ of the undecomposed resin is approximately 1.24-1.26 g./cm^3 and that of the char about the same. Statistically it appears that the density may increase slightly as the char becomes 30-40% decomposed, approaching the value for natural graphite.

The pore volume, V_p of the resin is 0.69-0.73 cm^3/g. and appears to remain approximately constant as decomposition progresses, perhaps increasing somewhat in the later stages.

The surface area, S, for the resin is approximately 2400 cm^2/g., a rather low value compared to catalyst substances (500 - 1000 m^2/g.), and as decomposition progresses the surface area appears to remain fairly constant; however there is considerable scatter in the data.

The average pore diameter, $\bar{d} = \frac{4V_p}{S}$ for the resin is about 12 microns, characterizing the pores as macro-pores rather than micro-pores, and consistent with the slight increase in pore volume in the later stages of decomposition; the average pore diameter appears to increase to 20-30 microns.

The permeability, K, for the resin is approximately 0.5-2 x 10^{-6} cm^2 and appears to increase in the later stages.

The pore size distribution for the resin and three chars at different stages of decomposition is presented by Figure 21. The majority of the pores are in the range of 10-80 microns diameter, shifting to the large end of this range as decomposition occurs, which should also increase the permeability.

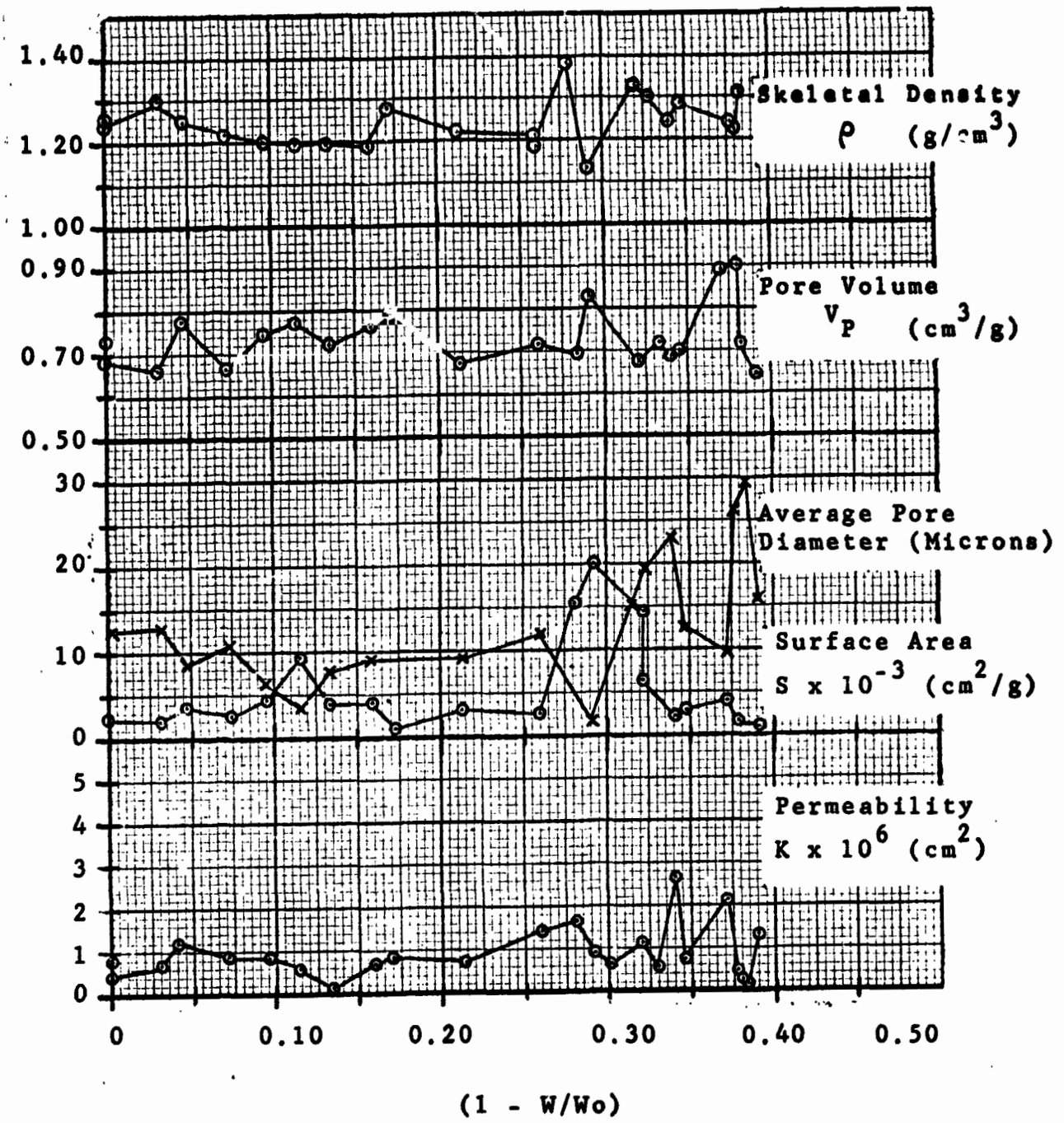

FIGURE 20 - PHYSICAL PROPERTIES OF SOLID

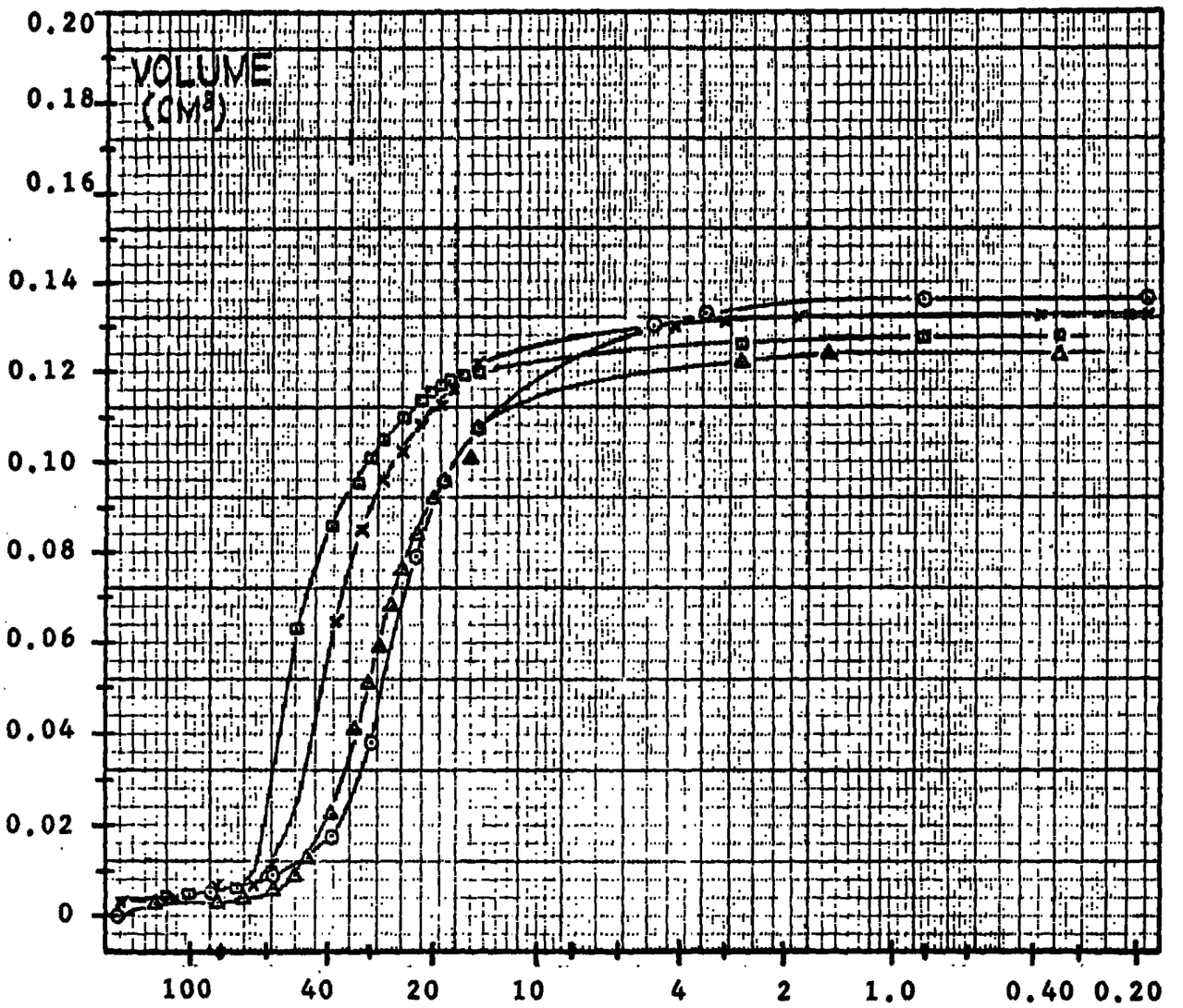

		$(1-W/Wo)$
● Resin	0.188 g. sample	0
▲ #67	0.176 g.	0.133
x #71	0.190 g.	0.259
■ #73	0.195 g.	0.320

FIGURE 21 - PORE SIZE DISTRIBUTIONS

C. DISAPPEARANCE OF OXYGEN AND CARBON FROM THE SOLID:

Insofar as the determination of the mechanism of decomposition is concerned, it appears that the oxygen disappearance from the solid, which occurs the most rapidly, would be the simplest approach, since oxygen occurs in only one group, phenolic-OH, (c.f. carbon which can come from numerous locations in the structure). If the polymer were completely cured and free of adsorbed water, etc., the oxygen content would be (16/112 = 0.143); however, analysis indicates some residual phenolic-OH (about 0.47%) and also some residual adsorbed water and air. Table VI presents a material balance of the C-1 resin with the appropriate parameters calculated and indicates $(^{Wox}/Wo)_g \cong 0.1627$ (including adsorbed nitrogen). The $(^{Wox}/Wo)_g$ isotherms are presented in Figure 22.

Consider the oxygen evolution into the gas phase; at low temperatures equation V-48 is applicable,

$$\left(\frac{W_{ox}}{W_o}\right)_g = \frac{16 n_o}{W_o}\left(\frac{n_{SRO}}{n_o}\xi_o + \xi_1^\circ - \eta_1\right) \qquad (V\text{-}48)$$

$$\left(\frac{W_{ox}}{W_o}\right)_g = 0.0243\,\xi_o + 0.1355\left(\xi_1^\circ - \eta_1\right)$$

Figure 22 presents $(^{Wox}/Wo)_g$ at three temperatures, 382°C (720°F), 498°C (928°F) and 605°C (1121°F), and indicates a very rapid initial rise; interpreted as rapid release of the adsorbed water, fixed gases and residual alcoholic-OH. Consequently ξ_o reaches unity almost instantaneously. Initially reaction occurs on the solid surface and,

$$\lim_{\theta \to 0}\left(\frac{W_{ox}}{W_o}\right)_g = 0.0243 + 0.1355\,\xi_1^\circ$$

$$\lambda_1 = \frac{1}{\theta}\ln\left\{\lim\left[\frac{1}{1-\left(\frac{\left(\frac{W_{ox}}{W_o}\right)_g - 0.0243}{0.1355}\right)}\right]\right\}$$

$$\lambda_1 \equiv \frac{k_1 V}{n_o} = \left(\frac{k_1 M_o}{\rho}\right) \qquad (VI\text{-}1)$$

TABLE VI. MATERIAL BALANCE ON C-1 RESIN:

				Component	Weight Fraction		Oxygen Contribution
1)	C-H, in Resin	0.8356	0.8109	C-H	0.8109	0.9497 (C-1 Resin)	--
2)	Oxygen (phenolic & alcoholic)	0.1644	0.1596	Phenolic Oxy.	0.1388		0.1388
				Ads. O_2 & N_2	0.0161		0.0161
3)	Adsorbed Air			Alc. OH	0.0047	0.0243	0.0047
4)	Adsorbed H_2O	0.0035Wo		Ads. H_2O	0.0035		0.0031
5)	Ash	0.0260Wo	0.0260	Ash	0.0260	0.0260	--
		Wo=1.00+0.0295Wo	1.0000		1.0000	1.0000	0.1627
		Wo=1.0304					

W_{ABCO}: $0.9497 = \left(\frac{W_{ABCO}}{W_o}\right)$; $\left(\frac{W_o}{n_o}\right) = M_{ABC}\left(1 + \frac{W_{ash}}{W_o} + \frac{W_{SRO}}{W_{ABCO}}\right) = 112\,(1.0530) = 118.0$

W_{ash}: $0.0260 = \left(\frac{W_{ash}}{W_o}\right)$

W_{SRO}: $0.0243 = \left(\frac{W_{SRO}}{W_o}\right)$

W_{ox}: $0.1627 = \left(\frac{W_{ox}}{W_o}\right)$

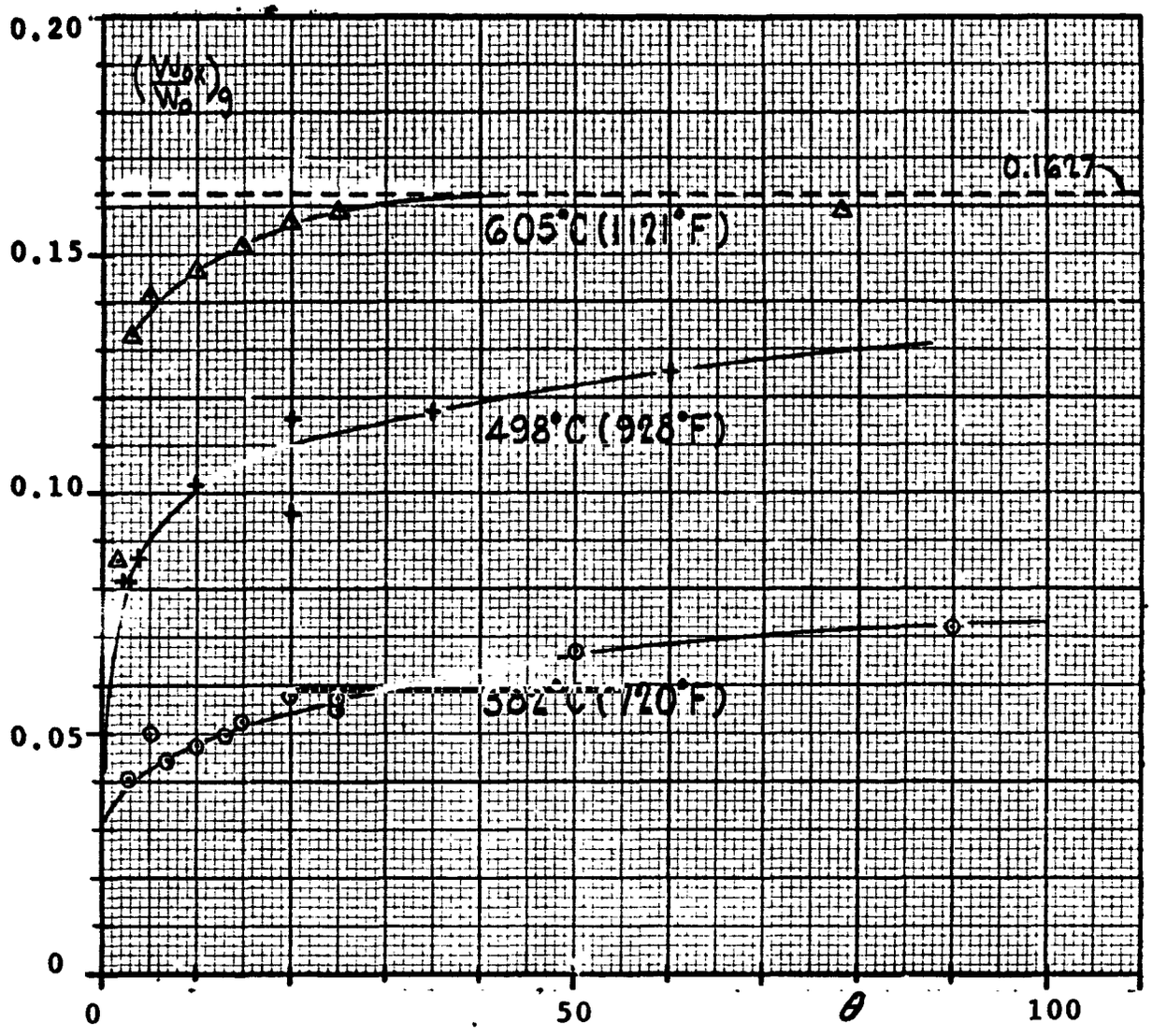

FIGURE 22 - OXYGEN DISAPPEARANCE

using the data at 382°C, λ_1, can be calculated,

θ	$\lambda_1 (min^{-1})$
3.0	0.0425
5.0	0.0410
7.0	0.0224
13.0	0.0160

Obviously the reaction is "slowing down", which is interpreted as the diffusion attenuation effect. Figure 23 presents a plot of ξ_1, ξ_1°, and $(\xi_1^\circ - \xi_1)$ vs θ, and it appears that $(\xi_1^\circ - \xi_1)$ is the same form as η, predicted by the theoretical development. η derived in Chapter 5-B assumes no buildup of product species at the surface; i.e., the sweep gas rate is sufficient to prevent buildup. However, in the actual case since the surface occurs in pores a concentration will build up at the surface and consequently slow down mass transfer into the bulk gas phase. The actual ξ_1-data does not extend beyond 100 mins., but qualitatively the effect is illustrated in Figure 23.

Figure 24 presents the curves for the carbon loss into the gas phase at 382, 498, and 605°C, and by the proposed model is the sum of the two reactions (characterized by k_2 and k_5) involving breakout of the $-CH_2$ bridges and the C_6-ring,

$$A\,|\,BC \xrightarrow{k_2} BC(s) + A(g) \qquad \text{(V-28)}$$

$$A\,|\,B\,|\,C \xrightarrow{k_5} A(g) + B(g) + C(g) \qquad \text{(V-30)}$$

The loss of total carbon into the gas phase is given by,

$$\left(\frac{W_c}{W_o}\right)_g = \left(\frac{18 n_o}{W_o}\right)\left(\frac{\lambda_1}{\lambda_{15}}\right)\xi_2 + \left(\frac{18 n_o}{W_o}\right)\beta_2\,\xi_{125} \qquad \text{(V-51)}$$

at 382°C the equation becomes,

$$\left(\frac{W_c}{W_o}\right)_g = 0.1899\left(\xi_2^\circ - \eta_2\right) + 0.05514\left(\xi_{125}^\circ - \eta_{125}\right)$$

$$(\lambda_2 = 0.0120\,;\ \alpha_2 = 18.00;\ \lambda_5 = 0.0054\,;\ \alpha_3 = 10.00) \qquad \text{(VI-2)}$$

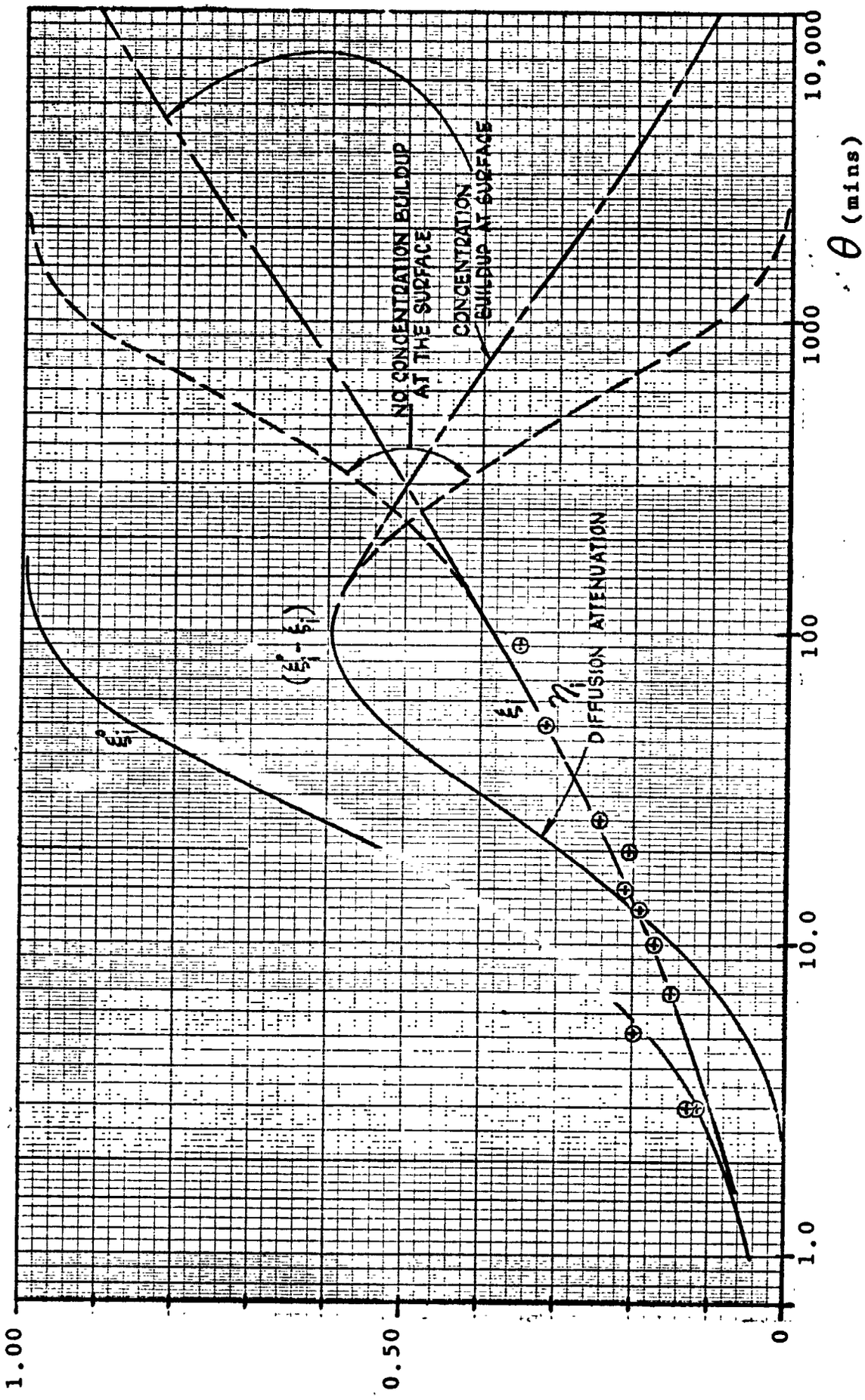

FIGURE 23 - OXYGEN DISAPPEARANCE MECHANISM

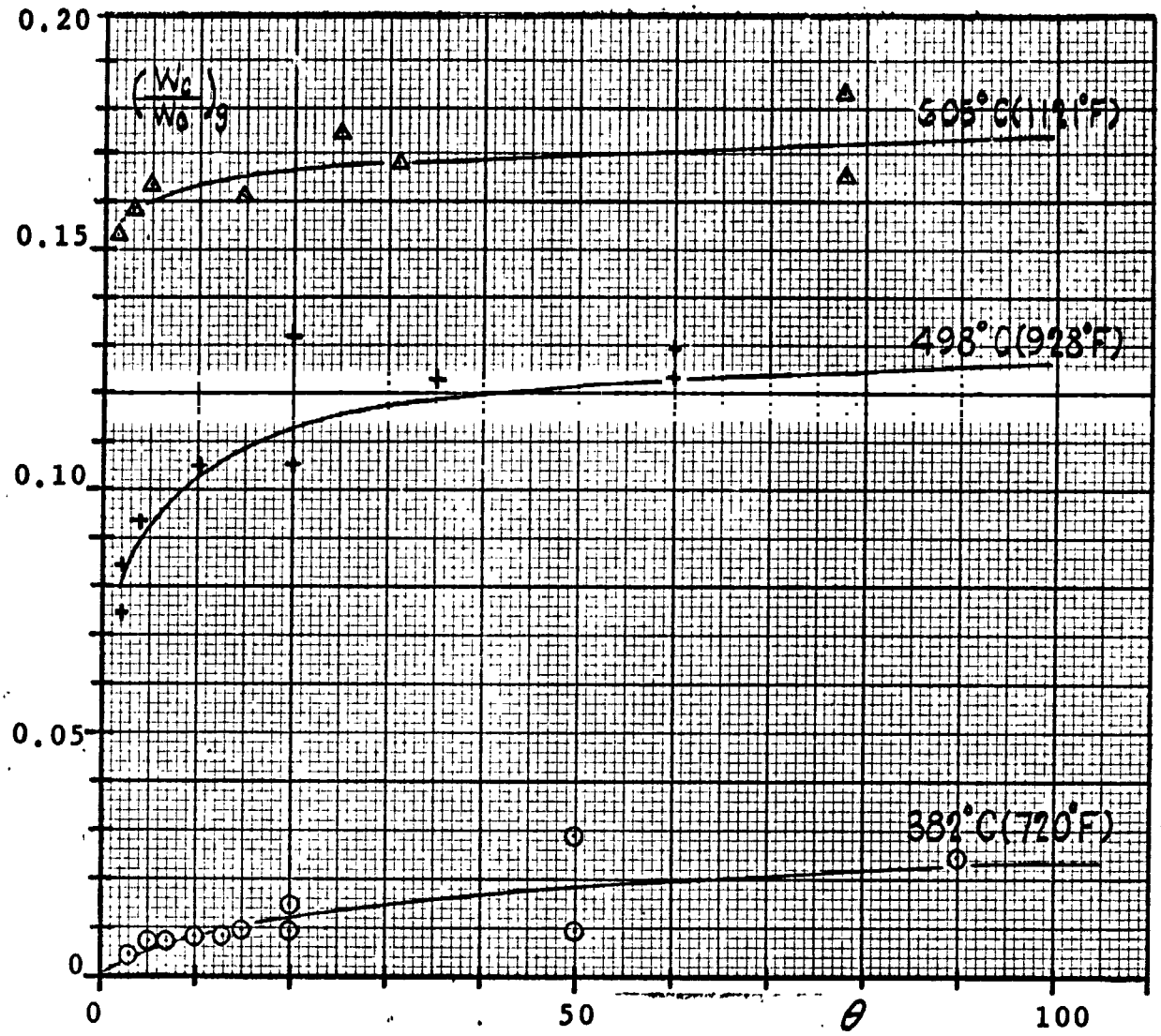

FIGURE 24 - CARBON DISAPPEARANCE

at 498°C,

$$\left(\frac{Wc}{Wo}\right)_g = 0.1086\left(\xi_2^\circ - \eta_2\right) + 0.07171\left(\xi_{125}^\circ - \eta_{125}\right)$$

$$(\lambda_2 = 1.344\,;\ \alpha_2 = 10.72\,;\ \lambda_5 = 0.0728\,;\ \alpha_3 = 1.200) \qquad \text{(VI-3)}$$

at 605°C,

$$\left(\frac{Wc}{Wo}\right)_g = 0.08392\left(\xi_2^\circ - \eta_2\right) + 0.07914\left(\xi_{125}^\circ - \eta_{125}\right)$$

$$(\lambda_2 = 30.10\,;\ \alpha_2 = 6.00\,;\ \lambda_5 = 0.5440\,;\ \alpha_3 = 0.250) \qquad \text{(VI-4)}$$

Note from the above equations and the values of the parameters (λ's and α's) that both the bridge and ring removal reactions increase rapidly with temperature (λ_2 = 0.0120 → 30.1; $\lambda 5$ = 0.0054 → 0.5440). On the other hand, the transport effect decreases with temperature (α_2 = 18.0 → 6.00; α 3 = 10.0 0.250); actually the diffusivities increase, but $\alpha = (\lambda/\mu)^{1/2}$ decreases.

Figure 25 illustrates how well the model satisfied the $(Wc/Wo)_g$ and $(^{1-W}/Wo)$ data at 605°C. It is interesting to note in equation (V-58) for $(^{1-W}/Wo)$ that the maximum value of the weight loss can be obtained by setting ξ_o, ξ_1, ξ_2, and ξ_{125} equal to unity, then,

$$\left(1 - W/W_o\right)_{max} = \left(\frac{18 n_{SRO}}{Wo}\right) + \left(\frac{17 n_o}{Wo}\right)\frac{\lambda_2}{\lambda_{25}} + \frac{21 n_o}{Wo}\left(\frac{\lambda_1}{\lambda_{15}}\right) + \left(\frac{16 n_o}{Wo}\right)\Phi 125$$

(VI-5)

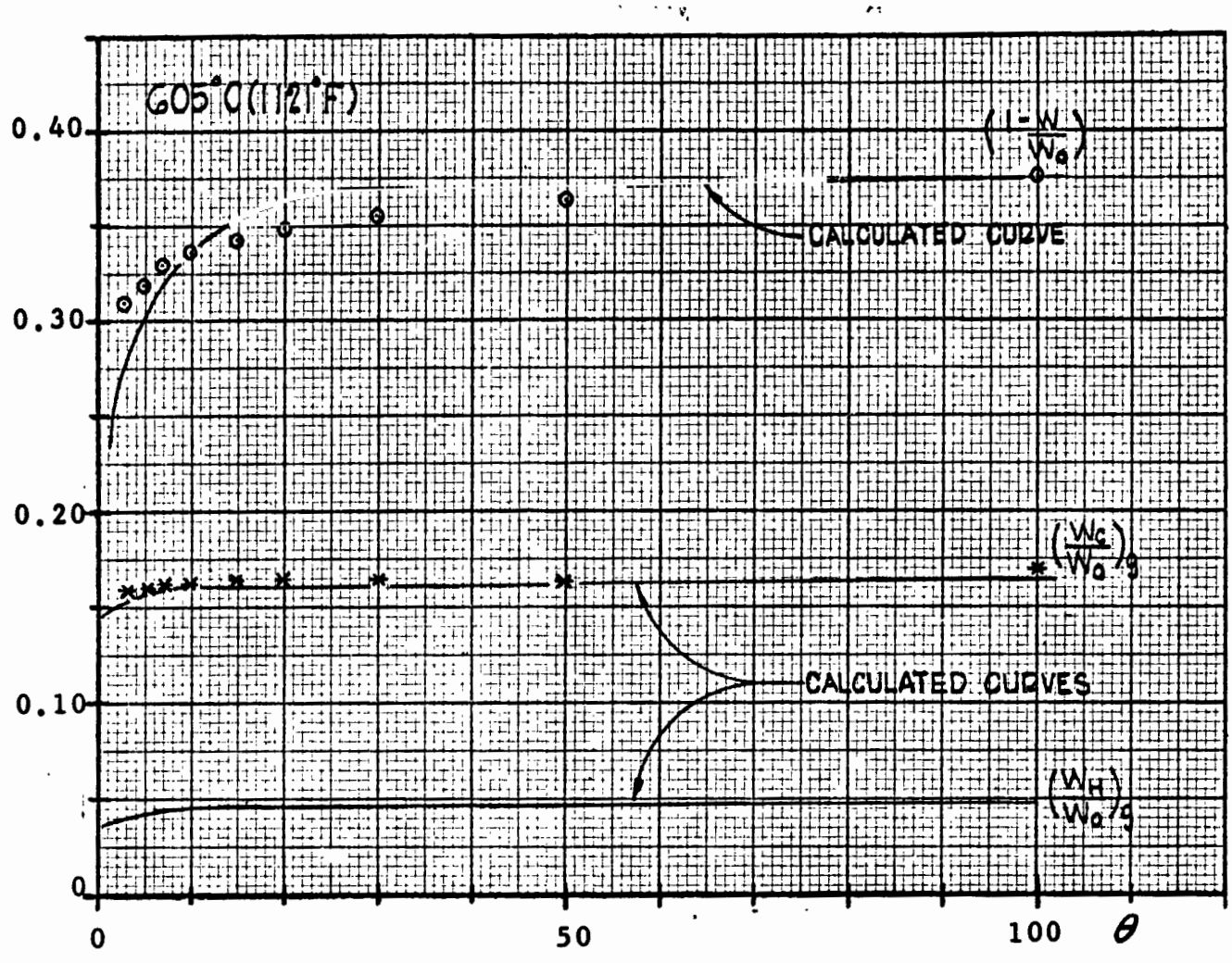

FIGURE 25 - CARBON DISAPPEARANCE, BY THE MODEL

Values are,

t °C	$(^{1-W}/Wo)$Max.
382	0.3916
498	0.3902
605	0.3720
800	0.3580
1000	0.3533

D. RATE AND TRANSPORT CONSTANTS:

In the mathematical model proposed (equations V-46, V-51, V-55, and V-58) there are four reaction rate constants k_o, k_1, k_2 and k_5, and three diffusivities, D_1, D_2, and D_5 involved. k_o is large, even at low temperatures, and since it is a surface reaction, $\eta o = 0$. For mathematical convenience, λ's, the reaction parameters, can be used instead of k's since they differ only by constants.

$$\lambda_i \equiv \left(\frac{k_i M_o}{\rho}\right) \qquad \text{(VI-5)}$$

and similarly μ's, the diffusion parameters can be used instead of D's,

$$\mu_i \equiv (D_i S^1 \rho^2) \qquad \text{(VI-6)}$$

As is well known, reaction rate constants can be represented by several temperature function forms, the simplest of which is the Arrhenius equation,

$$k_i = A e^{-Ek_i/RT}$$

$$\left(\frac{\kappa_i M_o}{\rho}\right) = \left(\frac{A M_o}{\rho}\right) e^{-Ek_i/RT}$$

$$\lambda_i = A\lambda_i \, e^{-E\lambda_i/RT} \qquad \text{(VI-7)}$$

Also, Shewmon (47) indicates that solid phase diffusivities can be represented by the same type of temperature function,

$$D_i = B e^{-E_{\kappa i}/RT}$$

$$(D_i S^2 \rho^2) = (B S^2 \rho^2)\, e^{-E_{\kappa i}/RT}$$

$$\mu_i = A_{\mu i}\, e^{-E_{\kappa i}/RT} \qquad \text{(VI-8)}$$

We note by equation (V-17) that, $\alpha_i = (\lambda_i/\mu_i)^{1/2}$; by substituting (VI-7) and (VI-8),

$$\alpha_i = \left[\frac{A_{\lambda i}\, e^{-E_{\lambda i}/RT}}{A_{\mu i}\, e^{-E_{\mu i}/RT}}\right]^{1/2} = A_{\alpha i}\, e^{-E_{\alpha i}/RT} \qquad \text{(VI-9)}$$

For purposes of calculations the most convenient parameters to work with will be the λ's and α's.

Using the model all isotherms were processed by computer program HRI65R002 (see Appendix C and Appendix D) to determine the "best fit" of the data and the values of the reaction rate parameters λ_1, λ_2 and λ_5, and the transport parameters, α_1, α_2 and α_3. The experimental values of the constants are presented in Tables VII and VIII; all "fits" were within an average deviation of 5%, except at the lower temperatures where diffusion is rate controlling.

Plots of the λ's, α's and D's are presented in Figures 26, 27 and 28. Least-squares fits of the experimental λ's and α's were made and the Arrhenius parameters A's and E's are presented in Table IX. It is interesting to note the magnitudes of the diffusivities; e.g. D_2, the diffusivity of the CH_2 - species is shown in Figure 27 and is the range of 10^{-13} to 10^{-8} cm^2/sec which is directly comparable to values reported in the literature and summarized in Table B-41 in Appendix B. Also, we note that the activation energy for the diffusion process is reasonable.

$$E_{\mu 2} = E_{\lambda 2} - 2E_{\alpha 2}$$

$$= 39.65 - 2(-5.69) = 51.03 \text{ K. cals./g. mole}$$

TABLE VII - EXPERIMENTAL VALUES OF λ's & k's AS A FUNCTION OF TEMPERATURE

t°C	382	436	498	533	571	605	666
t°F	720	819	928	991	1060	1121	1199
T°K	655	709	771	806	844	878	939
$\frac{1}{T} \times 10^3$	1.528	1.411	1.298	1.241	1.184	1.139	1.064
$RT(\frac{K.cals}{g.\ mol})$	1.302	1.410	1.530	1.601	1.676	1.744	1.864
$\lambda_1(min^{-1})$	0.060	0.095	0.180	0.260	0.410	0.666	1.40
$k_1(moles/sec\text{-}cm^3)$	1.09×10^{-5}	1.730×10^{-5}	3.28×10^{-5}	4.73×10^{-5}	7.47×10^{-5}	1.212×10^{-5}	2.55×10^{-5}
λ_2	0.0120	0.1700	1.334	5.40	12.2	30.1	134.0
k_2	2.18×10^{-6}	3.10×10^{-5}	2.43×10^{-4}	9.84×10^{-4}	2.22×10^{-3}	5.48×10^{-3}	2.44×10^{-2}
λ_5	0.0054	0.0150	0.0728	0.160	0.300	0.544	1.60
k_5	9.84×10^{-7}	2.73×10^{-6}	1.326×10^{-5}	2.91×10^{-5}	5.46×10^{-5}	9.91×10^{-5}	2.91×10^{-4}

$$k_i = \frac{\lambda_i \eta_{Ao}}{60V} = \frac{\lambda_i \rho}{60\ M_{resin}} = (1.820 \times 10^{-4})\ \lambda_i^{*};\quad (moles/sec - cm^3)$$

* Value of ρ from Table B-15, C-1 Run 2

TABLE VIII - EXPERIMENTAL VALUES OF α's & μ's AS A FUNCTION OF TEMPERATURE

t°C	382	436	498	533	571	605	666
t°F	720	819	928	991	1060	1121	1199
T°K	655	709	771	806	844	878	939
$\frac{1}{T} \times 10^3$	1.528	1.411	1.298	1.241	1.184	1.139	1.064
RT	1.302	1.410	1.530	1.601	1.676	1.744	1.864
α_1	20.6	13.6	7.56	6.56	4.50	3.40	2.30
$\mu_1 (min^{-1})$	1.413×10^{-4}	5.14×10^{-4}	3.16×10^{-3}	6.05×10^{-3}	2.02×10^{-2}	5.76×10^{-2}	0.265
$D_1 (\frac{cm^2}{sec})$	2.67×10^{-13}	0.974×10^{-12}	0.597×10^{-11}	1.144×10^{-11}	3.82×10^{-10}	1.09×10^{-10}	0.501×10^{-9}
α_2	18.0	14.0	10.72	8.00	7.00	6.00	5.08
$\mu_2 (min^{-1})$	0.370×10^{-4}	0.867×10^{-3}	1.155×10^{-3}	0.844×10^{-1}	0.249	0.836	5.19
$D_2 (\frac{cm^2}{sec})$	0.707×10^{-13}	1.64×10^{-12}	2.18×10^{-11}	1.594×10^{-10}	4.71×10^{-10}	1.582×10^{-9}	0.981×10^{-8}
α_3	10.0	3.60	1.20	0.720	0.400	0.250	0.130

$$D_i = \left(\frac{\mu_i}{60\ S^2\rho^2}\right) = (1.87\times10^{-9})\mu_i\ ^*;\quad \left(\frac{cm^2}{sec}\right)$$

* Values of S and ρ from Table B-15, C-1 run 2

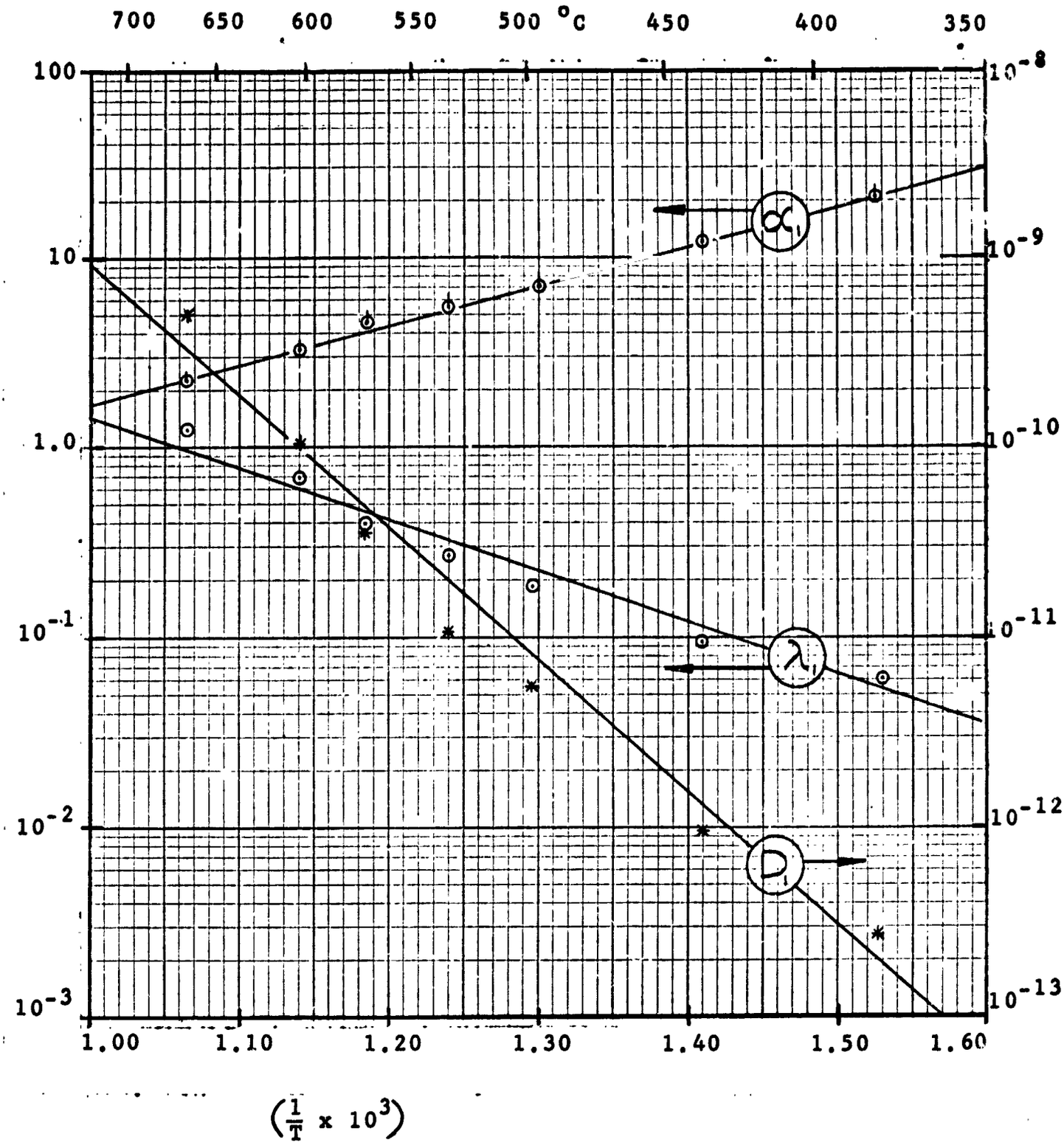

FIGURE 26 - RATE AND TRANSPORT PARAMETERS
OXYGEN DISAPPEARANCE

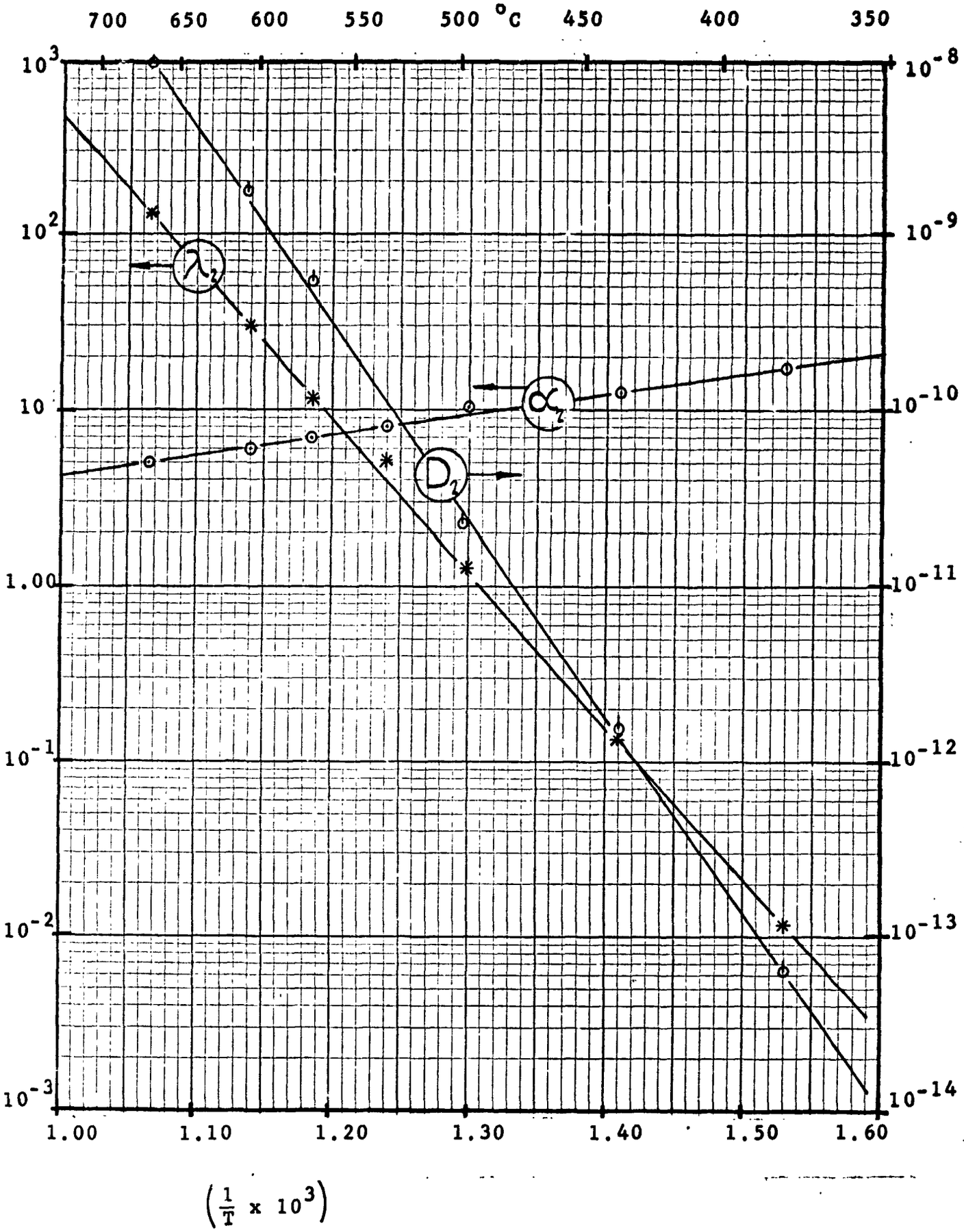

FIGURE 27 - RATE AND TRANSPORT PARAMETERS
CH_2 - DISAPPEARANCE

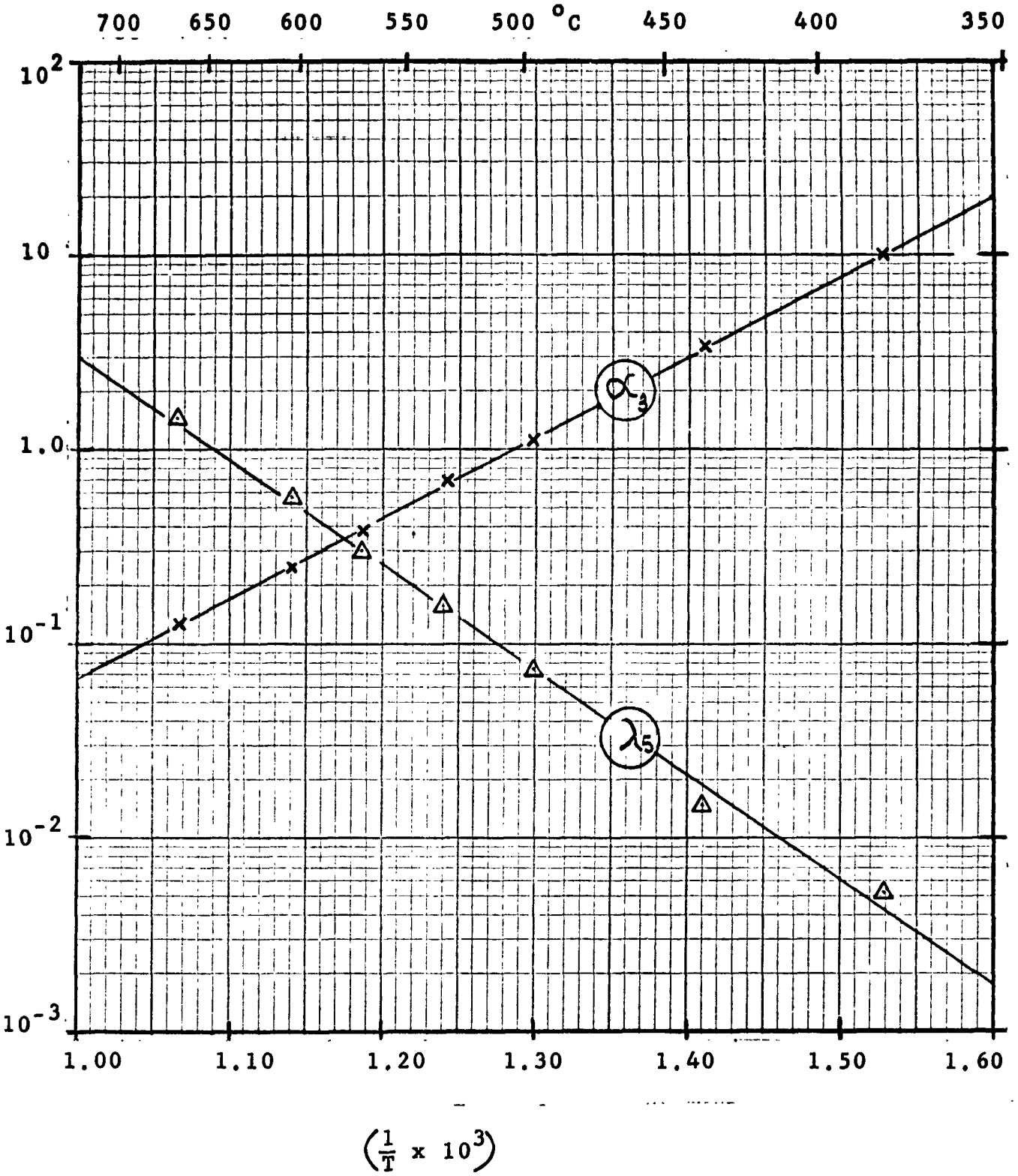

FIGURE 28 - RATE AND TRANSPORT PARAMETERS
RING DISAPPEARANCE

TABLE IX - TEMPERATURE FUNCTION PARAMETERS FOR λ's AND α's

$$\lambda_i = A_{\lambda i} e^{-E_{\lambda i}/RT} \qquad \text{(VI-7)}$$

$$\alpha_i = A_{\alpha i} e^{-E_{\alpha i}/RT} \qquad \text{(VI-9)}$$

		A_λ (min^{-1})	E_λ (K.Cals./g. mole)
(estimate)	λ_0	0.1700×10^{7}	12.65
	λ_1	0.13568×10^{4}	13.379
	λ_2	0.24058×10^{12}	39.648
	λ_5	0.84331×10^{6}	24.824

	A (dimensionless)	E_α (K.Cals./g. mole)
α_1	0.015442	-9.481
α_2	0.23829	-5.690
α_3	0.51945×10^{-5}	-18.891

It is interesting to note that a "chemical decomposition threshold temperature or incipient reaction temperature, T_r" can be calculated from the data obtained. Using equation (V-58), at low temperatures and $\theta = 0$,

$$\left(\frac{d\,W/W_0}{d\theta}\right) = \frac{-17 n_0 \lambda_1}{W_0} = \frac{-17 n_0 A_{\lambda 1}}{W_0} e^{-E_{\lambda i}/RT_r} \qquad \text{(VI-10)}$$

and arbitrarily defining the threshold of chemical reaction as the temperature at which 0.01% weight loss occurs per minute, i.e. $\left(\frac{d\ W/W_o}{d\theta}\right) = 0.0001$, then,

$$T_r = \frac{-E_{\lambda i}}{R \ln\left(\frac{0.0001\ A_2}{17 n_o A_{\lambda i}}\right)} \qquad \text{(VI-11)}$$

Substituting in values gives,

$$T_r = 506^{\circ}K = 233^{\circ}C = 387^{\circ}F$$

VII. PF PYROLYSIS GAS SPECIES

Figures 29, 30 and 31 present the product gas species distributions at 382, 498 and 605°C and indicate that at low temperatures the products are H_2O, CO, CO_2, with traces of H_2. At high temperatures, additional hydrocarbon species appear as a result of breakout of aromatic rings and their subsequent decomposition to lighter species. It must be remembered that we also see in the gaseous products the results of secondary reactions (and further) in the gas phase. The overall sequence might be visualized as indicated in Figure 32.

More specifically, the following considerations are pertinent:

1. The absence of light aromatics, condensed ring products, and H_2 in low temperature runs (382°C) indicates that water is the only product formed initially in substantial quantities and that a few bridges are also severed and further react producing CO and CO_2. This is very likely because elimination of water between the neighboring OH and CH_2 groups can proceed with ease.

2. The appearance of light aromatics and condensed ring structures in pyrolysis products at higher temperatures indicates fragmentation of the PF resin.

3. The mechanism by which CO, CO_2 and H_2 are formed can be illustrated by the following sequence of reactions:

$$H_2O \longrightarrow OH + H$$

$$2\ OH \longrightarrow H_2O + O$$

$$OH + O \longrightarrow HO_2$$

$$CH_2 + HO_2 \longrightarrow CH_3OO$$

$$CH_3OO + CH_2 \longrightarrow CH_3OOH + CH$$

$$CH_3OOH \longrightarrow CO + 2H_2 + O$$

$$CH + O \longrightarrow CHO$$

$$CHO + H_2O \longrightarrow CH_3OO$$

$$CO + H_2O \longrightarrow CO_2 + H_2$$

4. Amongst the light hydrocarbons CH_4, C_2H_6 and C_3H_8, methane is likely to be the result of two mechanisms while

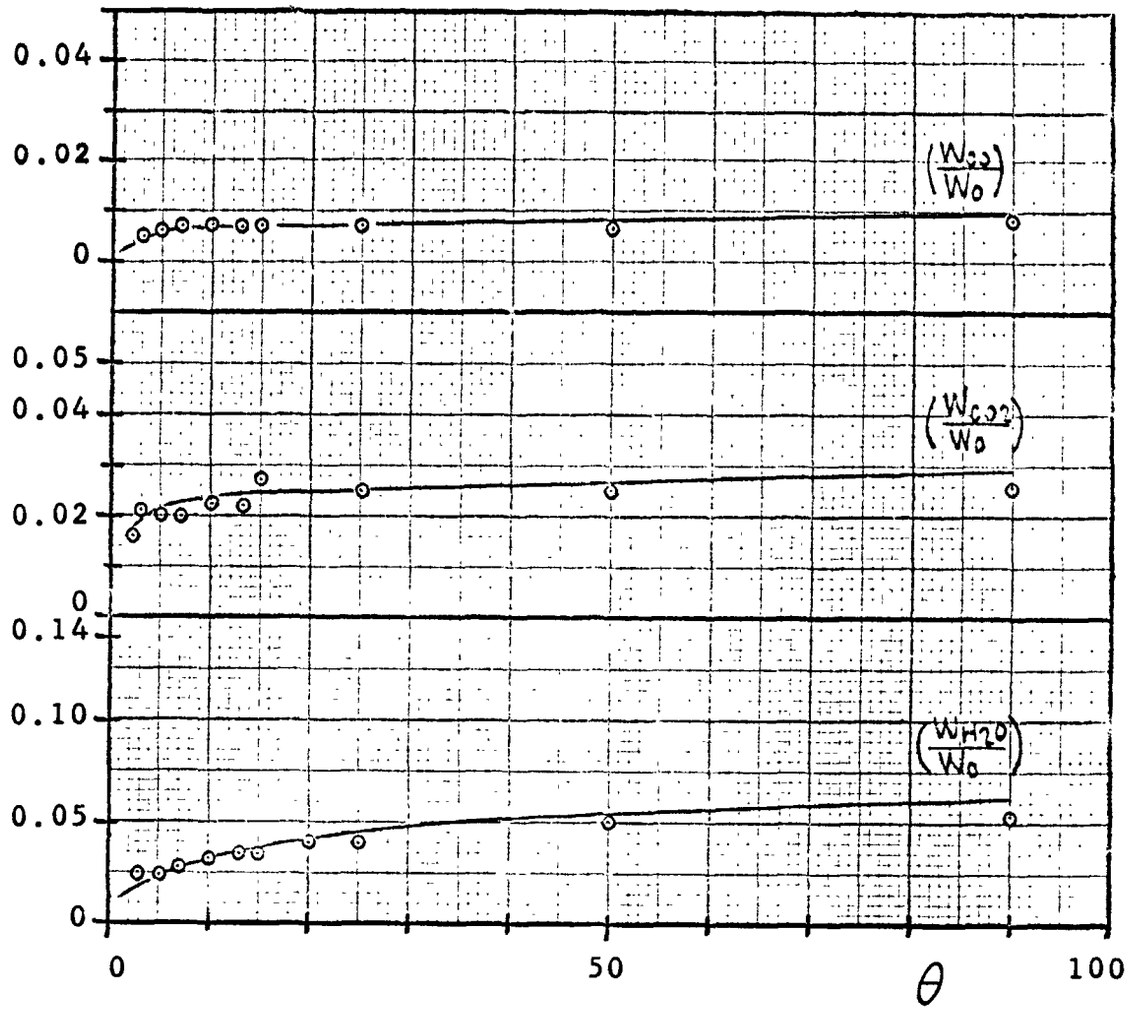

FIGURE 29 - GAS SPECIES DISTRIBUTION, 382°C

(No trace of H_2, condensed ring structures, or light aromatics, and only traces of light hydrocarbons)

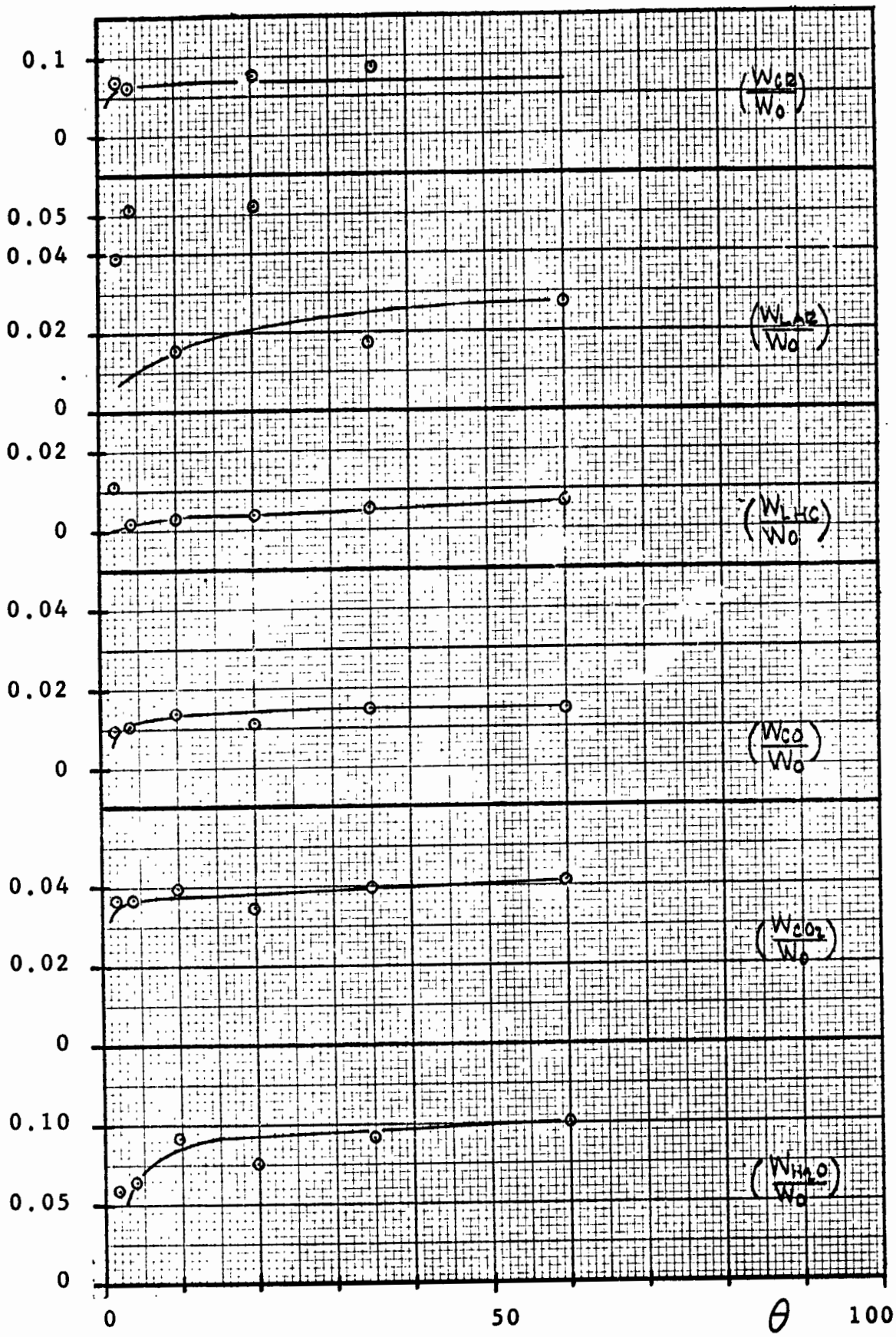

FIGURE 30 - GAS SPECIES DISTRIBUTION, 498°C

(Only a trace of H_2)

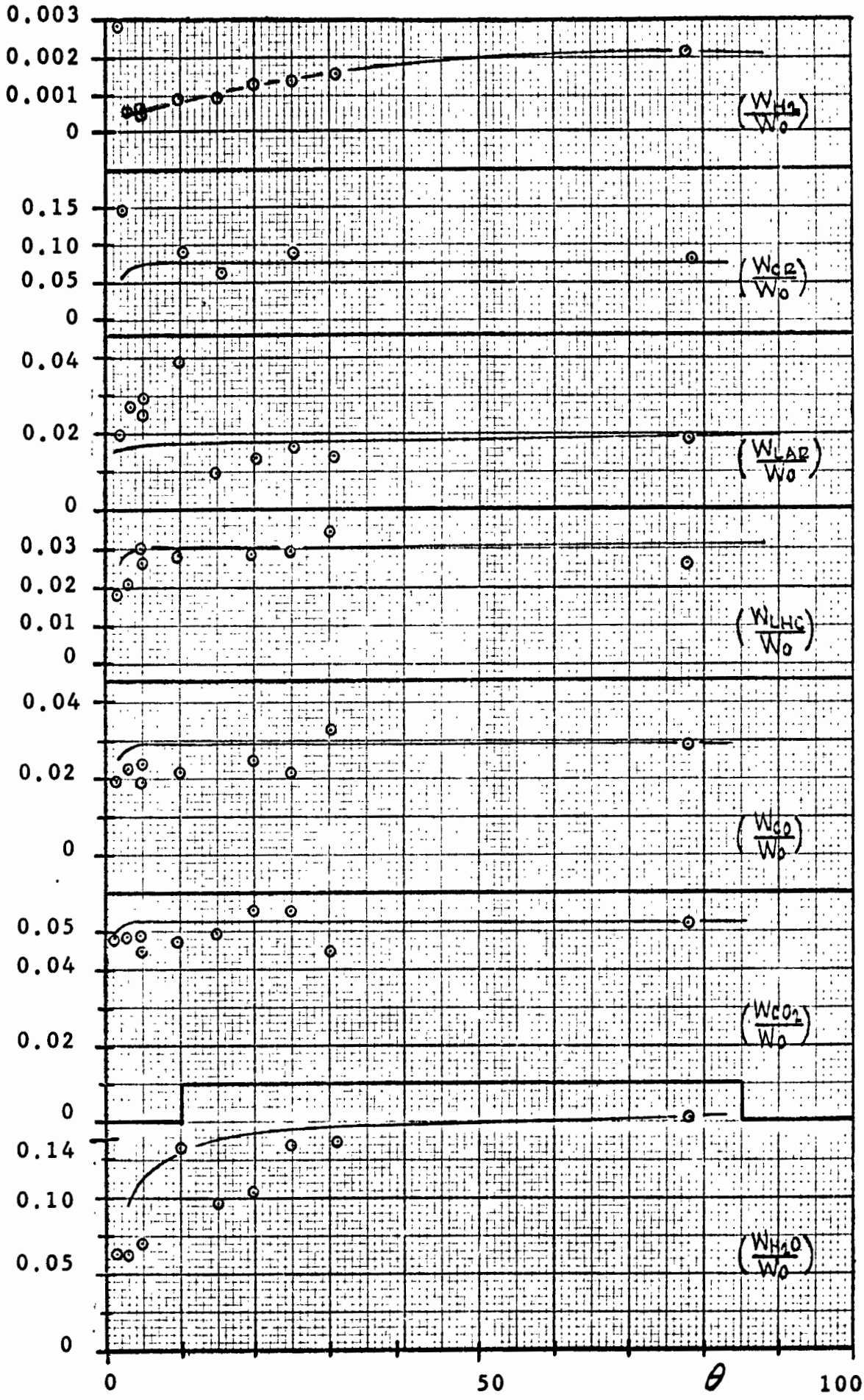

FIGURE 31 - GAS SPECIES DISTRIBUTION, 605°C

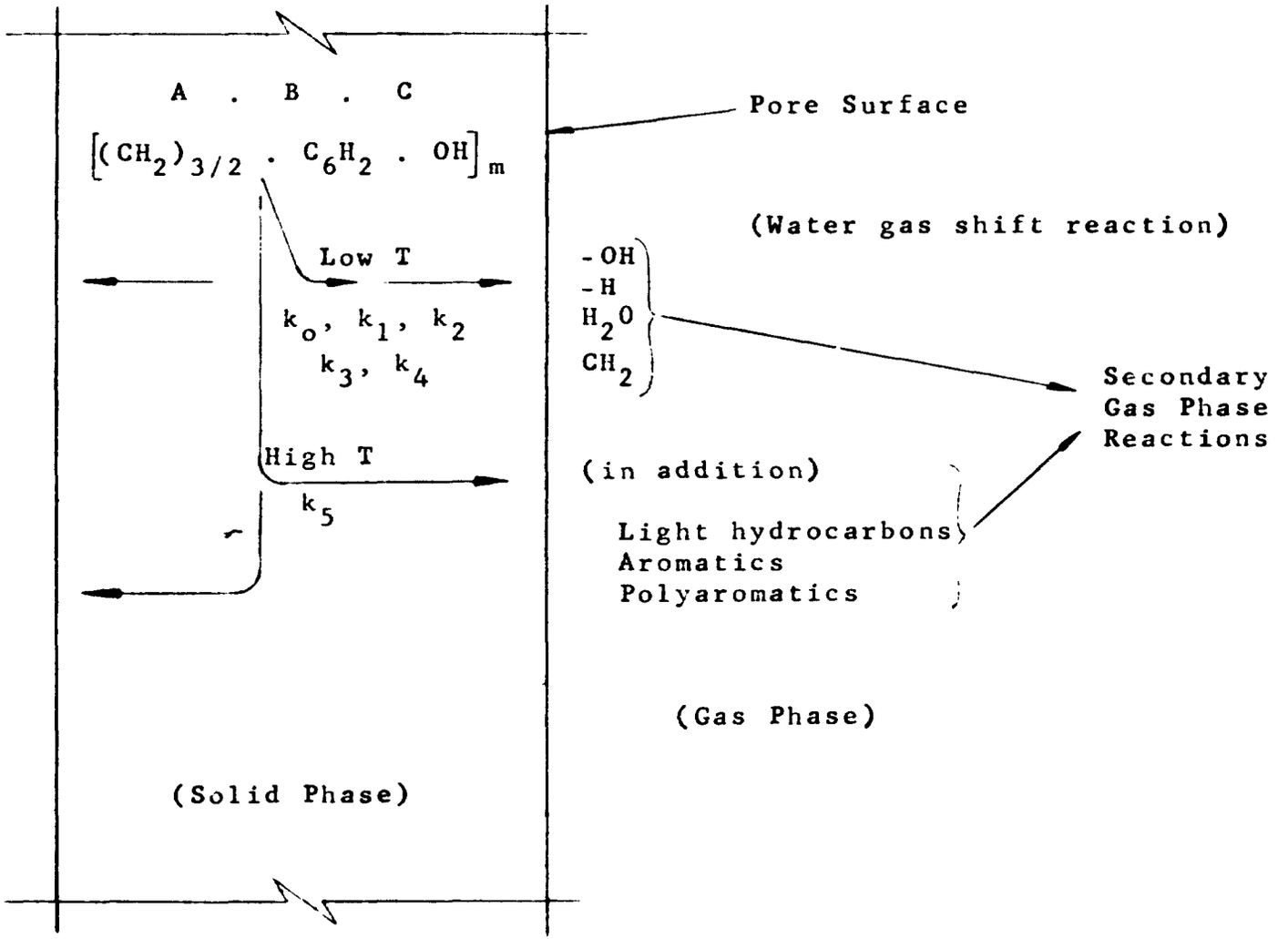

FIGURE 32 - SOLID & GAS PHASE REACTION MECHANISM

propane and ethane are primarily due to thermal cracking of ring structures (fragments) as indicated in the following sequence of reactions.

$$CH_2 + H_2 \longrightarrow CH_4$$

Methylene bridge

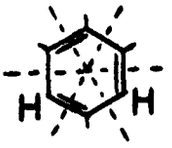

$$+ \; 11H_2 \longrightarrow 6\,CH_4$$

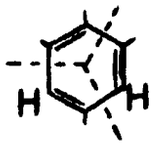

$$+ \; 8H_2 \longrightarrow 3C_2H_6$$

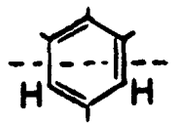

$$+ \; 7H_2 \longrightarrow 2C_3H_8$$

5. Toluene and Xylene found in the reaction products are probably due to ring fragments detaching from the resin with one or two CH_2 groups intact and reacting further with hydrogen.

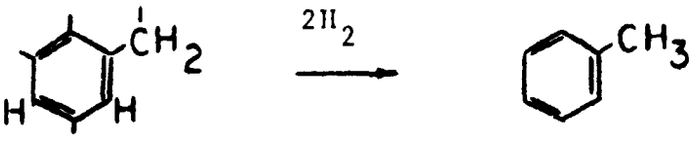

Toluene

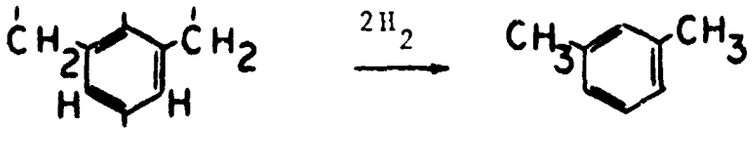

Xylene

From the product species produced it is evident that a number of simultaneous reactions are involved in the pyrolysis process. As a preliminary procedure, attention was focused on the water gas shift reaction and equilibrium constants were calculated from the kinetic data and compared with the values

calculated from free energy of formation data. The results are presented as follows:

$$CO + H_2O \rightleftharpoons CO_2 + H_2$$

Temp. 498°C				Temp. 605°C			
Run No.	$K^{(a)}$	$K'^{(b)}$	$K^{(c)}$	Run No.	$K^{(a)}$	$K'^{(b)}$	$K^{(c)}$
60	0	1.45	5.728	55	0.660	1.80	3.304
61	0	0.647		53	0.095	1.31	
59	0	0.478		49	0.101	1.25	
62	0	0.688		54	0.121	1.67	
63	0	0.645		58	0.086	0.735	
64	0	0.638		51	0.102	0.815	
				5[illegible]	0.154	0.950	
				57	0.144	0.865	
				52	0.086	0.425	
				56	0.151	0.528	

(a) Equilibrium constant, using H_2 analysis

(b) Equilibrium constant, using total hydrogen

(c) Equilibrium constant from thermodynamic data

The constants K and K' were both lower than the thermodynamic value, and were off by an order of magnitude at low temperatures and at higher temperature by a factor of 5. Values of K and K' are consistent (though small); the deviation may be due to the H_2 analysis which is not very accurate by the chromatograph using helium as sweep gas.

Table X compares gaseous species reported in the literature with a typical gas analysis from this investigation, selected to correspond as closely as possible to the pyrolysis conditions of the literature data. The values from Lee include a considerable amount of aldehydes, primarily formaldehyde, as would be expected from an acid catalyzed novolak (see Section III). An additional problem is that there is no indication of the total amount of material lost, and each product is reported as a fraction of the total products identified; because of this, comparison can be made only on a basis of relative amounts.

TABLE X

COMPARISON OF GASEOUS SPECIES

Component	Fractions of Weight Lost		
	Lee (26)* 450°C	HRI No. 63 (35 min. at 498°C)	Madorsky (55)** (30 min. at 500°C)
H_2	Trace	Trace	None Reported
H_2O	0.058	0.367	Included in Unidentified
CO_2	0.413	0.161	0.055
CO	0.346	0.059	0.035
Light Hydrocarbons	0.032	0.024	0.043
Light Aromatics	0.041	0 069	0.072
Unidentified	---	0.338	0.499
Acetone & Propanol	None Reported	None Found	0.287
Aldehydes	0.111	None Found	None Reported
Weight Loss/Sample Weight	Unknown	0.25	0.28

* Novolak. Fractions of products identified.

** Approximately 1:1 phenol-formaldehyde, CTL 91-LD

The values from Madorsky are expected to be more comparable to the present work because temperature, time, and weight loss correspond closely, even though the material is not exactly the same. The acetone and propanol is thought to come from a solvent used when the material was polymerized. Most of the other entries compare reasonably well with this work.

VIII. CALCULATIONAL MODEL

As indicated previously, the purpose of the model is to permit better design calculations by providing a more realistic description of the decomposition phenomena occurring.

The mechanism of ablation can be visualized as follows, (refer to Figure 33). Once heat has started to flow inward from the external surface raising the temperature of the ablator from T_o to T_r, the threshold or incipient reaction temperature, and after certain time has elapsed, the ablator layer may be visualized as consisting of four zones: a) a carbonized char zone, b) a char zone, c) a reaction zone, and d) a virgin material zone. The extent, temperature profile and physical characteristics of zones a, b, and c obviously change with time.

The purpose of the study described in this report is to provide a better understanding and develop a mathematical model for the pyrolysis occurring in zone c, the reaction zone. As mentioned previously, primary attention in this work was focused on the solid decomposition reactions and not on the subsequent secondary reactions of the product species.

In order to use the mathematical model for the desired calculations, a set of working equations is given in the following section.

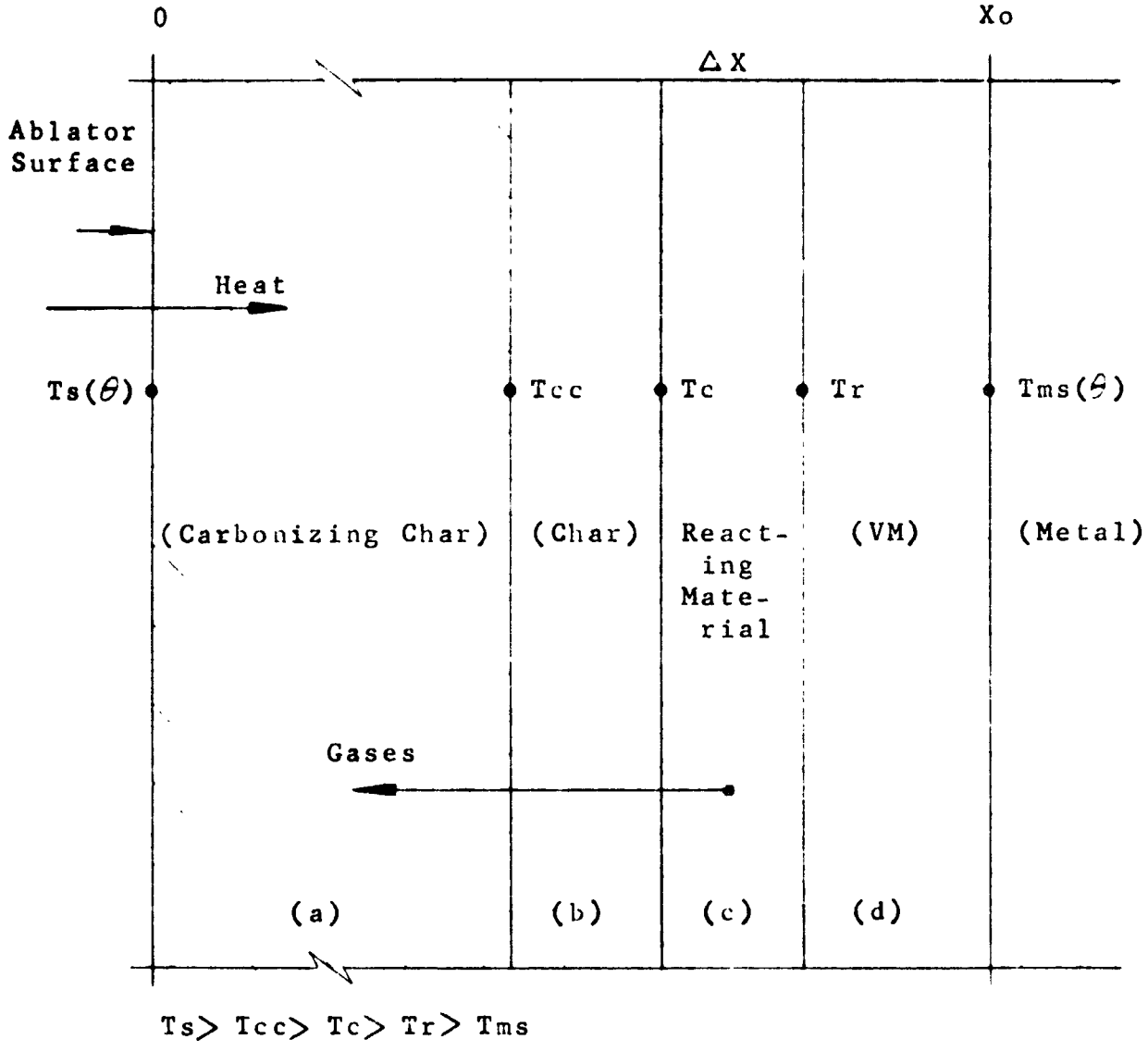

FIGURE 33 - VISUALIZATION OF THE ABLATION PROCESS

A. WORKING EQUATIONS:

$$\left(\frac{W_{ox}}{W_o}\right)_g = \left(\frac{W_o}{W_{PF}}\right)\left[\left(\frac{16n_{SRO}}{W_o}\right)\xi_0 + \left(\frac{16n_o}{W_o}\right)\left(\frac{\lambda_2}{\lambda_{25}}\right)\xi_1 + \left(\frac{16n_o}{W_o}\right)\beta_1\xi_{125}\right]$$

$$\left(\frac{W_c}{W_o}\right)_g = \left(\frac{W_o}{W_{PF}}\right)\left[+\frac{18n_o}{W_o}\left(\frac{\lambda_1}{\lambda_{15}}\right)\xi_2 + \left(\frac{18n_o}{W_o}\right)\beta_2\,\xi_{125}\right]$$

$$\left(\frac{W_H}{W_o}\right)_g = \left(\frac{W_o}{W_{PF}}\right)\left[\left(\frac{2n_{SRO}}{W_o}\right)\xi_0 + \left(\frac{n_o}{W_o}\right)\left(\frac{\lambda_2}{\lambda_{25}}\right)\xi_1 + \frac{3n_o}{W_o}\left(\frac{\lambda_1}{\lambda_{15}}\right)\xi_2 + \left(\frac{n_o}{W_o}\right)\beta_3\,\xi_{125}\right]$$

$$\left(1-\frac{W}{W_o}\right) = \left(\frac{W_o}{W_{PF}}\right)\left[\left(\frac{18n_{SRO}}{W_o}\right)\xi_0 + \left(\frac{17n_o}{W_o}\right)\left(\frac{\lambda_2}{\lambda_{25}}\right)\xi_1 + \left(\frac{21n_o}{W_o}\right)\left(\frac{\lambda_1}{\lambda_{15}}\right)\xi_2 + \left(\frac{16n_o}{W_o}\,\Phi_{125}\xi_{125}\right)\right] \qquad \text{(VIII-1)}$$

$$\beta_1 \equiv \left[\frac{1}{\left(1+\frac{\lambda_2}{\lambda_{15}}\right)} - \frac{1}{\left(1+\frac{\lambda_5}{\lambda_2}\right)\left(1+\frac{\lambda_2}{\lambda_1}+\frac{\lambda_5}{\lambda_1}\right)}\right]$$

$$\beta_2 \equiv \left[\frac{\lambda_2+5\lambda_5-\frac{\lambda_1\lambda_2}{\lambda_{15}}}{\lambda_{125}}\right]$$

$$\beta_3 \equiv \left[\frac{\lambda_1+3\lambda_2+4\lambda_5-\frac{3\lambda_1\lambda_2}{\lambda_{15}}-\frac{\lambda_1\lambda_2}{\lambda_{25}}}{\lambda_{125}}\right]$$

$$\Phi_{125} \equiv \left(\beta_1+\frac{9}{8}\beta_2+\frac{\beta_3}{16}\right) \qquad \text{(VIII-2)}$$

where, $\lambda_{15} = \lambda_1 + \lambda_5$; $\lambda_{25} = \lambda_2 + \lambda_5$; $\lambda_{125} = \lambda_1 + \lambda_2 + \lambda_5$

$$\xi_i = \xi_i^\circ(\tau_{ki}) - \eta_i(\alpha_i, \tau_{mi})$$

(VIII-3)

however, $[\eta_0 = 0]$

$$\tau_{ki} = \lambda_i \theta \; ; \quad \tau_{mi} = \mu_i \theta \; ; \quad \alpha_i = \left(\frac{\lambda_i}{\mu_i}\right)^{1/2} \qquad \text{(VIII-4)}$$

$$\xi_i^\circ(\tau_{ki}) = (1 - e^{-\tau_{ki}}) \qquad \text{(VIII-5)}$$

$$\eta_i(\alpha_i, \tau_{mi}) = \left[\frac{8}{\pi^2} \sum_{n=0}^{\infty} \frac{\left(1 - e^{-\frac{(2n+1)^2 \pi^2 \tau_{mi}}{4}}\right)}{(2n+1)^2 \left(\frac{(2n+1)^2 \pi^2}{4\alpha_i^2} - 1\right)} \right.$$

$$\left. + \left(1 - \frac{\tan \alpha_i}{\alpha_i}\right)\left(1 - e^{-\alpha_i^2 \tau_{mi}}\right) \right] \qquad \text{(VIII-6)}$$

$$\lambda_i = A_{\lambda i}\, e^{-E_{\lambda i}/RT} \qquad \text{(VIII-7)}$$

$$\alpha_i = A_{\alpha i}\, e^{-E_{\alpha i}/RT} \qquad \text{(VIII-8)}$$

B. CALCULATED TGA CURVE:

It is now possible by means of the working equations and for an assumed heating rate $(dT/d\theta) = R$ to calculate a weight loss curve for a changing temperature situation (simulated TGA curve).

By equation (VIII-1)

$$\frac{W}{W_o} = \Phi(\theta, T)$$

then

$$d\left(\frac{W}{W_o}\right) = \left[\frac{\partial(W/W_o)}{\partial\theta}\right]_T d\theta + \left[\frac{\partial(W/W_o)}{\partial T}\right]_\theta dT$$

and

$$\frac{d(W/W_o)}{d\theta} = \left[\frac{\partial(W/W_o)}{\partial\theta}\right]_T + R\left[\frac{\partial(W/W_o)}{\partial T}\right]_\theta$$

(VIII-9)

The derivatives can be obtained from the working equations and lead to the equation for the partial derivative with respect to time,

$$\left[\frac{\partial(W/W_o)}{\partial\theta}\right] = \frac{-W_o}{V_1\rho_F}\left[C_0\left(\frac{\partial\xi_0}{\partial\theta}\right)_T + C_1\left(\frac{\partial\xi_1}{\partial\theta}\right)_T + C_2\left(\frac{\partial\xi_2}{\partial\theta}\right)_T + C_3\left(\frac{\partial\xi_{125}}{\partial\theta}\right)_T\right]$$

(VIII-10)

where,

$$C_0 = \frac{2n_{SRO}}{W_o} \; ; \; C_1 = \frac{n_o}{W_o}\frac{\lambda_2}{\lambda_{25}} \; ; \; C_2 = \frac{2In_o}{W_o}\frac{\lambda_1}{\lambda_{15}} \; ; \; C_3 = \frac{n_o}{W_o}\Phi_{125}$$

(VIII-10a)

and,

$$\left(\frac{\partial \xi_i}{\partial \theta}\right)_T = \lambda_i e^{-\tau_{ki}} \frac{\tan\alpha}{\alpha} - 2\lambda_i \sum_{n=0}^{\infty} \frac{e^{-(2n+1)^2 \frac{\pi^2}{4} \tau_{mi}}}{(2n+1)^2 \frac{\pi^2}{4}\left[(2n+1)^2 \frac{\pi^2}{4} - \alpha_i^2\right]}$$

(VIII-106)

and the partial derivative with respect to temperature,

$$\left[\frac{\partial (W/W_o)}{\partial \theta}\right]_T = \frac{-W_o}{W_{pf}}\left[C_o\left(\frac{\partial \xi_{i,o}}{\partial T}\right) + C_1\left(\frac{\partial \xi_1}{\partial T}\right)_\theta + \xi_1 \frac{d(C_1)}{dT} + C_2\left(\frac{\partial \xi_2}{\partial T}\right)_\theta + \right.$$

$$\left. \xi_2 \frac{d(C_2)}{dT} + C_3\left(\frac{\partial \xi_{125}}{\partial T}\right)_\theta + \xi_{1-5} \frac{d(C_3)}{dT}\right]$$

(VIII-11)

where,

$$\left(\frac{\partial \xi_i}{\partial T}\right)_\theta = \theta e^{-\tau_{ki}}\left(\frac{d\lambda_i}{dT}\right)\frac{\tan\alpha_i}{\alpha_i} - 2\alpha_i^2\left(\frac{\partial \Sigma_i}{\partial T}\right)_\theta - \frac{4\alpha_i^2 E_{\alpha i}}{RT^2} \sum_i$$

$$+\left(1 - e^{-\tau_{ki}}\right)\frac{E_{\alpha i}}{RT^2}\left[\frac{1}{(\cos\alpha_i)^2} - \frac{\tan\alpha_i}{\alpha_i}\right]$$

(VIII-11a)

and for i = 0, 1, 2, 5:

$$\frac{d\lambda_i}{dT} = \frac{\lambda_i E_{\lambda_i}}{RT}$$

(VIII-11b)

but for i = 125:

$$\frac{d\lambda_{125}}{dT} = \frac{d\lambda_1}{dT} + \frac{d\lambda_2}{dT} + \frac{d\lambda_5}{dT}$$

(VIII-11c)

The definition of $\sum_i$ is given by,

$$\sum_i = \sum_{n=0}^{\infty} \frac{\left[1 - e^{-(2n+1)^2 \frac{\pi^2}{4} \tau_{m_i}}\right]}{(2n+1)^2 \frac{\pi^2}{4} \left[(2n+1)^2 \frac{\pi^2}{4} - \alpha_i^2\right]} \qquad \text{(VIII-11d)}$$

and,

$$\left(\frac{\partial \Sigma_i}{\partial T}\right)_\theta = \theta \frac{d\mu_i}{dT} \sum_{n=0}^{\infty} \frac{e^{-(2n+1)^2 \frac{\pi^2}{4} \tau_{m_i}}}{\left[(2n+1)^2 \frac{\pi^2}{4} - \alpha_i^2\right]} + \frac{2\alpha_i^2 E_{\alpha_i}}{RT^2} \sum_{n=0}^{\infty} \frac{\left[1 - e^{-(2n+1)^2 \frac{\pi^2}{4} \tau_{m_i}}\right]}{(2n+1)^2 \frac{\pi^2}{4} \left[(2n+1)^2 \frac{\pi^2}{4} - \alpha_i^2\right]^2} \qquad \text{(VIII-11e)}$$

where for i = 0, 1, 2, 5:

$$\frac{d\mu_i}{dT} = \frac{\lambda_i}{\alpha_i^2} \frac{E_{\lambda_i} - 2E_{\alpha_i}}{RT^2} \qquad \text{(VIII-11f)}$$

but for i = 125:

$$\frac{d\mu_{125}}{dT} = \frac{1}{\alpha_3^2} \left[\frac{\lambda_1 E_{\lambda_1} + \lambda_2 E_{\lambda_2} + \lambda_5 E_{\lambda_5} - 2\lambda_{125} E_{\alpha_3}}{RT^2}\right] \qquad \text{(VIII-11g)}$$

Also needed for (VIII-11),

$$\frac{dC_1}{dT} = \frac{17 n_0}{w_0} \frac{\lambda_2 \lambda_5}{\lambda_{25}^2} \left[\frac{E_{\lambda_2} - E_{\lambda_5}}{RT^2}\right]$$

$$\frac{dC_2}{dT} = \frac{21 n_o}{W_o} \frac{\lambda_1 \lambda_5}{\lambda_{15}^2} \left[\frac{E_{\lambda_1} - E_{\lambda_5}}{RT^2} \right]$$

$$\frac{dC_3}{dT} = \frac{n_o}{W_o} \left[\frac{d\beta_1}{dT} + \frac{9}{8} \frac{d\beta_2}{dT} + \frac{1}{16} \frac{d\beta_3}{dT} \right]$$

(VIII-11f)

where,

$$\frac{d\beta_1}{dT} = \frac{\lambda^2}{\lambda_{125}^2} \frac{(\lambda_1 E_{\lambda_1} + \lambda_5 E_{\lambda_5} - \lambda_{15} E_{\lambda_2})}{RT^2}$$

$$- \frac{\lambda_1 \lambda_2}{\lambda_{25} \lambda_{125}} \left[\frac{E_{\lambda_1} + E_{\lambda_2}}{RT^2} - \frac{\lambda_1 E_{\lambda_1} + \lambda_2 E_{\lambda_2} + \lambda_5 E_{\lambda_5}}{RT^2 \lambda_{125}} - \frac{\lambda_2 E_{\lambda_2} + \lambda_5 E_{\lambda_5}}{RT \lambda_{25}} \right]$$

$$\frac{d\beta_2}{dT} = \frac{1}{\lambda_{125}} \left(\frac{\lambda_2 E_{\lambda_2} + 5\lambda_5 E_{\lambda_5}}{RT^2} \right) - \frac{\lambda_2 + 5\lambda_5}{\lambda_{125}^2} \left(\frac{\lambda_1 E_{\lambda_1} + \lambda_2 E_{\lambda_2} + \lambda_5 E_{\lambda_5}}{RT^2} \right)$$

$$- \frac{\lambda_1 \lambda_2}{\lambda_{15} \lambda_{25}} \left[\left(\frac{E_{\lambda_1} + E_{\lambda_2}}{RT^2} \right) - \left(\frac{\lambda_1 E_{\lambda_1} + \lambda_2 E_{\lambda_2} + \lambda_5 E_{\lambda_5}}{\lambda_{125} RT^2} \right) - \left(\frac{\lambda_1 E_{\lambda_1} + \lambda_5 E_{\lambda_5}}{\lambda_{15} RT^2} \right) \right]$$

and,

$$\frac{d\beta_3}{dT} = \frac{d}{dT} \left(\frac{\lambda_1 + 3\lambda_2 + 4\lambda_5}{\lambda_{125}} \right) - \frac{d}{dT} \left(\frac{3\lambda_1 \lambda_2}{\lambda_{125}^2} \right) - \frac{d}{dT} \left(\frac{\lambda_1 \lambda_2}{\lambda_{25} \lambda_{125}} \right)$$

where,

$$\frac{d}{dT} \left(\frac{\lambda_1 + 3\lambda_2 + 4\lambda_5}{\lambda_{125}} \right) = \frac{(\lambda_1 E_{\lambda_1} + 3\lambda_2 E_{\lambda_2} + 4\lambda_5 E_{\lambda_5})}{\lambda_{125} RT^2}$$

$$- \frac{(\lambda_1 + 3\lambda_2 + 4\lambda_5)(\lambda_1 E_{\lambda_1} + \lambda_2 E_{\lambda_2} + \lambda_5 E_{\lambda_5})}{\lambda_{125}^2 RT^2}$$

$$\frac{d}{dT}\left(\frac{3\lambda_1\lambda_2}{\lambda^2_{125}}\right) = \frac{3\lambda_1\lambda_2}{\lambda^2_{125}}\left[\frac{(E_{\lambda_1} + E_{\lambda_2})}{RT^2} - \frac{2}{\lambda_{125}}\,\frac{(\lambda_1 E_{\lambda_1} + \lambda_2 E_{\lambda_2} + \lambda_5 E_{\lambda_5})}{R\,T^2}\right]$$

$$\frac{d}{dT}\left(\frac{\lambda_1\,\lambda_2}{\lambda_{25}\,\lambda_{125}}\right) = \frac{\lambda_1\,\lambda_2}{\lambda_{25}\,\lambda_{125}}\left[\frac{(E_{\lambda_1} + E_{\lambda_2})}{RT^2} - \frac{(\lambda_1 E_{\lambda_1} + \lambda_2 E_{\lambda_2} + \lambda_5 E_{\lambda_5})}{\lambda_{125}\,RT^2}\right.$$

$$\left. - \frac{(\lambda_2 E_{\lambda_2} + \lambda_5 E_{\lambda_5})}{\lambda_{25}\,RT^2}\right]$$

In order to illustrate the effect of various parameters on the TGA curves calculations have been made for:

a. Different heating rates, R = 1°C./min., 3°C./min., and 6°C./min.; curves shown on Figure 34.

b. Different water adsorptions, 0. w%, 2.74 w% and 11.4 w%; curves shown on Figure 35.

c. Different quartz contents, 0. w%, 10. w%, 28.8 w%, and 40. w%; curves shown on Figure 36.

In general, the same amount of weight can be lost for a short time period at a high temperature as for a longer time period at a lower temperature. The net effect is that the curves, although very similar to each other, appear to be displaced toward higher temperatures at higher heating rates, or toward lower temperatures at lower heating rates. Consideration on this basis tends to give a false impression of the situation. When it is realized that in Figure 34, the line for R = 6°C/min. reaches 1000°C at 150 minutes; 3°C/min. at 300 min.; and 1°C/min. at 900 min.; a truer perspective can be obtained, and it is obvious that the curves for lower heating rates are displaced toward lower temperatures because the material spends so much more time at lower temperatures.

The different water content curves of Figure 35 are easily interpreted. The water is released very quickly between 100-125°C and after that the curves are displaced to lower W/Wo by the amount of the original water fraction. The implication is that adsorbed water will not stay in the heat shield long enough to be of any real value during ablation.

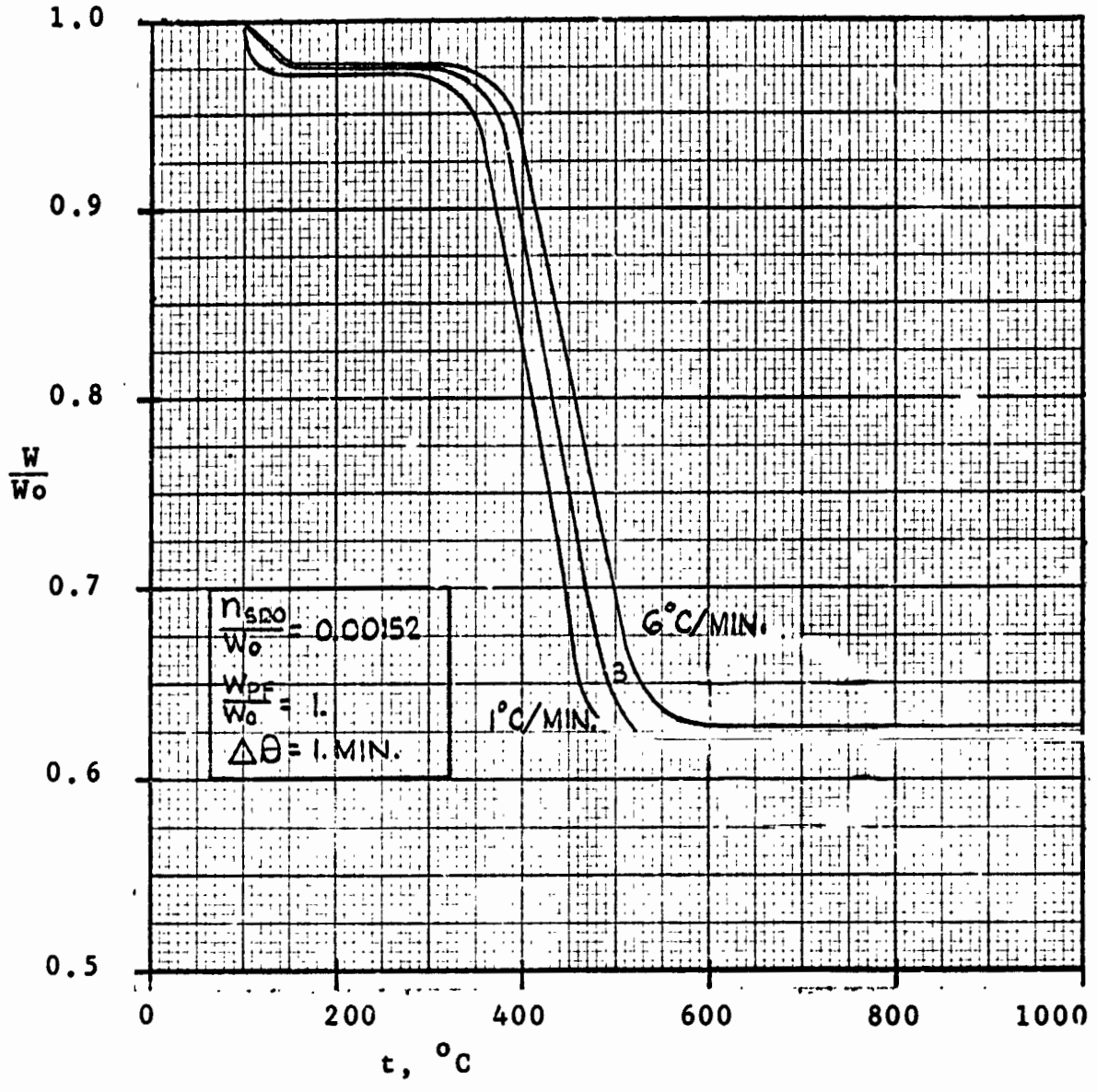

FIGURE 34 - EFFECT OF HEATING RATE ON TGA CURVE

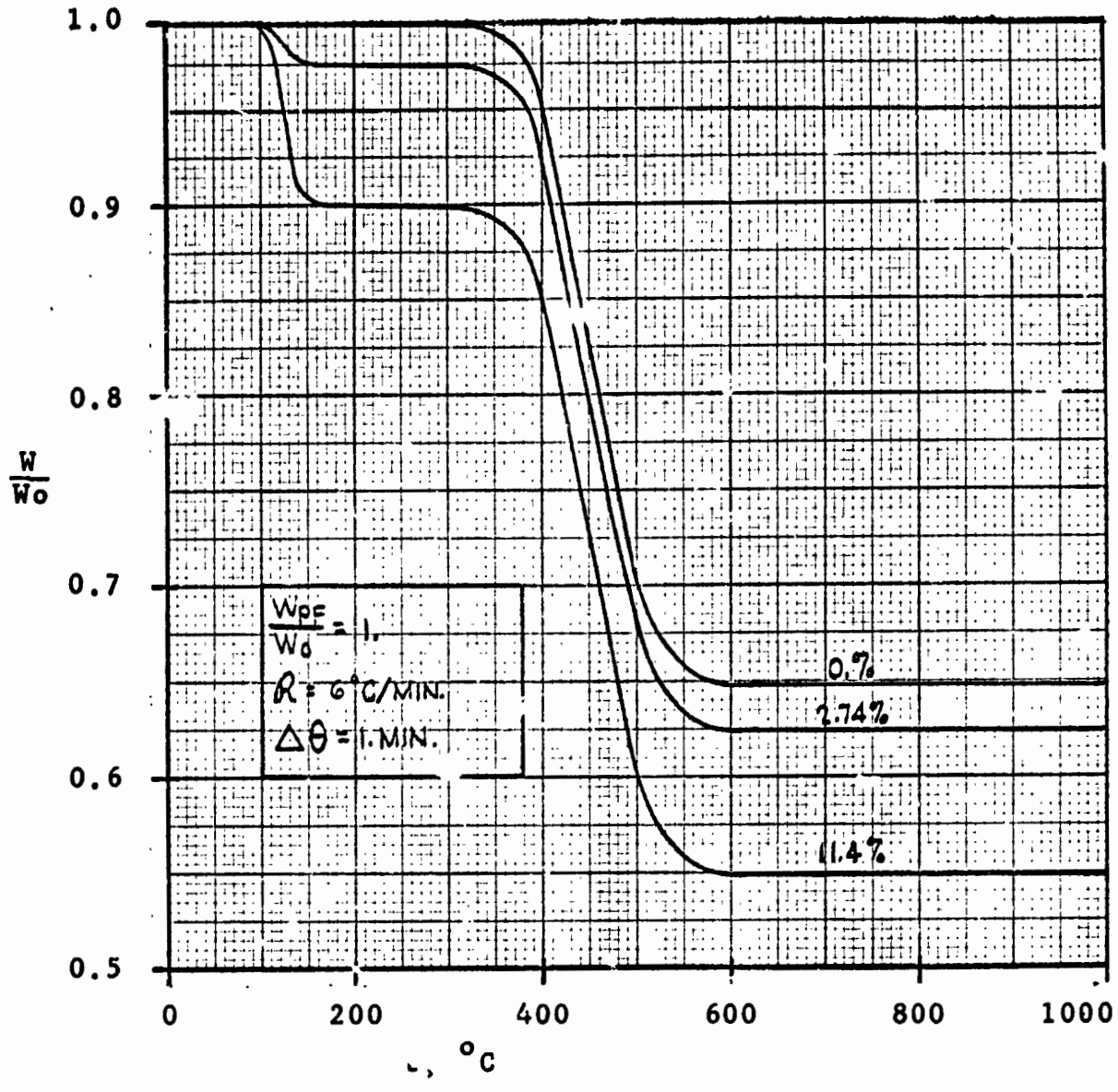

FIGURE 35 - EFFECT OF ADSORBED WATER ON TGA CURVE

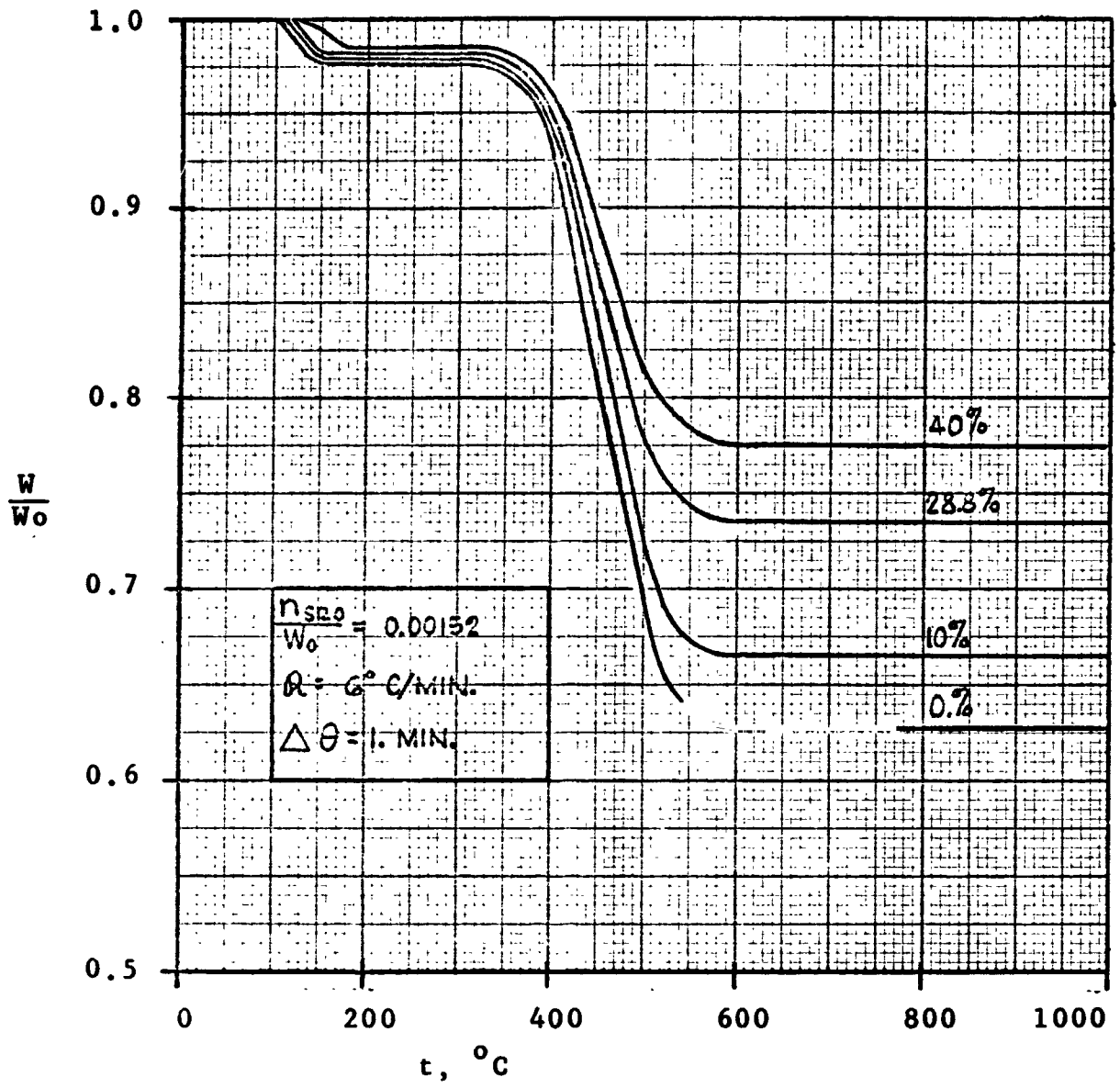

FIGURE 36 - EFFECT OF QUARTZ CONTENT ON TGA CURVE

Figure 36 presents a very simple picture of the effect of quartz content. The value of (1. - W/Wo) is directly proportional to (1. - quartz fraction) for any value of time (temperature) so long as the heating rate is constant.

Although Figures 34, 35, 36 were obtained using time increments of 1 minute, some calculations were made using $\Delta\Theta = 0.2$ min., but the results did not change appreciably from those of the 1 min. increments.

These results appear to be quite consistent with those reported by Friedman (14) or Farmer (12).

C. IN SITU DECOMPOSITION:

In the reaction zone of Figure 33, the degradation of the polymer material follows the pattern described previously, and we can now focus attention on the equations that must be solved in order to describe the actual ablation process in a protective layer.

Consider a slice element of the layer and assume a one dimensional flow process.

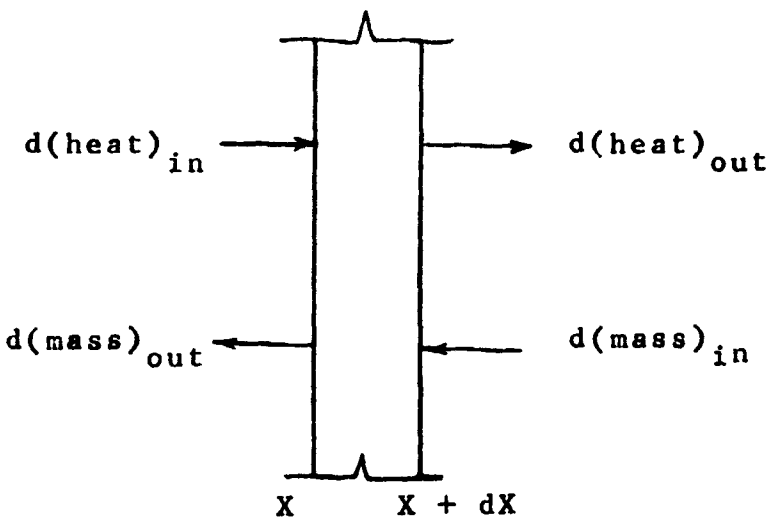

The equation for total heat transfer, based on flow of the product gases through the porous char at a given instant of time can be written as,

$$\left(\frac{k_s}{C_{p_s}\rho_s}\ \frac{\theta_T}{L^2}\right)\frac{\partial^2 T}{\partial X^2} - \frac{\partial T}{\partial \Theta} - \left(\frac{K}{\mu}\ \frac{P_o\,\theta_T}{L^2}\right)\left(\frac{C_p \rho_g}{C_{p_s}\rho_s}\right)\frac{\partial P}{\partial X}\ \frac{\partial T}{\partial X}$$

$$+\left[\left(\frac{\rho_{s_o} C_p}{C_{p_s} \rho_s}\right)\left(\tau - \tau_{datum}\right) - \frac{\Delta H_R \rho_{s_o}}{T_o C_{p_s} \rho_s}\right] \frac{d(W/W_o)}{d\Theta} = 0$$

(VIII-12)

where $d\left(\frac{W}{W_o}\right)/d\Theta$ is defined by equation (VIII-9) from the relation $\Theta = \frac{\Theta}{\Theta_T}$ and Θ_T is the total re-entry time. The first two terms are the usual Fourier differential equation for heat transfer, in dimensionless form; the third term is the heat loss due to mass flow through the element; and the fourth term is the contribution due to reaction and mass loss within the element. The density of the gas, $\rho_g = M/ZRT$. The parameters k_s, Cp_s, and ρ_s are properties of the solid. The permeability of the solid, K, is the sum of contributions from all types of gas flow. The parameters M, Cp, μ, and Z are properties of the gas dependent on composition; for Cp and μ, the property is the sum of the weight fraction of each component times the property of the pure component; for M and Z, the mole fraction is used. The sum of the energies of all reactions is represented by ΔH_R. All of the foregoing properties are to be evaluated at the proper temperature, T; the proper time, Θ; and total pressure, π; for the displacement from the surface, X. Dimensionless variables used are $\tau = T/T_o$; $\rho = \pi/P_o$; $\chi = X/L$; where T_o is the initial temperature of the material, P_o is a reference pressure of one atmosphere, and L is the thickness of the heat shield. The initial density of the ablation material is ρ_{s_o}, and R is the gas constant.

The corresponding mass flow differential equation can be written as,

$$\left(\frac{\rho_g}{\rho_{s_o}}\right)\left(\frac{K}{\mu}\,\frac{P_o\,\Theta_T}{L^2}\right)\left[\frac{\partial^2 \rho}{\partial \chi^2} + \frac{1}{\rho}\left(\frac{\partial \rho}{\partial \chi}\right)^2 - \frac{1}{\tau}\,\frac{\partial \rho}{\partial \chi}\,\frac{\partial \tau}{\partial \chi}\right] + \frac{d(W/W_o)}{d\Theta} = 0$$

(VIII-13)

The differential equations for heat and mass transfer must be solved simultaneously by numerical methods, using appropriate boundary conditions, in order to obtain the temperature profile through the reaction zone after each of the selected time increments.

IX. LITERATURE CITED

(1) American Society of Metals, Atom Movements, Seminar, 32nd National Metal Congress, Chicago, October 1950

(2) Anderson, H. C., U. S. Naval Ordnance Lab. TR 62-59, October (1962)

(3) Boquist, C. W. and Nielsen, E. R., WADD TR 61-72, Vol. XV, AD 418 260, July 1963

(4) Carslaw, H. S.; Jaeger, J. C., Conduction of Heat in Solids, 2nd Edition, Oxford University Press, (1959)

(5) Carswell, T. S., "Chemical Structure of the Phenoplasts," in "Phenoplasts: Their Structure Properties and Chemical Technology," Interscience, New York (1947)

(6) Coffman, J. A., WADD TR 60-646, Part II; AD 297 946, January 1963

(7) Coffman, J. A., and Friedman, H. L., WADD TR 60-646; AD 433 021, February 1964

(8) Conley, R. T. and Bieron, J. F., J. Applied Science, 7, 103, 171 (1963)

(9) Dienes, G. J., J. Appl. Phys., 23, 1194, (1952)

(10) Directorate of Engineering Test, Wright-Patterson AFB, WADC TR 59-523, Part IV; N63-32019, October 1962

(11) Farmer, Rex W., WADD TR 60-314, AD 249 275, September 1960

(12) Farmer, Rex W., ML-TDR64-133, AD-441 142, January 1964

(13) Feldman, M. H.; Goeddel, W. V.; Dienes, G. J., Grossen, W., J. Appl. Phys., 23, 1200, (1952)

(14) Friedman, H. L., G. E. Space Sciences Lab. Report ER61SD145, August (1961) N63-13464

(15) Friedman, H. L., G. E. Space Sciences Lab. Report ER 62SD57, December (1962) AD 297237

(16) Good, G. M.; Voge, H. H.; and Greensfelder, B. S., Ind. Eng. Chem., 39, 1032 (1947)

(17) Greensfelder, B. S., and Voge, H. H., Ibid., 37, 514, 983, 1038 (1945)

(18) Greensfelder, B. S.; Voge, H. H.; and Good, G. M., Ibid., 37, 1168 (1945); Ibid., 41, 2573 (1945)

(19) Howse, Paul T., Jr., Pears, C. D. and Oglesby, Sabert, Jr., WADD TR 60-657; AD 260 065, January 1961

(20) Jenkins, R. J. and Parker, W. J., WADD TR 61-95; AD 268 752, June 1961

(21) Johnson, R. D. and Havlik, A. J., JPL SPS No. 37-22, August 31, 1963

(22) Kinney, C. R., and DelBel, E., Ind. Eng. Chem., 46, 548 (1954)

(23) Kinney, C. R., and Slysh, R. S., "Proceedings of the Fourth Conference on Carbon," p. 301, Pergamon, New York (1960)

(24) Kotlensky, W. V., JPL SPS No. 37-21, p. 42 ff, June 30, 1963

(25) Lapple, C. E., Brady, A. P. and Chamberlain, D. L., Jr., ASD TR 61-204; AD 268 946, September 1961

(26) Lee, L. H., J. Polymer Science, A3, 859 (1965)

(27) Lewis, I. C., and Edstrom, T., WADD TR 61-72, Vol. XXVII, November (1963) AD 427 129

(28) Lincoln, K. A., USNRDL TR 617; AD 401 875, 23 January 1963

(29) Madorsky, Samuel L., and Straus, Sidney, WADC TR 59-64, Part I; AD 215 852, June 1959

(30) Martin, Stanley B., and Ramstad, Robert W., Analytical Chemistry, 33, 982, (1961)

(31) Mason, Donald R., Kulwicki, Bernard M., Barnes, Charles E., and Rose, Gerald D., Michigan #2900-146-R, N63 22421, September 1963

(32) Mathews, B. E. and Perdue, G. F., WADC TR 59-523, Part III; AD 276 384; N63-13960, May 1962

(33) McAllister, L. E.; Bolger, J. C.; McCaffery, E. L.; Roy, P. J.; Ward, F. W.; and Walker, A. C., Jr. Chem. Eng. Progr. Symposium Series 40, 59, 17 (1963)

(34) Meyer, R. A. and Burr, J. G., J. Am. Chem. Soc., 85, 478 (1963)

(35) Mixer, R. Y., and Marynowski, C. W., WADC TR 59-668, Part I; AD 237 242, February 1960

(36) Nagler, Robert G., JPL TR #32-552, January 20, 1964

(37) Nelson, L. S., Science, 136, 296 (1962)

(38) Ouchi, K., and Honda, H., Fuel, 38, 429 (1959)

(39) Reid, R. C.; Sherwood, T. K., The Properties of Gases and Liquids, McGraw-Hill, (1958)

(40) Rudkin, R. L., ASD TDR 62-24, Part II; AD 413 005, June 1963

(41) Scala, S. M., and Gilbert, L. M., ARS Journal, June, 917 (1962)

(42) Schmidt, D. L., WADD TR 60-862; AD 268 078, August 1961

(43) Schmidt, D. L., ASD-TR-61-650, February (1962) N62-12763

(44) Schmidt, D. L., and Schwartz, H. S., ASD TR 61-691, March 1962

(45) Schwartz, H. S., Schmidt, D. L., Marolo, S. A., and Starks, D. F., WADD TN 60-286; AD 260 071, January 1961

(46) Schwartz, H. S., ASD TR 61-517; N62-10952, January 1962

(47) Shewmon, P. G., Diffusion in Solids, McGraw-Hill, (1963)

(48) Singer, L. A., and Lewis, I. S., WADD TR-61 72, Vol. XVI; AD 414 491, June 1963

(49) Space Sciences Lab - General Electric, Final Report - Mark 3 Advanced Re-Entry Vehicle Program Applied Research, 30 June 1961

(50) Stehling, F. C.; Frazee, J. D.; and Anderson, R. C., "Eighth Symposium (International) on Combustion," p. 774, Williams and Wilkins, Baltimore (1962)

(51) Sutton, G. W., J. Aero/Space Sci., 27 (5), 377 (1960)

(52) Wacks, Morton E., ASD TDR 62-372; AD 287 790, May 1962

(53) Wolfs, P. M. J.; van Krevelen, D. W.; and Waterman, H. I., Fuel, 39, 25 (1960)

(54) Sherwood, T. K.; Reid, R. C., The Properties of Gases and Liquids, McGraw-Hill, (1958)

(55) Madorsky, S. L. and Straus, S., Modern Plastics, 38, No. 6, February, 134 (1961)

° APPENDIX °

APPENDIX A

EXPERIMENTAL PROCEDURES

The following are the procedures for the supplementary analyses. The operations of the major pieces of equipment are described in Section IV.

1. Elemental Analysis:

The equipment required consists of a combustion furnace with a fused silica or vycor glass tube, combustion boats, push rod, flow indicator, and two adsorption tubes. The reagents required are cupric oxide (wire form), dehydrite (magnesium perchlorate, granular), ascarite (or carbasorb) 14 mesh, and pure dry oxygen.

Before starting a series of analyses after an extensive shut-down, a pre-conditioning routine must be followed. The furnace tube is packed with cupric oxide for about four inches at the exhaust end. One adsorption tube is filled with dehydrite and connected to the exhaust of the furnace tube; the other adsorption tube is filled with ascarite and connected to the exhaust of the first adsorption tube. The furnace is heated to 800°C and an empty boat is pushed into the furnace. Oxygen is allowed to pass through the furnace tube and through the adsorption tubes for 4 to 5 hours, or until the adsorption tubes attain constant weight.

A run is made by weighing 300-500 milligrams of sample in a pre-conditioned boat and adding about 1/2 gram of cupric oxide to cover the sample. The oxygen flow is adjusted to 300-400 cc./min. The ads. tubes are removed, wiped thoroughly with lint free adsorbent paper, and weighed. The tubes are re-connected, dehydrite to the furnace tube, ascarite to the dehydrite, and the boat with sample is pushed to the center of the furnace tube. Pass oxygen through the tubes for 15 minutes, remove the adsorption tubes and let them cool at room temperature for 15 minutes. Remove the boat from the furnace tube and clean the cupric oxide from the boat. After the adsorption tubes are cool, they are wiped and weighed again. The gain of weight by the dehydrite tube represents the water generated by burning the resin, and the gain of the ascarite tube is carbon dioxide.

Elemental analysis is calculated on a dry ash free basis by,

$$\%C = \frac{0.2729}{F} \left(\frac{\text{wt. of } CO_2}{\text{wt. of sample}} \right)$$

$$\%H = \frac{0.1119}{F}\left(\frac{\text{wt. of } H_2O}{\text{wt. of sample}} - \frac{\%\text{ moisture in resin}}{100}\right)$$

and,

$$\%\,O = 100 - \%C - \%H$$

where,

$$F = \left(1 - \frac{\%\text{ ash in resin}}{100(W/Wo)} - \frac{\%\text{ moisture in sample}}{100}\right)$$

These equations hold whether the sample is undecomposed resin or a char, and whether the sample is phenolic or epoxy.

Loss of individual elements can be calculated from the results of the elemental analysis by,

$$\frac{Wc}{Wo} = \frac{\%C\text{ in resin}}{100}(A) - \frac{\%C\text{ in char}}{100}(B)$$

$$\frac{W_H}{Wo} = \frac{\%H\text{ in resin}}{100}(A) - \frac{\%H\text{ in char}}{100}(B)$$

$$\frac{Wox}{Wo} = \frac{\%O\text{ in resin}}{100}(A) - \frac{\%O\text{ in char}}{100}(B)$$

where,

$$A = \left(1 - \frac{\%\text{ ash in resin}}{100} - \frac{\%\text{ moisture in resin}}{100}\right)$$

$$B = \left(\frac{W}{Wo} - \frac{\%\text{ ash in resin}}{100} - \frac{\%\text{ moisture in char}}{100}\right)$$

2. Ash determination:

The equipment required consists of a muffle furnace, a fused silica or vycor glass crucible with lid, and a burette. The reagents required are standard HCL soln. and phenolphthalein indicator.

Before making a run, the crucible must be heated in a muffle furnace at 800°C until it attains a constant weight. One gram of resin is weighed into the crucible and covered with the lid. The crucible is placed in a muffle furnace at 400°C for 1/2 hour; the lid is removed and the furnace temperature is raised to 800°C for one hour, or until constant weight is attained.

$$\%\text{ ash} = \frac{\text{weight of residue}}{\text{weight of sample}} \times 100$$

If a fixed alkali catalyst is used in the polymerization of the resin (as is the case for the phenol-formaldehyde used in this investigation), it is necessary to determine the alkali content of the ash. The ash is leached out by boiling with distilled water for 1-2 hours. The washings are titrated with 1 N HCL to a phenolphthalein end point. Alkali is calculated as Na_2O.

$$\% \ Na_2O = \frac{(\text{mls. of 1 N HCL})(3.10)}{\text{weight of sample}}$$

3. Karl Fisher analysis for moisture:

The equipment required is described in detail in Appendix E. The reagents required are stabilized Karl Fisher reagent, Karl Fisher diluent, methanol and sodium tartrate dihydrate, reagent grade. The reagent is diluted approximately 1:4 with the diluent. The resulting diluted reagent is standardized by titrating a weighed amount of sodium tartrate dihydrate in methanol, using the technique of operation described in Section IV-B. The calibration factor is calculated by,

$$C_F = \frac{(\text{mg. sodium tartrate}) \times 0.1566}{\text{ml. KF reagent}}$$

When the unknown sample is titrated, the moisture content is calculated by,

$$\%H_2O = \frac{C_F \times (\text{ml. KF reagent})}{(\text{grams of sample}) \times 10}$$

4. Alcoholic hydroxide determination:

The equipment required consists of a 125 ml. flask with ground glass joint and matching reflux condenser, hot plate or heating mantle to fit the flask, thermometer, 10 ml. pipette, and burette. Reagents required are pyridine, acetic anhydride, fused sodium acetate and standardized sodium hydroxide soln. and phenolphthalein indicator (all ACS or AR quality). A stock reagent is prepared from one volume of acetic anhydride to 19 volumes of pyridine.

A 0.25 gram sample is weighed into the flask. The pipette is used to add 10 ml of the stock reagent to the flask. Approximately 2 gm. sodium acetate is added, and the reaction mass is refluxed for 10 hours at 100°C. After acetylation, 30-50 ml. of CO_2 - free distilled water is used to wash down the wall of the condenser into the flask. The solution is titrated with standard sodium hydroxide to the phenolphthalein end point.

Simultaneously a blank is run which consists of the same reagents and treatment, but without a sample being added to the flask.

$$\%OH = \frac{1.701(\text{titre for blank} - \text{titre for sample})(\text{Normality of NaOH})}{\text{sample weight}}$$

APPENDIX B

EXPERIMENTAL DATA

The following tables contain data pertinent to this report. Tables B-1 to B-40 contain experimental data obtained by this investigation. Data in Table B-41 was obtained from the literature for comparison purposes.

TABLE B-1: THERMAL DECOMPOSITION DATA, 378°C (712°F), PHENOL-FORMALDEHYDE ABLATOR C-1

Run	X7	X8	X9	X10	X11
Time (mins)	5.00	10.0	20.0	30.0	80.0
(W/W_o)	0.948	0.945	0.932	0.926	0.908
$(1-W/W_o)$	0.052	0.055	0.068	0.074	0.092

TABLE B-2: 387°C (729°F)

Run	4	5	6	7	X2	X3
Time (mins)	5.00	5.00	5.00	10.0	10.0	15.0
(W/W_o)	0.941	0.937	0.942	0.932	0.934	0.931
$(1-W/W_o)$	0.059	0.063	0.058	0.068	0.066	0.069

Run	8	9	X4	X5	X1
Time (mins)	15.0	20.0	20.0	20.0	25.0
(W/W_o)	0.927	0.925	0.926	0.923	0.920
$(1-W/W_o)$	0.073	0.075	0.074	0.077	0.080

TABLE B-3: THERMAL DECOMPOSITION DATA, 382°C (720°F), PHENOL-FORMALDEHYDE ABLATOR C-1

	Run	41		36		42	
	Time (mins)	3.0		5.0		7.0	
	(W/W_o)	0.953		0.946		0.931	
	$(1-W/W_o)$	0.047		0.054		0.061	
(GAS)	(W_{H_2O}/W_o)	0.025		0.024		0.027	
	(W_{CO}/W_o)	0.005		0.0061		0.0069	
	(W_{CO_2}/W_o)	0.021		0.020		0.020	
	(W_{CH_4}/W_o)	2.05×10^{-5}		3.3×10^{-5}		3.7×10^{-5}	
		(0.051)		(0.0501)		(0.0539)	
		(GA)	(EA)	(GA)	(EA)	(GA)	(EA)
	(W_C/W_o)	0.0078	0.0240	0.0081	0.005	0.0085	0.007
	(W_{ox}/W_o)	0.0404	0.0197	0.0494	0.0439	0.0440	0.0695
	(W_H/W_o)	0.0028	0.0016	0.0027	0.0037	0.030	--
(SOLID-ASH FREE)	(W_C/W)		0.793		0.820		0.831
	(W_{ox}/W)		0.151		0.126		0.100
	(W_H/W)		0.056		0.054		0.070
	Total $(\frac{W_{ox}}{W_o})$	0.1804	0.1597	0.1654	0.1589	0.1345	0.1600

TABLE B-3 (CONTINUED)

	Run	44		43		37	
	Time (mins)	13.0		10.0		15.0	
	(W/W_o)	0.932		0.935		0.931	
	$(1-W/W_o)$	0.068		0.065		0.069	
(GAS)	(W_{H_2O}/W_o)	0.0340		0.0310		0.0340	
	(W_{CO}/W_o)	0.0062		0.0064		0.0065	
	(W_{CO_2}/W_o)	0.0220		0.0220		0.0270	
	(W_{CH_4}/W_o)	4.5×10^{-5}		3.8×10^{-5}		5.7×10^{-5}	
		(0.0622)		(0.0594)		(0.0675)	
		(GA)	(EA)	(GA)	(EA)	(GA)	(EA)
	(W_C/W_o)	0.0087		0.0087	0.0430	0.0102	0.0160
	(W_{ox}/W_o)	0.0497		0.0473	--	0.0522	0.0467
	(W_H/W_o)	0.0038		0.0034	0.0028	0.0038	0.0046
(SOLID-ASH FREE)	(W_C/W)	--			0.7880		0.821
	(W_{ox}/W)	--			0.1565		0.125
	(W_H/W)	--			0.0555		0.054
	Total $\left(\frac{W_{ox}}{W_o}\right)$	--		0.1893		0.1652	

TABLE B-3 (CONTINUED)

	Run	45	38		39	
	Time (mins)	20.0	25.0		50.0	
	(W/W_o)	0.925	0.924		0.911	
	$(1-W/W_o)$	0.075	0.076		0.089	
(GAS)	(W_{H2O}/W_o)	0.039	0.0390		0.0510	
	(W_{CO}/W_o)	--	0.0068		0.0060	
	(W_{CO_2}/W_o)	0.020	0.0250		0.0250	
	(W_{CH_4}/W_o)	--	6.8×10^{-5}		8.9×10^{-5}	
			(0.0708)		(0.0820)	
		(EA)	(GA)	(EA)	(GA)	(EA)
	(W_C/W_o)	0.005	0.0097	0.0150	0.0094	0.0290
	(W_{ox}/W_o)	0.0706	0.0569	0.0538	0.0671	0.0534
	(W_H/W_o)	--	0.0043	0.0049	0.0057	0.0035
(SOLID-ASH FREE)	(W_C/W)	0.839		0.828		0.825
	(W_{ox}/W)	0.100		0.054		0.119
	(W_H/W)	0.061		0.118		0.056
	Total $(\frac{W_{ox}}{W_o})$	0.1605	0.1054		0.1725	0.1676

TABLE B-3 (CONTINUED)

	Run	40 (384°C)		47 (384°C)		46 (384°C)	
	Time (mins)	90.0		3.0		20.0	
	(W/W_o)	0.901		0.951		0.924	
	$(1-W/W_o)$	0.099		0.049		0.076	
(GAS)	(W_{H_2O}/W_o)	0.0540		0.0260		0.0400	
	(W_{CO}/W_o)	0.0081		0.0063		0.0086	
	(W_{CO_2}/W_o)	0.0260		0.0200		0.0250	
	(W_{CH_4}/W_o)	10.5×10^{-5}		2.5×10^{-5}		7.2×10^{-5}	
		(0.0881)		(0.0523)		(0.0836)	
		(GA)	(EA)	(GA)	(EA)	(GA)	(EA)
	(W_C/W_o)	0.0106	0.0250	0.0080	--	0.0105	0.020
	(W_{ox}/W_o)	0.0716	0.0653	0.0412	0.0687	0.0587	0.0516
	(W_H/W_o)	0.0060	0.0061	0.0029	--	0.0045	0.0028
(SOLID-ASH FREE)	(W_C/W)		0.838		0.843		0.823
	(W_{ox}/W)		0.108		0.099		0.121
	(W_H/W)		0.054		0.058		0.056
	Total $(\frac{W_{ox}}{W_o})$	0.1661	0.1598	0.1328	0.1603	0.1672	0.1604

TABLE B-4: THERMAL DECOMPOSITION DATA, 436°C (819°F), PHENOL-FORMALDEHYDE ABLATOR C-1

Run	65	66	67	68	69	70
Time (mins)	2.0	5.0	10.0	20.0	41.0	90.0
(W/W_o)	0.905	0.885	0.867	0.857	0.842	0.828
$(1-W/W_o)$	0.095	0.115	0.133	0.143	0.158	0.172

TABLE B-5: THERMAL DECOMPOSITION DATA, 533°C (991°F), PHENOL-FORMALDEHYDE ABLATOR C-1

Run	83	84	85	86
Time (mins)	2.0	10.0	30.0	60.0
(W/W_o)	0.787	0.740	0.718	0.709
$(1-W/W_o)$	0.213	0.260	0.282	0.291

TABLE B-6: THERMAL DECOMPOSITION DATA, 571°C (1060°F), PHENOL-FORMALDEHYDE ABLATOR C-1

Run	71	72	73	74	75	76
Time (mins)	1.0	3.00	8.00	16.0	32.0	70.0
(W/W_o)	0.741	0.698	0.680	0.671	0.660	0.655
$(1-W/W_o)$	0.259	0.302	0.320	0.329	0.340	0.345

TABLE B-7: THERMAL DECOMPOSITION DATA, 498°C (928°F), PHENOL-FORMALDEHYDE ABLATOR C-1

	Run	60		61		59	
	Time (mins)	2.00		4.00		10.00	
	(W/W_o)	0.823		0.811		0.782	
	$(1-W/W_o)$	0.177		0.189		0.218	
(GAS)	(W_{H_2O}/W_o)	0.0550		0.0590		0.0739	
	(W_{CO}/W_o)	0.0103		0.0112		0.0138	
	(W_{CO_2}/W_o)	0.0373		0.0368		0.0386	
	(W_{CH_4}/W_o)	0.0087		0.0012		0.0032	
	(W_{rg}/W_o)*	0.0001		0.0001		0.0001	
	(W_{org}/W_o)**	0.0715		0.0673		0.0752	
		(0.183)		(0.176)		(0.205)	
(SOLID-ASH FREE)		(GA)	(EA)	(GA)	(EA)	(GA)	(EA)
	(W_C/W_o)	0.0850	0.0750	0.094	0.0950	0.105	0.1180
	(W_{ox}/W_o)	0.0820	0.0999	0.0858	0.1024	0.102	0.0854
	(W_H/W_o)	0.0102	0.0085	0.0087	0.0092	0.011	0.0141
		(0.1772)		(0.1885)		(0.218)	
	(W_C/W)		0.8680		0.8760		0.8500
	(W_{ox}/W)		0.0754		0.0665		0.0982
	(W_H/W)		0.0566		0.0575		0.0578
	Total $(\frac{W_{ox}}{W_o})$	0.1421	0.1601	0.1380	0.1546	0.1762	0.1597

* Residual gas - see Table B-14
** Organic "tar" - see Table B-13

TABLE B-7 (CONTINUED)

	Run	62		63		64	
	Time (mins)	20.00		35.00		60.00	
	(W/W_o)	0.762		0.746		0.736	
	$(1-W/W_o)$	0.238		0.254		0.264	
(GAS)	(W_{H2O}/W_o)	0.0706		0.0887		0.0968	
	(W_{CO}/W_o)	0.0115		0.0148		0.0156	
	(W_{CO_2}/W_o)	0.0348		0.0404		0.0417	
	(W_{CH_4}/W_o)	0.0033		0.0057		0.0070	
	(W_{rg}/W_o)	0.0001		0.0001		0.0001	
	(W_{org}/W_o)	0.0798		0.0885		0.0835	
		(0.2000)		(0.2382)		(0.2447)	
		(GA)	(EA)	(GA)	(EA)	(GA)	(EA)
	(W_C/W_o)	0.1324	0.1050	0.1237	0.1430	0.1237	0.1300
	(W_{ox}/W_o)	0.0948	0.1158	0.1168	0.1038	0.1253	0.1206
	(W_H/W_o)	0.0108	0.0090	0.0136	0.0102	0.0149	0.0173
		(0.2380)		(0.2541)		(0.2639)	
(SOLID-ASH FREE)	(W_C/W)		0.8820		0.8620		0.8940
	(W_{ox}/W)		0.0587		0.0778		0.0550
	(W_H/W)		0.0593		0.0602		0.0510
	Total $(\frac{W_{ox}}{W_o})$	0.1380	0.1590	0.1728	0.1598	0.1644	0.1597

TABLE B-8: THERMAL DECOMPOSITION DATA, 605°C (1121°F), PHENOL-FORMALDEHYDE ABLATOR C-1

Run	55		53		49	
Time (mins)	1.50		3.00		5.00	
(W/W_o)	0.680		0.680		0.680	
$(1-W/W_o)$	0.320		0.320		0.320	
(W_{H_2O}/W_o)	0.0436		0.0436		0.0515	
(W_{CO}/W_o)	0.0195		0.0223		0.0243	
(W_{CO_2}/W_o)	0.0483		0.0492		0.0490	
(W_{CH_4}/W_o)	0.0141		0.0162		0.0214	
(W_{rg}/W_o)	0.0002		0.0002		0.0002	
(GAS) (W_{org}/W_o)	0.1690		0.0915		0.0850	
	(0.292)		(0.223)		(0.231)	
	(GA)	(EA)	(GA)	(EA)	(GA)	(EA)
(W_C/W_o)	0.1965	0.1530		0.1580	0.1225	0.1640
(W_{ox}/W_o)	0.0862	0.1516	0.0884	0.1328	0.0953	0.1407
(W_H/W_o)	0.0129	0.0228	0.0114	0.0263	0.0134	0.0288
(SOLID-ASH FREE) (W_C/W)		0.9410		0.9180		0.9330
(W_{ox}/W)		0.0116		0.0410		0.0289
(W_p/W)		0.0474		0.0410		0.0381
Total$\left(\frac{W_{ox}}{W_o}\right)$		0.1592		0.1597		0.1596

TABLE B-8 (CONTINUED)

	Run	54		51		50	
	Time (mins)	5.00		15.00		20.00	
	(W/W_o)	0.667		0.661		0.658	
	$(1-W/W_o)$	0.333		0.339		0.342	
(GAS)	(W_{H_2O}/W_o)	0.0525		0.0788		0.0887	
	(W_{CO}/W_o)	0.0198		0.0289		0.0252	
	(W_{CO_2}/W_o)	0.0453		0.0502		0.0561	
	(W_{CH_4}/W_o)	0.0190		0.0233		0.0233	
	(W_{rg}/W_o)	0.0002		0.0002		0.0002	
	(W_{org}/W_o)	0.1640		0.0750		0.0708	
		(0.301)		(0.256)		(0.261)	
		(GA)	(EA)	(GA)	(EA)	(GA)	(EA)
	(W_C/W_o)	0.1947	0.1690	0.1996	0.1610	0.1900	0.1530
	(W_{ox}/W_o)	0.0900	0.1420	0.1231	0.1515	0.1342	0.1578
	(W_H/W_o)	0.0149	0.0245	0.0165	0.0266	0.0175	0.0282
				(0.339)		(0.342)	
(SOLID-ASH FREE)	(W_C/W)		0.9280		0.9460		0.9580
	(W_{ox}/W)		0.0270		0.0121		0.0027
	(W_H/W)		0.0450		0.0419		0.0393
	Total $(\frac{W_{ox}}{W_o})$		0.1593		0.1592		0.1595

TABLE B-8 (CONTINUED)

	Run	57		52		56	
	Time (mins)	25.00		31.00		78.00	
	(W/W_o)	0.648		0.653		0.637	
	$(1-W/W_o)$	0.352		0.347		0.363	
(GAS)	(W_{H_2O}/W_o)	0.1200		0.1200		0.1350	
	(W_{CO}/W_o)	0.0214		0.0333		0.0290	
	(W_{CO_2}/W_o)	0.0550		0.0455		0.0522	
	(W_{CH_4}/W_o)	0.0205		0.0237		0.0204	
	(W_{rg}/W_o)	0.0002		0.0002		0.0002	
	(W_{org}/W_o)	0.1090		0.0590		0.1000	
		(0.326)		(0.282)		(0.337)	
		(GA)	(EA)	(GA)	(EA)	(GA)	(EA)
	(W_C/W_o)	0.1717	0.1750	0.1673	0.1680	0.1656	0.1841
	(W_{ox}/W_o)	0.1590	0.1591	0.1589	0.1463	0.1746	0.1591
	(W_H/W_o)	0.0213	0.0328	0.0208	0.0324	0.0228	0.0374
		(0.352)		(0.347)			
(SOLID-ASH FREE)	(W_C/W)		0.9665		0.9440		0.9735
	(W_{ox}/W)		0.0000		0.0212		0.0000
	(W_H/W)		0.0335		0.0348		0.0265
	Total $(\frac{W_{ox}}{W_o})$		0.1591		0.1594		0.1591

TABLE B-8 (CONTINUED)

Run	58	
Time (mins)	10.00	
(W/W_o)	0.656	
$(1-W/W_o)$	0.344	
(W_{H_2O}/W_o)	0.1130	
(W_{CO}/W_o)	0.0218	
(W_{CO_2}/W_o)	0.0468	
(W_{CH_4}/W_o)	0.0199	
(W_{rg}/W_o)	0.0002	
(GAS) (W_{org}/W_o)	0.1160	
	(0.317)	
	(GA)	(EA)
(W_C/W_o)	0.1499	0.1780
(W_{ox}/W_o)	0.1470	0.1534
(W_H/W_o)	0.0206	0.0318
(SOLID-ASH FREE) (W_C/W)		0.9555
(W_{ox}/W)		0.0095
(W_H/W)		0.0350
Total $(\frac{W_{ox}}{W_o})$		0.1594

TABLE B-9: THERMAL DECOMPOSITION DATA, 666°C (1199°F), PHENOL-FORMALDEHYDE ABLATOR C-1

Run	77	78	79	80	81	82
Time (mins)	2	4	8	16	32	72
W/W_o	0.628	0.624	0.622	0.618	0.612	0.607
$1-W/W_o$	0.372	0.376	0.378	0.382	0.388	0.393

TABLE B-10: THERMAL DECOMPOSITION DATA, 388°C (730.4°F), PHENOL-FORMALDEHYDE-QUARTZ* ABLATOR C-3

Run	105		109		106	
Time (mins)	2		5		10	
(W/W_o)	0.976		0.966		0.960	
$(1-W/W_o)$	0.024		0.034		0.040	
(GAS) (W_{H_2O}/W_o)	0.01860		0.02600		0.03100	
(GAS) (W_{CO}/W_o)	0.00284		0.00376		0.00477	
(GAS) (W_{CO_2}/W_o)	0.0021		0.00560		0.00520	
	(0.0235)		(0.0354)		(0.0410)	
	(GA)	(EA)	(GA)	(EA)	(GA)	(EA)
(W_C/W_o)	0.00176	0.007	0.00314	0.023	0.00346	0.017
(W_{ox}/W_o)	0.01364	0.0260	0.02930	0.0213	0.03409	0.0310
(W_H/W_o)	0.00206	--	0.00284	--	0.00344	--
(SOLID-ASH FREE) (W_C/W)		0.800		0.788		0.802
(SOLID-ASH FREE) (W_{ox}/W)		0.1318		0.1410		0.1270
(SOLID-ASH FREE) (W_H/W)		0.0682		0.0710		0.0710

* 28.8 W% Quartz

TABLE B-10 (CONTINUED)

	Run	110		12		113 (Mixture)	114
	Time (mins)	30		60		2	60
	(W/W_o)	0.943		0.929		0.968	0.927
	$(1-W/W_o)$	0.057		0.071		0.0316	0.0727
(G A S)	(W_{H_2O}/W_o)	0.04970		0.05720		0.01850	0.05800
	(W_{CO}/W_o)	0.00480		0.00490		0.00305	0.01690
	(W_{CO_2}/W_o)	0.00370		0.00580		0.00890	--
		(0.0582)		(0.0679)		(0.03045)	(0.0749)
		(GA)	(EA)	(GA)	(EA)	(GA)	(GA)
(SOLID-ASH FREE)	(W_C/W_o)	0.00306	0.033	0.00368	0.034	0.00155	(0.0072)*
	(W_{ox}/W_o)	0.04773	0.0418	0.05791	0.0400	0.0247	(0.0613)*
	(W_H/W_o)	0.00552	--	0.00635	--	0.0021	0.0064
	(W_C/W)		0.800		0.817		
	(W_{ox}/W)		0.1298		0.119		
	(W_H/W)		0.0702		0.0640		

* Contributions from CO_2 not included.

TABLE B-11: THERMAL DECOMPOSITION DATA, 316°C (560°F), EPOXY-NOVOLAK ABLATOR

Run	214		215		207	
Time (mins)	2		5		10	
(W/W_o)	0.950		0.943		0.934	
$(1-W/W_o)$	0.050		0.057		0.066	
(W_{H_2O}/W_o)	0.0364		0.0348		0.0470	
(W_{CO}/W_o)	trace		trace		trace	
(W_{CO_2}/W_o)	0.0045		0.0070		0.0048	
(GAS) (W_{tar}/W_o)*	0.0045		0.0104		0.0119	
	(0.0454		(0.0522)		(0.0637)	
	(GA)	(EA)	(GA)	(EA)	(GA)	(EA)
(W_C/W_o)	0.0056	0.0140	0.0120	0.0170	0.0129	0.0350
(W_{ox}/W_o)	0.0357	0.0040	0.0361	--	0.0453	0.0040
(W_H/W_o)	0.0041	--	0.0042	--	0.0055	--
(SOLID-ASH FREE) (W_C/W)		0.6870		0.6840		0.6800
(W_{ox}/W)		0.2200		0.2310		0.2237
(W_H/W)		0.0930		0.0850		0.0963

* No detailed analysis attempted.

TABLE B-11 (CONTINUED)

Run	213		208		216	
Time (mins)	20		30		60	
(W/W_o)	0.917		0.902		0.867	
$(1-W/W_o)$	0.083		0.098		0.133	
(W_{H_2O}/W_o)	0.0479		0.0482		0.0610	
(W_{CO}/W_o)	trace		trace		trace	
(W_{CO_2}/W_o)	0.0064		0.0072		0.0127	
(GAS) (W_{tar}/W_o)	0.0179		0.0144		0.0162	
	(0.0722)		(0.0698)		(0.0899)	
	(GA)	(EA)	(GA)	(EA)	(GA)	(EA)
(W_C/W_o)	0.0192	0.0320	0.0160	0.0170	0.0192	0.0310
(W_{ox}/W_o)	0.0473	0.0110	0.0480	0.0435	0.0634	0.0552
(W_H/W_o)	0.0058	--	0.0057	--	0.0072	--
(SOLID-ASH FREE) (W_C/W)		0.6840		0.7120		0.7240
(W_{ox}/W)		0.2178		0.1860		0.1802
(W_H/W)		0.0982		0.1020		0.0958

TABLE B-12: THERMAL DECOMPOSITION DATA, 388°C (730.4°F) EPOXY-NOVOLAK ABLATOR

	Run	202		201		203	
	Time (mins)	2		5		10	
	(W/W_o)	0.811		0.680		0.577	
	$(1-W/W_o)$	0.189		0.320		0.423	
(GAS)	(W_{H_2O}/W_o)	0.0750		0.0980		0.1260	
	(W_{CO}/W_o)	0.0039		0.0079		0.0119	
	(W_{CO_2}/W_o)	0.0680		0.0270		0.0430	
	(W_{tar}/W_o)	0.0430		0.0260		0.1040	
		(0.1899)		(0.1589)		(0.2849)	
		(GA)	(EA)	(GA)	(EA)	(GA)	(EA)
	(W_C/W_o)	0.0620	0.0960	0.0371	0.1720	0.1171	0.2550
	(W_{ox}/W_o)	0.1177	0.0480	0.1103	0.1107	0.1490	0.1278
	(W_H/W_o)	0.0095	0.0050	0.0119	0.0213	0.0168	0.0228
(SOLID-ASH FREE)	(W_C/W)		0.7040		0.7560		0.7440
	(W_{ox}/W)		0.2040		0.1552		0.1533
	(W_H/W)		0.0920		0.0880		0.1027

TABLE B-12 (CONTINUED)

Run	204		205		206	
Time (mins)	20		30		60	
(W/W_o)	0.470		0.406		0.305	
$(1-W/W_o)$	0.530		0.594		0.695	
(W_{H_2O}/W_o)	0.1540		0.1560		0.1650	
(W_{CO}/W_o)	0.0166		0.0166		0.0205	
(W_{CO_2}/W_o)	0.0590		0.0670		0.0760	
(GAS) (W_{tar}/W_o)	0.1230		0.1310		0.1170	
	(0.3526)		(0.3706)		(0.3785)	
	(GA)	(EA)	(GA)	(EA)	(GA)	(EA)
(W_C/W_o)	0.1429	0.3070	0.1528	0.3440	0.1434	0.4380
(W_{ox}/W_o)	0.1878	0.1907	0.1953	0.2041	0.2121	0.1957
(W_H/W_o)	0.0203	0.0379	0.0208	0.0407	0.0215	0.0544
(SOLID-ASH FREE) (W_C/W)		0.8540		0.8780		0.8510
(W_{ox}/W)		0.0474		0.0162		0.0561
(W_H/W)		0.0986		0.1058		0.0929

TABLE B-13: TAR ANALYSIS, PF RUNS

Run	51	55	56	57	58
		Component Weight Fraction of W_o			
Ethane	3.24×10^{-4}	4.98×10^{-4}	6.83×10^{-4}	4.62×10^{-4}	4.18×10^{-4}
Propane	--	1.56×10^{-5}	2.15×10^{-5}	Trace	Trace
Water	1.66×10^{-2}	1.95×10^{-2}	1.80×10^{-2}	1.64×10^{-2}	2.08×10^{-2}
Xylene	3.16×10^{-5}	4.43×10^{-5}	6.40×10^{-6}	5.69×10^{-5}	4.27×10^{-5}
Toluene	--	--	--	--	--
Unident	6.84×10^{-2}	14.95×10^{-2}	8.20×10^{-2}	9.25×10^{-2}	9.52×10^{-2}
Total	7.50×10^{-2}	16.9×10^{-2}	10.0×10^{-2}	10.9×10^{-2}	11.6×10^{-2}
Temp °C	605	605	605	605	605
$(1-W/W_o)$	0.339	0.320	0.363	0.352	0.344
$\frac{W_{(und)}}{W_C}$	0.343	0.761	0.495	0.538	0.535

TABLE B-13 (CONTINUED)

Run	59	60	61	62	63
		Component Weight Fraction of W_o			
Ethane	3.91×10^{-4}	2.74×10^{-3}	2.00×10^{-4}	3.17×10^{-4}	3.15×10^{-4}
Propane	Trace	9.10×10^{-5}	Trace	--	5.14×10^{-6}
Water	1.99×10^{-2}	3.68×10^{-3}	4.51×10^{-3}	4.97×10^{-3}	3.56×10^{-3}
Xylene	Trace	1.78×10^{-5}	Trace	1.89×10^{-6}	1.61×10^{-6}
Toluene	--	Trace	Trace	Trace	Trace
Unident	5.53×10^{-2}	6.78×10^{-2}	6.28×10^{-2}	7.48×10^{-2}	8.48×10^{-2}
	7.52×10^{-2}	7.15×10^{-2}	6.73×10^{-2}	7.98×10^{-2}	8.85×10^{-2}
Temp °C	498	498	498	498	498
$(1-W/W_o)$	0.218	0.177	0.189	0.238	0.254
$\frac{W_{(und)}}{W_C}$	0.527	0.798	0.668	0.564	0.59?

TABLE B-14: ANALYSIS OF RESIDUAL GAS, PF RUNS

Run	49	50	51	52
	(Weight Fraction of W_o)			
H_2	6.24×10^{-4}	1.26×10^{-3}	9.77×10^{-4}	1.53×10^{-3}
C_2H_6	5.13×10^{-3}	1.84×10^{-3}	1.85×10^{-3}	1.88×10^{-3}
C_2H_4	Trace Only			
C_3H_8	1.79×10^{-3}	1.36×10^{-3}	2.79×10^{-3}	6.58×10^{-3}
ϕCH_3	2.35×10^{-2}	3.26×10^{-3}	2.46×10^{-3}	3.53×10^{-3}
$\phi(CH_3)_2$	5.23×10^{-3}	9.82×10^{-3}	6.94×10^{-3}	1.01×10^{-2}

Run	53	54	55	56
	(Weight Fraction of W_o)			
H_2	4.78×10^{-4}	6.68×10^{-4}	2.93×10^{-3}	2.25×10^{-8}
C_2H_6	1.65×10^{-3}	1.52×10^{-3}	1.34×10^{-3}	1.85×10^{-3}
C_2H_4	Trace Only			
C_3H_8	1.80×10^{-3}	9.05×10^{-3}	1.05×10^{-3}	1.29×10^{-2}
ϕCH_3	2.13×10^{-2}	1.82×10^{-2}	1.94×10^{-2}	--
$\phi(CH_3)_2$	5.23×10^{-3}	6.80×10^{-3}	5.05×10^{-3}	1.77×10^{-2}

TABLE B-14 (CONTINUED)

Run	57	58	59	60
	(Weight Fraction of W_o)			
H_2	1.33×10^{-3}	9.41×10^{-4}	--	--
C_2H_6	1.79×10^{-3}	1.55×10^{-3}	4.22×10^{-4}	1.68×10^{-3}
C_2H_4	Trace Only			
C_3H_8	5.72×10^{-3}	4.95×10^{-3}	2.96×10^{-3}	6.20×10^{-3}
ϕCH_3	3.96×10^{-3}	2.92×10^{-2}	1.07×10^{-2}	2.92×10^{-2}
$\phi(CH_3)_2$	1.18×10^{-2}	9.24×10^{-3}	9.25×10^{-3}	9.53×10^{-3}

Run	61	62	63	64
	(Weight Fraction of W_o)			
H_2	--	--	--	-
C_2H_6	2.30×10^{-3}	5.53×10^{-4}	6.55×10^{-4}	6.14×10^{-4}
C_2H_4	Trace Only			
C_3H_8	6.85×10^{-3}	2.92×10^{-2}	5.20×10^{-3}	8.87×10^{-3}
ϕCH_3	3.82×10^{-2}	1.04×10^{-2}	1.15×10^{-2}	1.80×10^{-2}
$\phi(CH_3)_2$	1.27×10^{-2}	4.18×10^{-2}	5.89×10^{-3}	9.55×10^{-3}

TABLE B-15 - PHYSICAL PROPERTIES OF SOLID (PF)

(1-W/Wo)	Run No.	ϵ Porosity	ρ_B (g/cm^2)	ρ (g/cm^3)	V_P (cm^3/g)	S x 10^{-3} (cm^2/g)	$\bar{d}$ (Microns)	K x 10^6 (cm^2)
0	(C-1 resin) Run 2	0.473	0.648	1.225	0.729	2.437	11.97	0.413
0.032	P-1	0.459	0.701	1.298	0.656	1.987	13.2	0.738
0.047	P-2	0.485	0.628	1.220	0.773	3.516	8.80	1.235
0.0734	#33	0.446	0.676	1.220	0.659	2.386	11.0	0.942
0.095	#65	0.4692	0.6371	1.200	0.7365	4.545	6.48	0.914
0.133	#67	0.4612	0.6424	1.192	0.7179	3.573	8.00	0.413
0.158	#69	0.4750	0.6247	1.190	0.7603	3.628	8.37	0.781
0.171	#70	0.484	0.623	1.234	0.793	1.027	30.9	0.900
0.213	#83	0.486	0.678	1.320	0.717	3.245	8.83	0.991
0.259	#71	0.4610	0.6536	1.213	0.7053	2.337	12.4	1.528
0.260	#84	0.452	0.641	1.160	0.706	2.314	12.22	1.320
0.282	#85	0.454	0.660	1.205	0.687	3.614	7.60	1.338
0.340	#75	0.445	0.677	1.220	0.658	1.167	22.6	2.80
0.345	#76	0.470	0.678	1.278	0.693	2.274	12.20	0.844
0.376	#78	0.548	0.560	1.240	0.980	1.504	26.10	0.530
0.378	#79	0.539	0.597	1.292	0.902	0.8924	40.5	0.196
0.382	#80	0.484	0.679	1.314	0.7132	0.9612	29.7	0.119
0.388	#81	0.515	0.7802	1.514	0.622	1.734	14.3	1.081

$$\bar{d} = \frac{4V_p}{S}$$

TABLE B-16

MERCURY POROSIMETER DETERMINATION OF PORE VOLUME, SURFACE AREA, AND PERMEABILITY

Sample Identification: Phenol-formaldehyde resin, C-1, Run 1

Sample weight, grams	0.2180
Bulk density, grams/cm^3	0.6737
Skeletal density, grams/cm^3	1.256
Fraction porosity	0.4635

PORE VOLUME, CM3/G	PORE DIAMETER, MICRONS	D2/16VT X10 TO+8, CM-1	2/D X10 TO-4, CM-1	SURFACE AREA, CM2/G	PERMEAB. X10 TO+8, CM2
.0000	372.340	12592.409	.0054	.0	.00
.0275	134.615	1645.954	.0149	2.8	90.82
.0321	112.179	1143.024	.0178	3.5	93.78
.0413	85.784	668.412	.0233	5.4	97.63
.0459	73.529	491.078	.0272	6.6	98.87
.0550	65.789	393.135	.0304	9.2	100.75
.0596	59.524	321.818	.0336	10.7	101.51
.0780	50.143	228.378	.0399	17.4	103.85
.0872	45.103	184.774	.0443	21.3	104.73
.1147	37.634	128.647	.0531	34.7	106.72
.1440	34.585	108.643	.0578	51.3	108.36
.2110	30.329	83.551	.0659	92.4	111.33
.3119	26.718	64.837	.0749	163.5	114.80
.3945	23.087	48.413	.0866	230.1	116.96
.4879	19.423	34.265	.1030	299.7	118.37
.5646	17.623	28.210	.1135	339.4	118.90
.5459	14.957	20.320	.1337	390.5	119.37
.6101	2.705	.665	.7394	670.8	119.68
.6697	.343	.011	5.8251	2628.1	119.69
.6789	.218	.004	9.1771	3316.3	119.69
.6835	.174	.003	11.4629	3789.7	119.69
.6835	.058	.000	34.3200	3789.7	119.69
.6861	.050	.000	40.0343	5495.1	119.69
.6881	.012	.000	171.4286	5495.1	119.69

TABLE B-17

MERCURY POROSIMETER DETERMINATION OF PORE VOLUME, SURFACE AREA, AND PERMEABILITY

Sample Identification: Phenol-formaldehyde Resin (C-1), Run 2

Sample weight, grams	.188
Bulk density, grams/cm^3	.648
Skeletal density, grams/cm^3	1.225
Fraction porosity	.473

PORE VOLUME, CM3/G	PORE DIAMETER, MICRONS	D2/16VT X10 TO+8, CM-1	2/D X10 TO-4, CM-1	SURFACE AREA, CM2/G	PERMEAB. X10 TO+8, CM2
.0000	159.672	2185.785	.0125	.0	.00
.0266	86.164	636.515	.0232	4.8	17.75
.0479	56.726	275.879	.0353	11.0	22.34
.0851	40.230	138.755	.0497	26.8	25.99
.2021	30.435	79.413	.0657	94.3	32.03
.4202	22.537	43.546	.0887	262.8	38.37
.5106	18.717	30.033	.1069	351.2	39.95
.5718	14.957	19.180	.1337	424.8	40.66
.6915	4.768	1.949	.4194	755.8	41.26
.7074	3.385	.982	.5909	836.4	41.27
.7234	.825	.058	2.4229	1076.8	41.27
.7234	.192	.003	10.4229	1076.8	41.27
.7261	.087	.001	22.9943	1521.2	41.27
.7287	.044	.000	45.8514	2436.7	41.27
.7287	.012	.000	171.5657	2436.7	41.27

TABLE B-18

MERCURY POROSIMETER DETERMINATION OF PORE VOLUME, SURFACE AREA, AND PERMEABILITY

Sample Identification: Phenol-formaldehyde Char # P1

(1 - W/Wo) = 0.032 (2½ min at 385°C)

Sample weight, grams	.122
Bulk density, grams/cm^3	.701
Skeletal density, grams/cm^3	1.298
Fraction porosity	.459

PORE VOLUME, CM3/G	PORE DIAMETER, MICRONS	D2/16VT X10 TO+8, CM-1	2/D X10 TO-4, CM-1	SURFACE AREA, CM2/G	PERMEAB. X10 TO+8, CM2
.0000	182.292	3165.992	.0110	.0	.00
.0410	102.041	992.028	.0196	6.3	39.11
.0656	77.640	574.307	.0258	11.8	47.95
.0984	58.725	328.564	.0341	21.6	54.74
.1311	47.814	217.816	.0418	34.1	58.85
.1516	40.907	159.430	.0489	43.4	60.63
.2131	34.247	111.740	.0584	76.4	64.45
.2787	29.863	84.968	.0670	117.5	67.41
.3607	24.964	59.377	.0801	177.7	70.13
.4631	19.094	34.737	.1047	272.4	72.34
.4262	21.525	44.144	.0929	236.0	71.67
.5205	15.926	24.167	.1256	339.0	73.15
.6311	4.464	1.899	.4480	656.3	73.81
.6393	3.557	1.205	.5623	697.7	73.82
.6475	.829	.065	2.4137	819.7	73.82
.6516	.342	.011	5.8423	988.9	73.82
.6516	.146	.002	13.7257	988.9	73.82
.6557	.057	.000	34.9829	1987.0	73.82
.6557	.012	.000	171.5543	1987.0	73.82

TABLE B-19

MERCURY POROSIMETER DETERMINATION OF PORE VOLUME, SURFACE AREA, AND PERMEABILITY

Sample Identification: Phenol-formaldehyde Char #P-2

(1 - W/Wo) = 0.047 (4½ min. at 385°C)

Sample weight, grams	.130
Bulk density, grams/cm^3	.628
Skeletal density, grams/cm^3	1.220
Fraction porosity	.485

PORE VOLUME, CM3/G	PORE DIAMETER, MICRONS	D2/16VT X10 TO+8, CM-1	2/D X10 TO-4, CM-1	SURFACE AREA, CM2/G	PERMEAB. X10 TO+8, CM2
.0000	221.519	3967.550	.0090	.0	.00
.0615	135.240	1478.795	.0148	7.3	81.28
.0923	86.207	600.876	.0232	13.2	96.79
.1192	65.250	344.238	.0307	20.4	102.96
.1385	53.191	228.762	.0376	27.0	105.64
.2000	41.371	138.387	.0483	53.4	111.12
.2692	34.483	96.140	.0580	90.2	115.05
.3308	28.950	67.762	.0691	129.3	117.50
.4000	24.407	48.166	.0819	181.6	119.44
.4769	21.135	36.117	.0946	249.5	121.02
.5508	18.647	28.113	.1073	303.9	121.86
.6077	15.576	19.617	.1284	394.5	122.75
.7015	1.530	.189	1.3074	1499.0	123.49
.7692	.825	.055	2.4229	1642.5	123.49
.7092	.044	.000	45.8514	1642.5	123.49
.7751	.039	.000	51.5657	3515.9	123.49
.7731	.012	.000	171.5657	3515.9	123.49

TABLE B-20

MERCURY POROSIMETER DETERMINATION OF PORE VOLUME, SURFACE AREA, AND PERMEABILITY

Sample Identification: Phenol-formaldehyde Char #33

(1-W/Wo) = .0734 (15 min at 389°C)

Sample weight, grams	.088
Bulk density, grams/cm^3	.676
Skeletal density, grams/cm^3	1.220
Fraction porosity	.446

PORE VOLUME, CM3/G	PORE DIAMETER, MICRONS	D2/16VT X10 TO+8, CM-1	2/D X10 TO-4, CM-1	SURFACE AREA, CM2/G	PERMEAB. X10 TO+8, CM2
.0000	282.258	7555.919	.0071	.0	.00
.0227	182.292	3151.579	.0110	2.1	54.27
.0341	84.175	671.988	.0238	4.0	63.96
.0455	68.843	449.490	.0291	7.0	66.80
.0739	57.302	311.410	.0349	16.1	71.62
.0909	51.110	247.744	.0391	22.4	73.74
.1304	43.424	178.838	.0461	41.8	78.07
.1932	38.168	138.163	.0524	69.8	82.09
.2614	33.144	104.184	.0603	108.2	85.77
.3182	29.561	82.876	.0677	144.6	88.14
.4091	24.964	59.106	.0801	211.7	91.02
.4602	21.772	44.955	.0919	255.7	92.21
.5000	19.189	34.921	.1042	294.7	92.91
.5568	16.151	24.741	.1238	359.5	93.67
.6364	5.303	2.667	.3771	558.7	94.16
.6477	1.591	.240	1.2571	651.6	94.16
.6534	.426	.017	4.6971	820.7	94.16
.6534	.097	.001	20.6971	820.7	94.16
.6591	.058	.000	34.4114	2386.3	94.16
.6591	.012	.000	171.5543	2386.3	94.16

TABLE B-21

MERCURY POROSIMETER DETERMINATION OF PORE VOLUME, SURFACE AREA, AND PERMEABILITY

Sample Identification: Phenol-formaldehyde Char #65; (1-W/Wo) = 0.095; (2 min at 436°C)

Sample weight, grams	0.148
Bulk density, grams/cm^3	0.6371
Skeletal density, grams/cm^3	1.2003
Fraction porosity	0.4692

PORE VOLUME, CM3/G	PORE DIAMETER, MICRONS	D2/16VT X10 TO+8, CM-1	2/D X10 TO-4, CM-1	SURFACE AREA, CM2/G	PERMEAB. X10 TO+8, CM2
.0000	416.667	14732.782	.0048	.0	.00
.0135	143.914	1757.584	.0139	1.3	52.28
.0203	115.971	1141.313	.0172	2.3	56.87
.0270	96.048	782.865	.0208	3.6	59.92
.0372	74.754	474.221	.0268	6.0	62.91
.0405	64.386	351.791	.0311	7.0	63.57
.0541	56.379	269.737	.0355	11.5	65.54
.0777	49.688	209.510	.0403	20.4	68.20
.1216	44.081	164.893	.0454	39.2	72.05
.1892	39.503	132.427	.0506	71.7	76.77
.2635	34.757	102.514	.0575	111.9	80.86
.3784	28.548	69.161	.0701	185.2	85.49
.4122	28.067	66.851	.0713	209.0	86.57
.4662	25.907	56.955	.0772	249.2	88.14
.4966	23.966	48.742	.0835	273.6	88.89
.5338	21.672	39.856	.0923	306.2	89.66
.5608	20.290	34.935	.0986	332.0	90.14
.5811	19.022	30.705	.1051	352.7	90.45
.5946	17.986	27.451	.1112	367.3	90.64
.6115	16.816	23.996	.1189	386.7	90.84
.6216	15.311	19.893	.1306	399.4	90.94
.7095	4.300	1.569	.4651	661.0	91.39
.7196	1.530	.199	1.3074	750.9	91.39
.7230	1.054	.094	1.8971	805.0	91.39
.7264	.660	.037	3.0286	888.2	91.39
.7297	.342	.010	5.8514	1038.2	91.39
.7297	.116	.001	17.2800	1038.2	91.39
.7331	.035	.000	57.2800	2297.6	91.39
.7331	.032	.000	62.9943	2297.6	91.39
.7365	.029	.000	70.0800	4545.5	91.39
.7365	.012	.000	171.5657	4545.5	91.39

TABLE B-22

MERCURY POROSIMETER DETERMINATION OF PORE VOLUME, SURFACE AREA, AND PERMEABILITY

Sample Identification: Phenol-formaldehyde Char #66

(1-W/Wo) = 0.115; (5 min at 436°C)

Sample weight, grams	0.152
Bulk density, grams/cm^3	0.6227
Skeletal density, grams/cm^3	1.1959
Fraction porosity	0.4793

PORE VOLUME, CM3/G	PORE DIAMETER, MICRONS	D2/16VT X10 TO+8, CM-1	2/D X10 TO-4, CM-1	SURFACE AREA, CM2/G	PERMEAB. X10 TO+8, CM2
.0000	182.292	2698.312	.0110	.0	.00
.0329	114.007	1055.402	.0175	4.7	29.59
.0461	89.240	646.665	.0224	7.3	34.96
.0526	75.301	460.429	.0266	8.9	36.70
.0625	63.337	325.741	.0316	11.8	38.56
.0724	55.292	248.249	.0362	15.1	39.92
.0921	47.814	185.640	.0418	22.8	41.97
.2072	39.124	124.290	.0511	76.3	50.52
.2829	34.415	96.173	.0581	117.7	54.52
.4013	28.998	68.278	.0690	192.9	59.19
.4770	25.480	52.720	.0785	248.7	61.38
.5428	22.327	40.478	.0896	304.0	62.85
.5921	19.774	31.750	.1011	351.0	63.71
.6250	17.065	23.646	.1172	386.9	64.14
.6579	14.957	18.166	.1337	428.2	64.47
.7500	.324	.009	6.1714	3331.9	64.87
.7566	.170	.002	11.7714	3922.1	64.87
.7632	.087	.001	23.0857	5068.7	64.87
.7632	.058	.000	34.2857	5068.7	64.87
.7664	.049	.000	40.5714	6299.9	64.87
.7664	.022	.000	91.4286	6299.9	64.87
.7697	.019	.000	102.8571	9495.4	64.87
.7697	.012	.000	171.4286	9495.4	64.87

TABLE B-23

MERCURY POROSIMETER DETERMINATION OF PORE VOLUME, SURFACE AREA, AND PERMEABILITY

Sample Identification: Phenol-formaldehyde Char #67

(1-W/Wo) = 0.133; (10 min. at 436°C)

Sample weight, grams	0.1755
Bulk density, grams/cm^3	0.6424
Skeletal density, grams/cm^3	1.1923
Fraction porosity	0.4612

PORE VOLUME, CM3/G	PORE DIAMETER, MICRONS	D2/16VT X10 TO+8, CM-1	2/D X10 TO-4, CM-1	SURFACE AREA, CM2/G	PERMEAB. X10 TO+8, CM2
.0000	190.217	3150.043	.0105	.0	.00
.0114	125.358	1368.111	.0160	1.5	11.87
.0171	82.586	593.786	.0242	2.7	14.45
.0228	69.389	419.181	.0288	4.2	15.78
.0342	57.040	283.258	.0351	7.8	17.63
.0513	50.186	219.275	.0399	14.2	19.61
.0769	45.776	182.425	.0437	24.9	21.98
.1254	39.503	135.858	.0506	47.8	25.54
.2336	33.686	98.792	.0594	107.3	31.40
.2906	30.648	81.775	.0653	142.8	33.77
.3362	28.595	71.185	.0699	173.6	35.38
.3875	26.515	61.207	.0754	210.9	36.94
.4387	24.289	51.360	.0823	251.4	38.27
.4766	22.321	43.377	.0896	285.6	39.15
.5242	20.115	35.225	.0994	328.7	39.97
.5470	18.837	30.893	.1062	352.2	40.32
.5698	15.880	21.955	.1259	378.6	40.60
.6066	14.957	19.477	.1337	426.7	40.95
.7009	2.624	.599	.7623	847.9	41.39
.7066	1.526	.203	1.3109	907.0	41.39
.7094	.342	.010	5.8514	1009.0	41.39
.7094	.192	.003	10.4229	1009.0	41.39
.7123	.173	.003	11.5314	1321.7	41.39
.7123	.087	.001	22.9943	1321.7	41.39
.7151	.048	.000	41.2800	2237.3	41.39
.7179	.038	.000	52.4800	3572.9	41.39
.7179	.012	.000	171.5657	3572.9	41.39

TABLE B-24

MERCURY POROSIMETER DETERMINATION OF PORE VOLUME, SURFACE AREA, AND PERMEABILITY

Sample Identification: Phenol-formaldehyde Char #69

(1 - W/Wo) = 0.158; (41 min. at 436°C)

Sample weight, grams	0.1210
Bulk density, grams/cm^3	0.6247
Skeletal density, grams/cm^3	1.1898
Fraction porosity	0.4750

PORE VOLUME, CM3/G	PORE DIAMETER, MICRONS	D2/16VT X10 TO+8, CM-1	2/D X10 TO-4, CM-1	SURFACE AREA, CM2/G	PERMEAB. X10 TO+8, CM2
.0000	291.667	6993.082	.0069	.0	.00
.0165	175.000	2517.509	.0114	1.5	37.33
.0248	116.667	1118.893	.0171	2.7	44.47
.0331	88.384	642.156	.0226	4.3	47.93
.0496	57.377	270.627	.0349	9.1	51.51
.0744	46.419	177.128	.0431	18.7	54.15
.1818	43.323	133.657	.0496	68.5	62.08
.2562	36.008	106.586	.0555	107.6	66.32
.3471	31.646	82.323	.0632	161.6	70.40
.4050	28.548	66.996	.0701	200.2	72.45
.4628	26.080	55.915	.0767	242.6	74.14
.4959	24.272	48.428	.0824	268.9	74.96
.5455	22.350	41.063	.0895	311.5	76.02
.5765	20.833	35.679	.0960	342.2	76.62
.6116	18.421	27.895	.1086	376.0	77.12
.6446	17.123	24.103	.1168	413.2	77.53
.7438	2.814	.651	.7109	823.7	78.11
.7479	.352	.010	5.6800	955.7	78.11
.7521	.289	.007	6.9257	1216.1	78.11
.7562	.070	.000	28.6857	1951.9	78.11
.7603	.038	.000	52.4571	3628.4	78.11
.7603	.012	.000	171.5429	3628.4	78.11

TABLE B-25

MERCURY POROSIMETER DETERMINATION OF PORE VOLUME, SURFACE AREA, AND PERMEABILITY

Sample Identification: Phenol-formaldehyde Char #70

(1-W/Wo) = 0.172; (90 min. at 436°C)

Sample weight, grams	.1185
Bulk density, grams/cm^3	.623
Skeletal density, grams/cm^3	1.234
Fraction porosity	.484

PORE VOLUME, CM3/G	PORE DIAMETER, MICRONS	D2/16VT X10 TO+8, CM-1	2/D X10 TO-4, CM-1	SURFACE AREA, CM2/G	PERMEAB. X10 TO+8, CM2
.0000	339.147	9065.328	.0059	.0	.00
.0084	162.187	2073.194	.0123	.8	22.75
.0506	86.462	589.199	.0231	8.3	49.93
.0970	55.520	242.946	.0360	22.0	59.28
.3038	37.634	111.629	.0531	114.2	77.02
.5063	28.090	62.188	.0712	240.1	85.54
.6076	22.096	38.480	.0905	322.0	88.01
.6582	18.229	26.190	.1097	372.6	88.80
.7089	15.432	18.770	.1296	433.2	89.35
.7679	4.442	1.555	.4503	604.5	89.64
.7764	3.405	.914	.5874	648.3	89.65
.7848	1.571	.194	1.2731	726.8	89.65
.7932	.342	.009	5.8514	1027.4	89.65
.7932	.012	.000	171.5657	1027.4	89.65

TABLE B-26

MERCURY POROSIMETER DETERMINATION OF PORE VOLUME, SURFACE AREA, AND PERMEABILITY

Sample Identification: Phenol-formaldehyde Char #71

(1-W/Wo) = 0.259; (1 min. at 571°C)

Sample weight, grams	0.1900
Bulk density, grams/cm^3	0.6530
Skeletal density, grams/cm^3	1.2125
Fraction porosity	0.4610

PORE VOLUME, CM3/G	PORE DIAMETER, MICRONS	D2/16VT X10 TO+8, CM-1	2/D X10 TO-4, CM-1	SURFACE AREA, CM2/G	PERMEAB. X10 TO+8, CM2
.0000	546.375	26502.221	.0037	.0	.00
.0158	153.644	2091.870	.0130	1.3	104.07
.0211	107.891	1031.527	.0185	2.1	107.86
.0316	83.413	616.554	.0240	4.4	111.86
.0368	64.552	369.252	.0310	5.8	113.05
.0526	55.911	277.009	.0358	11.1	115.40
.3421	38.168	129.095	.0524	138.7	142.50
.4447	32.181	91.771	.0621	197.5	147.72
.5053	27.822	68.593	.0719	238.1	149.96
.5368	24.579	53.533	.0814	262.3	150.85
.5684	22.013	42.939	.0909	289.5	151.55
.5947	19.663	34.261	.1017	314.8	152.02
.6105	17.766	27.971	.1126	331.7	152.25
.6395	14.957	19.825	.1337	367.4	152.57
.0842	4.197	1.561	.4766	503.9	152.79
.6895	2.931	.761	.6823	534.4	152.79
.6947	1.868	.309	1.0709	580.5	152.79
.6947	.483	.021	4.1371	580.5	152.79
.6974	.385	.013	5.2000	703.4	152.79
.6974	.214	.004	9.3371	703.4	152.79
.7000	.194	.003	10.3086	961.9	152.79
.7000	.116	.001	17.2800	961.9	152.79
.7026	.084	.001	23.9086	1503.8	152.79
.7026	.070	.000	28.7086	1503.8	152.79
.7053	.058	.000	34.6514	2337.5	152.79
.7053	.012	.000	171.5657	2337.5	152.79

TABLE B-27

MERCURY POROSIMETER DETERMINATION OF PORE VOLUME, SURFACE AREA, AND PERMEABILITY

Sample Identification: Phenol-formaldehyde Char #72

(1 - W/Wo) = 0.302; (3 min. at 571°C)

Sample weight, grams	.1515
Bulk density, grams/cm^3	.659
Skeletal density, grams/cm^3	1.680
Fraction porosity	.609

PORE VOLUME, CM3/G	PORE DIAMETER, MICRONS	D2/16VT X10 TO+8, CM-1	2/D X10 TO-4, CM-1	SURFACE AREA, CM2/G	PERMEAB. X10 TO+8, CM2
.0000	233.333	3682.660	.0086	.0	.00
.0132	126.537	1083.028	.0158	1.6	19.16
.0264	81.699	451.487	.0245	4.3	25.33
.0462	62.927	267.844	.0318	9.8	29.66
.1584	47.425	152.136	.0422	51.3	44.01
.3234	35.971	87.522	.0556	132.0	56.06
.4224	29.362	58.317	.0681	193.2	60.45
.4950	24.221	39.683	.0826	247.9	62.62
.5413	20.420	28.205	.0979	289.7	63.57
.5677	18.154	22.291	.1102	317.1	63.98
.6007	15.331	15.898	.1305	356.8	64.36
.6601	5.193	1.824	.3851	510.0	64.68
.7591	1.562	.165	1.2800	1334.3	64.74
.7921	.709	.034	2.8229	2011.4	64.75
.7921	.116	.001	17.2800	2011.4	64.75
.8581	.057	.000	34.9943	19263.6	64.75
.8581	.044	.000	45.8514	19263.6	64.75
.8911	.029	.000	68.7086	38167.9	64.75
.9241	.014	.000	141.8514	72913.7	64.75
.9241	.012	.000	171.5657	72913.7	64.75

TABLE B-28

MERCURY POROSIMETER DETERMINATION OF PORE VOLUME, SURFACE AREA, AND PERMEABILITY

Sample Identification: Phenol-formaldehyde Char #73

(1 - W/Wo) = 0.320; (8 min. - 571°C)

Sample weight, grams	0.1948
Bulk density, grams/cm^3	0.7010
Skeletal density, grams/cm^3	1.3261
Fraction porosity	0.4714

PORE VOLUME, CM3/G	PORE DIAMETER, MICRONS	D2/16VT X10 TO+8, CM-1	2/D X10 TO-4, CM-1	SURFACE AREA, CM2/G	PERMEAB. X10 TO+8, CM2
.0000	261.194	6340.364	.0077	.0	.00
.0154	182.432	3094.757	.0110	1.4	34.25
.0205	118.084	1295.888	.0169	2.1	39.56
.0231	98.370	899.315	.0203	2.6	40.89
.0359	72.584	489.632	.0276	5.7	45.09
.3234	48.679	220.225	.0411	104.4	93.19
.4415	39.150	142.446	.0511	158.8	103.28
.4625	34.385	111.164	.0578	181.1	105.74
.5133	30.435	86.085	.0657	200.2	107.17
.5390	28.000	72.862	.0714	217.8	108.13
.5547	24.646	56.461	.0811	237.3	108.91
.5652	22.293	46.188	.0897	254.9	109.41
.5903	20.735	39.956	.0965	259.7	109.51
.6006	19.063	33.774	.1049	270.0	109.69
.6057	17.748	29.276	.1127	275.6	109.77
.6109	16.463	25.188	.1215	281.6	109.83
.6160	14.957	20.792	.1337	288.2	109.89
.6468	2.705	.680	.7394	422.6	110.05
.6520	.825	.063	2.4229	503.8	110.05
.6571	.344	.011	5.8057	715.0	110.05
.6622	.031	.000	64.1371	2510.2	110.05
.6648	.020	.000	97.9657	4590.6	110.05
.6674	.019	.000	103.1086	7171.1	110.05
.6725	.012	.000	169.2800	14162.6	110.05
.6725	.012	.000	171.5657	14162.6	110.05

TABLE B-29

MERCURY POROSIMETER DETERMINATION OF PORE VOLUME, SURFACE AREA, AND PERMEABILITY

Sample Identification: Phenol-formaldehyde Char #74

(1 - W/Wo) = .329; (16 min at 571°C)

Sample weight, grams	0.146
Bulk density, grams/cm^3	.673
Skeletal density, grams/cm^3	1.297
Fraction porosity	.482

PORE VOLUME, CM3/G	PORE DIAMETER, MICRONS	D2/16VT X10 TO+8, CM-1	2/D X10 TO-4, CM-1	SURFACE AREA, CM2/G	PERMEAB. X10 TO+8, CM2
.0000	307.018	8230.857	.0065	.0	.00
.0137	162.639	2309.778	.0123	1.3	34.80
.0265	107.428	1007.749	.0186	2.3	40.27
.0542	76.586	512.180	.0261	5.4	45.29
.0548	61.533	330.625	.0325	11.4	49.47
.1644	46.667	190.166	.0429	52.7	63.22
.3002	38.846	131.767	.0515	120.6	74.38
.4178	32.022	89.539	.0625	183.0	80.23
.4795	27.778	67.377	.0720	224.5	82.56
.5274	23.793	49.434	.0841	261.9	83.91
.5479	21.793	41.473	.0918	279.9	84.36
.5753	19.252	32.364	.1039	306.7	84.84
.6027	16.572	23.981	.1207	337.5	85.22
.6164	15.351	20.577	.1303	354.7	85.36
.6849	4.442	1.723	.4503	553.5	85.73
.6849	2.850	.709	.7017	553.5	85.73
.6918	1.516	.201	1.3189	622.7	85.73
.6918	.426	.016	4.6971	622.7	85.73
.6966	.346	.010	5.7829	981.6	85.73
.6966	.039	.000	51.5543	981.6	85.73
.7055	.032	.000	62.9829	4904.1	85.73
.7069	.019	.000	102.9829	7746.0	85.73
.7123	.017	.000	114.4114	11468.5	85.73
.7158	.012	.000	171.5543	16365.2	85.73

TABLE B-30

MERCURY POROSIMETER DETERMINATION OF PORE VOLUME, SURFACE AREA, AND PERMEABILITY

Sample Identification: Phenol-formaldehyde Char #75

(1 - W/Wo) = .340; (32 min. at 571°C)

Sample weight, grams	.1360
Bulk density, grams/cm^3	.677
Skeletal density, grams/cm^3	1.220
Fraction porosity	.445

PORE VOLUME, CM3/G	PORE DIAMETER, MICRONS	D2/16VT X10 TO+8, CM-1	2/D X10 TO-4, CM-1	SURFACE AREA, CM2/G	PERMEAB. X10 TO+8, CM2
.0000	579.470	31894.539	.0035	.0	.00
.0294	176.569	2961.985	.0113	2.2	228.11
.0551	82.547	647.230	.0242	6.7	248.77
.0772	55.644	294.096	.0359	13.4	253.39
.2132	40.491	155.726	.0494	71.4	267.01
.3713	29.561	83.002	.0677	163.9	275.40
.4743	22.422	47.751	.0892	244.7	278.40
.5551	15.597	23.107	.1282	332.6	279.67
.6267	7.511	5.358	.2663	477.7	280.14
.6434	3.263	1.024	.6091	542.0	280.16
.6507	.828	.065	2.4149	653.2	280.16
.6581	.173	.003	11.5543	1166.8	280.16
.6581	.012	.000	171.5543	1166.8	280.16

TABLE B-31

MERCURY POROSIMETER DETERMINATION OF PORE VOLUME, SURFACE AREA, AND PERMEABILITY

Sample Identification: Phenol-formaldehyde Char #76

(1 - W/Wo) = .345; (70 min. at 571°C)

Sample weight, grams	.137
Bulk density, grams/cm^3	.678
Skeletal density, grams/cm^3	1.278
Fraction porosity	.470

PORE VOLUME, CM3/G	PORE DIAMETER, MICRONS	D2/16VT X10 TO+8, CM-1	2/D X10 TO-4, CM-1	SURFACE AREA, CM2/G	PERMEAB. X10 TO+8, CM2
.0000	237.772	5098.79:	.0084	.0	.00
.0292	105.932	1012.052	.0189	4.0	41.93
.0657	56.180	284.647	.0356	13.9	53.05
.3358	31.250	88.074	.0640	148.4	76.71
.4818	25.399	58.181	.0787	252.6	81.72
.5401	20.612	38.318	.0970	303.9	83.05
.5839	17.310	27.022	.1155	350.5	83.72
.6058	15.453	21.535	.1294	377.3	83.97
.6715	5.556	2.784	.3600	538.1	84.34
.6788	4.207	1.596	.4754	568.6	84.35
.6861	1.454	.186	1.3943	636.8	84.36
.6861	.192	.003	10.4229	636.8	84.36
.6934	.058	.000	34.4229	2273.5	84.36
.6934	.012	.000	171.5657	2273.5	84.36

TABLE B-32

MERCURY POROSIMETER DETERMINATION OF PORE VOLUME, SURFACE AREA, AND PERMEABILITY

Sample Identification: Phenol-formaldehyde Char #77

(1 - W/Wo) = 0.372; (2 min. at 666°C)

Sample weight, grams	.1180
Bulk density, grams/cm^3	.620
Skeletal density, grams/cm^3	1.322
Fraction porosity	.469

PORE VOLUME, CM3/G	PORE DIAMETER, MICRONS	D2/16VT X10 TO+8, CM-1	2/D X10 TO-4, CM-1	SURFACE AREA, CM2/G	PERMEAB. X10 TO+8, CM2
.0000	223.785	4140.195	.0089	.0	.00
.0678	122.378	1238.118	.0163	8.6	85.51
.1186	73.529	446.972	.0272	19.6	105.60
.1864	50.872	213.953	.0393	42.2	116.11
.4492	34.861	100.458	.0574	169.2	135.48
.5763	27.822	63.993	.0719	251.3	140.38
.6441	22.698	42.592	.0881	305.6	142.07
.6949	19.551	31.537	.1024	354.0	142.96
.7203	16.900	23.612	.1183	382.1	143.29
.7575	15.331	19.430	.1305	403.2	143.46
.8136	5.892	2.870	.3394	582.4	143.86
.8220	2.931	.710	.6823	625.6	143.86
.8305	1.462	.177	1.3680	712.5	143.86
.8390	.174	.003	11.4743	1256.7	143.87
.8390	.087	.001	22.9943	1256.7	143.87
.8475	.035	.000	57.2800	4658.1	143.87
.8475	.017	.000	114.4229	4658.1	143.87
.8559	.014	.000	144.7086	15638.3	143.87
.8559	.012	.000	171.5657	15638.3	143.87

TABLE B-33

MERCURY POROSIMETER DETERMINATION OF PORE VOLUME, SURFACE AREA, AND PERMEABILITY

Sample Identification: Phenol-formaldehyde Char #78

(1 - W/Wo) = .376; (4 min. at 666°C)

Sample weight, grams	.102
Bulk density, grams/cm^3	.560
Skeletal density, grams/cm^3	1.240
Fraction porosity	.548

PORE VOLUME, CM3/G	PORE DIAMETER, MICRONS	D2/16VT X10 TO+8, CM-1	2/D X10 TO-4, CM-1	SURFACE AREA, CM2/G	PERMEAB. X10 TO+8, CM2
.0000	96.899	598.818	.0206	.0	.00
.1176	56.452	203.239	.0354	33.0	25.85
.2745	38.210	93.111	.0523	101.8	38.59
.4510	28.974	53.537	.0690	208.9	45.68
.6275	22.996	33.726	.0870	346.6	49.90
.7451	18.479	21.779	.1082	461.4	51.69
.8157	15.453	15.228	.1294	542.9	52.39
.9412	5.556	1.968	.3600	854.8	52.99
.9608	3.199	.653	.6251	951.4	53.00
.9706	1.080	.074	1.8514	1072.8	53.00
.9755	.603	.028	3.0171	1192.1	53.00
.9755	.425	.012	4.7086	1192.1	53.00
.9804	.249	.004	8.0229	1504.2	53.00
.9804	.012	.000	171.5657	1504.2	53.00

TABLE B-34

MERCURY POROSIMETER DETERMINATION OF PORE VOLUME, SURFACE AREA, AND PERMEABILITY

Sample Identification: Phenol-formaldehyde Char #79

(1 - W/Wo) = .378; (8 min. at 666°C)

Sample weight, grams	.1230
Bulk density, grams/cm^3	.597
Skeletal density, grams/cm^3	1.292
Fraction porosity	.539

PORE VOLUME, CM3/G	PORE DIAMETER, MICRONS	D2/16VT X10 TO+8, CM-1	2/D X10 TO-4, CM-1	SURFACE AREA, CM2/G	PERMEAB. X10 TO+8, CM2
.0000	230.263	3672.230	.0087	.0	.00
.1057	129.630	1163.830	.0154	12.7	137.75
.1870	73.222	371.331	.0273	30.1	171.39
.2520	47.425	155.777	.0422	52.7	180.62
.3659	28.455	56.080	.0703	116.7	187.12
.5285	25.811	46.142	.0775	236.9	191.60
.6504	20.290	28.513	.0986	344.2	194.06
.7256	17.073	20.189	.1171	423.1	195.02
.7724	14.957	15.495	.1337	484.3	195.49
.8862	4.768	1.575	.4194	799.1	196.01
.9024	2.747	.523	.7280	892.4	196.02
.9024	.012	.000	171.5657	892.4	196.02

TABLE B-35

MERCURY POROSIMETER DETERMINATION OF PORE VOLUME, SURFACE AREA, AND PERMEABILITY

Sample Identification: Phenol-formaldehyde Char #80

(1 - W/Wo) = .382; (16 min. at 666°C)

Sample weight, grams	.129
Bulk density, grams/cm^3	.679
Skeletal density, grams/cm^3	1.314
Fraction porosity	.484

PORE VOLUME, CM3/G	PORE DIAMETER, MICRONS	D2/16VT X10 TO+8, CM-1	2/D X10 TO-4, CM-1	SURFACE AREA, CM2/G	PERMEAB. X10 TO+8, CM2
.0000	226.460	4575.189	.0088	.0	.00
.0543	104.979	966.041	.0191	7.5	72.77
.1085	61.169	328.197	.0327	21.6	89.76
.2481	39.663	139.296	.0502	79.4	105.55
.4341	28.926	73.343	.0691	190.4	115.12
.5116	22.379	43.899	.0894	251.8	117.32
.5736	18.207	29.251	.1095	313.5	118.42
.6124	15.535	21.155	.1287	359.6	118.89
.6899	4.226	1.565	.4733	593.0	119.32
.6977	2.384	.498	.8389	643.9	119.32
.7054	1.509	.200	1.3257	727.8	119.32
.7132	.426	.016	4.6971	961.2	119.32
.7132	.012	.000	171.5543	961.2	119.32

TABLE B-36

MERCURY POROSIMETER DETERMINATION OF PORE VOLUME, SURFACE AREA, AND PERMEABILITY

Sample Identification: Phenol-formaldehyde **Phenolic Char #81**

(1 - W/Wo) = 0.388; (32 min. at 666°C)

Sample weight, grams	0.1519
Bulk density, grams/cm^3	0.7802
Skeletal density, grams/cm^3	1.514
Fraction porosity	.515

PORE VOLUME, CM3/G	PORE DIAME R, MICRONS	D2/16VT X10 TO+8, CM-1	2/D X10 TO-4, CM-1	SURFACE AREA, CM2/G	PERMEAB. X10 TO+8, CM2
.0000	266.656	4298.879	.0097	.0	.00
.0529	126.720	1613.275	.0158	4.2	50.11
.0527	97.222	949.622	.0206	7.8	63.15
.0692	73.933	549.161	.0271	11.7	69.50
.1440	52.063	272.532	.0384	36.5	85.52
.2107	39.503	156.779	.0506	65.8	92.79
.3016	28.926	84.059	.0691	168.3	103.41
.4042	23.360	54.918	.0855	224.3	106.00
.4672	20.444	41.990	.0978	254.5	106.82
.5201	17.199	29.719	.1163	289.7	107.43
.5552	15.494	24.117	.1291	305.9	107.61
.6168	1.443	.209	1.3863	954.3	108.15
.6221	.044	.000	45.9543	1733.5	108.15
.6221	.012	.000	171.5657	1733.5	108.15

TABLE B-37

MERCURY POROSIMETER DETERMINATION OF PORE VOLUME, SURFACE AREA, AND PERMEABILITY

Sample Identification: Phenol-formaldehyde Char #83

(1 - W/Wo) = 0.213; (2 min. at 533°C)

Sample weight, grams	.129
Bulk density, grams/cm^3	.678
Skeletal density, grams/cm^3	1.320
Fraction porosity	.486

PORE VOLUME, CM3/G	PORE DIAMETER, MICRONS	D2/16VT X10 TO+8, CM-1	2/D X10 TO-4, CM-1	SURFACE AREA, CM2/G	PERMEAB. X10 TO+8, CM2
.0000	233.333	4745.854	.0086	.0	.00
.0233	124.202	1344.668	.0161	2.9	34.42
.0543	84.094	616.443	.0238	9.1	49.20
.1434	54.062	254.772	.0370	36.1	68.07
.3721	38.210	127.264	.0523	138.3	89.30
.4805	30.702	82.165	.0651	202.0	94.82
.5426	25.849	58.245	.0774	246.2	96.94
.5969	20.673	37.255	.0967	293.5	98.20
.6279	16.966	25.090	.1179	326.8	98.67
.6395	15.503	20.951	.1290	341.1	98.80
.6977	4.442	1.720	.4503	509.5	99.12
.7054	1.571	.215	1.2731	576.3	99.12
.7152	.435	.016	4.5989	803.9	99.12
.7132	.044	.000	45.8400	803.9	99.12
.7171	.025	.000	80.1257	3245.1	99.12
.7171	.012	.000	171.5543	3245.1	99.12

TABLE B-38

MERCURY POROSIMETER DETERMINATION OF PORE VOLUME, SURFACE AREA, AND PERMEABILITY

Sample Identification: Phenol-formaldehyde Char #84

(1 - W/Wo) = .260; (10 min. at 533°C)

Sample weight, grams	.141
Bulk density, grams/cm^3	.641
Skeletal density, grams/cm^3	1.160
Fraction porosity	.452

PORE VOLUME, CM3/G	PORE DIAMETER, MICRONS	D2/16VT X10 TO+8, CM-1	2/D X10 TO-4, CM-1	SURFACE AREA, CM2/G	PERMEAB. X10 TO+8, CM2
.0000	413.712	15152.025	.0048	.0	.00
.0213	156.802	2232.483	.0126	1.9	83.59
.0355	84.210	627.856	.0237	4.4	92.76
.0709	54.945	267.259	.0364	15.1	99.94
.3830	33.207	97.618	.0602	165.9	125.67
.4965	25.234	56.371	.0793	245.0	129.62
.5562	20.673	37.835	.0967	294.9	130.83
.6176	15.391	20.972	.1299	367.3	131.67
.6773	5.556	2.732	.3600	515.0	132.00
.6879	3.528	1.102	.5669	564.3	132.01
.6950	1.434	.182	1.3943	633.8	132.01
.7021	.173	.003	11.5657	1093.4	132.01
.7057	.035	.000	57.2800	2314.0	132.01
.7057	.012	.000	171.5657	2314.0	132.01

TABLE B-39

MERCURY POROSIMETER DETERMINATION OF PORE VOLUME, SURFACE AREA, AND PERMEABILITY

Sample Identification: Phenol-formaldehyde Char #85

(1 - W/Wo) = .282; (30 min. at 533°C)

Sample weight, grams	.128
Bulk density, grams/cm^3	.660
Skeletal density, grams/cm^3	1.205
Fraction porosity	.454

PORE VOLUME, CM3/G	PORE DIAMETER, MICRONS	D2/16VT X10 TO+8, CM-1	2/D X10 TO-4, CM-1	SURFACE AREA, CM2/G	PERMEAB. X10 TO+8, CM2
.0000	372.340	12612.572	.0054	.0	.00
.0156	228.460	47[illegible].340	.0088	1.1	61.58
.0313	155.971	2213.164	.0128	2.8	86.27
.0469	88.923	719.365	.0225	5.5	96.67
.0859	58.824	314.793	.0340	16.6	105.84
.2168	40.696	159.682	.0491	71.8	119.87
.3672	31.503	90.286	.0635	155.4	127.99
.4531	25.622	59.725	.0781	216.2	130.92
.5204	21.097	40.492	.0948	277.0	132.52
.5625	17.006	28.199	.1136	317.7	133.13
.5859	15.660	22.310	.1277	346.0	133.40
.6563	5.102	2.368	.3920	528.7	133.79
.6719	3.550	1.146	.5634	603.3	133.80
.6719	.829	.063	2.4114	603.3	133.80
.6797	.342	.011	5.8400	925.6	133.80
.6797	.116	.001	17.2686	925.6	133.80
.6875	.039	.000	51.5543	3614.0	133.80
.6875	.012	.000	171.5543	3614.0	133.80

TABLE B-40

MERCURY POROSIMETER DETERMINATION OF PORE VOLUME, SURFACE AREA, AND PERMEABILITY

Sample Identification: Phenol-formaldehyde Char #86

(1 - W/Wo) = .291; (60 min. at 533°C)

Sample weight, grams	.110
Bulk density, grams/cm^3	.603
Skeletal density, grams/cm^3	1.132
Fraction porosity	.466

PORE VOLUME, CM3/G	PORE DIAMETER, MICRONS	D2/16VT X10 TO+8, CM-1	2/D X10 TO-4, CM-1	SURFACE AREA, CM2/G	PERMEAB. X10 TO+8, CM2
.0000	300.172	7294.604	.0067	.0	.00
.0136	167.946	2283.512	.0119	1.3	30.43
.0364	84.337	575.841	.0237	5.3	45.57
.1727	50.215	204.142	.0398	48.6	70.36
.4273	32.895	87.602	.0608	176.7	87.66
.5273	26.475	56.746	.0755	244.9	91.02
.5909	20.933	35.475	.0955	299.3	92.39
.6273	17.713	25.399	.1129	337.2	92.91
.6500	15.712	19.986	.1273	364.5	93.15
.7318	4.453	1.605	.4491	600.3	93.56
.7364	2.722	.600	.7349	627.2	93.56
.7455	1.505	.183	1.3291	721.1	93.56
.7455	.216	.004	9.2720	721.1	93.56
.7545	.083	.001	24.1257	2239.1	93.56
.7545	.035	.000	57.2686	2239.1	93.56
.7636	.020	.000	99.5543	9367.5	93.56
.7727	.014	.000	145.2686	20495.8	93.56
.7727	.012	.000	171.5543	20495.8	93.56

TABLE B-41 - MAGNITUDE OF DIFFUSIVITIES

			D $\frac{cm^2}{sec}$	Ref.
Gases:				
1)	327°C	CO_2 in Air	0.555	Sherwood & Reid (39)
2)	300°C	H_2O in Air	0.849	
Liquids:				
1)	18°C	CO_2 in Water	1.71×10^{-5}	Sherwood & Reid (39)
2)	25°C	H_2 in Water	3.36×10^{-5}	
3)	25°C	O_2 in Water	2.60×10^{-5}	
4)	22°C	N_2 in Water	2.02×10^{-5}	
5)	15°C	Phenol in Methanol	1.40×10^{-5}	
Solids:				
1)	350°C	Na in NaCl	7×10^{-13}	Shewmon (47)
	400°C		1.5×10^{-12}	
	500°C		9×10^{-12}	
2)	800°C	Fe in FeO	8×10^{-9}	
3)	1000°C	C in Austenite	$2.7\text{-}7.8 \times 10^{-7}$	American Soc. Metals (1)
4)	800°C	Nitrogen in α-Iron	7.3×10^{-7}	
5)	1100°C	Oxygen in γ-Iron	1×10^{-9}	
6)	1050°C	Hydrogen in γ-Iron	1.6×10^{-4}	

APPENDIX C

COMPUTER PROGRAMS

The computer programs which follow were used to perform the majority of calculations and data processing which were necessary for this investigation. A short description, flow chart and print out of the source deck are presented for each program.

° COMPUTER PROGRAM HRI65R002 °

CALCULATION OF RATE AND TRANSPORT CONSTANTS FROM EXPERIMENTAL DATA

The purpose of the program is to calculate the best values of the kinetic constants (λ's) and transport constants (α's) from experimental data.

The working equations consist of: (V-46), (V-51), (V-55), (V-58), (VIII-2), (VIII-3 to VIII-8 incl.), and

$$Y_1,\ Y_2,\ Y_3,\ Y_4 = \left(\frac{Wox}{Wo}\right)_g, \left(\frac{Wc}{Wo}\right)_g, \left(\frac{W_H}{Wo}\right)_g,$$

(1-W/Wo) respectively.

$$F\delta = \left(\frac{Y_{calc}}{Y_{exptl}} - 1\right)$$

$$\overline{F\delta} = \frac{1}{m}\sum_{1}^{m}|F\delta|$$

$$\delta^2 = (F\delta)^2$$

The input consists of:

1) $Y_1,\ Y_2,\ Y_3,\ Y_4$ vs. θ
2) The constants, $(^nSRO/Wo)$, (n_o/Wo), λ_o, α_o
3) First approximations of λ_1, λ_2, λ_5 and α_1, α_2, and α_3.
4) Coarse mesh increments of λ_1, λ_2, λ_5. and the number of mesh points. The same for α's.
5) Medium mesh increments and number of mesh points.
6) Fine mesh increments and number of mesh points.

The calculational procedure consists of searching for the best fit of the function by "narrowing down" from a coarse to a fine mesh of values, starting with certain first approximations. See also Appendix D.

The computer program follows.

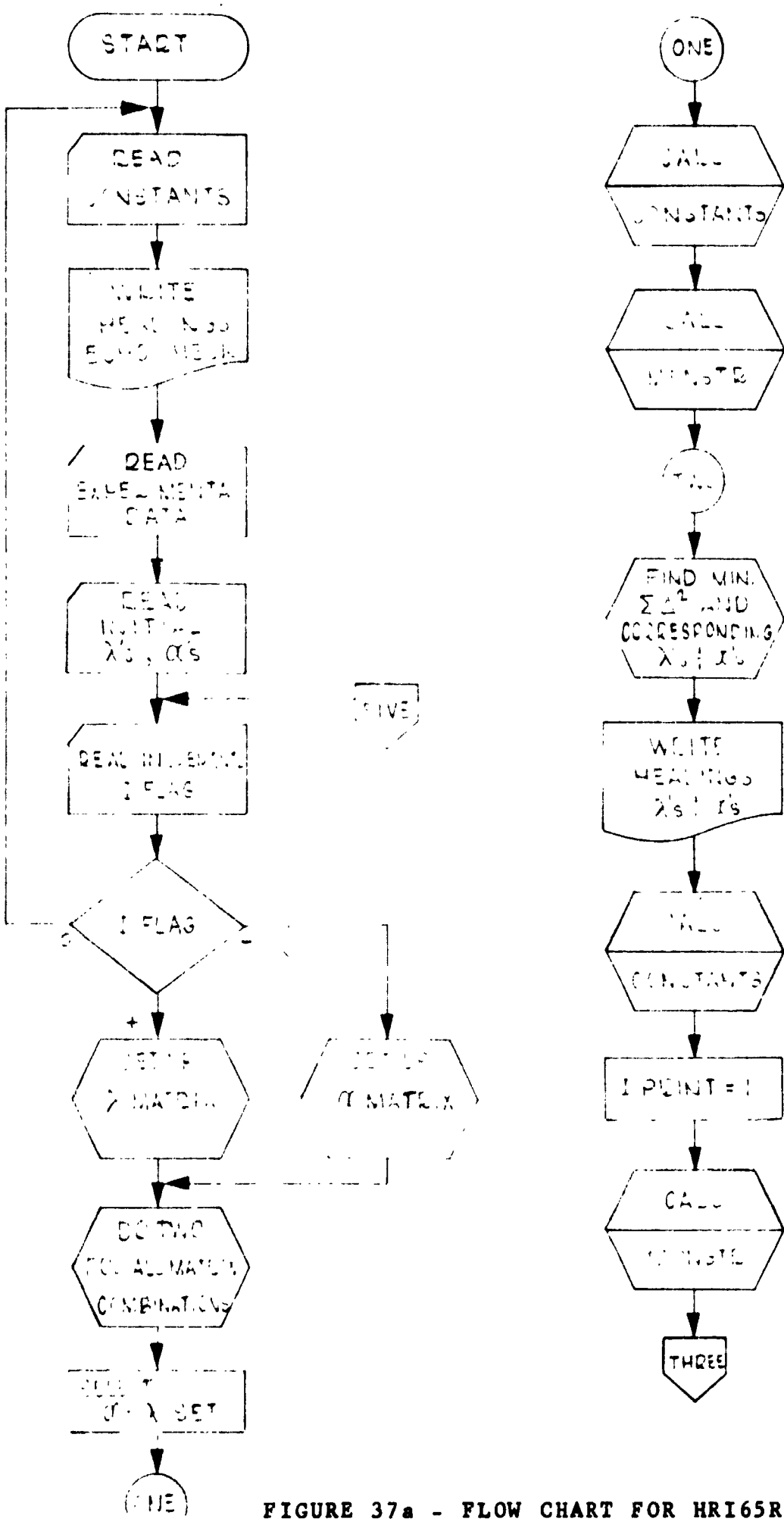

FIGURE 37a - FLOW CHART FOR HRI65R002

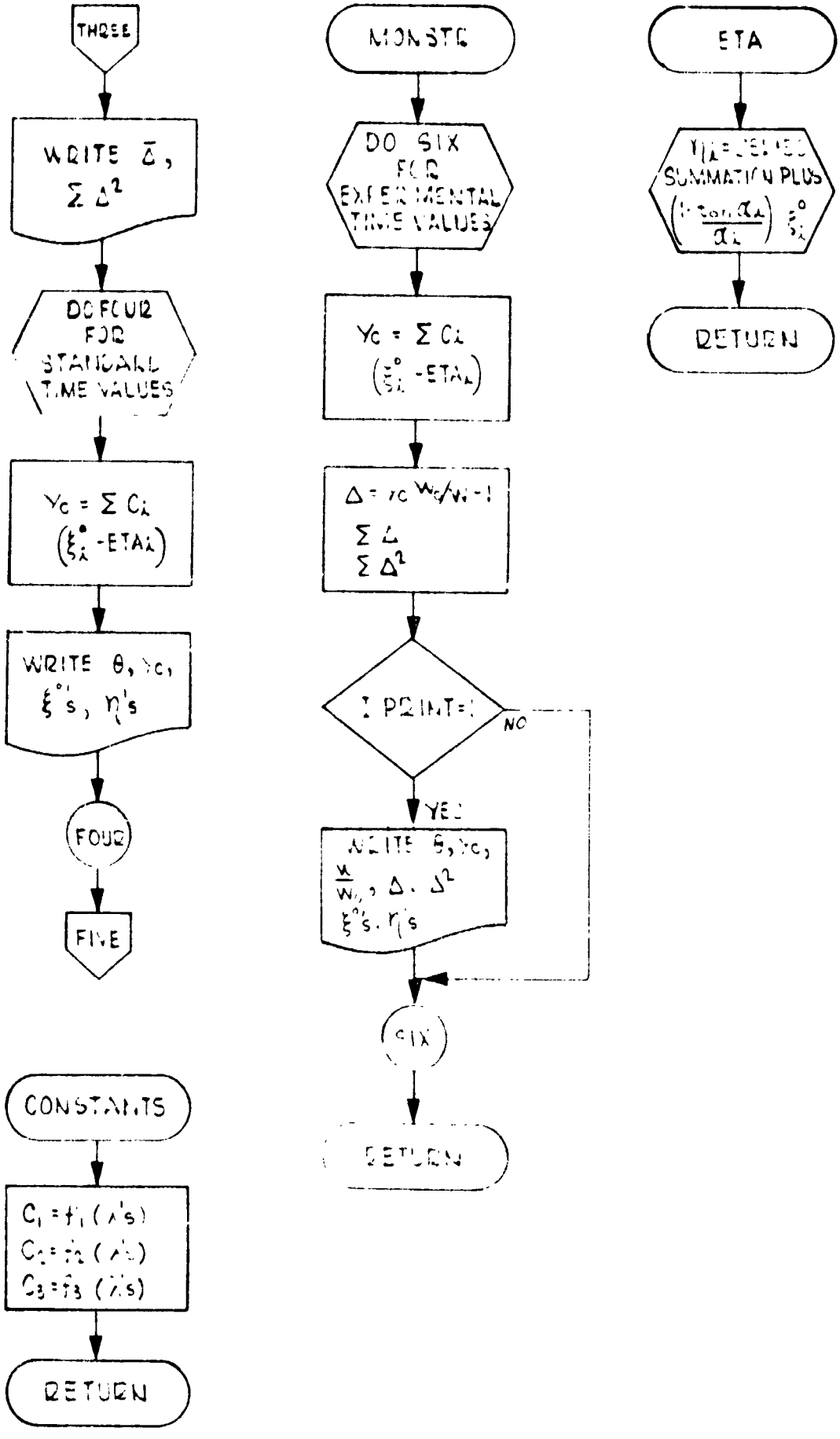

FIGURE 37b - FLOW CHART FOR HRI65R002

```
      DIMENSION C(5),SDELSQ(1000),                              ALAMB(6)
     1,THETA(50),WOWO(50),UM(6),ETAI(6),XII (6),ALPHA(6),STDTHE(50),
     2          CON(4),WEXP(200),VLAM1(1000),VLAM2(1000),VLAM3(1000),
     3VALP1(1000),VALP2(1000),VALP3(1000),SUMSQI(1000)
  222 FORMAT(68H1DATA PROCESSING - CALCULATION OF RATE AND TRANSPORT CON
     1STANTS FOR PYROLYSIS OF ABLATORS//27H HRI PROGRAM NO. HRI65R002,,3
     29HTYPE OF MATERIAL IS PHENOL-FORMALDEHYDE,5X,9HDATA SET-,I4//)
  111 READ(5,1) IY,N,ID,TEMP, (CON(I),I=1,4)
    1 FORMAT(I1,I2,I7  ,7F10.5)
      READ(5,221)IPRINT,IT,(STDTHE(I),I=1,IT)
  221 FORMAT(I1,I4,15F5.4 /16F5.4/16F5.4)
      WRITE(6,222) ID
      WRITE(6,343)TEMP,     (CON(I),I=1,4)
      ALAMBO=CON(3)
      ALPHAO=CON(4)
  343 FORMAT(14H TEMP. DEG. C=,F5.0,5X,4HC/S=,7F10.5///)
      DO 3 J=1,50
      READ(5,2)THETA(J),WEXP(J),WEXP(J+50),WEXP(J+100),WEXP(J+150)
    2 FORMAT(5F10.5)
      IF(THETA(J) )4,3,3
    3 CONTINUE
    4 JN=J-1
      DO 440 J=1,JN
      JDEX=(IY-1)*50+J
  440 WOWO(J)=WEXP(JDEX)
      EM=FLOAT(JN)
      READ(5,555)ALAMB1,ALAM32,ALAMB5,ALPH1,ALPH2,ALPH3
  553 READ(5,556)DLAM1,DLAM2,DLAM5,INLAM1,INLAM2,INLAM5 ,IFLAG
  555 FORMAT(6F10.5)
  556 FORMAT(5F10.5,3(I1,9X),I2)
      IF (IFLAG) 889,111,554
  554 ALPHA(1)=ALPH1
      ALPHA(2)=ALPH2
      ALPHA(3)=ALPH3
      ALAMB1=ALAMB1-DLAM1*FLOAT((INLAM1-1)/2)
      ALAMB2=ALAMB2-DLAM2*FLOAT((INLAM2-1)/2)
      ALAMB5=ALAMB5-DLAM5*FLOAT((INLAM5-1)/2)
      ALAMB(2)=ALAMB2
      ALAMB(3)=ALAMB5
      KK=0
      DO 888 I=1,INLAM1
      ALAMB2=ALAMB(2)
      DO 887 J=1,INLAM2
      ALAMB5=ALAMB(3)
      DO 886 K=1,INLAM5
      KK=KK+1
      VLAM3(KK)=ALAMB1+ALAMB2+ALAMB5
      VLAM2(KK)=ALAMB2
      VLAM1(KK)=ALAMB1
  886 ALAMB5=ALAMB5+DLAM5
  887 ALAMB2=ALAMB2+DLAM2
  888 ALAMB1=ALAMB1+DLAM1
  904 CONTINUE
      DO 99 K=1,KK
      IF(IFLAG.EQ.(-1))GO TO 905
      ALAMB(1)=VLAM1(K)
      ALAMB(2)=VLAM2(K)
```

```
      ALAMB(3)=VLAM3(K)
      CALL       CONSTS (IY,ALAMB,CON,CO,C)
  906 CONTINUE
      DO 9 I=1,3
    9 UM(I)=ALAMB(1)/ALPHA(I)/ALPHA(I)
      UMO=ALAMBO/ALPHAO/ALPHAO
      IF (IPRINT) 999,999,6
    6 ALAMB5=ALAMB(3)-ALAMB(1)-ALAMB(2)
      WRITE(6,7)ALAMBO,ALAMB(1),ALAMB(2),ALAMB5
    7 FORMAT(7H LAMBA=,6F10.4)
      WRITE(6,8)ALPHAO,(ALPHA(I),I=1,3)
    8 FORMAT(7H ALPHA=,6F10.4)
      WRITE(6,10) UMO,(UM(I),I=1,3)
   10 FORMAT(7H MU=   ,6E10.3//)
   11 WRITE(6,120) IY,IY
  120 FORMAT(1H /6H THETA,2X,2(2HY(,I1,1H),4X),
     14HFDEL,9X,5HDELSQ,5X,3HXI0,5X,5HXI1/0,
     2   3X,4HETA1,4X,5HXI2/0,3X,4HETA2,4X,5HXI3/0,3X,4HETA3)
   20 WRITE(6,21)
   21 FORMAT(8X,13HEXPER.  CALC.//)
  999 CALL       MONSTR(N,CO,C,ALAMBO,ALAMB,ALPHAO,ALPHA,THETA,WOWO,JN,
     1EM,SUMDEL,SUMSQ,IPRINT,UMO,UM)
      SUMSQI(K)=SUMSQ
      SDELSQ(K)=SUMDEL
   99 CONTINUE
      WRITE(6,101)
  101 FORMAT(10H SUM DELSQ,4X,6HLAMBA0,4X,6HALPHA0,4X,6HLAMBA1,4X,6HALPH
     1A1,4X,6HLAMBA2,4X,6HALPHA2,4X,6HLAMBA3,4X,6HALPHA3//)
      DO 102 K=1,KK
      IF (IFLAG.EQ.(-1)) GO TO 907
      ALAMB(1)=VLAM1( K)
      ALAMB(2)=VLAM2( K)
      ALAMB(3)=VLAM3( K)
  102 WRITE(6,103) SUMSQI(K),ALAMBO,ALPHAO,((ALAMB(I),ALPHA(I)),I=1,3)
  103 FORMAT(1X,E9.4,12(2X,F8.4))
      MK=1
      EXDLSQ=SUMSQI(1)
      DO 104 K=2,KK
      IF(EXDLSQ.LT.SUMSQI(K))GO TO 104
      MK=K
      EXDLSQ =SUMSQI(K)
  104 CONTINUE
      IF (IFLAG.EQ.(-1))GO TO 908
      ALAMB(1)=VLAM1(MK)
      ALAMB(2)=VLAM2(MK)
      ALAMB(3)=VLAM3(MK)
  909 CONTINUE
      DO 105 I=1,3
  105 UM(I)=ALAMB(I)/ALPHA(I)/ALPHA(I)
      ALAMB5=ALAMB(3)-ALAMB(2)-ALAMB(1)
      WRITE(6,7) ALAMBO,ALAMB(1),ALAMB(2),ALAMB5
      WRITE(6,8)ALPHAO,(ALPHA(I),I=1,3)
      WRITE(6,10) UMO,(UM(I),I=1,3)
      CALL       CONSTS (IY,ALAMB,CON,CO,C)
      WRITE(6,120) IY,IY
      NPRINT=1
      CALL       MONSTR(N,CO,C,ALAMBO,ALAMB,ALPHAO,ALPHA,THETA,WOWO,JN,
     1EM,SUMDEL,SUMSQ,NPRINT,UMO,UM)
```

```
      WRITE(6,98) SUMDEL,SUMSQ
   98 FORMAT(1H /10H DEL BAR=,F8.5,10X,10HSUM DELSQ=,E10.3/////)
      WRITE(6,150)IY
  150 FORMAT(6H THETA,4X,2HY(,I1,1H)                    ,5X,3HXI0,6X,5HXI1
     1/0,4X,4HETA1 5X,5HXI2/0,4X,4HETA2,5X,5HXI3/0,4X,4HETA3)
      DO 107 J=1,IT
      T=STOTHE(J)
      TAU=UMO  *T
      XI=1.-EXP(-ALAMBO  *T)
      XI0=XI
      YC=CO*(XI-ETA(ALPHAO  ,TAU,XI))
      DO 106 I=1,3
      TAU=UM(I)*T
      XI=1.-EXP(-ALAMB(I)*T)
      XII(I)=XI
      ETAII=ETA(ALPHA(I),TAU,XI)
      ETAI(I)=ETAII
  106 YC=C(I  ) *(XI-ETAII)+YC
  107 WRITE(6,108)T,YC,XI0,((XII(I),ETAI(I)),I=1,3)
  108 FORMAT(1X,F7.3,2X,F6.5          , 7(2X,F7.5))
      ALPH1=ALPHA(1)
      ALPH2=ALPHA(2)
      ALPH3=ALPHA(3)
      ALAM1=ALAMB(1)
      ALAM2=ALAMB(2)
      GO TO 553
  889 ALPH1=ALPH1-DLAM1*FLOAT((INLAM1-1)/2)
      ALPH2=ALPH2-DLAM2*FLOAT((INLAM2-1)/2)
      ALPH3=ALPH3-DLAM3*FLOAT((INLAM3-1)/2)
      ALPHA(2)=ALPH2
      ALPHA(3)=ALPH3
      KK=0
      DO 903 I=1,INLAM1
      ALPH2=ALPHA(2)
      DO 902 J=1,INLAM2
      ALPH3=ALPHA(3)
      DO 901 K=1,INLAM3
      KK=KK+1
      VALP3(KK)=ALPH3
      VALP2(KK)=ALPH2
      VALP1(KK)=ALPH1
  901 ALPH3=ALPH3+DLAM3
  902 ALPH2=ALPH2+DLAM2
  903 ALPH1=ALPH1+DLAM1
DIAGNOSTIC*  102
DIAGNOSTIC*  906
      CALL CONSTS(IY,ALAMB,CON,CO,C)
      GO TO 904
  905 ALPHA(1)=VALP1(K)
      ALPHA(2)=VALP2(K)
      ALPHA(3)=VALP3(K)
      GO TO 906
  907 ALPHA(1)=VALP1(K)
      ALPHA(2)=VALP2(K)
      ALPHA(3)=VALP3(K)
      GO TO 102
  908 ALPHA(1)=VALP1(MK)
      ALPHA(2)=VALP2(MK)
```

```
      ALPHA(3)=VALP3(MK)
      GO TO 909
      END
```

• SUBROUTINES •

```
      SUBROUTINE CONSTS (IY,ALAMB,CON,CO,C)
      DIMENSION ALAMB(6),CON(4),C(5)
      IF(IY.EQ. 1) GO TO 771
      IF(IY.EQ. 2) GO TO 772
      IF(IY.EQ. 3) GO TO 773
      CO=18.*CON(1)
      C(1)=17.*CON(2)*ALAMB(2)/(ALAMB(3)-ALAMB(1))
      C(2)=21.*CON(2)*ALAMB(1)/(ALAMB(3)-ALAMB(2))
      BETA1=1.-ALAMB(2)/ALAMB(3)*(1.-ALAMB(1)/(ALAMB(3)-ALAMB(1)))
      BETA2=(ALAMB(2)+5.*(ALAMB(3)-ALAMB(1)-ALAMB(2))-ALAMB(1)*ALAMB(2)/
     1(ALAMB(3)-ALAMB(2)))/ALAMB(3)
      PHI3=BETA1+1.125*BETA2+(4.*ALAMB(3)-ALAMB(2)-3.*ALAMB(1)-ALAMB(1)*
     1ALAMB(2)*
     2(3./ALAMB(3)+1./(ALAMB(3)-ALAMB(1))))/ALAMB(3)/16.
      C(3)=16.*CON(2)*PHI3
      GO TO 774
  771 CO=16.*CON(1)
      C(1)=16.*CON(2)*ALAMB(2)/(ALAMB(3)-ALAMB(1))
      C(2)=0.
      BETA1=1.-ALAMB(2)/ALAMB(3)*(1.-ALAMB(1)/(ALAMB(3)-ALAMB(1)))
      C(3)=16.*CON(2)*BETA1
      GO TO 774
  772 CO=0.
      C(1)=0.
      C(2)=18.*CON(2)
      BETA2=(ALAMB(2)+5.*(ALAMB(3)-ALAMB(1)-ALAMB(2))-ALAMB(1)*ALAMB(2)/
     1(ALAMB(3)-ALAMB(2)))/ALAMB(3)
      C(3)=12.*CON(2)*BETA2
      GO TO 774
  773 CO=2.*CON(1)
      C(1)=CON(2)*ALAMB(2)/(ALAMB(3)-ALAMB(1))
      C(2)=3.*CON(2)*ALAMB(1)/(ALAMB(3)-ALAMB(2))
      C(3)=0.
  774 RETURN
      END
```

```
      FUNCTION ETA(ALPHAI,TAU,XI)
      ETAKIN=SIN(ALPHAI)/COS(ALPHAI)/ALPHAI
      ALPHSQ=ALPHAI*ALPHAI
      SUM=0.
      EN=-1.
      DO 333 NN=1,99
      EN=EN+1.
      ENS=2.*EN+1.
      ENS=ENS*ENS*2.4674
      TERM=(1.-EXP(-ENS*TAU))/ENS/(1.-ENS/ALPHSQ)
      SUM=SUM+TERM
DIAGNOSTIC*  THE TEST FOR EQUALITY BETWEEN NON-INTEGERS MAY NOT BE MEANINGFUL.
      IF(ABS(TERM/SUM).LE..001)GO TO 334
  333 CONTINUE
  334 SUM=2.*SUM*(-1.)
  444 ETA=SUM-(ETAKIN-1.)*XI
      RETURN
      END
```

```
      SUBROUTINE MONSTR(N,CO,C,ALAMBO,ALAMB,ALPHAO,ALPHA,THETA,WOWO,JN,
     1EM,SUMDEL,SUMSQ,IPRINT,UMO,UM)
      DIMENSION C(5),ALAMB(6),ALPHA(6),THETA(50),WOWO(50),UM(6),
     1 XII(6),ETAI(6)
      SUMDEL=0.
      SUMSQ=0.
      DO 30 J=1,JN
      T=THETA(J)
      XIO=1.-EXP(-ALAMBO*T)
      TAU=UMO*T
      ETAO=ETA(ALPHAO,TAU,XIO)
      YC=     C(1)*(XIO-ETAO)
      DO 25 I=2,N
      TAU=UM(I)*T
      XI=1.-EXP(-ALAMB(I)*T)
      ETAII=ETA(ALPHA(I),TAU,XI)
      XII(I)=XI
      YC=YC+C(I)*(XI-ETAII)
   25 ETAI(I)=ETAII
      WOW=WOWO(J)
      DEL=YC-WOW
      DEL=DEL/WOW
      DELSQ=DEL*DEL
      SUMSQ=SUMSQ+DELSQ
      SUMDEL=SUMDEL+ABS(DEL)
      IF (IPRINT) 30,30,930
  930 WRITE(6,31) T,WOW,YC,DEL  ,DELSQ,XIO,((XII(I),ETAI(I)),I=1,N)
   31 FORMAT(1X,F5.1,2(2X,F6.5),2X,F8.5,2X,E10.3,7(2X,F6.4))
   30 CONTINUE
      SUMDEL=SUMDEL/EM
      RETURN
      END
```

° COMPUTER PROGRAM HRI65R003 °

CALCULATION OF SURFACE AREA AND PERMEABILITY FROM EXPERIMENTAL POROSITY DATA

A derivation has been made which shows that the surface area of the pores is of the form,

$$A_p = 2 \int_0^{V_T} \frac{dV}{D}$$

where V_T is the total pore volume, and D is the pore diameter. Permeability can be obtained from,

$$K = \int_0^{V_T} \frac{D^2 \, dV}{6 V_T}$$

This program takes the porosity data in the form of tabulated pressure and pore volume values and performs the required integrations by the trapezoid method after calculating pore diameter by,

$$D \text{ (microns)} = \frac{175}{P \text{ (psia)}}$$

The computer program follows.

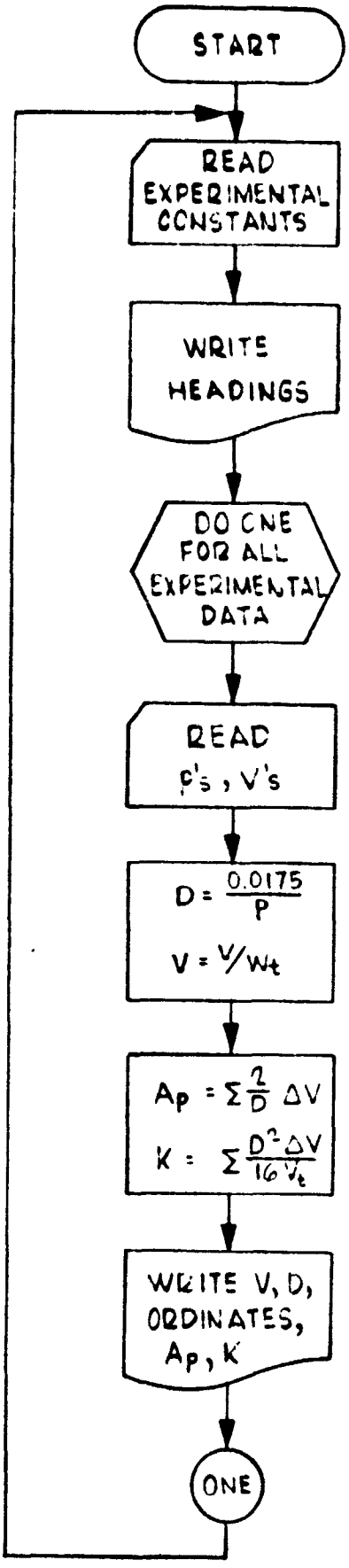

FIGURE 38 - FLOW CHART FOR HRI65R003

```
      DIMENSION V(100),D(100),DSQ(100),TWOD(100)
  111 WRITE(6,10)
   10 FORMAT(1H1)
      READ(5,11)ID,WT,VT,PHI
   11 FORMAT(I10,3F10.5)
      WRITE(6,1)
    1 FORMAT(1H0,9X,48HSURFACE AREA AND PERMEABILITY FROM POROSITY DATA/
     1/)
      WRITE(6,2)ID
    2 FORMAT(10X,10HSAMPLE NO.,I5,//)
      DO 5 I=1,100
      READ(5,3)P,VEE
    3 FORMAT(2F10.5)
      IF (P) 6,6,4
    4 V(I)=VEE/WT
      DEE=175.E-4/P
      D(I)=DEE
      DSQ(I)=DEE*DEE/16./VT
    5 TWOD(I)=2./DEE
    6 WRITE(6,7)
    7 FORMAT(10X,4HPORE,8X,4HPORE,7X,7HD2/16VT,7X,3H2/D,8X,7HSURFACE,4X,
     18HPERMEAB./10X,7HVOLUME,,5X,9HDIAMETER,,2X,9HX10 TO+8,,5X,9HX10 TO
     2-4,,2X,5HAREA,,6X,9HX10 TO+8,/10X,5HCM3/G,7X,7HMICRONS,4X,4HCM-1,1
     30X,4HCM-1,7X,5HCM2/G,6X,3HCM2//)
      N=I-1
      SUR=0.
      PER=0.
      VPRE=V(1)
      DSQPRE=DSQ(1)
      TWDPRE=TWOD(1)
      PR=0.
      TP=TWDPRE*1.E-4
      DD=DSQPRE*1.E8
      DI=1.E4*D(1)
      WRITE(6,9)VPRE,DI   ,DD,TP,SUR,PR
      DO 8 I=2,N
      VEE=V(I)
      DELV=(VEE-VPRE)*.5
      DS=DSQ(I)
      PER=PER+DELV*(DS+DSQPRE)*PHI
      TD=TWOD(I)
      SUR=SUR+DELV*(TD+TWDPRE)
      VPRE=VEE
      DSQPRE=DS
      TWDPRE=TD
      PR=PER*1.E8
      TP=TWDPRE*1.E-4
      DD=DSQPRE*1.E8
      DI=1.E4*D(I)
    8 WRITE(6,9)VPRE,DI   ,DD,TP,SUR,PR
    9 FORMAT(F16.4,F13.3,F13.3,F13.4,F10.1,F11.2)
      GO TO 111
      END
```

WRT65:003

○ COMPUTER PROGRAM HRI65R004 ○

MATHEMATICAL SIMULATION OF TGA CURVES

The purpose of this program is to simulate the thermogravimetric analysis of phenol-formaldehyde resin of the type used in this investigation. Equation (VIII-9) is used in the finite difference form,

$$\Delta\left(\frac{W}{W_o}\right) = \left\{\left[\frac{\partial(W/W_o)}{\partial\theta}\right]_T + R\left[\frac{\partial(W/W_o)}{\partial T}\right]_\theta\right\}\Delta\theta$$

for a convenient time increment, $\Delta\theta$, and a selected value of heating rate, R. The partial derivatives are given by equations (VIII-10) and (VIII-11). The increments of W/Wo are negative, and as each is calculated, it is summed with the current value of W/Wo.

The input consists of:

1) Constants, $\left(\frac{n_{SRQ}}{W_o}\right)$, $\left(\frac{n_o}{W_o}\right)$, $\left(\frac{W_{PF}}{W_o}\right)$, R, $\Delta\theta$, initial and final temperatures.

2) A_{λ_o}, E_{λ_o}, A_{λ_1}, E_{λ_1}, A_{λ_2}, E_{λ_2}, A_{λ_5}, E_{λ_5};
A_{α_1}, E_{α_1}, A_{α_2}, E_{α_2}, A_{α_3}, E_{α_3}.

The computer program follows.

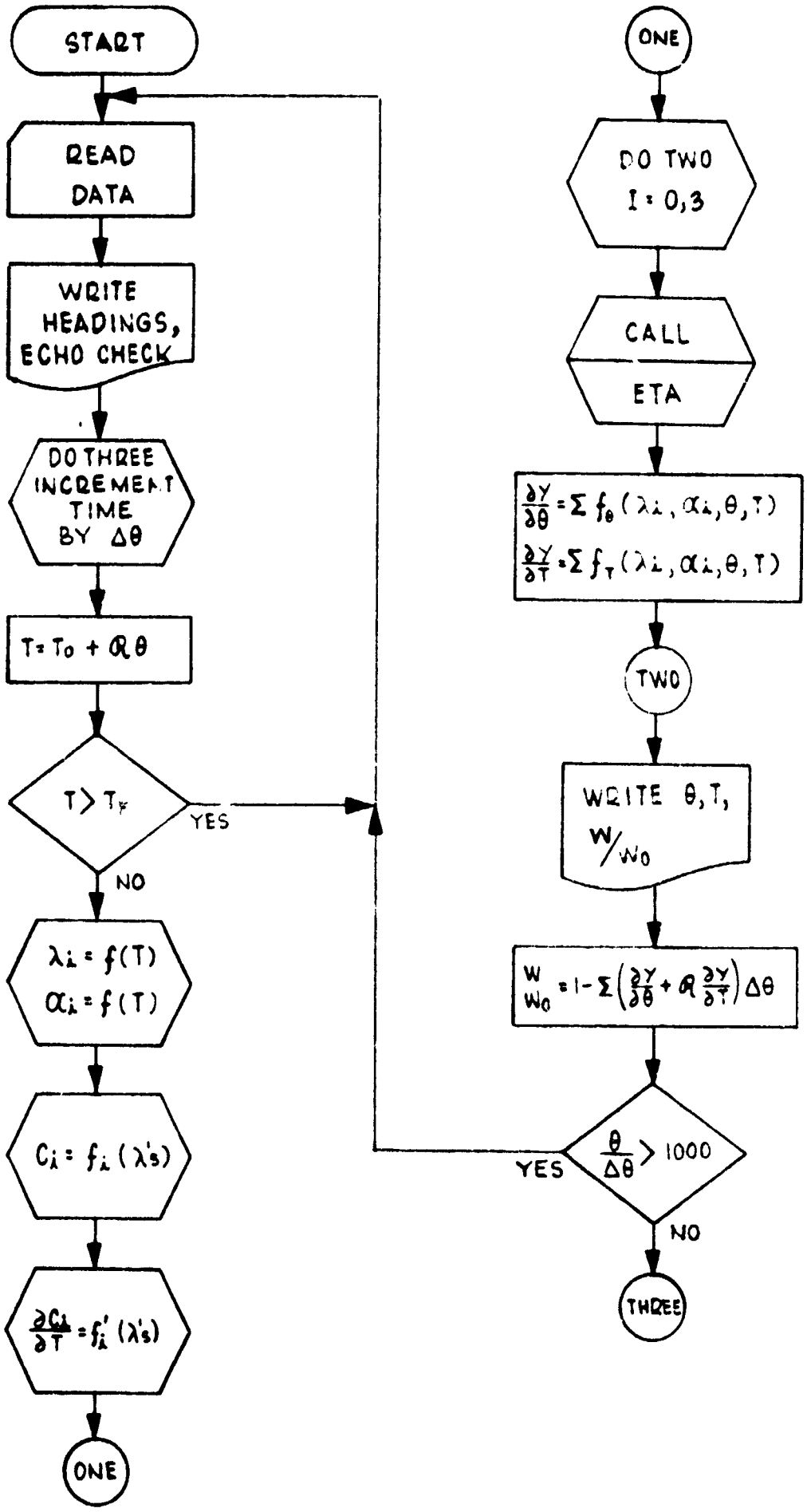

FIGURE 39a - FLOW CHART FOR HRI65R004

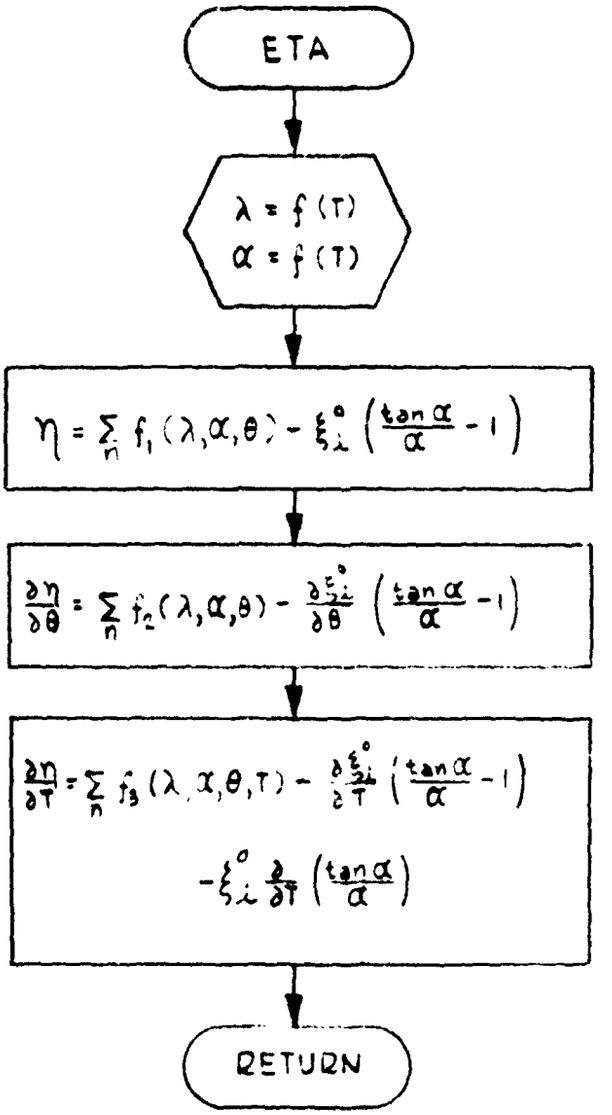

FIGURE 39b - FLOW CHART FOR HRI65R004

```
      2 FORMAT(27H1TGA FROM KINETIC CONSTANTS//67H HRI PROGRAM NO. HRI65R0
     1 04, TYPE OF MATERIAL IS PHENOL-FORMALDEHYDE//10H DATA SET-,I4//)
  111 READ (5,1)ID,TO,RH,DELTH,WPFOWO,ENSRO,ENO,TF
    1 FORMAT(I10,7F10.5)
      WLOWO=1.-WPFOWO
      READ (5,9)AL0,EL0,AL1,EL1,AL2,EL2,AL5,EL5
    9 FORMAT(8E10.3)
      READ (5,9)AA0,EA0,AA1,EA1,AA2,EA2,AA3,EA3
      WRITE(6,2)ID
      WRITE(6,1)ID,TO,RH,DELTH,WPFOWO,ENSRO,ENO,TF
      WRITE(6,9)AL0,EL0,AL1,EL1,AL2,EL2,AL5,EL5
      WRITE(6,9)AA0,EA0,AA1,EA1,AA2,EA2,AA3,EA3
      WRITE(6,3)
    3 FORMAT(1H /6H TIME,,5X,6HTEMP.,,4X,4HW/W0,6X,9HDY/DTHETA,6X,5HDY/D
     1T/5H MIN.,6X,6HDEG. C//)
      TO=TO+273.
      TF=TF+273.
      CO=18.*ENSRO
      THETA=-DELTH
      WOWO=1.
      DO 222 I=1,1000
      ENTH=1.
      IF(I.LT. 21) ENTH=.1
      IF(I.LT. 12) ENTH=.01
      IF(I.LT. 2 ) ENTH=1.
      THETA=THETA+DELTH *ENTH
      T=TO+RH*THETA
      RT=1.987*T
      IF (T.GT. TF)    GO TO 223
      ALAMB0=AL0*EXM(-EL0/RT)
      ALAMB1=AL1*EXM(-EL1/RT)
      ALAMB2=AL2*EXM(-EL2/RT)
      ALAMB5=AL5*EXM(-EL5/RT)
      C1=17.*ENO*ALAMB2/(ALAMB2+ALAMB5)
      C2=21.*ENO*ALAMB1/(ALAMB1+ALAMB5)
      ALAMB3=ALAMB1+ALAMB2+ALAMB5
      BETA1=1.-ALAMB2  /ALAMB3  *(1.+ALAMB1  /(ALAMB3  -ALAMB1  ))
      BETA2=(ALAMB2  +5.*(ALAMB5                    )-ALAMB1  *ALAMB2  /
     1(ALAMB3  -ALAMB2  ))/ALAMB3
      PHI3=BETA1+1.125*BETA2+(4.*ALAMB3  -ALAMB2  -3.*ALAMB1  -ALAMB1  *
     1ALAMB2*
     2(3./ALAMB3  +1./(ALAMB3  -ALAMB1  )))/ALAMB3  /16.
      C3=18.*ENO*PHI3
      RTSQ=RT*T
      DLAMB0=ALAMB0*EL0/RTSQ
      DLAMB1=ALAMB1*EL1/RTSQ
      DLAMB2=ALAMB2*EL2/RTSQ
      DLAMB5=ALAMB5*EL5/RTSQ
      ALAM25=ALAMB2+ALAMB5
      ALAM15=ALAMB1+ALAMB5
      DC1=17.*ENO*(ALAMB5*DLAMB2-ALAMB2*DLAMB5)/ALAM25/ALAM25
      DC2=21.*ENO*(ALAMB5*DLAMB1-ALAMB1*DLAMB5)/ALAM15/ALAM15
```

```
      DBETA1=(ALAMB2*(DLAMB1+DLAMB5)-ALAM15*DLAMB2)/ALAMB3/ALAMB3-(ALAM2
     15*ALAMB3*(ALAMB1*DLAMB2 +ALAMB2*DLAMB1)-ALAMB1*ALAMB2*(ALAM25*(DLA
     2MB1+DLAMB2+DLAMB5)+ALAMB3*(DLAMB2+DLAMB5)))/ALAM25/ALAM25/ALAMB3/A
     3LAMB3
      DBETA2=(ALAMB3*(DLAMB2+5.*DLAMB5
     1                                -ALAMB1*ALAMB2*(ALAM15*(EL1+EL2)/RT
     2SQ-DLAMB1-DLAMB5)/ALAM15/ALAM15)-(ALAMB2+5.*ALAMB5-ALAMB1*ALAMB2/A
     3LAM15)*(DLAMB1+DLAMB2+DLAMB5))/ALAMB3/ALAMB3
      DBETAA=ALAMB1*(2.*DLAMB2+3.*DLAMB5)+ALAMB2*(DLAMB5-2.*DLAMB1)-ALAM
     1B5*(3.*DLAMB1+DLAMB2)
      DBETAB=ALAMB1*ALAMB2*(3.*(EL1+EL2)/RTSQ-6.*(DLAMB1+DLAMB2+DLAMB5)/
     1ALAMB3)
      DBETAC=ALAMB1*ALAMB2*((EL1+EL2)/RTSQ-(DLAMB1+DLAMB2+DLAMB5)/ALAMB3
     1-(DLAMB2+DLAMB5)/ALAM25)/ALAM25
      DBETA3=((DBETAA-DBETAB)/ALAMB3-DBETAC)/ALAMB3
      DC3=16.*ENO*(DBETA1+1.125*DBETA2+DBETA3/16.)
      DYDTH=0.
      DYDT=0.
      CALL ETA (T,THETA,AA0,EA0,AL0,EL0,ETA0,DETDT,DETDTH)
      XIEXP=EXP(-ALAMB0*THETA)
      DLDTH=C0*(ALAMB0*XIEXP-DETDTH)
      DLDT=C0*(THETA*DLAMB0*XIEXP-DETDT)
      DYDTH=DYDTH+DLDTH
      DYDT=DYDT+DLDT
      CALL ETA (T,THETA,AA1,EA1,AL1,EL1,ETA1,DETDT,DETDTH)
      XIEXP=EXP(-ALAMB1*THETA)
      DLDTH=C1*(ALAMB1*XIEXP-DETDTH)
      DLDT=C1*(THETA*DLAMB1*XIEXP-DETDT)          +DC1*(1.-XIEXP-ETA1)
      DYDTH=DYDTH+DLDTH
      DYDT=DYDT+DLDT
      CALL ETA (T,THETA,AA2,EA2,AL2,EL2,ETA2,DETDT,DETDTH)
      XIEXP=EXP(-ALAMB2*THETA)
      DLDTH=C2*(ALAMB2*XIEXP-DETDTH)
      DLDT=C2*(THETA*DLAMB2*XIEXP-DETDT)          +DC2*(1.-XIEXP-ETA2)
      DYDTH=DYDTH+DLDTH
      DYDT=DYDT+DLDT
      CALL ATE (T,THETA,AA3,EA3,AL1,EL1,AL2,EL2,AL5,EL5,ETA3,DETDT,DETDT
     1H)
      XIEXP=EXP(-ALAMB3*THETA)
      DLAMB3=DLAMB1+DLAMB2+DLAMB5
      DLDTH=C3*(ALAMB3*XIEXP-DETDTH)
      DLDT=C3*(THETA*DLAMB3*XIEXP-DETDT)       +DC3*(1.-XIEXP-ETA3)
      DYDTH=DYDTH+DLDTH
      DYDT=DYDT+DLDT
      S=T-273.
      WRITE(6,221) THETA,S,WOWO,DYDTH,DYDT,ETA0,ETA1,ETA2,ETA3
  221 FORMAT(1X,F7.2,3X,F7.2,3X,F6.4,6X,E10.3,5X,E10.3,4(5X,E10.3))
      IF(DYDTH.LT. 0.)DYDTH=0.
      IF(DYDT .LT. 0.)DYDT =0.
      DELW=      WPFOWO*(DYDTH+DYDT*RH) *DELTH *ENTH
      IF(S.GT. 360.)GO TO 224
  220 WOWO=WOWO-DELW
  220 DELPRE=DELW
```

```
      IF(WOWO .LT. WLOWO) WOWO= WLOWO
  222 CONTINUE
  225 CONTINUE
      GO TO 111
  224 IF(DELW.GT. 3.*DELPRE)GO TO 225
      GO TO 220
  225 WOWO=WOWO-DELPRE
      GO TO 226
      END
```

° SUBROUTINES °

```
      SUBROUTINE ETA (T,THETA,AA,EA,AL,EL,EIGHTA,DETDT,DETDTH)
      RT=1.987*T
      ALPHA=AA*EXM(-EA/RT)
      ALAMB=AL*EXM(-EL/RT)
      UM=ALAMB/ALPHA/ALPHA
      RTSQ=RT*T
      DLAMBA=ALAMB *EL/RTSQ
      DALPHA=ALPHA*EA/RTSQ
      DMU=UM*(EL-2.*EA)/RTSQ
      XIEXP=EXP(-ALAMB *THETA)
      DXIODT=DLAMBA*THETA*XIEXP
      XIO=1.-XIEXP
      COSINE=COS(ALPHA)
      TANALP=SIN(ALPHA)/COSINE
      SUM1=0.
      SUM2=0.
      SUM3=0.
      EN=-1.
      TAOAM1=TANALP/ALPHA-1.
      ALPHSQ=ALPHA*ALPHA
      DO 888 I=1,99
      EN=EN+1.
      ENS=2.*EN+1.
      ENS=ENS*2.4674*ENS
      UMEXP=EXP(-ENS*UM*THETA)
      DENOM=ENS-ALPHSQ
      TERM1=UMEXP/DENOM
      SUM1=SUM1+TERM1
      TERM=(1.-UMEXP)/DENOM/ENS
      SUM2=SUM2+TERM
      TERM3=TERM/DENOM
      SUM3=SUM3+TERM3
      IF(ABS(TERM/SUM2).LT. .001 .AND. ABS(TERM1/SUM1).LT. .001 .AND.
     1 ABS(TERM3/SUM3).LT. .001) GO TO 889
  888 CONTINUE
  889 DSIGMA=DMU*SUM1*THETA+2.*ALPHA*DALPHA*SUM3
      EIGHTA=2.*ALPHSQ*SUM2-XIO*TAOAM1
      IF(EIGHTA .LT. 0.) EIGHTA=0.
```

```
      H'T65'00/
```

```
      DETDTH=(2.*SUM1-TAOAM1*XIEXP)*ALAMB
      COSINE=COSINE*COSINE
      DETDT=2.*ALPHSQ*DSIGMA+4.*ALPHA*SUM2*DALPHA-XIO*DALPHA*(ALPHA/COSI
     1NE-TANALP)/ALPHSQ-TAOAM1*THETA*DLAMBA*XIEXP
      RETURN
      END


      SUBROUTINE ATE (T,THETA,AA ,EA ,AL1,EL1,AL2,EL2,AL5,EL5,EIGHTA,DET
     1DT,DETDTH)
      RT=1.987*T
      ALPHA=AA*EXM(-EA/RT)
      ALAMB1=AL1*EXM(-EL1/RT)
      ALAMB2=AL2*EXM(-EL2/RT)
      ALAMB5=AL5*EXM(-EL5/RT)
      ALAMB=ALAMB1+ALAMB2+ALAMB5
      UM=ALAMB/ALPHA/ALPHA
      RTSQ=RT*T
      DLAMB1=ALAMB1*EL1/RTSQ
      DLAMB2=ALAMB2*EL2/RTSQ
      DLAMB5=ALAMB5*EL5/RTSQ
      DLAMBA=DLAMB1+DLAMB2+DLAMB5
      DALPHA=ALPHA*EA/RTSQ
      DMU=(DLAMB1+DLAMB2+DLAMB5-2.*ALAMB*DALPHA/ALPHA)/ALPHA/ALPHA
      XIEXP=EXP(-ALAMB *THETA)
      DXIODT=DLAMBA*THETA*XIEXP
      XIO=1.-XIEXP
      COSINE=COS(ALPHA)
      TANALP=SIN(ALPHA)/COSINE
      SUM1=0.
      SUM2=0.
      SUM3=0.
      EN=-1.
      TAOAM1=TANALP/ALPHA-1.
      ALPHSQ=ALPHA*ALPHA
      DO 998 I=1,99
      EN=EN+1.
      ENS=2.*EN+1.
      ENS=ENS*2.4674*ENS
      UMEXP=EXP(-ENS*UM*THETA)
      DENOM=ENS-ALPHSQ
      TERM1=UMEXP/DENOM
      SUM1=SUM1+TERM1
      TERM=(1.-UMEXP)/DENOM/ENS
      SUM2=SUM2+TERM
      TERM3=TERM/DENOM
      SUM3=SUM3+TERM3
      IF(ABS(TERM/SUM2).LT. .001 .AND. ABS(TERM1/SUM1).LT. .001 .AND.
     1 ABS( TERM3/SUM3).LT. .001) GO TO 999
  998 CONTINUE
  999 DSIGMA=DMU*SUM1*THETA+2.*ALPHA*DALPHA*SUM3
```

```
      EIGHTA=2.*ALPHSQ*SUM2-XIO*TAOAM1
      IF(EIGHTA .LT. 0.) EIGHTA=0.
      DETDTH=(2.*SUM1-TAOAM1*XIEXP)*ALAMB
      COSINE=COSINE*COSINE
      DETDT=2.*ALPHSQ*DSIGMA+4.*ALPHA*SUM2*DALPHA-XIO*DALPHA*(ALPHA/COSI
     1NE-TANALP)/ALPHSQ-TAOAM1*THETA*DLAMBA*XIEXP
      RETURN
      END
```

```
      FUNCTION EXM(X)
      DO 96 I=1,10
      IF (ABS(X).LT. 10.) GO TO 97
   96 X=X/2.
   97 II=I-1
      EXM=EXP(X)
      IF(II.EQ. 0) GO TO 99
      DO 98 I=1,II
   98 EXM=EXM*EXM
   99 CONTINUE
      RETURN
      END
```

o COMPUTER PROGRAM HRI65R005 o

CALCULATION OF ISOTHERMAL DECOMPOSITION OF PF/QUARTZ ABLATORS

The object of this program is to calculate the decomposition functions $(1 - W/Wo)$, $\left(\frac{Wox}{Wo}\right)_g$, $\left(\frac{Wc}{Wo}\right)_g$, and $\left(\frac{W_H}{Wo}\right)$ at certain specified temperatures by either of two options.

(A) - For sets of specified values of the rate and transport parameters or,

(B) - For specified rate and transport parameter functions.

The following equations are used in the calculations: VIII-1 to VIII-8 incl.

The input consists of:

1) Constants, $(^nSRO/Wo)$, (n_o/Wo), (W_{pf}/Wo).

2) Option one: tabular values of λ_o, λ_1, λ_2, λ_5 and α_o, α_1, α_2, α_3 at specified temperatures.

3) Option two: A_{λ_o}, A_{λ_1}, A_{λ_2}, A_{λ_5}; E_{λ_o}, E_{λ_1}, E_{λ_2}, E_{λ_5}; A_{α_1}, A_{α_2}, A_{α_3}; E_{α_1}, E_{α_2}, E_{α_3}.

The computer program follows.

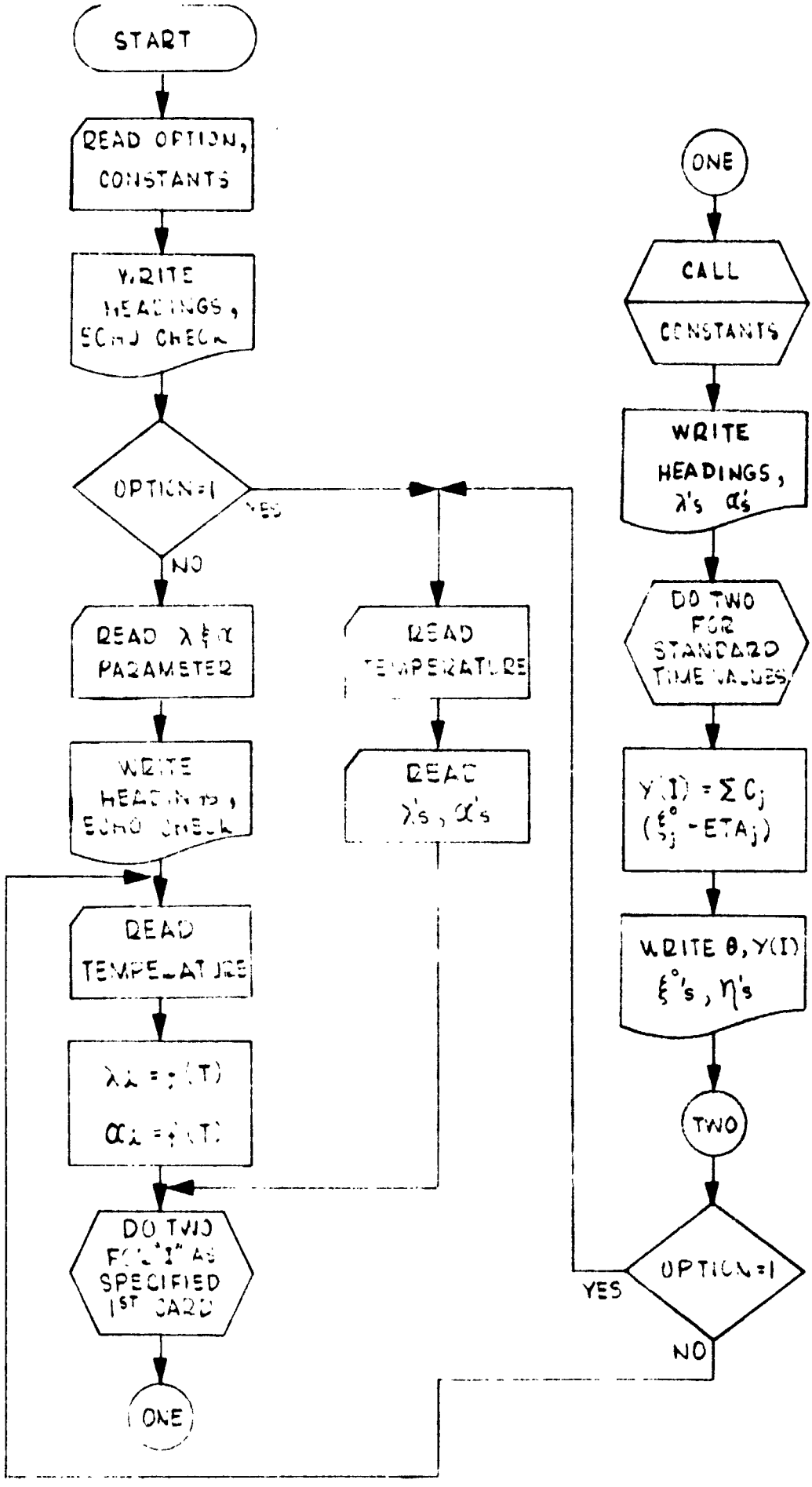
START
READ OPTION, CONSTANTS
WRITE HEADINGS, ECHO CHECK
OPTION=1
YES
NO
READ λ & α PARAMETER
WRITE HEADINGS, ECHO CHECK
READ TEMPERATURE
λλ = f(T)
αλ = f(T)
DO TWO FOR "I" AS SPECIFIED 1ST CARD
ONE
READ TEMPERATURE
READ λ's, α's
ONE
CALL CONSTANTS
WRITE HEADINGS, λ's α's
DO TWO FOR STANDARD TIME VALUES
Y(I) = Σ Cj (ξj° - ETAj)
WRITE θ, Y(I) ξ°'s, η's
TWO
OPTION=1
YES
NO

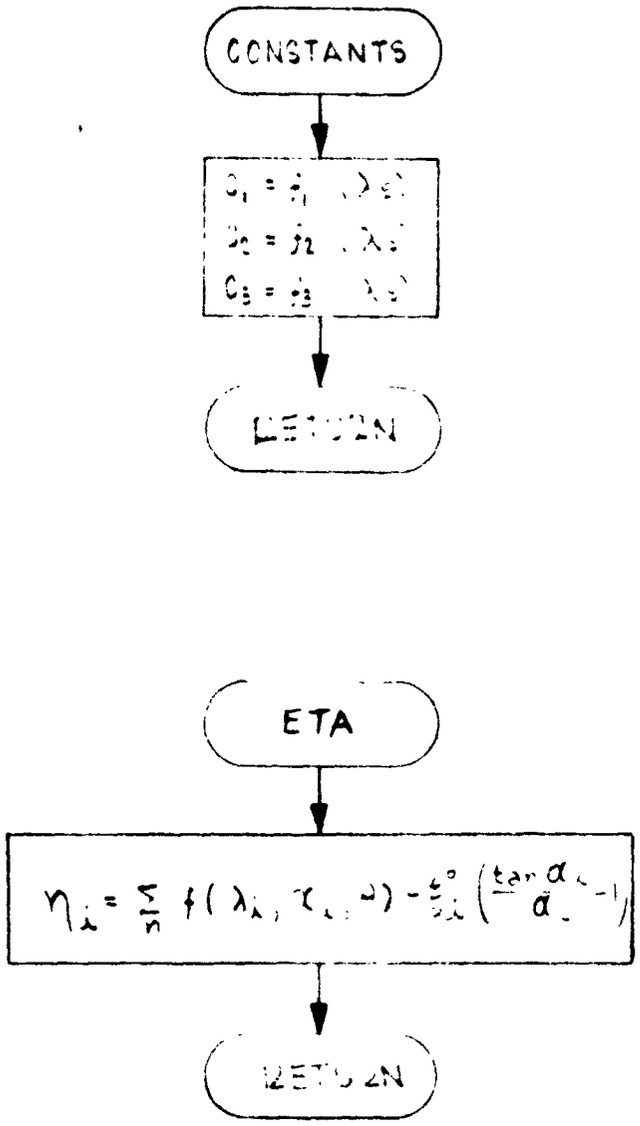

FIGURE 40b - FLOW CHART FOR HRI65R005

```
1.      222 FORMAT(34H1DATA PROCESSING - CALCULATION OF ,     25HISOTHERMAL DE
 .         1COMPOSITION ,     11HOF ABLATORS//27H HRI PROGRAM NO. HRI65R005,,3
3.         29HTYPE OF MATERIAL IS PHENOL-FORMALDEHYDE,5X,9HCALC. NO.,I4//)
4.          DIMENSION C(5),IYVEC(4),CON(4), TM(4),                 ALAMB(6)
5.         1,THETA(50),WOWO(50),UM(6),ETAI(6),XII (6),ALPHA(6),STDTHE(50)
6.      111 READ(5,1) ID,IOPT,CON(1),CON(2),CON(3),(IYVEC(I),I=1,4)
7.        1 FORMAT(2I5,3F10.5,4I1)
8.          READ(5,221)        IT,(STDTHE(I),I=1,IT)
9.      221 FORMAT(    I5,15F5.4 /16F5.4/16F5.4)
0.          WRITE(6,222)ID
1.          WRITE(6,223)CON(1),CON(2),CON(3)
2.      223 FORMAT(9H NSRO/WO=, F8.5,5X,6HNO/WO=,F10.5,5X,7HWPF/WO=,F10.5)
3.          IF (IOPT.EQ. 1) GO TO 301
4.          READ (5,9)AL0,EL0,AL1,EL1,AL2,EL2,AL5,EL5
5.        9 FORMAT(8E10.3)
6.          READ (5,9)AA0,EA0,AA1,EA1,AA2,EA2,AA3,EA3
7.          WRITE(6,224)
8.      224 FORMAT(1H /16H LAMBA CONSTANTS)
9.          WRITE(6,9)AL0,EL0,AL1,EL1,AL2,EL2,AL5,EL5
0.          WRITE(6,225)
1.      225 FORMAT(16H ALPHA CONSTANTS)
2.          WRITE(6,9)AA0,EA0,AA1,EA1,AA2,EA2,AA3,EA3
3.      302 READ(5,227)TEMP
4.      227 FORMAT(F10.5)
5.          IF (TEMP) 111,111,228
6.      228 RT=1.987*(TEMP+2.3.)
7.          EORT=-EL0/RT
8.          ALAMBO  =AL0*EXM( EORT)
9.          EORT=-EL1/RT
0.          ALAMB(1)=AL1*EXM( EORT)
1.          EORT=-EL2/RT
2.          ALAMB(2)=AL2*EXM( EORT)
3.          EORT=-EL5/RT
4.          ALAMB(5)=AL5*EXM( EORT)
5.          EORT=-EA0/RT
6.          ALPHAO  =AA0*EXM( EORT)
7.          EORT=-EA1/RT
8.          ALPHA(1)=AA1*EXM( EORT)
9.          EORT=-EA2/RT
0.          ALPHA(2)=AA2*EXM( EORT)
1.          EORT=-EA3/RT
2.          ALPHA(3)=AA3*EXM( EORT)
3.          GO TO 231
4.      301 READ(5,230)TEMP,ALAMBO,ALPHAO,ALAMB(1),ALPHA(1),ALAMB(2),ALPHA(2),
5.         1ALAMB(5),ALPHA(3)
6.      230 FORMAT(F10.5/8F10.5)
7.          IF(TEMP)111,111,231
8.      231 ALAMB(3)=ALAMB(1)+ALAMB(2)+ALAMB(5)
9.          DO 401 K=1,4
0.          IY=IYVEC(K)
1.          IF(IY.EQ. 0) GO TO 401
2.          CALL        CONSTS (IY,ALAMB,CON,CO,C)
3.          WRITE(6,500)
4.      500 FORMAT(1H ////)
5.          WRITE(6,501) TEMP
6.      501 FORMAT(13H TEMPERATURE=,F5.0,7H DEG. C)
7.          WRITE(6,502) CO,C(1),C(2),C(3)
```

```
      DO 105 I=1,3
  105 UM(I)=ALAMB(I)/ALPHA(I)/ALPHA(I)
      WRITE(6,7) ALAMBO,ALAMB(1),ALAMB(2),ALAMB(5)
    7 FORMAT(7H LAMBA=,6F10.4)
      WRITE(6,8)ALPHAO,(ALPHA(I),I=1,3)
    8 FORMAT(7H ALPHA=,6F10.4)
      WRITE(6,10) UMO,(UM(I),I=1,3)
   10 FORMAT(7H MU=   ,6E10.3//)
      GO TO (601,602,149,149),IY
  149 WRITE(6,150)IY
  150 FORMAT(6H THETA,4X,2HY(,I1,1H),5X,3HXI0,6X,4HTM/0,5X,5HXI1/0,4X,4H
     1ETA1,5X,4HTM/1,5X,5HXI2/0,4X,4HETA2,5X,4HTM/2,5X,5HXI3/0,4X,4HETA3
     2,5X,4HTM/3)
  151 DO 400 J=1,IT
      T=STDTHE(J)
      TAU=UMO  *T
      XI=1.-EXP(-ALAMBO  *T)
      XIO=XI
      TMO=  (XI-ETA(ALPHAO  ,TAU,XI))*CO
      YC=TMO
      DO 106 I=1,3
      TAU=UM(I)*T
      XI=1.-EXP(-ALAMB(I)*T)
      XII(I)=XI
      ETAII=ETA(ALPHA(I),TAU,XI)
      ETAI(I)=ETAII
      TM(I)=C(I)*(XI-ETAII)
  106 YC=YC+TM(I)
      GO TO (701,702,107,107),IY
  107 WRITE(6,108)T,YC,XIO,TMO,((XII(I),ETAI(I),TM(I)),I=1,3)
  108 FORMAT(1X,F7.3,2X,F6.5            ,11(2X,F7,5))
  400 CONTINUE
  401 CONTINUE
IAGNOSTIC*  151
IAGNOSTIC*  400
      IF(IOPT.EQ. 1) GO TO 301
      GO TO 302
  601 WRITE(6,610)IY
  610 FORMAT(6H THETA,4X,2HY(,I1,1H),5X,3HXI0,6X,4HTM/0,5X,5HXI1/0,4X,4H
     1ETA1,5X,4HTM/1,5X,5HXI3/0,4X,4HETA3,5X,4HTM/3)
      GO TO 151
  602 WRITE(6,620)IY
  620 FORMAT(6H THETA,4X,2HY(,I1,1H),5X,5HXI2/0,4X,4HETA2,5X,4HTM/2,5X,5
     1HXI3/0,4X,4HETA3,5X,4HTM/3)
      GO TO 151
  701 WRITE(6,108)T,YC,XIO,TMO,XII(1),ETAI(1),TM(1),XII(3),ETAI(3),TM(3)
      GO TO 400
  702 WRITE(6,108)T,YC,XII(2),ETAI(2),TM(2),XII(3),ETAI(3),TM(3)
      GO TO 400
      END
```

° SUBROUTINES °

```
      FUNCTION ETA(ALPHAI,TAU,XI)
      ETAKIN=SIN(ALPHAI)/COS(ALPHAI)/ALPHAI
      ALPHSQ=ALPHAI*ALPHAI
      SUM=0.
      EN=-1.
      DO 333 NN=1,99
      EN=EN+1.
      ENS=2.*EN+1.
      ENS=ENS*ENS*2.4674
      TERM=(1.-EXP(-ENS*TAU))/ENS/(1.-ENS/ALPHSQ)
      SUM=SUM+TERM
IAGNOSTIC*  THE TEST FOR EQUALITY BETWEEN NON-INTEGERS MAY NOT BE MEANINGFUL.
      IF(ABS(TERM/SUM).LE..001)GO TO 334
  333 CONTINUE
  334 SUM=2.*SUM*(-1.)
  444 ETA=SUM-(ETAKIN-1.)*XI
      RETURN
      END
```

```
      SUBROUTINE CONSTS (IY,ALAMB,CON,CO,C)
      DIMENSION ALAMB(6),CON(4),C(5)
      IF(IY.EQ. 1) GO TO 771
      IF(IY.EQ. 2) GO TO 772
      IF(IY.EQ. 3) GO TO 773
      CO=18.*CON(1)/CON(3)
      C(1)=17.*CON(2)*ALAMB(2)/(ALAMB(3)-ALAMB(1))/CON(3)
      C(2)=21.*CON(2)*ALAMB(1)/(ALAMB(3)-ALAMB(2))/CON(3)
      BETA1=1.-ALAMB(2)/ALAMB(3)*(1.+ALAMB(1)/(ALAMB(3)-ALAMB(1)))
      BETA2=(ALAMB(2)+5.*(ALAMB(3)-ALAMB(1)-ALAMB(2))-ALAMB(1)*ALAMB(2)/
     1(ALAMB(3)-ALAMB(2)))/ALAMB(3)
      PHI3=BETA1+1.125*BETA2+(4.*ALAMB(3)-ALAMB(2)-3.*ALAMB(1)-ALAMB(1)*
     1ALAMB(2)*
     2(3./ALAMB(3)+1./(ALAMB(3)-ALAMB(1))))/ALAMB(3)/16.
      C(3)=16.*CON(2)*PHI3 /CON(3)
      GO TO 774
  771 CO=16.*CON(1) /CON(3)
      C(1)=16.*CON(2)*ALAMB(2)/(ALAMB(3)-ALAMB(1))/CON(3)
      C(2)=0.
      BETA1=1.-ALAMB(2)/ALAMB(3)*(1.+ALAMB(1)/(ALAMB(3)-ALAMB(1)))
      C(3)=16.*CON(2)*BETA1 /CON(3)
      GO TO 774
  772 CO=0.
      C(1)=0.
      C(2)=18.*CON(2)  /CON(3)*ALAMB(1)/(ALAMB(1)+ALAMB(5))
      BETA2=(ALAMB(2)+5.*(ALAMB(3)-ALAMB(1)-ALAMB(2))-ALAMB(1)*ALAMB(2)/
     1(ALAMB(3)-ALAMB(2)))/ALAMB(3)
      C(3)=18.*CON(2)*BETA2/CON(3)
      GO TO 774
  773 CO=2.*CON(1) /CON(3)
      C(1)=CON(2)*ALAMB(2)/(ALAMB(3)-ALAMB(1))/CON(3)
      C(2)=3.*CON(2)*ALAMB(1)/(ALAMB(3)-ALAMB(2)) /CON(3)
      BETA3=                    (4.*ALAMB(3)-ALAMB(2)-3.*ALAMB(1)-ALAMB(1)*
     1ALAMB(2)*
     2(3./ALAMB(3)+1./(ALAMB(3)-ALAMB(1))))/ALAMB(3)
```

```
      C(3)=CON(2)*BETA3/CON(3)
  774 RETURN
      END
```

```
      FUNCTION EXM(X)
      DO 96 I=1,10
      IF (ABS(X).LT. 10.) GO TO 97
   96 X=X/2.
   97 II=I-1
      EXM=EXP(X)
      IF(II.EQ. 0) GO TO 99
      DO 98 I=1,II
   98 EXM=EXM*EXM
   99 CONTINUE
      RETURN
      END
```

APPENDIX D

CALCULATION OF KINETIC AND DIFFUSION PARAMETERS

To illustrate the calculation of such parameters as λ, μ, D, k, and ξ, the path of calculation is followed for the smoothed values of weight loss (1 - W/Wo) at 605°C as taken from Figure 16. The actual calculations are made by computer program HRI65R002 (Appendix C), but this section will follow the calculations as closely as possible.

The theory of this operation is to calculate (1 - W/Wo) by equation (VIII-1) (or calculate Wox/Wo, Wc/Wo, or W_H/Wo by the appropriate equations if the data is based on the individual elements) for the specified values of time at the given temperature. The individual values calculated for (1 - W/Wo) have the corresponding experimental values substracted, and the differences are squared and summed. Since values of λ's and α's are required to calculate (1 - W/Wo) (where $\alpha = (\lambda/\mu)^{\frac{1}{2}}$), the correct values of λ's and α's should allow the calculated weight loss to match the experimental weight loss, and the sum of the squares of the difference, $\sum\Delta^2$, will be zero. A logically arranged series of "guesses" of sets of values for λ's and α's must be initiated, bearing in mind that the more correct the values in a set are, the smaller will be the sum of the squares of the differences between calculated and experimental values of weight loss. In principle, when $\sum\Delta^2 = 0$, the correct values will have been found for all λ's and α's, but in an actual case, the experimental values have inherent errors, and $\sum\Delta^2 = 0$ can not be reached. A compromise must be made so that the best values of λ's and α's, giving a minimum for $\sum\Delta^2$, will be taken as correct for the temperature of the experimental points.

The selection of the series of successive approximations of sets of λ's and α's follows a simple pattern. A first approximation set must be selected, but there are no rules governing the selection, and unfortunately only individual experience in the field of reaction kinetics is of any help in this selection. Regardless of how far the first approximation is from the correct set, given enough successive approximations the process should converge to give the correct set of λ's and α's. In the case of HRI65R002, some simplification is possible. The desorption of water is thought to be very fast even at low temperatures so that λ_o is high, and is strictly a surface reaction so that α_o is negligible. These are arbitrarily set at λ_o = 100/min. and α_o = 0.0001. For these sample calculations, λ_1 = 0.6/min., λ_2 = 27.0/min., λ_5 = 0.7/min., α_1 = 3.2, α_2 = 6.0, and α_3 = 0.05.

A three dimensional matrix is set up for the λ's which centers around the initial values of λ's. An arbitrary number

of points is selected for each direction; in this case, five points for each direction. The size of the increments of λ in each direction are selected to define the volume of space to be investigated; in this case $\Delta\lambda_1 = 0.05$, $\Delta\lambda_2 = 1.0$, $\Delta\lambda_5 = 0.05$. The space is therefore defined as $\lambda_1 = 0.5, 0.55, 0.6, 0.65, 0.7$; $\lambda_2 = 25., 26., 27., 28., 29.$; $\lambda_5 = 0.6, 0.65, 0.7, 0.75, 0.8$. Each of these 125 combinations of λ's is used with the values of $\lambda_o, \alpha_o, \alpha_1, \alpha_2, \alpha_3$ to calculate a $\Sigma\Delta^2$ for the set of experimental data. The combination giving the smallest $\Sigma\Delta^2$ is $\lambda_1 = 0.7$, $\lambda_2 = 29.0$, $\lambda_5 = 0.6$; plus the values $\lambda_o = 100.$, $\alpha_o = 0.0001$, $\alpha_1 = 3.2$, $\alpha_2 = 6.0$, and $\alpha_3 = 0.05$. Sample calculations will therefore be made for this set, and at the time, $\theta = 3$ min.

From equation (VIII-1), it can be seen that four terms contribute to (1 - W/Wo) and the second term, involving ξ_1, will be examined as the most significant in this instance. Since by equation (VIII-3), ξ_1 is made up of two parts, ξ_1^o will be calculated first. By combining (VIII-4) and (VIII-5),

$$\xi_1^o = 1 - e^{-\lambda\theta} = 1 - e^{-0.7(3)} = 0.8775$$

By combining (VIII-4), (VIII-5), (VIII-6),

$$\eta_1 = \sum_{n=0}^{\infty} \frac{2\left[1 - e^{-(2n+1)^2\pi^2\mu_1\theta/4}\right]}{(2n+1)^2\frac{\pi^2}{4}\left[\frac{(2n+1)^2}{\alpha_1^2}\frac{\pi^2}{4} - 1\right]} + \left(1 - \frac{\tan\alpha_1}{\alpha_1}\right)\xi_1^o$$

where $\mu_1 = \dfrac{\lambda_1}{\alpha_1^2} = \dfrac{0.7}{(3.2)^2} = 0.0683$

The first term of the series will be for $n = 0$,

$$\frac{2\left[1 - e^{-(0+1)^2\pi^2(0.0683)(3.)/4}\right]}{(0+1)^2\frac{\pi^2}{4}\left[\frac{(0+1)}{(3.2)^2}\frac{\pi^2}{4} - 1\right]} = -0.422$$

The second term, for $n = 1$, is 0.075; the third for $n = 2$ is 0.006; all of the following terms are positive but drop off rapidly in value, and the sum of the series is - 0.3390. The second term of η_1 contains,

$$1 - \frac{\text{Tan}\,\alpha_1}{\alpha_1} = 1 - \frac{\text{Tan}\,3.2}{3.2} = 0.9818$$

So,

$$\eta_1 = -0.3390 + (0.9818)\ 0.8775 = 0.5225$$

From (VIII-3),

$$\xi_1 = \xi_1^\circ - \eta_1\ , = 0.8775 - 0.5225 = 0.3550$$

The coefficient of ξ_1 is,

$$17\left(\frac{n_o}{W_o}\right)\frac{\lambda_2}{\lambda_2+\lambda_5} = 17(0.00847)\frac{29.}{29.+0.6} = 0.1411$$

where (no/Wo) is determined from the structure of the p-f resin and the ash content. Since the structure is represented by equation (V-25), $(CH_2)_{3/2}\ (C_6H_2)\ OH$, one gram mole of resin would weigh 112.12 grams. Since the material, resin plus ash plus adsorbed species, is 94.97 w% resin, an initial weight of 100 grams gives 94.97 grams of resin or 0.847 gram moles, and (no/Wo) = (0.847/100) = 0.00847.

The second term is therefore,

$$17\left(\frac{no}{Wo}\right)\frac{\lambda_2}{\lambda_{25}}\xi_1 = (0.1411)(0.3550) = 0.05001$$

Similarly, the coefficient of ξ_o is 0.02736, $\xi_o^\circ = 1.0$, and $\eta_o = 0$. So the first term is 0.02736. The coefficient of ξ_2 is 0.09578, $\xi_2^\circ = 1.0$, and $\eta_2 = 0.00104$, so the third term is 0.09568. The coefficient of ξ_{125} is 0.10962. $\xi_{125}^\circ = 1.0$, and $\eta_{125} = 0$. So the last term is 0.10962. The sum of the four terms is 0.2828, and since no inert filler was added, $(W_o/W_{pf}) = 1$. Therefore (1 - W/Wo) = 0.2828 calculated by equation (VIII-1) at $\theta = 3$ min. The experimental value is 0.3100 (Figure 16); the difference, $\Delta = -0.0879$; the difference squared, $\Delta^2 = 0.00773$.

For all of the points from $\theta = 0$ to $\theta = 100$ the sum of the squares of the differences, $\Sigma\Delta^2 = 0.0198$, for the set $\lambda_o = 100.$, $\alpha_o = 0.0001$, $\lambda_1 = 0.7$, $\alpha_1 = 3.2$, $\lambda_2 = 29.0$, $\alpha_2 = 6.0$, $\lambda_5 = 0.6$, $\alpha_3 = 0.05$. Other sets from the possible combinations have $\Sigma\Delta^2$ as high as 0.03717, but since none of the sets has a lower $\Sigma\Delta^2$, these values of λ_1, λ_2, λ_5 are used in the next step.

The second phase of the operation is a minimization of $\Sigma\Delta^2$ by variation of α's in exactly the same fashion as was just done with variation of λ's. The number of points in each direction is chosen to be five. The size of the increments are chosen as $\Delta\alpha_1 = 0.50$, $\Delta\alpha_2 = 0.50$, $\Delta\alpha_3 = 0.05$, and from this the α matrix of $\alpha_1 = 2.2, 2.7, 3.2, 3.7, 4.2$; $\alpha_2 = 5.0, 5.5, 6.0, 6.5, 7.0$; and $\alpha_3 = 0.15, 0.20, 0.25, 0.30, 0.35$, is set up with the previous "best" α's in the center of the matrix. Each of the 125 combinations of α's is used in a set with the previously determined best set of λ's and λ_o and α_o. From this series of calculations $\Sigma\Delta^2$ as high as 0.03416 and as low as 0.0197 are obtained. Corresponding to the minimum $\Sigma\Delta^2$ are $\alpha_1 = 3.2$, $\alpha_2 = 5.0$, $\alpha_3 = 0.15$ and these "best" values are used in the next step.

The third phase is a repetition of the first phase which minimizes $\Sigma\Delta^2$ by variation of λ's again, but this time smaller λ increments are used and the λ matrix generated is a "medium mesh" matrix in the volume of the "coarse mesh" matrix generated in the first phase. The minimum $\Sigma\Delta^2 = 0.0189$ is calculated with $\lambda_1 = 0.74$, $\lambda_2 = 29.8$, $\lambda_5 = 0.56$ which are now taken as the new "best" values of λ's to be used in the next step.

The fourth phase is a repetition of the second phase and minimizes $\Sigma\Delta^2$ by using values from a "medium mesh" α matrix. Minimum $\Sigma\Delta^2 = 0.0189$ is calculated with $\alpha_1 = 3.2$, $\alpha_2 = 4.6$, $\alpha_3 = 0.11$ which become the new "best" α's.

Repeating with a "fine mesh" matrix of λ's gives a minimum $\Sigma\Delta^2 = 0.0189$, and following with a "fine mesh" α matrix gives a minimum $\Sigma\Delta^2 = 0.0186$. In principle this alternately improving λ's and α's is continued until $\Sigma\Delta^2$ no longer gets substantially smaller, and then the current "best" values of λ's and α's are taken as correct for the temperature of the data. In practice it is unwise to have the computer continue automatically beyond three repetitions of λ's and three of α's, or possibly even less for the first few submissions of the program. The reason for this is that the "correct" values of λ's and α's may not be within the volume originally started with. This is the case for this example; by viewing the computer output in its entirety, it can be seen that the minimum

$\Sigma\Delta^2$ always occurs at the boundary of the matrix being used. This means that better values of λ's and a's can probably be obtained by shifting the volume of investigation and repeating the process starting with a new coarse mesh matrix. When this is done, the parameters finally selected are $\lambda_o = 100$, $a_o = 0.0001$, $\lambda_1 = 0.666$, $a_1 = 3.40$, $\lambda_2 = 30.1$, $a_2 = 6.00$, $\lambda_5 = 0.544$, $a_3 = 0.250$ for 605°C. The values at other temperatures are presented in Tables VII and VIII. A least squares fit is then used to evaluate the constants for equations (VIII-7) and (VIII-8) so that λ's and a's can be calculated at intermediate temperatures.

The λ's can be converted to k's by the simple relation given in Table VII,

$$k = \frac{\lambda_i \rho}{60\, M_{resin}} = \frac{1.225\,\lambda_i}{60(112.12)} = (1.820\times10^{-4})\lambda_i^{*};\ \frac{g.mole}{sec\text{-}cm^3}$$

and values of k's so obtained are tabulated in Table VII.

For each λ_i a_i pair, a value for μ_i can be calculated by,

$$\mu_i = \frac{\lambda_i}{a_i^2}$$

and the diffusivities can be calculated by the relation given in Table VIII,

$$D_i = \frac{\mu_i}{60 S^2 \rho^2} = \frac{\mu_i}{60(2437)^2(1.225)^2} = (1.87\times10^{-9})\mu_i^{*};\ \frac{cm^2}{sec}$$

and values of μ's and D's are tabulated in Table VIII.

* Values of S and ρ from Table B-15, C-1 Run 2.

APPENDIX E

EXPERIMENTAL EQUIPMENT

1. Kinetic equipment:

The configuration of the kinetic equipment is discussed in Section IV. The chief item is a Perkin-Elmer model 800 gas chromatograph, which has a differential flame ionization detector, and is shown in Figure 41. An auxiliary thermal conductivity (hot wire) detector is installed in a separate oven and can be controlled at temperatures from 50-400°C. It is possible to operate the chromatograph so that both detectors are in use at the same time. The duel columns are in a proportional controlled oven which can be temperature programmed from ambic to 400°C. The dual liquid injector system can be operated up to 500°C. The gas sampling valve allows the introduction of a reproducible volume of sample gas in the nominal amounts of 25 ml., 5 ml., 1 ml., and 0.25 ml.

The output from the chromatograph goes to a Texas Instruments two channel Servo-Writer recorder, Model FWD-1MVE-5MVE-05-A16-BT, which is zener regulated, has 1/2 sec. response, and has 12 chart speeds. Channel A is 1 mv. and is connected to the hot wire detector. Channel B is 5 mv. and is connected to the flame detector.

The pyrolysis furnace, Figure 42, is a Lindberg-Heviduty type 54031, rated at 800 watts for 115/230 v. and can be operated to 1850°F. The furnace tube is custom made of vycor glass by Scientific Glass Blowing Company. The furnace temperature is controlled by a Honeywell Versa-Tronic indicating and controlling potentiometer, model R7161B-1468, which will operate over the range 0-1000°C. The controller activates a P & B relay #KA11AG, 10A. DPDT 115V. coil, which connects the furnace to the output of a 20A. 120V. Powerstat. The furnace temperature is obtained by means of an L & N #8686 millivolt potentiometer, which has multiple ranges to 100.100 millivolts, by means of a chromel-alumel thermocouple inserted down the furnace tube.

The vacuum for the furnace tube is provided by a Welch Disto-Pump model 1399, rated at 15 μ, Hg, and absolute pressure up to 240 mm Hg is indicated by a Bennert type vacuum manometer.

The adsorption tubes are 100 ml. Swartz drying tubes with 1215 ball and socket joints.

2. Karl Fisher apparatus:

The construction diagram of the apparatus is shown, Dwg. C-1001-19,700. The stirrer is a Lab-Line Magnestir #1250.

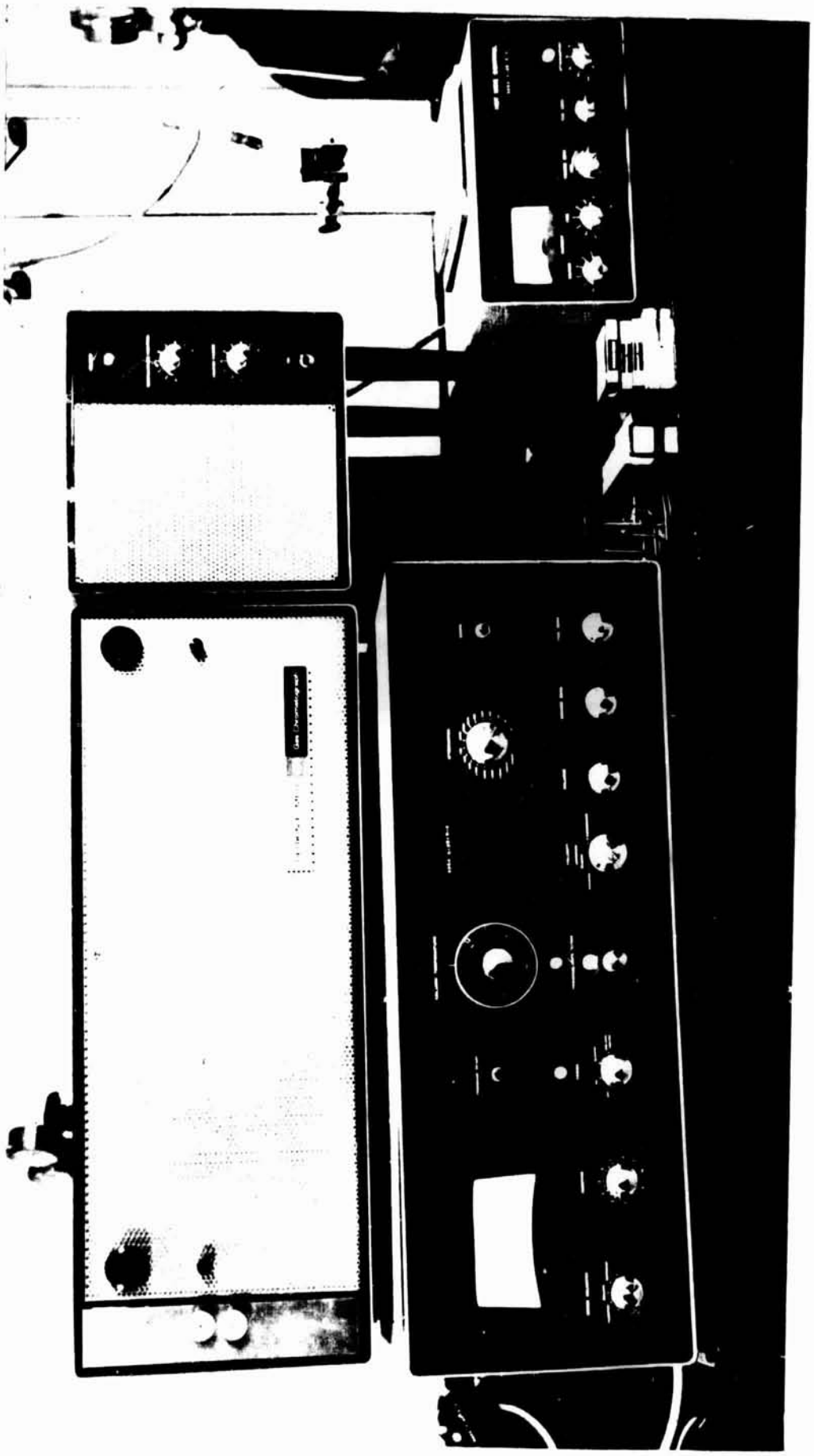

FIGURE 41 - GAS CHROMATOGRAPH

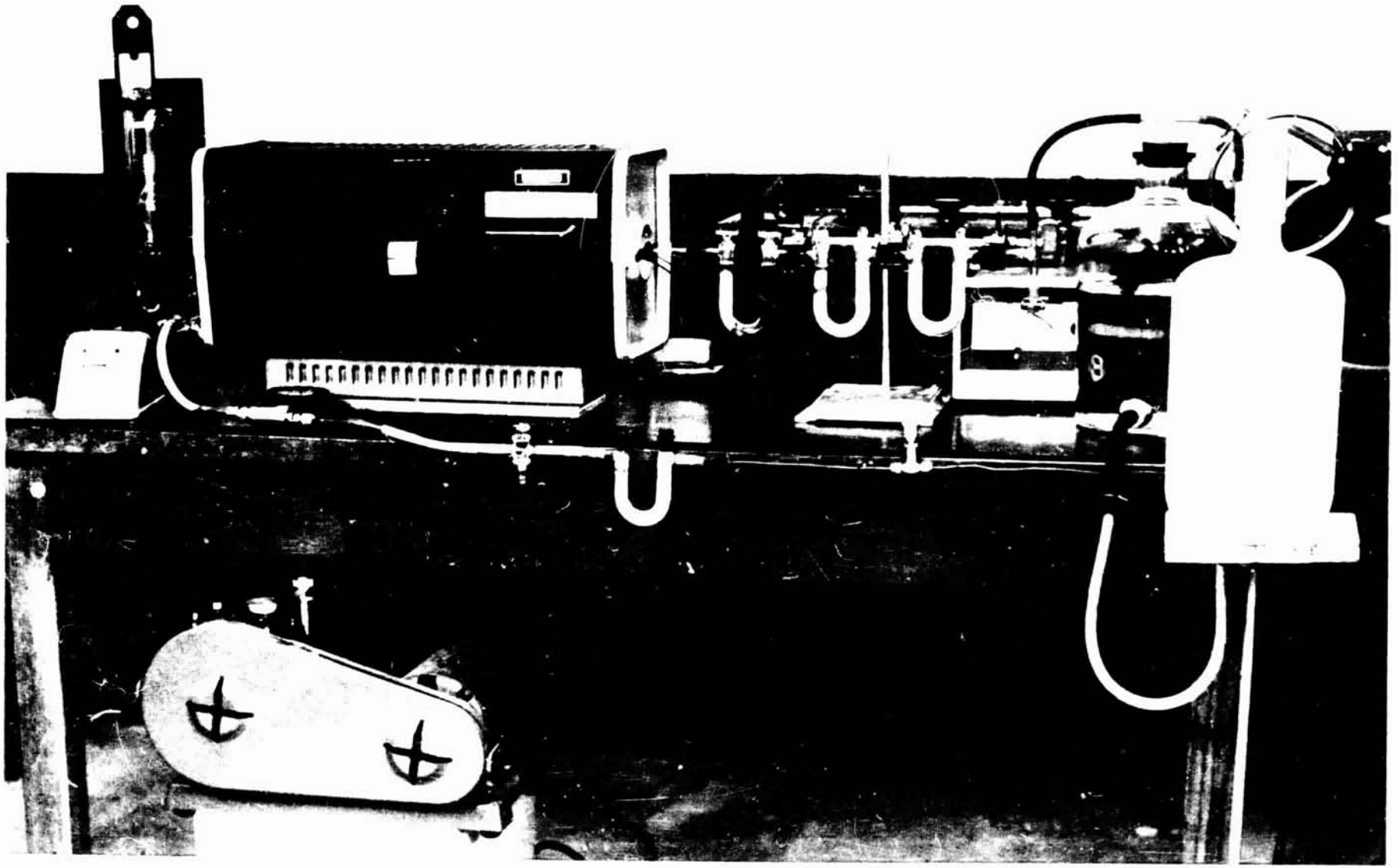

FIGURE 42 - PYROLYSIS FURNACE

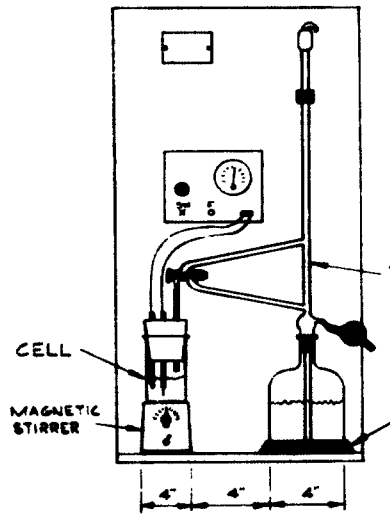

ASSEMBLY

SCALE: NONE

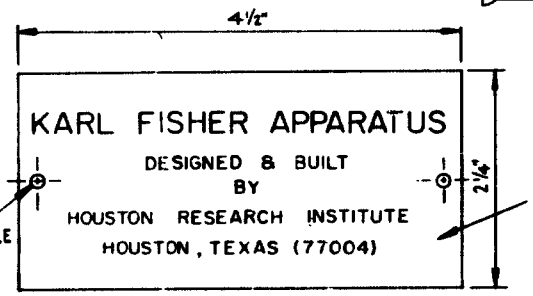

NAME PLATE DETAIL

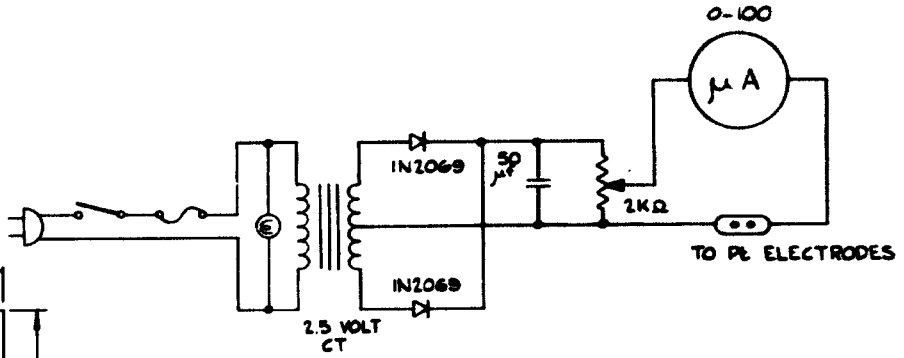

WIRING SCHEMATIC

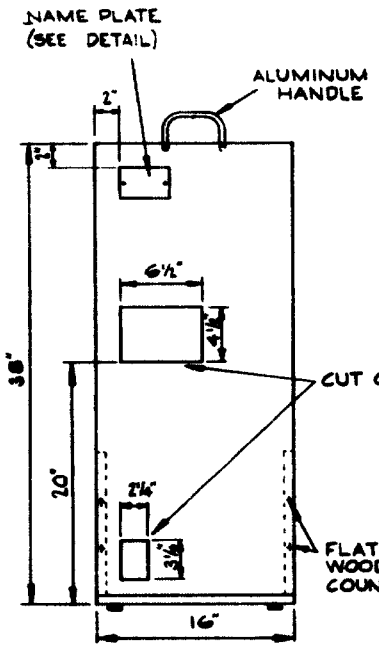

FRONT ELEV.

SCALE: NONE

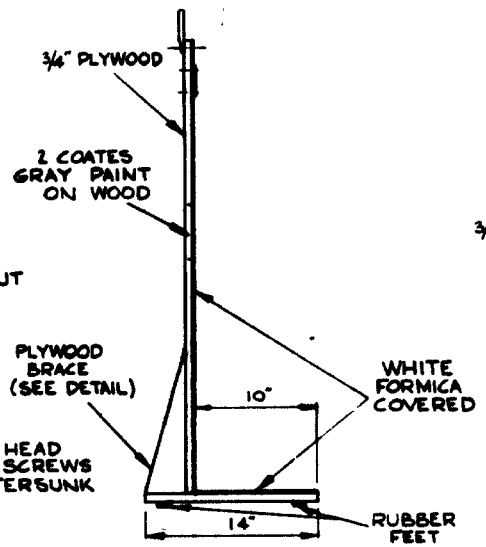

SIDE ELEV.

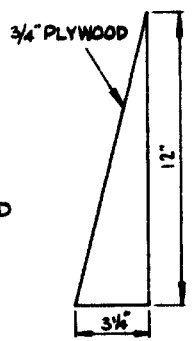

BRACE DETAIL

ITEM	QUAN.	DESCRIPTION

HOUSTON RESEARCH INSTITUTE, INC.

PREVIOUS DWG. NO. C-1001-19,700

MARK	REVISION	DATE

MANNED SPACECRAFT CENTER

KARL FISHER APPARATUS

DESIGNED BY	SCALE
CEI	NONE
DWN'D	DATE
TRACED	APP'D

PROJECT-19,700(NAS -2516) REV.

The automatic burette is manufactured by Kimax to meet the requirements of NBS Circular 602; the reservoir is 1000 ml.; the burette capacity is 25 ml. with 0.1 ml. subdivisions.

3. Vacuum desorption apparatus:

The construction diagram of the apparatus is shown, DWG. C-1002-19,700; vacuum oven is a National Appliance Company model 5830, and draws 550 watts at 115/220 V.; vacuum down to an absolute pressure of 1 μ Hg can be held, and temperature can be controlled from ambic to 200°C within 0.5°C. The vacuum for the oven is provided by a Welch Disto-Pump model 1399, rated at 15 μ Hg, and absolute pressure up to 240 mm Hg is indicated by a Bennert type vacuum manometer.

4. Winslow Mercury Porosimeter:

The porosimeter, pictured in Figure 10, is American Instrument's 15,000 psi model and was supplied completely equipped except for the following accessories which were obtained separately: a Hastings DV3, TC type vacuum gauge for absolute pressures below 1000 μ Hg.; and a Welch Disto-Pump model 1399 vacuum pump, rated at 15 μ Hg.

LET	DATE	REVISIONS	BY

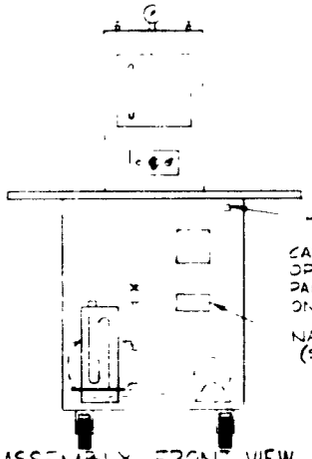

ASSEMBLY FRONT VIEW

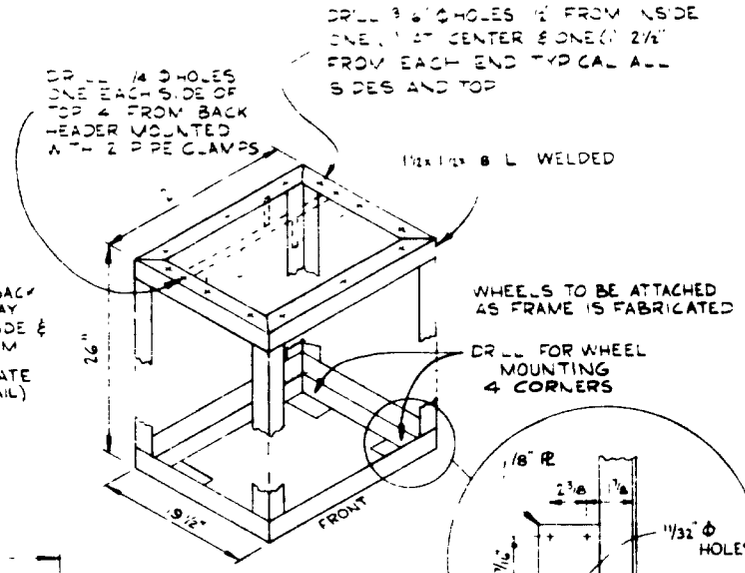

FRAME

NOTE: FINISHED FRAME TO BE PAINTED WITH ONE COAT SHOP PRIMER

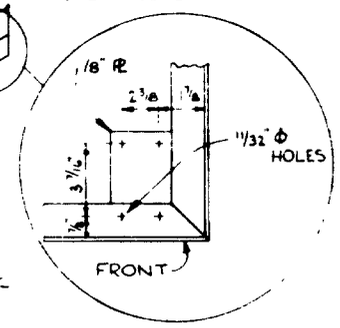

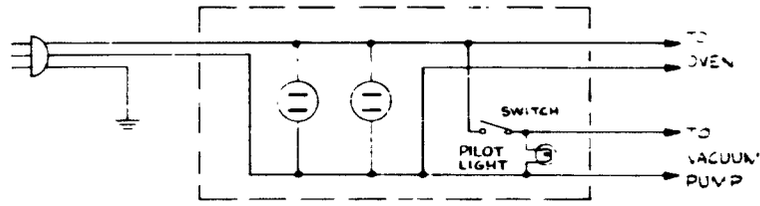

WIRING SCHEMATIC

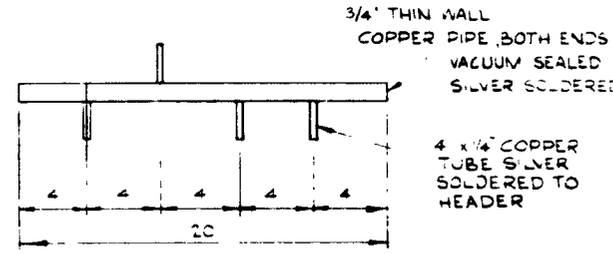

HEADER DETAIL

SCALE: NONE

VACUUM DESORPTION APPARATUS

DESIGNED & BUILT BY

HOUSTON RESEARCH INSTITUTE
HOUSTON, TEXAS (77004)

4"

2¼"

NAME PLATE

FULL SCALE

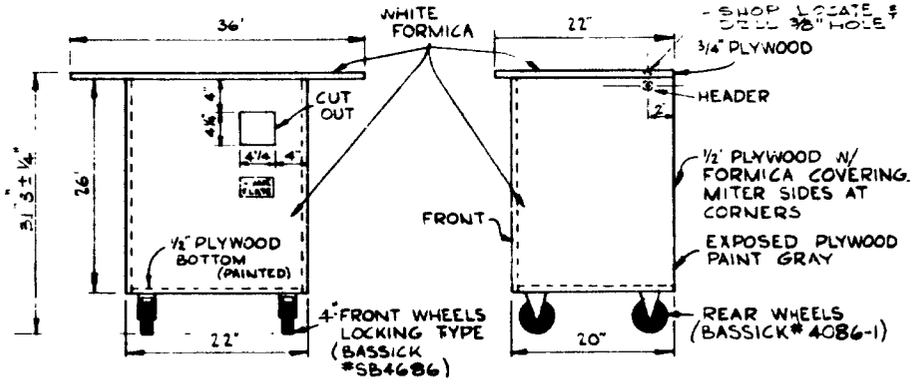

FRONT ELEV.

SCALE: 1" = 1'

SIDE ELEV.

SCALE = 1'

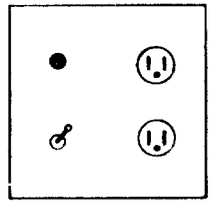

COVER PLATE DETAIL

DOUBLE 3-PRONG RECEPTICAL, SWITCH & PILOT LIGHT.

ASSEMBLY TO BE PLACED IN 4¼" x 4¼" CUTOUT

ITEM	REQD.	DESCRIPTION

HOUSTON RESEARCH INSTITUTE, INC.
PRENGLE DUKLER & CRUMP, INC TECHNO-SCIENCE, INC

NRI DWG NO C-002-9700

MARK	REVISION	DATE

DRAWN BY CEI SCALE AS NOTED
CHK'D DATE
TRACED APP'D

MANNED SPACECRAFT CENTER
HOUSTON, TEXAS

VACUUM DESORPTION APPARATUS

PROJECT 9700, NAS-9-2516 REV.